CHARLES UNIVERSITY IN PRAGUE

FACULTY OF SCIENCE

DEPARTMENT OF GENETICS AND MICROBIOLOGY

Mgr. Petra Beznosková

The role of translation initiation factor 3 (eIF3) in translation termination.

Úloha translačního iniciačního faktoru 3 (eIF3) v terminaci translace.

PhD Thesis

Supervisor: Leoš Valášek, Ph.D.

INSTITUTE OF MICROBIOLOGY AS CR

Prague, 2016

Declaration:

With this, I declare that I have written this work on my own, appropriately acknowledged citations, and used no other than the listed resources and aids.

Prague ..... **.....**

Mgr. Petra Beznosková

ACKNOWLEDGEMENTS

I would like to thank to my supervisor Leoš Valášek, Ph.D., for his patient guidance and support throughout all the years of my studies and for the opportunity to be a part of a great collective of the Laboratory of Regulation of Gene Expression, Institute of Microbiology AS CR. I would also like to thank to all the current and former members of our lab for their help, advices and long discussions which helped me greatly during my studies.

Many thanks belongs also to the members of Libor Krásný, Ph.D., Doc. David Staněk, Ph.D. and Doc. Petr Svoboda, Ph.D. laboratories for their constructive criticism, great questions and suggestions, which helped me to gain perspective and to look at my projects from different angles.

Special thanks I dedicate to my family for their patience and support, emotional and financial, during my studies, and all my friends who always encouraged and motivated me when I needed it.

This work was supported by the Wellcome Trust (grant number 090812/B/09/Z and 075438), Howard Hughes Medical Institute, the Centrum of Excellence Grant (P305/12/G034) awarded by the Czech Science Foundation, Czech Science Foundation (GA14-05394S); Charles University in Prague, project GA UK (762513 and 323415).

TABLE OF CONTENTS

ACKNOWLEDGEMENTS **2**

ABBREVIATIONS **5**

ABSTRACT **6**

ABSTRAKT **7**

INTRODUCTION **8**

Protein synthesis in eukaryotes *8*

Translation termination *9*

Stop codon readthrough *10*

Programmed stop codon readthrough *12*

Readthrough at a premature termination codon *14*

Ribosomal recycling *15*

Reinitiation – gene-specific mechanism of translational control *15*

AIMS OF THE STUDY **20**

MATERIALS AND METHODS **21**

RESULTS **22**

List of publications in chronological order *22*

Translation Initiation Factors eIF3 and HCR1 Control Translation Termination and Stop Codon Read-Through in Yeast Cells *24*

Structural integrity of the PCI domain of eIF3a/TIF32 is required for mRNA recruitment to the 43S pre-initiation complexes *26*

Translation Initiation Factor eIF3 Promotes Programmed Stop Codon Readthrough *27*

Rules of UGA-N decoding by near-cognate tRNAs and analysis of readthrough on short uORFs in yeast *28*

In-depth analysis of cis-determinants that either promote or inhibit reinitiation on GCN4 after translation of its four short uORFs *30*

DISCUSSION **31**

CONCLUSIONS **36**

REFERENCES 37

PUBLICATIONS I-V 42

ABBREVIATIONS

CTD	C-terminal domain
eIF	Eukaryotic initiation factor
IC	Initiation complex
Met-tRNAi	Methionyl initiator tRNA
MFC	Multifactor complex
mRNA	Messenger RNA
nc	Near-cognate
NMD	Nonsense mediated decay
NTD	N-terminal domain
PIC	Pre-initiation complex
post-TC	Post-termination complex
pre-TC	Pre-termination complex
PTC	Peptidyl transferase center
PTC	Premature termination codon
REI	Reinitiation
RPE	Reinitiation promoting element
RRM	RNA recognition motif
rRNA	Ribosomal RNA
TC	Ternary complex
uORF	Upstream open reading frame
WT	Wild type

ABSTRACT

Protein synthesis is a tightly regulated process of gene expression. Each gene has its start and its stop, which is determined by one of the three stop codons. Many recent articles describe ribosomes that purposely bypass stops on specific mRNAs to extend the nascent polypeptide to alter its properties. It is called programmed stop codon readthrough. Since over 15% of human genetic diseases are caused by so called premature termination codons (PTC) that halt translation and produce truncated proteins, this mechanism has a great potential implication in medical research. Numerous labs search for non-toxic drugs specifically increasing readthrough at PTCs; however, the success of this effort requires identification and understanding of all factors that are involved in this process. Here, we present one such factor eukaryotic initiation factor 3 (eIF3) and describe its ability to induce readthrough on stop codons in termination non-favorable context during programmed readthrough and also the consequences of its action on translation regulation. We additionally analyzed which near-cognate (nc) tRNAs are incorporated at UGA stop codons depending on the nucleotide that immediately follows them (so called +4 base). This way we established new rules for stop codon decoding and identified so called readthrough inducing tRNAs for each UGAN stop codon. We believe that the progress we have achieved in characterizing the regulation of translation termination will contribute to the overall intention of many researchers from the translation control field to fully understand the process of protein synthesis on a molecular level in order to improve human health.

ABSTRAKT

Syntéza proteinů v buňce je velmi regulovaný proces během genové exprese. Každý gen má svůj vlastní začátek a též jeden konec, který je určován přítomností jednoho ze tří stop kodónů. Mnoho současných článků popisuje ribosomy, které záměrně přechází přes stop signál u některých vybraných mRNA, aby prodloužily vznikající polypeptid a změnily jeho vlastnosti. Tento regulační proces se nazývá programované pročítání stop kodónu. Výzkum této regulace má potenciál se uplatnit i v lékařství, neboť přibližně 15% všech dědičných chorob je způsobeno přítomností takzvaného předčasného terminačního kodónu (PTC), který zastaví translaci a vznikne tak zkrácený nefunkční protein. Mnohé laboratoře již hledají netoxické látky, které by zvyšovaly pročítání předčasného terminačního kodónu. Bohužel k úspěšnému naplnění jejich záměru je třeba identifikovat a porozumět všem faktorům, které tento process ovlivňují. V této disertační práci představujeme jeden takový faktor- eukaryotický iniciační faktor 3 (eIF3). Demonstrujeme jeho schopnost indukovat pročítání terminačních kodónů, které jsou v kontextu nukleotidů nevhodných pro efektivní terminaci. Taktéž jsme vytvořili analýzu „nearcognate“ tRNA a ukázali, jak jsou inkorporovány na stop kodón, za kterým následují různé nukleotidy. Díky tomu jsme byli schopni rozšířit genetický kód o nová pravidla a přesně určit tRNA, které incorporují na různých UGAN terminačních kodónech. Pokroky, které jsme udělali během našeho studia regulace terminace translace, pomůžou mnohým výzkumníkům z oboru regulace translace porozumět procesu syntézy proteinů na molekulární úrovni.

INTRODUCTION

PROTEIN SYNTHESIS IN EUKARYOTES

Protein synthesis (translation) utilizes genetic information carriers, mRNAs, as templates for the production of proteins of various cellular functions. Typically it is divided into four phases: initiation, elongation, termination and ribosomal recycling. Although these four phases are distinct in time, there is a longstanding notion for some form of communication among them. Notably, several initiation factors and related proteins have been proposed to function in more than one phase. These include ABCE1/RLI1 and GLE1, which are believed to promote both the initiation and termination phases by a mechanism that remains to be elucidated (8, 14, 36), eIF5A proposed to stimulate all three major phases (62), and the *bona fide* translation initiation factor eIF3, which has been recently suggested to promote the recycling phase, at least in a mammalian *in vitro* reconstituted system (54, 56).

The beginning of a translational cycle involves a series of steps that culminate in the assembly of the 80S initiation complex (IC) on the AUG start codon (reviewed in (72)). These steps include 1) Met-tRNA$_i^{Met}$ recruitment to the 40S subunit to form the 43S pre-initiation complex (PIC), 2) mRNA recruitment to the 43S PIC to form the 48S PIC, 3) scanning of the 48S PIC to the first recognized start codon, and 4) joining of the 60 subunit to commit the resulting 80S IC to the elongation phase. The translation initiation factor eIF3, which in yeast consists of five essential core subunits (eIF3a/TIF32, b/PRT1, c/NIP1, i/TIF34 and g/TIF35) and one transiently associated, non-essential subunit (eIF3j/HCR1), is actively involved in regulation of the first three of these steps (72). In the PIC assembly steps, the action of eIF3 is further stimulated by one of its interacting partners, the ATP-binding cassette protein ABCE1/RLI1, by an unknown mechanism (14). In contrast to the most of eIFs, eIF3 interacts with the solvent-exposed side of the small ribosomal subunit (72) and as such it was proposed to be able to interact with active 80S ribosomes post-initiation (47, 57, 67).

The end of a translational cycle involves another series of steps that culminate in the release of a newly synthesized polypeptide from the translating ribosome (the termination phase), and in the dissolution of the ribosome:tRNA:mRNA complex (the recycling phase).

TRANSLATION TERMINATION

Termination begins when a stop codon enters the ribosomal A-site, forming a pre-termination complex (pre-TC) (1). In eukaryotes, all three stop codons are decoded by the eukaryotic release factor 1 (eRF1) (Figure 1). According to recent models (2, 64), eRF1 enters the ribosomal A-site in complex with a second release factor, eRF3, in its GTP bound form. Recognition of a stop codon triggers GTPase activity of eRF3, which leads to its dissociation from the complex in its GDP bound form. eRF1 is then free to activate the ribosomal peptidyl transferase centre (PTC), which hydrolyses the bond between the P-site tRNA and the nascent polypeptide. Importantly, these steps are promoted by RLI1 in an ATP-independent manner; i.e. by the same factor that also somehow stimulates the eIF3 function in the initiation phase. Molecular details of this RLI1 role in termination are similarly not known, nevertheless, the proposed active role of RLI1 in stop codon recognition is consistent with observations that conditional down regulation of RLI1 protein levels increases stop codon read-through in yeast (36). Based on the most recent structural model, RLI1 binds to the same site on the terminating ribosome as eRF3 (thus their binding is mutually exclusive), and its 4Fe-4S domain interacts with the C-terminal domain of eRF1 to push the conserved GGQ motif in the middle domain of eRF1 to the PTC next to the acceptor stem of the P-site tRNA to trigger polypeptide release (2).

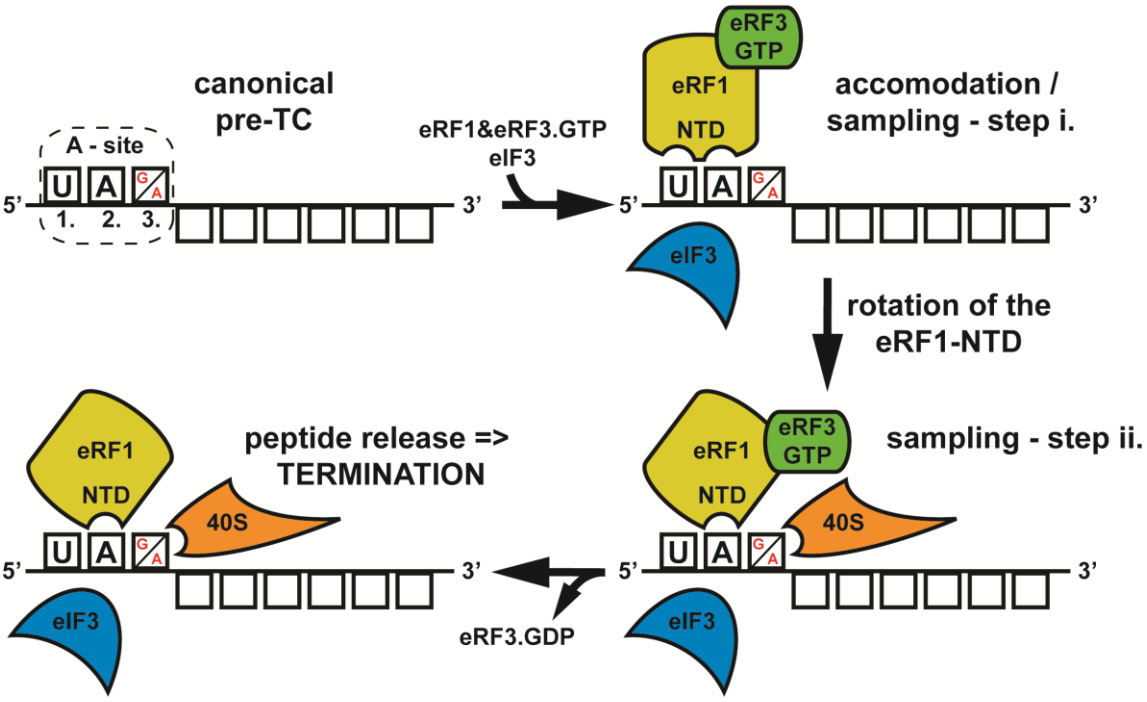

Figure 1: Stop codon recognition by eRF1; stop codon in the termination favorable context appears in the A-site (only UAG and UAA stop codons are indicated for illustration purposes; UGA works by the same mechanism), eRF1 in complex with eRF3.GTP binds to it and samples the codon in a two-step process including conformational re-arrangements of the eRF1-NTD. During the second step the ribosome by itself co-participates in this accommodation phase that ultimately leads to GTP hydrolysis on eRF3, polypeptide release and ribosomal recycling ((5)).

STOP CODON READTHROUGH

As indicated above, the stop codon is decoded by the release factor 1 (eRF1) that enters the A-site of the 80S ribosome in complex with the GTP-binding protein eRF3 during canonical termination (reviewed in (32)). In eukaryotes, eRF1 recognizes all three stop codons (UAA, UAG and UGA) with high precision. However, in some specific cases, not all stop codons signal the proper end of translation, which can thus continue beyond to the next stop codon. Generally speaking, translation termination can be viewed as a competition between stop codon recognition by release factors and stop codon decoding by near-cognate tRNAs. This competition differs genome-

wide in its efficiency. The efficiency can be influenced by the identity of the stop codon (30, 50, 60), the nucleotide context of the stop codon (9, 10, 41), the identity of the last two amino acids incorporated into the polypeptide chain (33), the identity of the P-site tRNA (45) and the presence of stimulatory elements downstream from the stop codon (25, 48, 65). All these features increase the odds of the stop codon being decoded by a near-cognate, natural suppressor tRNA rather than by eRF1, resulting in the process termed stop codon readthrough or nonsense suppressions which occurs when a near-cognate aminoacyl-tRNA or a suppressor tRNA is incorporated and accepted at a given stop codon (11). This allows production of C-terminally extended polypeptides with new or at least modified biological roles compared to their shorter, original versions. The mechanism whereby near-cognate tRNAs outcompete conventional stop codon recognition by eRF1 was not yet known, nor was which protein factors, if any, might be functionally important for stop codon readthrough.

Taken all this into account it is important to investigate which nc-tRNAs can decode individual stop codons and under what circumstances. The Namy's group has only recently made a great progress in this direction by experimentally demonstrating *in vivo* that tyrosine or glutamine preferentially incorporates at UAA (with similar frequencies), tyrosine predominantly inserts at UAG, and tryptophan or cysteine at UGA . Lysine and arginine were also shown to incorporate at UAA/UAG and UGA stop codons, respectively, and glutamine at UAG, but at very low rates. Soon after that the Jacobson's group extended these findings by a comprehensive *in vivo* analysis of termination readthrough from a PTC under different readthrough-inducing conditions (61). Their work identified exactly the same amino acid residues that are being inserted during readthrough, only with the predominant frequencies of incorporation for glutamine and not for tyrosine at UAG. However, what determines which of the amino acid residues that are specific for each stop codon incorporates at a given stop codon at a given frequency is not known.

It was previously demonstrated that the identity of a nucleotide immediately following any stop codon (the +4 nucleotide) fine tunes its termination efficiency; i.e. determines its permissiveness for readthrough (for an overview see (11)). For example, efficiency of readthrough on UGA determined by the +4 nucleotide identity follows this order of tetranucleotides: UGA-C>UGA-A>UGA-G>UGA-U (5). In fact, C at the +4 position is the strongest readthrough inducer among all four bases at all three stop codons (11). Hence it was possible that in addition to the stop codon, it is also the +4 base that influences what nc-tRNA gets preferentially accepted by the A-site during readthrough. It can be “spontaneous” and thus relatively infrequent (the order of spontaneous stop codon leakiness is UGA>UAG>UAA). Or it can be programmed to C-terminally extend the protein of interest as a response to for example specific environmental changes demanding an alteration of the corresponding protein’s properties (for more details see (13)).

PROGRAMMED STOP CODON READTHROUGH

Programmed stop codon readthrough is a post-transcriptional regulatory mechanism specifically increasing proteome diversity by creating a pool of C-terminally extended proteins. During this process, the stop codon is decoded as a sense codon by a near-cognate tRNA, which programs the ribosome to continue elongation (Figure 2). The efficiency of competition for the stop codon between release factors (eRFs) and near-cognate tRNAs is largely dependent on its nucleotide context; however, the molecular mechanism underlying this process is unknown. In recent years several groups have proposed that the stop codon readthrough mechanism is specifically regulated by cis-acting RNA elements downstream of the first stop codon that may exist to generate proteome diversity in response to changing environmental conditions. The rapidly growing list of cellular genes under the control of this “programmed stop codon readthrough” mechanism, the typical, long standing example of which is from the tobacco mosaic virus

(TMV) genome (65), strongly suggests that programmed stop codon readthrough is an important contributor to general translational control in all kingdoms of life (for review; see (6, 15, 49, 73). A recent ribosome profiling study detected many readthrough events occurring at biologically relevant levels in budding yeast, fruit fly, and human data sets, suggesting that this mechanism is highly conserved (16).

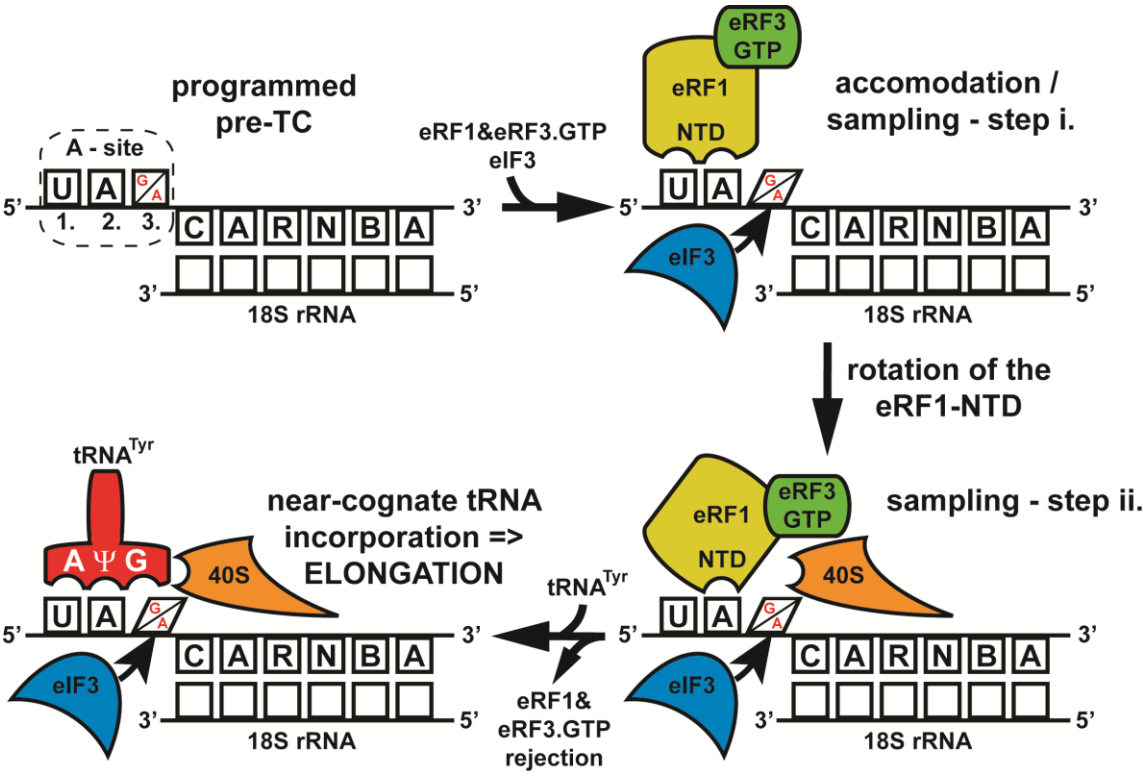

Figure 2: Programmed stop codon readthrough; stop codon occurs in the unfavorable termination context bearing specific consensus sequences like CAR-NBA in its 3' UTR – in this particular case proposed to base-pair with 18S rRNA. The eIF3 presence in the pre-TC – perhaps in co-operation with these sequences – alters the decoding property of the nucleotide at the 3rd stop codon position. This prevents its proper decoding during the second sampling step and subsequently, after the eRF1-eRF3.GTP complex rejection, allows incorporation of near-cognate tRNAs with the mismatch at the 3rd position to read through the stop codon and continue with elongation ((5)).

As mentioned above, we recently showed that one of the key translation initiation factors – eIF3 – interacts with pre-termination complexes

(pre-TCs) and controls translation termination and readthrough (3). In particular, it interferes with the eRF1 ability to recognize the third/wobble position of any programmed stop codon leading to the rejection of the eRF1-eRF3.GTP complex from pre-TCs. At the same time eIF3 promotes incorporation of nc-tRNAs with a mismatch at the same position and thus represents one of the key players in programmed stop codon readthrough (5). For UGA there are two nc-tRNAs with the mismatch at the third/wobble position, Trp- and Cys-tRNAs. The third and last nc-tRNA with the wobble mismatch, Tyr-tRNA, is shared by the UAA and UAG stop codons. Incorporation of all of these three nc-tRNAs is promoted by eIF3 and, in fact, we provided evidence that efficient readthrough at UGA is enabled exclusively by the former two nc-tRNAs with the mismatch at the third/wobble position (5). This does not seem to apply to the other two stop codons, however, because other studies based on different approaches that were mentioned above showed that in addition to Tyr-tRNA, UAA and UAG can be also recoded by Gln- and Lys-tRNAs; i.e. nc-tRNAs with the mismatch at the first position (7, 61). The UGA stop codon has two nc-tRNAs with the first position mismatch, Gly- and Arg-tRNA, the latter of which was also suggested to insert at the A-site with low frequencies by these authors; however, it did not do so in our hands (5).

READTHROUGH AT A PREMATURE TERMINATION CODON

Stop codon readthrough can also occur at a premature termination codon (PTC) within the coding region of a given gene, which is desirable because it can prevent the action of nonsense mediated decay (NMD) pathway by ensuring the synthesis of a full-length protein (35). In fact, there are many diseases caused by PTCs that often occur in the termination non-favorable context making them good substrates for drug-stimulated programmed readthrough (39). Mainly from this point of view this topic is of a high importance also for medical reasons (37).

RIBOSOMAL RECYCLING

At some point translation will terminate and then the ribosomal recycling can occur. Recycling of eRF1-associated post-termination complexes (post-TCs) was recently shown to be also mediated by ABCE1/RLI1, this time, however, in an ATP-dependent manner (56, 64). It was hypothesized that RLI1, upon binding and hydrolyzing ATP, switches its conformation into a closed state, and the mechanochemical work generated by this switch splits post-TCs into free 60S subunits and deacylated tRNA- and mRNA-bound 40S subunits (40S-post-TC) (2). Finally, Pisarev *et al.* showed that the release of tRNA and mRNA from the 40S-post-TCs is *in vitro* ensured by the *bona fide* initiation factors eIF1, eIF1A and eIF3 (54, 56). eIF3, and in particular its j subunit (HCR1 in yeast), were suggested to play the key role in mRNA dissociation.

REINITIATION – GENE-SPECIFIC MECHANISM OF TRANSLATIONAL CONTROL

When the ribosomal recycling fails and 40S stays bound to mRNA after termination, all initiation factors can be re-recruited and the new 43S pre-initiation factor can reinitiate at the following AUG start codon of the same mRNA. This is a basic principle of reinitiation (REI) - a gene-specific mechanism of translational control exerted by some short upstream ORFs (uORFs) to fine tune the expression of the main ORF. eIF3 was shown to play a critical role in this process by making contacts with both the 40S subunit as well as sequences upstream of REI-permissive uORFs to stabilize their mutual interaction (23, 47, 67). The classical REI-dependent mRNA of *GCN4* containing together four short uORFs has been studied in great detail for several decades and found to rely mainly on the first REI-permissive uORF1 and the last REI-non-permissive uORF4 (reviewed in (28); Figure 3). The middle two uORFs were not considered to be important for the regulation of *GCN4* expression because the entire system could relatively effectively

function also in the uORF1–uORF4 minimalistic arrangement (43, 46). The exceptionally high REI potential of uORF1 has been ascribed to 1) the 5' sequence preceding the uORF1 AUG with an unknown molecular role (21); 2) the first 10 nt immediately following the uORF1 stop codon supposedly owing to their low GC content that would not permit strong base-pairing interactions with the 40S subunit and thus allow it to promptly resume scanning – in contrast to the corresponding GC-rich sequence of uORF4(20); and 3) the third coding triplet of uORF1 that, when mutated in combination with the replacement of the

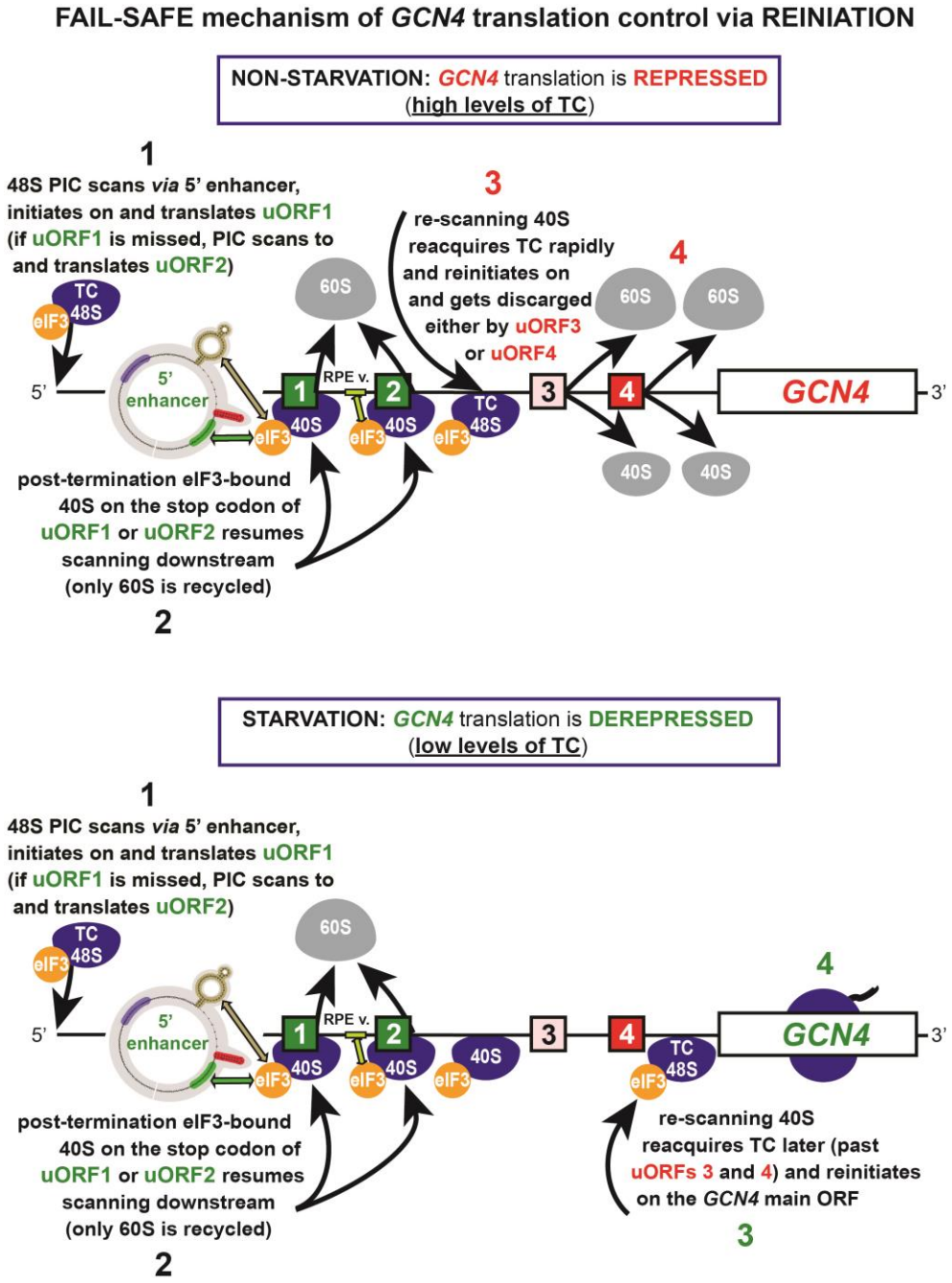

Figure 3: Model of the 'Fail-safe mechanism' of *GCN4* translational control adapted from (23). Schematic of the *GCN4* mRNA leader showing distribution of all four short uORFs, locations of the uORF1-specific and uORF2-specific RPEs, 40S-bound eIF3, and the description of the 'Fail-safe mechanism' of the *GCN4* translational control. Upper panel models the events on the *GCN4* mRNA leader occurring under non-starvation conditions with abundant TC levels—'*GCN4*-expression repressed state', the lower panel illustrates the steps that take place under starvation condition with limited supply of the TC—'*GCN4*-expression derepressed state' (23).

uORF1 3' sequence for that of uORF4, further exacerbated the negative impact of this replacement on REI efficiency (20). Based on these and other findings a detailed model of the *GCN4* translational control was proposed that was recently reviewed in our lab (28). Briefly, translational control of *GCN4* involves four short uORFs and is very sensitive to the TC levels that are changing in response to different nutrient conditions (12). The first of the four uORFs is efficiently translated under both nutritional replete and deplete conditions and after its translation, the post-termination 40S subunit remains attached to the mRNA – thanks to the functional interaction between uORF1's RPEs and the a/TIF32-NTD – and resumes scanning for REI downstream. In non-stressed cells, where the TC levels are high, nearly all of the rescanning ribosomes can rebind the TC before reaching one of the last two distant uORFs (uORFs 3 and 4), neither of which supports efficient REI. As a result, ribosomes terminating on these two uORFs undergo the full ribosomal recycling step, which prevents them from reaching and translating the main *GCN4* ORF. Under starvation conditions, the GCN2 kinase phosphorylates eIF2, which suspends formation of new TCs in the cytoplasm. Consequently, post-termination 40S ribosomes traveling from the uORF1 stop codon downstream will require more time to reacquire the TC to be able to recognize the next AUG start codon. This will allow a large proportion of them to bypass uORF3 and uORF4 and rebind the TC downstream of uORF4 but still upstream of the *GCN4* start codon. Thus, whereas the global protein synthesis is significantly down-regulated under nutrient deplete conditions; protein expression of the GCN4 transcriptional activator is concurrently induced. The second REI permissive uORF, uORF2, occurring only 56nt downstream of uORF1 and also utilizing the RPEs, then serves as a backup of uORF1 to capture all ribosomes that leaky scanned the uORF1 AUG, especially during stress conditions that seem to increase the frequency of leaky scanning in general (38, 52, 59, 66) to ensure that the maximum capacity of this intriguing regulatory system is met. Similarly, two consecutive uORFs with minimal or no REI-promoting potential occurring

further downstream (uORF3 and uORF4) also prevent leakiness of this system but during nutrient replete conditions (23).

Hence both processes – readthrough and reinitiation – are dependent on the physical presence of eIF3 in termination complexes, yet from the regulatory point of view they act against each other. In other words, increased readthrough will prevent reinitiation. Since to our knowledge virtually nothing is known about readthrough on short uORFs, we recently investigated the mutual functional relationship of readthrough and reinitiation during termination on uORFs that are set in regulatory networks relying on high levels of REI. This is the case of for example the *GCN4* mRNA (23), where the integrated regulatory output provided by its four short uORFs could be largely influenced by increased readthrough.

AIMS OF THE STUDY

The main goal of this pioneer study was first to demonstrate if there is a functional interaction between translation initiation factor eIF3 and factors involved in translation termination and then to determine the molecular role of the eIF3 factor in this process. Next I also sought to gain new knowledge regarding the molecular mechanism of translation termination in general and factors involved in its regulation. I also tried to address our question whether eIF3 role in termination somehow influences the already established eIF3-dependent activation of transcription factor GCN4 under stress conditions via its re-initiation-promoting activity, which was never considered before. Several specific objectives were postulated in order to explore these interesting biological questions:

- To uncover the role of the eIF3-associated factor HCR1 in translation termination and/or recycling
- To demonstrate the presence of eIF3 core subunits on the pre-termination 80S ribosome *in vivo*
- To demonstrate that the eIF3 stimulation of stop codon readthrough is dependent on its association with pre-termination 80S complexes *in vivo*
- To analyze the readthrough effects of eIF3 on stop codons in various nucleotide contexts
- To determine how eIF3 affects stop codon decoding by cognate, near-cognate or non-cognate factors
- To reveal the molecular base of differential termination efficiencies between UGAN stop codon tetranucleotides
- To analyze the readthrough efficiency on all four short uORFs from the GCN4 mRNA leader and to establish how the readthrough influences their re-initiation potential

MATERIALS AND METHODS

All experiments were carried out on a model organism of budding yeast *Saccharomyces cerevisiae* with exception of one experiment which was carried out in HeLa cells.

List of methods:

1% HCHO-crosslinking, WCE preparation, and fractionation of extracts for analysis of pre-termination complexes
Beta-galactosidase assay
Co-immunoprecipitation and affinity tag pull downs
Dual luciferase assay
Glutathione S-transferase (GST) pull-down experiments
Northern blot analysis
Polysome profile analysis
Polysome gradient analysis
Preparation of antibodies
Protein purifications
Resedimentation analysis of termination complexes
Western blot analysis

RESULTS

LIST OF PUBLICATIONS IN CHRONOLOGICAL ORDER

Translation Initiation Factors eIF3 and HCR1 Control Translation Termination and Stop Codon Read-Through in Yeast Cells

Petra Beznosková*, Lucie Cuchalová*, Susan Wagner, Christopher J. Shoemaker, Stanislava Gunišová, Tobias von der Haar, Leoš Shivaya Valášek

PLoS Genet. 2013 November; 9(11):e1003962

PMID:24278036 *These authors contributed equally to this work

IF_{2013} 8.167

Contribution of the author: 45%; I conceived and designed the experiments, performed one half of them, analyzed the data and also contributed to writing the publication.

Structural integrity of the PCI domain of eIF3a/TIF32 is required for mRNA recruitment to the 43S pre-initiation complexes

Sohail Khoshnevis, Stanislava Gunišová, Vladislava Vlčková, Tomáš Kouba, Piotr Neumann, Petra Beznosková, Ralf Ficner, and Leoš Shivaya Valášek

Nucleic Acids Res. 2014 April 42(6): 4123–4139.

PMID: 24423867

IF_{2014} 9.112

Contribution of the author: 5%; I helped to setup the RNA-binding assay.

Translation Initiation Factor eIF3 Promotes Programmed Stop Codon Readthrough

Petra Beznosková, Susan Wagner, Myrte Esmeralda Jansen, Tobias von der Haar and Leoš Shivaya Valášek

Nucleic Acids Res. 2015 May 26; 43(10):5099-111

PMID: 25925566

IF_{2015} 9.112

Contribution of the author: 80%; I conceived and designed the experiments, performed the majority of them, analyzed the data and also wrote the manuscript.

Rules of UGA-N decoding by near-cognate tRNAs and analysis of readthrough on short uORFs in yeast

Petra Beznosková, Stanislava Gunišová and Leoš Shivaya Valášek

RNA. 2016 Mar;22(3):456-66

PMID: 26759455

IF_{2015} 4.936

Contribution of the author: 90%; I conceived, designed and performed all experiments, analyzed the data, created the layout of the manuscript and contributed to writing the publication.

In-depth analysis of cis-determinants that either promote or inhibit reinitiation on GCN4 after translation of its four short uORFs

Stanislava Gunišová, Petra Beznosková, Mahabub Pasha Mohammad, Vladislava Vlčková, and Leoš Shivaya Valášek

RNA. 2016 Apr;22(4):542-58

PMID: 26822200

IF_{2015} 4.936

Contribution of the author: 10%; I performed the experiment shown in Figure 7B and help with writing of parts in the manuscript connected to the topic of my expertise (i.e. stop codon readthrough).

TRANSLATION INITIATION FACTORS eIF3 AND HCR1 CONTROL TRANSLATION TERMINATION AND STOP CODON READ-THROUGH IN YEAST CELLS

Petra Beznosková*, Lucie Cuchalová*, Susan Wagner, Christopher J. Shoemaker, Stanislava Gunišová, Tobias von der Haar, Leoš Shivaya Valášek

PLoS Genet. 2013 November; 9(11):e1003962

PMDI:24278036

*These authors contributed equally to this work

In this study we are presenting the ground breaking evidence that the key translation initiation factor eIF3 is involved in the regulation of the last phase of translation – translation termination. In particular, we are showing that i) various mutations reducing the activity of translation initiation factor eIF3 and its associated factor HCR1 affect stop codon read-through; ii) complexes containing eIF3, HCR1, ABCE1/RLI1 and both eRFs occur *in vivo* free of ribosomes and RNA; iii) there is a direct interaction between two eIF3 subunits and eRF1; iv) eIF3 associates with 80S couples isolated from heavy polysomes in an eRF1-dependent manner; and finally v) eIF3 mutants genetically interact with release factor mutants. In this study we also go deeper into understanding the role of HCR1 protein which is required for stringent selection of AUG and until now was believed to be non-essential subunit of eIF3 complex. Here, we provide an evidence that i) deletion of *HCR1* increases readthrough; ii) increased gene dosage of ABCE/RLI1 suppresses the slow growth and read-through defects of *hcr1* deletion strain; iii) Deletion of *hcr1* results in accumulation of eRF3 in heavy polysomes; iv) the sup45^{Y410S} mutation prevents stable association of eRF3 and HCR1 with polyribosomes; and v) the sup45^{Y410S} mutation eliminates the negative impact of hcr1Δ on read-through and growth rates. Based on our results we propose that HCR1 should be considered as a termination factor rather than an initiation factor and a subunit of eIF3.

To summarize our observations we proposed a model of eIF3 and HCR1 involvement in yeast translation termination. Upon stop codon entry into the ribosomal A-site the pre-TC forms, composed of the canonical release factors eRF1 and eRF3·GTP, and eIF3 and HCR1. eRFs and eIF3 may associate with the pre-TC as a pre-formed unit or alone. In the pre-TC, eIF3 interacts with the N domain of eRF1, *via* its two small g/TIF35 and i/TI34 subunits, and modulates, perhaps inhibits its stop codon recognition activity during the proofreading step. Upon stop codon recognition the GTP molecule on eRF3 is hydrolyzed. Subsequently, HCR1 promotes eRF3·GDP ejection to allow the ABCE1/RLI1·ATP recruitment to begin the accommodation phase of termination – the eRF1 GGQ motif is pushed to the peptidyl-transferase center (PTC) – during which HCR1 interacts with ABCE1/RLI1. Subsequently, both factors together with eIF3 participate in ribosomal recycling to enable and promote initiation of the next translational cycle.

STRUCTURAL INTEGRITY OF THE PCI DOMAIN OF eIF3A/TIF32 IS REQUIRED FOR mRNA RECRUITMENT TO THE 43S PRE-INITIATION COMPLEXES

Sohail Khoshnevis, Stanislava Gunišová, Vladislava Vlčková, Tomáš Kouba, Piotr Neumann, Petra Beznosková, Ralf Ficner, and Leoš Shivaya Valášek

Nucleic Acids Res. 2014 April 42(6): 4123–4139.
PMID: 24423867

This is an important study bringing more structural insight into yeast eIF3 complex. There is not any new information regarding the eIF3 role in translation termination. However, it contributes to characterization of mutants used in Beznosková et al. 2013 and Beznosková et al. 2015 (3, 5).

TRANSLATION INITIATION FACTOR eIF3 PROMOTES PROGRAMMED STOP CODON READTHROUGH

Petra Beznosková, Susan Wagner, Myrte Esmeralda Jansen, Tobias von der Haar and Leoš Shivaya Valášek

Nucleic Acids Res. 2015 May 26; 43(10):5099-111

PMID: 25925566

This study focuses on the eIF3 complex and its function during the translation termination step. We discovered that eIF3 actually promotes readthrough only on stop codons in termination non-favorable context, which has been known to be connected with the regulatory process called programmed readthrough. We showed that the eIF3 stimulation of stop codon readthrough is dependent on its association with pre-termination 80S complexes *in vivo.* Regarding the mechanism of eIF3 actions we discovered that eIF3 interferes with decoding of the 3rd position of the stop codon allowing incorporation of near-cognate tRNAs with the mismatch at the same position. The most of the work was done in yeast; however, we demonstrated that also human eIF3 promotes stop codon readthrough suggesting that the eIF3 role in stop codon readthrough is conserved between yeast and humans. Based on our new results we proposed a model how translation initiation factor eIF3 promotes programmed stop codon readthrough. It should be noted that there has been a long-standing lack of knowledge regarding the precise mechanism of this recoding event; even though many groups have sought to identify factors promoting incorporation of tRNA on stop codon.

RULES OF UGA-N DECODING BY NEAR-COGNATE tRNAs AND ANALYSIS OF READTHROUGH ON SHORT uORFs IN YEAST

Petra Beznosková, Stanislava Gunišová and Leoš Shivaya Valášek

RNA. 2016 Mar;22(3):456-66
PMID: 26759455

In this study we established new rules for decoding of UGAN tetranucleotides and subsequently analyzed readthrough on short uORFs in yeast. Note, that these two parts are tightly interconnected through the eIF3 role in stop codon readthrough. First, we showed that cytosine immediately following any stop codon interferes with the eRF1 decoding *in vivo*, which in fact causes the highest readthrough among the rest of tetranucleotides. The highlight of this study is the result showing that the UGA-A tetranucleotide is preferentially read through by tryptophan nc-tRNA and the UGA-C and UGA-G tetranucleotides are preferentially read through by cysteine nc-tRNA. We also confirmed our observations with additional experiments. We investigated i) an effect of the miscoding agent paromomycin on hc tryptophan or cysteine nc-tRNA incorporation at UGA-N termination tetranucleotides; and ii) an effect of the eRF1 (sup45-M48I) mutation with impaired decoding ability on hc tryptophan or cysteine nc-tRNA incorporation at UGA-N termination tetranucleotides; and came to the conclusion that neither the eRF1 decoding ability nor the geometry of the decoding pocket determines the UGA-N tetranucleotide preference for specific nc-tRNAs.

In the second part we focused on readthrough measurements of stop codons in their natural nucleotide contexts taken from all four short uORFs in the *GCN4* mRNA leader and we studied if the readthrough is eIF3 dependent. We observed that the eIF3-promoted readthrough does not interfere with the eIF3-promoted reinitiation on REI-permissive uORF1 from the GCN4 mRNA leader indicating that the key uORF1 naturally evolved to ensure as efficient termination as possible to be able to promote potent REI

despite the constant presence of the readthrough-stimulating eIF3 complex, which is at the same time essential for efficient REI.

IN-DEPTH ANALYSIS OF CIS-DETERMINANTS THAT EITHER PROMOTE OR INHIBIT REINITIATION ON GCN4 AFTER TRANSLATION OF ITS FOUR SHORT uORFs

Stanislava Gunišová, Petra Beznosková, Mahabub Pasha Mohammad, Vladislava Vlčková, and Leoš Shivaya Valášek

RNA. 2016 Apr;22(4):542-58

PMID: 26822200

This is a comprehensive study which reveals several REI-promoting and inhibiting cis-determinants that contribute either autonomously or in synergy to the overall efficiency of reinitiation (REI) on *GCN4*. Part of many results which are not connected to the topic of my thesis, we demonstrated that poor termination efficiency at the uORF4 stop codon strongly contributes to its poorest REI efficiency and also to the difference in the REI efficiency between uORF3 and uORF4.

DISCUSSION

There is no doubt that eIF3 belongs to the most promiscuous initiation factors. It is involved in all steps of this particular phase, is a key factor in translation control of transcription factor GCN4 and also possesses the ability to link translation initiation to transcription (24), to mRNA export (8), and to NMD pathway (31, 63) and thus integrates all these processes into a delicately regulated high-order process. In addition, eIF3 has been also suggested to promote the recycling phase of translation, at least in mammalian *in vitro* reconstituted system (54, 56). Based on newly identified interaction partner RLI1 and its recently described function in translation termination (36) it become highly attractive to investigate the possible role of eIF3 in this process. To do that we had to first extend our methodology which was primary designed to study details of translation initiation. In our lab, we established routine readthrough measurements using well defined dual luciferase reporter system (34) and designed several new reporters to satisfy our scientific needs. It should be noted that this is actually the only functional *in vivo* assay for determination of translation termination efficiency. We also repurposed resedimentation protocol previously used to detect factors bound to 40S (71) to analyze factors bound to terminating ribosomes. We had to request various strains with specific functional mutations in release factors and thus diversify our yeast collection. For our work it was no less important to prepare antibodies against factors involved in termination. We have prepared SUP45 and RLI1 antibodies, others that we didn´t have we had to request.

Throughout discovering the area of translation termination it was a big advantage to do all these first steps with a help of our collaborator and friend Tobias von der Haar, who is an expert in this field. However, it did not save us from troubles we had while setting a right nomenclature connected to the translation termination. Read-through, or readthrough? As freshmen we looked up the amount of publications for the term “read-through” (n=1093 on 13.5.2016) and “readthrough” (n=1159 on 13.5.2016) at the NCBI web page

(https://www.ncbi.nlm.nih.gov/) and it seems to be used equally often. Tobias was not a big help in this decision making process because he used both terms in one of his papers (42). So, in our first paper (3) we agreed on using “read-through” because I liked the graphics better and I was, and I still am, using the abbreviation “r-t” in my notes. However, for the second paper I performed more precise analysis of usage of these two terms in the literature. First, when I have searched “translational read-through” (n= 144 on 13.5.2016) and “translational readthrough” (n=287 on 13.5.2016) the term “readthrough” become slightly favored. And since we wanted to demonstrate that eIF3 is involved in programmed readtrough it was only rational to count the occurrence of “programmed read-through” (n=12 on 13.5.2016) vs. “programmed readthrough” (n=32 on 13.5.2016). This time readthough became almost threefold more used than read-through. Next way how to decide what to use was to look up the web sites of laboratories which are devoted to study regulation of translation termination. Surprisingly, all of them use the term “readthrough”. Based on that we decided to join groups with an established termination research by switching the nomenclature from read-through (3) to readthrough (5) and continuously use this term (4, 22) .

With the right methodology and nomenclature it became easy to perform all necessary experiments and thanks to all results gain knowledge about a function of eIF3 in translation termination. Since it is a complex theme I took liberty to divide the following discussion into three important points. First two discuss independently basic roles of HCR1 and eIF3 in translation termination and readthrough. And the last section discusses the effect of newly established eIF3 role in promoting readthrough on the translation regulation on upstream short uORFs in the GCN4 leader which might or might not interfere with eIF3-dependent resumption of scanning.

HCR1 functions in ejection of eRF3.GDP from post-TCs resulting in an efficient RLI1 binding and consecutive polypeptide release

The HCR1 protein was originally isolated as a high copy suppressor of temperature sensitive phenotype of rpg1-1 allele of TIF32 (69). HCR1 was considered to be a nonessential substoichiometric subunit of eIF3 with dual function in translation initiation and in processing of 20S pre-rRNA (68). It can bind to 40S ribosomes independently of eIF3 and other components of the MFC (53) and only modestly it stimulates 40S binding of eIF3 (51), (17). In one of my papers (3) we showed that deletion of *hcr1* increases stop codon read-through, independently of its association with the rest of eIF3, and results in accumulation of eRF3 in heavy polysomes. Increased dosage of ribosomal recycling factor RLI1 then substitutes for the HCR1 roles in termination (but not in initiation) and in enabling efficient cell growth, which together implied that the HCR1 function in termination is more critical for optimal cell proliferation than its function in translation initiation. This is consistent with the fact that yeast HCR1 is only loosely associated with the core eIF3 complex (70) and that it was shown to interact with both sides of the 40S mRNA entry channel on its own (17). Similarly, its mammalian ortholog also appears to be the most loosely associated subunit of all 13 eIF3 subunits that is, in addition, often missing from the purified 12-subunit complex (27, 58, 74). Moreover, it was also shown to associate with the 40S ribosome completely independently of the rest of eIF3 and promote several translational steps practically on its own (see for example (19, 27, 40, 54, 55, 58, 74)). Taken together, we suggest considering eIF3j/HCR1 as an independent initiation factor (eIF) that associates and closely co-operates with eIF3 but it is not its integral part. We propose how HCR1 functions in translation termination. Following stop codon recognition and subsequent GTP hydrolysis on eRF3, HCR1 promotes eRF3·GDP ejection from the post-TCs to allow binding of its interacting partner RLI1 (36), which in turn stimulates polypeptide release – both eRF3 and RLI1 bind to the same site in the post-TC (2). Inability to complete this step may lead to a reduced stop codon recognition resulting in an increased read-through. In support, eRF1

was shown to associate more firmly with post-TCs in the presence of eRF3 (56), which led the authors to propose that after GTP hydrolysis, eRF3 might not dissociate entirely from ribosomal complexes on its own and its release thus might require a stimulus by an additional factor; in our opinion by the HCR1 protein.

eIF3 regulates translation termination by promoting incorporation of nearcognate tRNA during programmed stop codon readthrough

Programmed stop codon readthrough has recently emerged as an important contributor to proteomic diversity and has also been implicated in the replication of several pathogenic RNA virus families and thus represents an appealing target for antiviral therapies (18, 26, 29, 44). We demonstrate that the *bona fide* translation initiation factor eIF3, recently implicated in controlling translation termination besides its critical initiation roles (3), is one of the major trans-acting factors in programmed stop codon readthrough in yeast, and perhaps also in mammals. In particular, we show that the presence of eIF3 in pre-TC complexes increases readthrough on stop codons in unfavorable termination contexts in a manner that is independent of its role during initiation. More importantly, eIF3 is critically required for efficient readthrough on three mRNAs previously demonstrated to be under the control of the programmed stop codon readthrough pathway. More detailed analysis of the codon specificity of eIF3-mediated stop codon readthrough suggests that eIF3 promotes the incorporation of near-cognate tRNAs with mismatches at the third (wobble) position, perhaps via an interaction with the decoding center of the ribosome.

Programmed stop codon readthrough has also been proposed as a potential treatment for hereditary diseases caused by premature termination codons (PTCs), many of which occur in unfavorable termination contexts (for review see (35)). PTCs produce truncated proteins that are non-functional or even toxic and targeted, mRNA-specific increase in readthrough could restore the functionality of the affected genes and thus cure the disease,

provided that the exact molecular mechanism is known and can be purposefully exploited. Since we reveal in this study that the translation initiation factor eIF3 plays a crucial role in programmed stop codon readthrough and suggest a detailed molecular model for its role; our results open new avenues of inquiry for understanding this important biological event also with respect to human health.

eIF3-dependent readthrough contributes to the high complexity of the translational regulation of the transcription activator GCN4

The intriguing fact that the eIF3 presence in pre-TCs formed at stop codons of short uORFs can theoretically stimulate readthrough and REI at the same time, but both activities are by their nature antagonistic, prompted us to investigate their prospective mutual interference with help of the yeast transcriptional activator GCN4. We analyzed readthrough levels on all four short uORFs from GCN4 mRNA leader and demonstrated that eIF3-promoted readthrough does not interfere with eIF3-promoted reinitiation on REI-permissive uORF1 suggesting that uORF1 naturally evolved to ensure as efficient termination as possible to be able to promote potent REI despite the constant presence of the readthrough-stimulating eIF3 complex. In the same publication, we also showed that termination efficiency of uORF3 and uORF4 markedly differs (22). So, we focused on what are major contributors to the earlier observed difference in uORF3 and uORF4 REI-potential. Could it be the eIF3-dependent readthrough? And indeed, we found out two factors. The combination of the sequence composition of uORF3 and uORF4 second codon and the identity of the stop codon tetranucleotide is what makes the major contribution to the difference in the REI potential between these two uORFs. Thus our data point at an interesting phenomenon where two counter-acting regulatory processes exist, both are mediated by the same protein factor, yet their mutual interference is prevented in favor of only one of them.

CONCLUSIONS

In this work we described the role of eIF3 in translation termination. We demonstrated that eIF3 is a key factor in promoting programmed stop codon readthrough. And we proposed a model of the mechanism of this recoding event. We put an effort in developing or improving multiple methods in order to achieve main goals of this study. For example by connecting the overexpression of several tRNAs with regular readthrough measurements we were able to monitor which tRNA decodes which stop codon *in vivo*. Using this particular approach we reached behind the scope of this study and described new decoding rules for UGAN stop codons. We also showed that eIF3-promoted readthrough does not interfere with the eIF3-promoted reinitiation on REI-permissive uORF1 from the GCN4 mRNA leader; and demonstrated that poor termination efficiency at the uORF4 stop codon strongly contributes to the difference in the REI efficiency between uORF3 and uORF4. These both results contributed to the general idea that termination efficiency matters and since eIF3 controls this process, promoting readthrough may become one of main characteristics of eukaryotic initiation factor 3 in translation regulation.

REFERENCES

1. **Alkalaeva, E. Z., A. V. Pisarev, L. Y. Frolova, L. L. Kisselev, and T. V. Pestova. 2006. In vitro reconstitution of eukaryotic translation reveals cooperativity between release factors eRF1 and eRF3. Cell 125:1125-36.**
2. **Becker, T., S. Franckenberg, S. Wickles, C. J. Shoemaker, A. M. Anger, J. P. Armache, H. Sieber, C. Ungewickell, O. Berninghausen, I. Daberkow, A. Karcher, M. Thomm, K. P. Hopfner, R. Green, and R. Beckmann. 2012. Structural basis of highly conserved ribosome recycling in eukaryotes and archaea. Nature 482:501-6.**
3. **Beznosková, P., L. Cuchalová, S. Wagner, C. J. Shoemaker, S. Gunišová, T. Von der Haar, and L. S. Valášek. 2013. Translation initiation factors eIF3 and HCR1 control translation termination and stop codon read-through in yeast cells. PLoS Genet 9:e1003962.**
4. **Beznoskova, P., S. Gunisova, and L. S. Valasek. 2016. Rules of UGA-N decoding by near-cognate tRNAs and analysis of readthrough on short uORFs in yeast. RNA 22:456-66.**
5. **Beznoskova, P., S. Wagner, M. E. Jansen, T. von der Haar, and L. S. Valasek. 2015. Translation initiation factor eIF3 promotes programmed stop codon readthrough. Nucleic Acids Res 43:5099-111.**
6. **Bidou, L., J. P. Rousset, and O. Namy. 2010. Translational errors: from yeast to new therapeutic targets. FEMS Yeast Res 10:1070-82.**
7. **Blanchet, S., D. Cornu, M. Argentini, and O. Namy. 2014. New insights into the incorporation of natural suppressor tRNAs at stop codons in Saccharomyces cerevisiae. Nucleic Acids Res 42:10061-72.**
8. **Bolger, T. A., A. W. Folkmann, E. J. Tran, and S. R. Wente. 2008. The mRNA export factor Gle1 and inositol hexakisphosphate regulate distinct stages of translation. Cell 134:624-33.**
9. **Bonetti, B., L. Fu, J. Moon, and D. M. Bedwell. 1995. The efficiency of translation termination is determined by a synergistic interplay between upstream and downstream sequences in Saccharomyces cerevisiae. J Mol Biol 251:334-45.**
10. **Cassan, M., and J. P. Rousset. 2001. UAG readthrough in mammalian cells: effect of upstream and downstream stop codon contexts reveal different signals. BMC Mol Biol 2:3.**
11. **Dabrowski, M., Z. Bukowy-Bieryllo, and E. Zietkiewicz. 2015. Translational readthrough potential of natural termination codons in eucaryotes - The impact of RNA sequence. RNA Biol:in press.**
12. **Dever, T. E., L. Feng, R. C. Wek, A. M. Cigan, T. D. Donahue, and A. G. Hinnebusch. 1992. Phosphorylation of initiation factor 2α by protein kinase GCN2 mediates gene-specific translational control of *GCN4* in yeast. Cell 68:585-596.**
13. **Dinman, J. D. 2012. Control of gene expression by translational recoding. Adv Protein Chem Struct Biol 86:129-49.**
14. **Dong, J., R. Lai, K. Nielsen, C. A. Fekete, H. Qiu, and A. G. Hinnebusch. 2004. The essential ATP-binding cassette protein RLI1 functions in translation by promoting preinitiation complex assembly. J Biol Chem 279:42157-68.**
15. **Dreher, T. W., and W. A. Miller. 2006. Translational control in positive strand RNA plant viruses. Virology 344:185-97.**

16. **Dunn, J. G., C. K. Foo, N. G. Belletier, E. R. Gavis, and J. S. Weissman. 2013. Ribosome profiling reveals pervasive and regulated stop codon readthrough in Drosophila melanogaster. Elife 2:e01179.**
17. **ElAntak, L., S. Wagner, A. Herrmannová, M. Karásková, E. Rutkai, P. J. Lukavsky, and L. Valášek. 2010. The indispensable N-terminal half of eIF3j co-operates with its structurally conserved binding partner eIF3b-RRM and eIF1A in stringent AUG selection. J Mol Biol. 396:1097-1116.**
18. **Firth, A. E., and I. Brierley. 2012. Non-canonical translation in RNA viruses. J Gen Virol 93:1385-409.**
19. **Fraser, C. S., K. E. Berry, J. W. Hershey, and J. A. Doudna. 2007. 3j is located in the decoding center of the human 40S ribosomal subunit. Mol Cell 26:811-9.**
20. **Grant, C. M., and A. G. Hinnebusch. 1994. Effect of sequence context at stop codons on efficiency of reinitiation in *GCN4* translational control. Mol Cell Biol 14:606-618.**
21. **Grant, C. M., P. F. Miller, and A. G. Hinnebusch. 1995. Sequences 5' of the first upstream open reading frame in *GCN4* mRNA are required for efficient translational reinitiation. Nuc Acids Res 23:3980-3988.**
22. **Gunisova, S., P. Beznoskova, M. P. Mohammad, V. Vlckova, and L. S. Valasek. 2016. In-depth analysis of cis-determinants that either promote or inhibit reinitiation on GCN4 mRNA after translation of its four short uORFs. RNA 22:542-58.**
23. **Gunisova, S., and L. S. Valasek. 2014. Fail-safe mechanism of GCN4 translational control-uORF2 promotes reinitiation by analogous mechanism to uORF1 and thus secures its key role in GCN4 expression. Nucleic Acids Res 42:5880-93.**
24. **Harel-Sharvit, L., N. Eldad, G. Haimovich, O. Barkai, L. Duek, and M. Choder. 2010. RNA polymerase II subunits link transcription and mRNA decay to translation. Cell 143:552-63.**
25. **Harrell, L., U. Melcher, and J. F. Atkins. 2002. Predominance of six different hexanucleotide recoding signals 3' of read-through stop codons. Nucleic Acids Res 30:2011-7.**
26. **Hartmann, K. 2012. Clinical aspects of feline retroviruses: a review. Viruses 4:2684-710.**
27. **Hashem, Y., A. des Georges, V. Dhote, R. Langlois, H. Y. Liao, R. A. Grassucci, C. U. Hellen, T. V. Pestova, and J. Frank. 2013. Structure of the Mammalian Ribosomal 43S Preinitiation Complex Bound to the Scanning Factor DHX29. Cell 153:1108-19.**
28. **Hinnebusch, A. G. 2005. Translational regulation of GCN4 and the general amino acid control of yeast. Annu Rev Microbiol. 59:407-50.**
29. **Houck-Loomis, B., M. A. Durney, C. Salguero, N. Shankar, J. M. Nagle, S. P. Goff, and V. M. D'Souza. 2011. An equilibrium-dependent retroviral mRNA switch regulates translational recoding. Nature 480:561-4.**
30. **Chao, A. T., H. A. Dierick, T. M. Addy, and A. Bejsovec. 2003. Mutations in eukaryotic release factors 1 and 3 act as general nonsense suppressors in Drosophila. Genetics 165:601-12.**
31. **Isken, O., Y. K. Kim, N. Hosoda, G. L. Mayeur, J. W. B. Hershey, and L. E. Maquat. 2008. Upf1 Phosphorylation Triggers Translational Repression during Nonsense-Mediated mRNA Decay. Cell 133:314–327.**
32. **Jackson, R. J., C. U. Hellen, and T. V. Pestova. 2012. Termination and post-termination events in eukaryotic translation. Adv Protein Chem Struct Biol 86:45-93.**

33. Janzen, D. M., L. Frolova, and A. P. Geballe. 2002. Inhibition of translation termination mediated by an interaction of eukaryotic release factor 1 with a nascent peptidyl-tRNA. Mol Cell Biol 22:8562-70.
34. Keeling, K. M., J. Lanier, M. Du, J. Salas-Marco, L. Gao, A. Kaenjak-Angeletti, and D. M. Bedwell. 2004. Leaky termination at premature stop codons antagonizes nonsense-mediated mRNA decay in S. cerevisiae. RNA 10:691-703.
35. Keeling, K. M., X. Xue, G. Gunn, and D. M. Bedwell. 2014. Therapeutics based on stop codon readthrough. Annu Rev Genomics Hum Genet 15:371-94.
36. Khoshnevis, S., T. Gross, C. Rotte, C. Baierlein, R. Ficner, and H. Krebber. 2010. The iron-sulphur protein RNase L inhibitor functions in translation termination. EMBO Rep 11:214-219.
37. Lee, H. L., and J. P. Dougherty. 2012. Pharmaceutical therapies to recode nonsense mutations in inherited diseases. Pharmacol Ther 136:227-66.
38. Lee, Y. Y., R. C. Cevallos, and E. Jan. 2009. An upstream open reading frame regulates translation of GADD34 during cellular stresses that induce eIF2alpha phosphorylation. J Biol Chem 284:6661-73.
39. Linde, L., and B. Kerem. 2008. Introducing sense into nonsense in treatments of human genetic diseases. Trends Genet 24:552-63.
40. Masutani, M., N. Sonenberg, S. Yokoyama, and H. Imataka. 2007. Reconstitution reveals the functional core of mammalian eIF3. EMBO J. 26:3373-83.
41. McCaughan, K. K., C. M. Brown, M. E. Dalphin, M. J. Berry, and W. P. Tate. 1995. Translational termination efficiency in mammals is influenced by the base following the stop codon. Proc Natl Acad Sci U S A 92:5431-5.
42. Merritt, G. H., W. R. Naemi, P. Mugnier, H. M. Webb, M. F. Tuite, and T. von der Haar. 2010. Decoding accuracy in eRF1 mutants and its correlation with pleiotropic quantitative traits in yeast. Nucleic Acids Res 38:5479-92.
43. Miller, P. F., and A. G. Hinnebusch. 1989. Sequences that surround the stop codons of upstream open reading frames in *GCN4* mRNA determine their distinct functions in translational control. Genes and Development 3:1217-1225.
44. Mohd Jaafar, F., H. Attoui, P. De Micco, and X. De Lamballerie. 2004. Termination and read-through proteins encoded by genome segment 9 of Colorado tick fever virus. J Gen Virol 85:2237-44.
45. Mottagui-Tabar, S., M. F. Tuite, and L. A. Isaksson. 1998. The influence of 5' codon context on translation termination in Saccharomyces cerevisiae. Eur J Biochem 257:249-54.
46. Mueller, P. P., and A. G. Hinnebusch. 1986. Multiple upstream AUG codons mediate translational control of *GCN4*. Cell 45:201-207.
47. Munzarová, V., J. Pánek, S. Gunišová, I. Dányi, B. Szamecz, and L. S. Valášek. 2011. Translation Reinitiation Relies on the Interaction between eIF3a/TIF32 and Progressively Folded cis-Acting mRNA Elements Preceding Short uORFs. PLoS Genet 7:e1002137.
48. Namy, O., I. Hatin, and J. P. Rousset. 2001. Impact of the six nucleotides downstream of the stop codon on translation termination. EMBO Rep 2:787-93.
49. Namy, O., J. P. Rousset, S. Napthine, and I. Brierley. 2004. Reprogrammed genetic decoding in cellular gene expression. Mol Cell 13:157-68.
50. Napthine, S., C. Yek, M. L. Powell, T. D. Brown, and I. Brierley. 2012. Characterization of the stop codon readthrough signal of Colorado tick fever virus segment 9 RNA. RNA 18:241-52.

51. Nielsen, K. H., L. Valášek, C. Sykes, A. Jivotovskaya, and A. G. Hinnebusch. 2006. Interaction of the RNP1 motif in PRT1 with HCR1 promotes 40S binding of eukaryotic initiation factor 3 in yeast. Mol Cell Biol 26:2984-98.
52. Palam, L. R., T. D. Baird, and R. C. Wek. 2011. Phosphorylation of eIF2 facilitates ribosomal bypass of an inhibitory upstream ORF to enhance CHOP translation. J Biol Chem 286:10939-49.
53. Phan, L., L. W. Schoenfeld, L. Valášek, K. H. Nielsen, and A. G. Hinnebusch. 2001. A subcomplex of three eIF3 subunits binds eIF1 and eIF5 and stimulates ribosome binding of mRNA and $tRNA_i^{Met}$. EMBO J 20:2954-2965.
54. Pisarev, A. V., C. U. T. Hellen, and T. V. Pestova. 2007. Recycling of Eukaryotic Posttermination Ribosomal Complexes. Cell 131:286–299.
55. Pisarev, A. V., V. G. Kolupaeva, M. M. Yusupov, C. U. T. Hellen, and T. V. Pestova. 2008. Ribosomal position and contacts of mRNA in eukaryotic translation initiation complexes. EMBO J. 27:1609-21.
56. Pisarev, A. V., M. A. Skabkin, V. P. Pisareva, O. V. Skabkina, A. M. Rakotondrafara, M. W. Hentze, C. U. T. Hellen, and T. V. Pestova. 2010. The Role of ABCE1 in Eukaryotic Posttermination Ribosomal Recycling. Mol Cell 37:196-210.
57. Pöyry, T. A., A. Kaminski, and R. J. Jackson. 2004. What determines whether mammalian ribosomes resume scanning after translation of a short upstream open reading frame? Genes Dev. 18:62-75.
58. Querol-Audi, J., C. Sun, J. M. Vogan, M. D. Smith, Y. Gu, J. H. Cate, and E. Nogales. 2013. Architecture of human translation initiation factor 3. Structure 21:920-8.
59. Raveh-Amit, H., A. Maissel, J. Poller, L. Marom, O. Elroy-Stein, M. Shapira, and E. Livneh. 2009. Translational control of protein kinase Ceta by two upstream open reading frames. Mol Cell Biol 29:6140-8.
60. Robinson, D. N., and L. Cooley. 1997. Examination of the function of two kelch proteins generated by stop codon suppression. Development 124:1405-17.
61. Roy, B., J. D. Leszyk, D. A. Mangus, and A. Jacobson. 2015. Nonsense suppression by near-cognate tRNAs employs alternative base pairing at codon positions 1 and 3. Proc Natl Acad Sci U S A 112:3038-43.
62. Saini, P., D. E. Eyler, R. Green, and T. E. Dever. 2009. Hypusine-containing protein eIF5A promotes translation elongation. Nature 459:118-21.
63. Sha, Z., L. M. Brill, R. Cabrera, O. Kleifeld, J. S. Scheliga, M. H. Glickman, E. C. Chang, and D. A. Wolf. 2009. The eIF3 interactome reveals the translasome, a supercomplex linking protein synthesis and degradation machineries. Mol Cell 36:141-52.
64. Shoemaker, C. J., and R. Green. 2011. Kinetic analysis reveals the ordered coupling of translation termination and ribosome recycling in yeast. Proc Natl Acad Sci U S A 108:E1392-8.
65. Skuzeski, J. M., L. M. Nichols, R. F. Gesteland, and J. F. Atkins. 1991. The signal for a leaky UAG stop codon in several plant viruses includes the two downstream codons. J Mol Biol 218:365-73.
66. Sundaram, A., and C. M. Grant. 2014. A single inhibitory upstream open reading frame (uORF) is sufficient to regulate Candida albicans GCN4 translation in response to amino acid starvation conditions. RNA 20:559-67.
67. Szamecz, B., E. Rutkai, L. Cuchalova, V. Munzarova, A. Herrmannova, K. H. Nielsen, L. Burela, A. G. Hinnebusch, and L. Valášek. 2008. eIF3a cooperates with sequences 5' of uORF1 to promote resumption of scanning by post-termination ribosomes for reinitiation on GCN4 mRNA. Genes Dev 22:2414-2425.

68. **Valášek, L., J. Hašek, K. H. Nielsen, and A. G. Hinnebusch. 2001. Dual function of eIF3j/Hcr1p in processing 20 S Pre-rRNA and translation initiation. J Biol Chem 276:43351-43360.**

69. **Valášek, L., J. Hašek, H. Trachsel, E. M. Imre, and H. Ruis. 1999. The *Saccharomyces cerevisiae HCRI* gene encoding a homologue of the p35 subunit of human translation eukaryotic initiation factor 3 (eIF3) is a high copy suppressor of a temperature-sensitive mutation in the Rpg1p subunit of yeast eIF3. J Biol Chem 274:27567-27572.**

70. **Valášek, L., L. Phan, L. W. Schoenfeld, V. Valášková, and A. G. Hinnebusch. 2001. Related eIF3 subunits TIF32 and HCR1 interact with an RNA recoginition motif in PRT1 required for eIF3 integrity and ribosome binding. EMBO J 20:891-904.**

71. **Valášek, L., B. Szamecz, A. G. Hinnebusch, and K. H. Nielsen. 2007. In vivo stabilization of preinitiation complexes by formaldehyde cross-linking. Methods Enzymol 429:163-83.**

72. **Valášek, L. S. 2012. 'Ribozoomin' – Translation Initiation from the Perspective of the Ribosome-bound Eukaryotic Initiation Factors (eIFs). Curr Protein Pept Sci. 13:305-330.**

73. **von der Haar, T., and M. F. Tuite. 2007. Regulated translational bypass of stop codons in yeast. Trends Microbiol 15:78-86.**

74. **Zhou, M., A. M. Sandercock, C. S. Fraser, G. Ridlova, E. Stephens, M. R. Schenauer, T. Yokoi-Fong, D. Barsky, J. A. Leary, J. W. Hershey, J. A. Doudna, and C. V. Robinson. 2008. Mass spectrometry reveals modularity and a complete subunit interaction map of the eukaryotic translation factor eIF3. Proc Natl Acad Sci USA 105:18139-44.**

PUBLICATIONS I-V

PUBLICATION I

OPEN ACCESS Freely available online

PLOS | GENETICS

Translation Initiation Factors eIF3 and HCR1 Control Translation Termination and Stop Codon Read-Through in Yeast Cells

Petra Beznosková[1☯], Lucie Cuchalová[1☯¤], Susan Wagner[1], Christopher J. Shoemaker[2], Stanislava Gunišová[1], Tobias von der Haar[3], Leoš Shivaya Valášek[1]*

1 Laboratory of Regulation of Gene Expression, Institute of Microbiology ASCR, Videnska, Prague, the Czech Republic, **2** Howard Hughes Medical Institute, Johns Hopkins University School of Medicine, Baltimore, Maryland, United States of America, **3** School of Biosciences, University of Kent, Kent, United Kingdom

Abstract

Translation is divided into initiation, elongation, termination and ribosome recycling. Earlier work implicated several eukaryotic initiation factors (eIFs) in ribosomal recycling *in vitro*. Here, we uncover roles for HCR1 and eIF3 in translation termination *in vivo*. A substantial proportion of eIF3, HCR1 and eukaryotic release factor 3 (eRF3) but not eIF5 (a well-defined "initiation-specific" binding partner of eIF3) specifically co-sediments with 80S couples isolated from RNase-treated heavy polysomes in an eRF1-dependent manner, indicating the presence of eIF3 and HCR1 on terminating ribosomes. eIF3 and HCR1 also occur in ribosome- and RNA-free complexes with both eRFs and the recycling factor ABCE1/RLI1. Several eIF3 mutations reduce rates of stop codon read-through and genetically interact with mutant eRFs. In contrast, a slow growing deletion of *hcr1* increases read-through and accumulates eRF3 in heavy polysomes in a manner suppressible by overexpressed ABCE1/RLI1. Based on these and other findings we propose that upon stop codon recognition, HCR1 promotes eRF3·GDP ejection from the post-termination complexes to allow binding of its interacting partner ABCE1/RLI1. Furthermore, the fact that high dosage of ABCE1/RLI1 fully suppresses the slow growth phenotype of *hcr1Δ* as well as its termination but not initiation defects implies that the termination function of HCR1 is more critical for optimal proliferation than its function in translation initiation. Based on these and other observations we suggest that the assignment of HCR1 as a *bona fide* eIF3 subunit should be reconsidered. Together our work characterizes novel roles of eIF3 and HCR1 in stop codon recognition, defining a communication bridge between the initiation and termination/recycling phases of translation.

Citation: Beznosková P, Cuchalová L, Wagner S, Shoemaker CJ, Gunišová S, et al. (2013) Translation Initiation Factors eIF3 and HCR1 Control Translation Termination and Stop Codon Read-Through in Yeast Cells. PLoS Genet 9(11): e1003962. doi:10.1371/journal.pgen.1003962

Editor: Alan G. Hinnebusch, National Institute of Child Health and Human Development, NIH, United States of America

Received July 16, 2013; **Accepted** October 1, 2013; **Published** November 21, 2013

Funding: This research was supported for the most part by The Wellcome Trust Grant 090812/Z/09/Z, and partly also by the Howard Hughes Medical Institute and the Centrum of Excellence Grant (P305/12/G034) awarded by the Czech Science Foundation (all to LSV); and by Wellcome Trust Grant 075438 (to TvdH). The funders had no role in study design, data collection and analysis, decision to publish, or preparation of the manuscript.

Competing Interests: The authors have declared that no competing interests exist.

* E-mail: valasekl@biomed.cas.cz

☯ These authors contributed equally to this work.

¤ Current address: Institute of Macromolecular Chemistry AS CR, Prague, the Czech Republic.

Introduction

Protein synthesis or mRNA translation is a complex and highly conserved process that can be separated into initiation, elongation, termination and ribosome recycling phases. Although these four phases are distinct in time, there is a longstanding notion for some form of communication among them. Notably, several initiation factors and related proteins have been proposed to function in more than one phase. These include ABCE1/RLI1 and GLE1, which are believed to promote both the initiation and termination phases by a mechanism that remains to be elucidated [1–3], eIF5A proposed to stimulate all three major phases [4], and the *bona fide* translation initiation factor eIF3, which has been recently suggested to promote the recycling phase, at least in a mammalian *in vitro* reconstituted system [5,6].

The beginning of a translational cycle involves a series of steps that culminate in the assembly of the 80S initiation complex (IC) on the AUG start codon (reviewed in [7]). These steps include 1) Met-tRNA$_i^{Met}$ recruitment to the 40S subunit to form the 43S pre-initiation complex (PIC), 2) mRNA recruitment to the 43S PIC to form the 48S PIC, 3) scanning of the 48S PIC to the first recognized start codon, and 4) joining of the 60 subunit to commit the resulting 80S IC to the elongation phase. The translation initiation factor eIF3, which in yeast consists of five essential core subunits (eIF3a/TIF32, b/PRT1, c/NIP1, i/TIF34 and g/TIF35) and one transiently associated, non-essential subunit (eIF3j/HCR1), is actively involved in regulation of the first three of these steps [7]. In the PIC assembly steps, the action of eIF3 is further stimulated by one of its interacting partners, the ATP-binding cassette protein ABCE1/RLI1, by an unknown mechanism [1]. In contrast to the most of eIFs, eIF3 interacts with the solvent-exposed side of the small ribosomal subunit [7] and as such it was proposed to be able to interact with active 80S ribosomes post-initiation [8–10].

Author Summary

Protein synthesis (translation) utilizes genetic information carriers, mRNAs, as templates for the production of proteins of various cellular functions. Typically it is divided into four phases: initiation, elongation, termination and ribosomal recycling. In this article we argue that the strict mechanistic separation of translation into its individual phases should be reconsidered in the light of "multitasking" of initiation factors eIF3, HCR1 and ABCE1/RLI1. In detail, we show that eIF3 and HCR1 not only promote the initiation phase but also specifically act at the other end of the translational cycle during termination. We present genetic and biochemical data linking eIF3 and HCR1 with both eukaryotic release factors (eRF1 and eRF3) and the ribosomal recycling factor ABCE1/RLI1, and propose a model for how all these factors co-operate with each other to ensure stringent selection of the stop codon. Collectively, our findings suggest that changes in one phase of translation are promptly communicated to and coordinated with changes in the other phases to maintain cellular homeostasis of all ongoing processes.

The end of a translational cycle involves another series of steps that culminate in the release of a newly synthesized polypeptide from the translating ribosome (the termination phase), and in the dissolution of the ribosome:tRNA:mRNA complex (the recycling phase). Termination begins when a stop codon enters the ribosomal A-site, forming a pre-termination complex (pre-TC) [11]. In eukaryotes, all three stop codons are decoded by the eukaryotic release factor 1 (eRF1). According to recent models [12,13], eRF1 enters the ribosomal A-site in complex with a second release factor, eRF3, in its GTP bound form. Recognition of a stop codon triggers GTPase activity of eRF3, which leads to its dissociation from the complex in its GDP bound form. eRF1 is then free to activate the ribosomal peptidyl transferase centre (PTC), which hydrolyses the bond between the P-site tRNA and the nascent polypeptide. Importantly, these steps are promoted by RLI1 in an ATP-independent manner; i.e. by the same factor that also somehow stimulates the eIF3 function in the initiation phase. Molecular details of this RLI1 role in termination are similarly not known, nevertheless, the proposed active role of RLI1 in stop codon recognition is consistent with observations that conditional down regulation of RLI1 protein levels increases stop codon read-through in yeast [2]. Based on the most recent structural model, RLI1 binds to the same site on the terminating ribosome as eRF3 (thus their binding is mutually exclusive), and its 4Fe-4S domain interacts with the C-terminal domain of eRF1 to push the conserved GGQ motif in the middle domain of eRF1 to the PTC next to the acceptor stem of the P-site tRNA to trigger polypeptide release [13].

Recycling of eRF1-associated post-termination complexes (post-TCs) is also mediated by ABCE1/RLI1, this time, however, in an ATP-dependent manner [6,12]. It was hypothesized that RLI1, upon binding and hydrolyzing ATP, switches its conformation into a closed state, and the mechanochemical work generated by this switch splits post-TCs into free 60S subunits and deacylated tRNA- and mRNA-bound 40S subunits (40S-post-TC) [13]. Finally, Pisarev *et al.* showed that the release of tRNA and mRNA from the 40S-post-TCs is *in vitro* ensured by the *bona fide* initiation factors eIF1, eIF1A and eIF3 [5,6]. eIF3, and in particular its j subunit (HCR1 in yeast), were suggested to play the key role in mRNA dissociation.

Since the implication of eIF3 in the recycling process was deduced only from experiments carried out with 11-codon long model mRNAs in mammalian *in vitro* reconstituted systems, we decided to investigate whether or not eIF3 also plays a direct role in translation termination and/or ribosomal recycling in the living cell. Here we show that the five core eIF3 subunits and HCR1 control translation termination and stop codon read-through in yeast, although in the opposite manner. HCR1 specifically cooperates with eRF3 and RLI1 and based on our and previous findings we propose that HCR1 and its mammalian orthologue should no longer be considered as *bona fide* subunits of eIF3. In any case, involvement of the canonical translation initiation factor eIF3 in termination strongly supports the idea that there is a highly coordinated communication between individual translational phases.

Results

Mutations in eIF3 subunits and hcr1 deletion affect stop codon read-through

eIF3 and the eIF3-core-associated factors like HCR1 and RLI1 play a role in ribosome recycling – at least *in vitro* [5,6], while only RLI1 is to date known to somehow promote also the preceding translation termination step [2]. In order to address whether eIF3 itself is likewise functionally involved in translation termination, we first measured the frequency of stop codon read-through in a collection of eIF3 mutants using an established dual-luciferase reporter assay, specifically designed to be independent of mRNA levels [14]. This reporter system is similar to the one which was also used to demonstrate increased stop codon read-through upon conditional down-regulation of RLI1 [2]. The [*psi*$^-$] strain background used in these initial experiments contains a genome-encoded UGA suppressor tRNA leading to unusually high basal UGA read-through levels of 3–4%, which is however ideal for studying stop-codon read-through effects. Importantly, as shown below, the results we obtained are independent of the presence of this suppressor tRNA.

The eIF3 mutants that were chosen for read-through analysis were previously shown to affect multiple initiation steps, from the 43 PIC assembly (due to reduced 40S-binding affinity of eIF3) to scanning for AUG recognition (with wild-type 40S-binding affinity of eIF3); summarized in Table S1. Strikingly, the majority of mutations in the core eIF3 subunits that we tested showed a significant reduction in stop-codon read-through (Figure 1) that thus could not be simply attributed to the reduced eIF3 association with ribosomes. Also, since the effect of eIF3 mutations on translation initiation does not correlate well with the observed translation termination defect (such as, for example, in case of *prt1-W674A vs. tif34-DD/KK* or *tif35-TKMQ vs. tif35-RLFT* mutants), we conclude that the impact of these mutations on translation initiation vs. termination is genetically separable. Importantly, in contrast to all core eIF3 subunits, deletion of the non-essential *hcr1* gene encoding eIF3j resulted in significantly increased stop-codon read-through (Figure 1), similar to that reported for RLI1 down-regulation [2]. Neither eIF3 mutations nor *hcr1Δ* have any impact on eRF1, eRF3 and RLI1 protein levels.

In order to confirm this unexpected result and to explore whether the observed effect on translation termination was specific to eIF3 or common to all other members of the Multifactor complex (MFC; composed of eIF1, eIF2, eIF3 and eIF5) and their closely co-operating factor eIF1A, we used partial depletion alleles (DaMP alleles) for these essential factors from the genome-wide DaMP collection [15]. DaMP alleles contain a selectable marker cassette inserted into the 3′-UTR of a gene, leading to

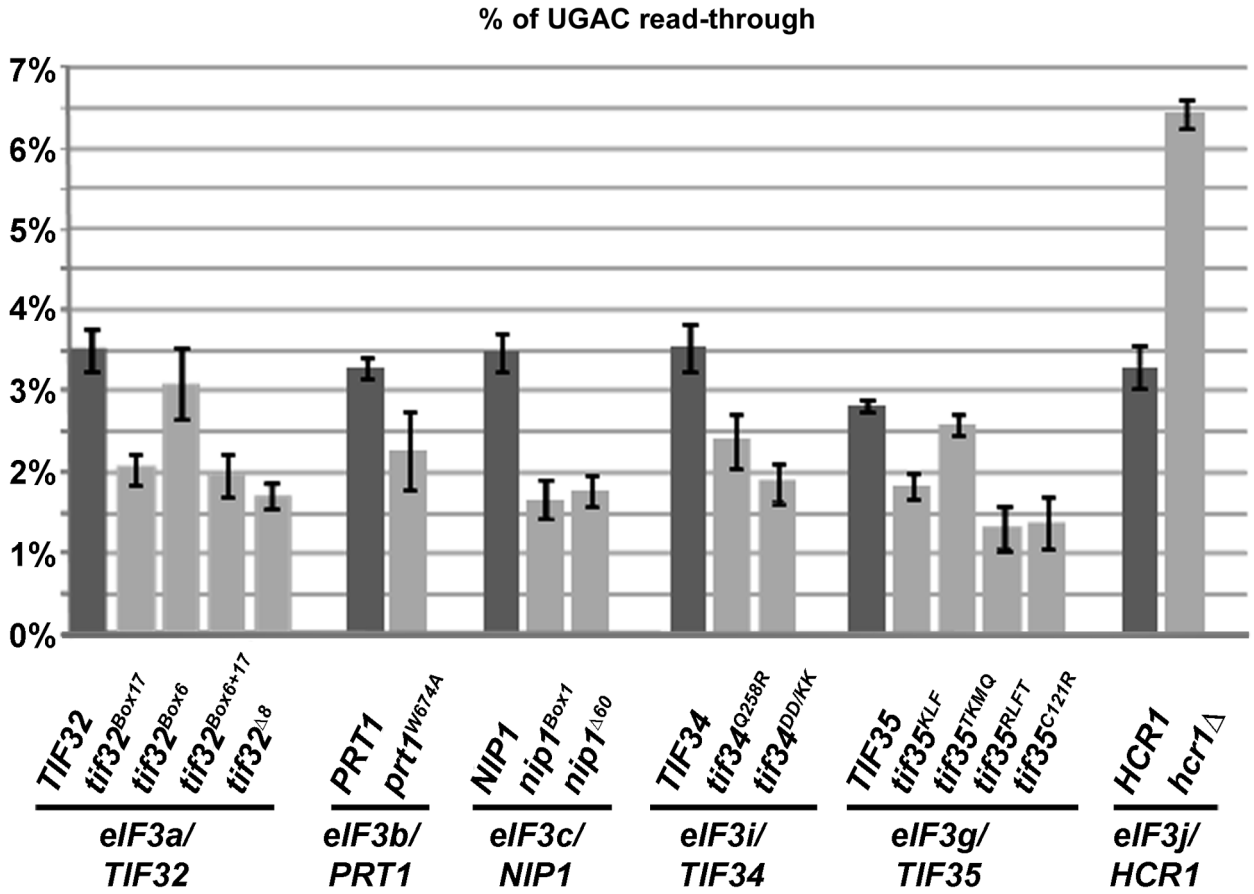

Figure 1. Mutations reducing the activity of translation initiation factor eIF3 and HCR1 affect stop codon read-through. Stop codon read-through was measured using dual luciferase reporter constructs as described in the main text. Plasmid-born mutant alleles of genes encoding eIF3 subunits and HCR1 were introduced into their respective shuffling strains, which are derived from a common strain background (for details please see Text S1 and Table S1). The wt strain background has unusually high levels of UGA read-through, due to the presence of an opal (UGA) suppressor tRNA in the genome. For each independently derived shuffling strain, read-through is shown for pairs of strains shuffled with wt or the indicated mutant alleles of the gene in question. For the non-essential HCR1 subunit, the H3675 *hcr1Δ* strain is shown. All investigated mutants showed significant ($p<0.05$) reductions in the level of stop codon read-through, with the exception of *tif35*^{TKMQ}, which showed no significant difference, and *Δhcr1* which showed strong and significant increase in stop codon read-through.
doi:10.1371/journal.pgen.1003962.g001

destabilization of the respective mRNA *via* the nonsense mediated decay pathway (NMD).

By their nature, DaMP alleles show varying degrees of depletion for different genes, and data obtained with DaMP alleles have to be interpreted with this in mind. Since the depleted genes are all essential, loss of the corresponding gene product below a critical level will affect growth, and demonstration of reduced growth for an individual strain can thus be taken as a reliable indicator for depletion below a critical threshold. In contrast, an absence of growth phenotypes cannot be unambiguously interpreted, as depletion of the gene product may have occurred but may have remained above a level where fitness is detectably affected. It should be noted that growth phenotypes are a better indicator of functional depletion than assessment of physical expression levels by Western blotting, since the relationship between translation factor abundance and translation rates is non-linear and generally not predictable [16]. Finally, since the DaMP strain background does not contain a UGA suppressor tRNA in the genome, these data also exclude possible suppressor tRNA effects on the eIF3 mutants in the initial experiments.

When we compared growth rates of the MFC DaMP alleles to the corresponding wild type (wt) strain (Figure S1), we observed that most non-eIF3 MFC factors but only one of the eIF3 strains (*TIF35*) showed a growth phenotype indicative of a significant depletion. When we proceeded to assess stop codon read-through in these strains, we observed that the one eIF3 strain for which the growth assay indicated significant depletion (about 2.5-fold as determined by Western blotting) also showed significantly reduced stop codon read-through. In addition, the *NIP1* depletion strain also showed modest but significant reduction in stop-codon read-through, which may be caused by depletion of the gene product to a level that does not yet affect growth rates. In contrast, none of the depletion alleles for the non-eIF3 MFC component showed a reduction in read-through, although eIF1A and eIF2α showed small but significant increases in stop codon read-through and, interestingly, eIF2γ showed even higher increase (~2-fold) that is similar to *hcr1Δ*. While the mechanism behind the increased read-through in the eIF1A and eIF2 alleles is yet to be explored, these observations demonstrate that i) reductions in eIF3 activity reliably lead to reductions in stop-codon read-through levels, whether this reduction is caused by point mutations or other gene ablation alleles, ii) this effect is specific to core eIF3 subunits, whereas other MFC components and HCR1 display either none or the opposite phenotype, and iii) general reduction in the initiation rates does

not automatically affect the precision of translation termination – see for example the read-through data for eIF1 (Figure S1), the protein levels of which were depleted by ~5-fold – suggesting that the reduced levels of read-through displayed by eIF3 mutants do not necessarily occur as an indirect consequence of an overall compromised protein synthesis. Interestingly, a similar phenotype (reduced read-through) was also observed for overexpression of eRF1 in otherwise wt cells (Figure S2; combined overexpression of eRF1 and 3 led to further, modest exacerbation), indicating that the eIF3 mutants may somehow affect the availability of eRFs for the stop codon in the A-site.

Overexpression of ABCE1/RLI1 fully suppresses the growth and read-through but not the initiation defects of the *hcr1* deletion strain

Next we wished to explore a molecular mechanism of the increased stop-codon read-through phenotype displayed by deletion of the non-essential *hcr1* gene (Figure 1), which sharply contrasted with the opposite termination phenotype of mutant core eIF3 subunits (Figure 1). As discussed above, recent reports suggested that the ABCE1/RLI1 protein not only critically promotes ribosomal recycling [6,12,17] but is also somehow involved in translation termination, as its conditional depletion produced an increased read-through defect [2]. Moreover, RLI1 was also implicated in biogenesis and transport of pre-ribosomes from the nucleolus [18] and in stimulating translation initiation by promoting assembly of 43S PICs together with eIF3 [1]. The striking resemblance of the latter effects with the previously reported functions of HCR1 [18–24] plus the earlier observations that RLI1 directly interacts with HCR1 *via* its ABC2 domain [2] and that combination of *hcr1Δ* with the TAP-tagged RLI1 results in synthetic lethality [18] prompted us to test a potential functional redundancy between these two proteins.

Strikingly, we found that overexpression of RLI1 (about 2.5-fold) fully suppressed the slow growth defect of an *hcr1Δ* strain (Figure 2A). Moreover, high copy (hc) *RLI1* also fully suppressed the increased read-through phenotype of this strain (Figure 2B). By way of control, we overexpressed elongation factor eEF3 (encoded by *YEF3*) as an independent ABC cassette-containing protein engaged in translation, which had no effect on the growth or read-through phenotypes of the *hcr1Δ* strain (Figure S3A and B). In addition, hc RLI1 did not suppress the increased read-through defect of the DaMP eIF2γ mutant (data not shown), further underscoring the novelty of the proposed role for HCR1 and eIF3 in termination.

Importantly, no hc suppression was observed when either the formation of the RLI1 N-terminal 4Fe-4S clusters (C25S and C61S mutants) or the ATP binding by its ABC cassettes (K116L, K391L, G224D G225D and G470D G471D mutants) were compromised (Figure 2B and data not shown). The integrity of the crucial N-terminal region of RLI1 as well as its intact ATPase activity are therefore critically required for a functional replacement of HCR1. In the opposite arrangement, hc *HCR1* suppressed neither the slow growth nor the increased read-through phenotype of the *Tet::RLI1* conditional depletion strain (Figure S4). It is noteworthy that in agreement with earlier results [2,12,17], the intact N-terminal 4Fe-4S clusters and the ability of RLI1 to bind and hydrolyze ATP were absolutely essential for restoration of the read-through defect in the *Tet::RLI1* cells (Figure S4).

In order to find out if HCR1 acts independently of eIF3 in the termination process, we examined the read-through phenotype of *hcr1* mutations, which are known to eliminate binding of full length HCR1 to eIF3 [21,22]. As shown in Figure 2B (mutations *hcr1-Box-NTA, -Box6* and *-Box6+R/I*), no effect was observed implying that the HCR1 function in termination does not require its physical association with eIF3.

One of the major initiation phenotypes of *hcr1Δ* is a leaky scanning defect (a decreased ability to recognize AUG as the translational start site resulting in increased scanning past it), which can be suppressed by hc eIF1A [21]. As can be seen in Figure 2B, neither hc eIF1A nor eIF1 suppressed the read-though defect of *hcr1Δ*. Similarly, hc *RLI1* did not suppress the leaky scanning defect of *hcr1Δ* (Figure S5). Hence, these findings clearly suggest that the *hcr1Δ* defects in initiation and termination are genetically separable and that RLI1 cannot replace HCR1 in all of its functions. Importantly, however, since hc eIF1A suppressed the *hcr1Δ* growth defect only partially [21], as opposed to the full suppression by hc *RLI1* (Figure 2A), we propose that the major contributor to the *hcr1Δ* slow growth phenotype is not a defect in initiation, as previously believed, but a defect related to translation termination. Altogether it seems that this substoichiometric "subunit" of eIF3 works more independently of the core eIF3 than previously thought and therefore we suggest not considering HCR1 as a *bona fide* eIF3 subunit anymore (see Discussion for more details).

Complexes containing eIF3, HCR1, ABCE1/RLI1 and both eRFs, free of ribosomes and RNA, occur *in vivo*

If eIF3 and HCR1 are indeed involved in translation termination as our read-through data indicate (Figure 1), it should be possible to detect a complex between these molecules and the release factors *in vivo*. We therefore carried out a series of *in vivo* pull down experiments using Myc-tagged RLI1, or TAP-tagged HCR1, a/TIF32 or eRF3 as baits. To stabilize presumably only transient interactions between eIF3 and termination/recycling factors, the TAP-tag experiments were performed after modest (1%) pre-treatment of growing cells with formaldehyde as described in [25]. As shown in Figure 3A, Myc-tagged RLI1 specifically pulled down selected eIF3 subunits (~51±1% of the input for a/TIF32 and ~43±2.6% for g/TIF35) and HCR1, as shown before [1]. In addition and in contrast to the latter study, we also observed significant co-precipitation of both release factors (~22±1.7% for eRF1 and ~13±3.9% for eRF3). The TAP-tagged HCR1 repeatedly co-purified with selected eIF3 subunits, as expected, but also with RLI1 (~58±5.8%) and small but specific amounts of eRF3 (9±0.2%) and eRF1 (~2±0.2%) (Figure 3B; eRF1 is indicated by an asterisk). eRF3 also co-precipitated with TAP-tagged a/TIF32 (~16±4.7%), and, importantly, TAP-tagged eRF3 reproducibly and specifically brought down small but significant amounts of core eIF3 subunits (~6.4±0.7% for a/TIF32 and ~18±5.8% for g/TIF35) but no other MFC-members such as eIF1 (Figure 3C and D; note that the mobility of a/TIF32 and eRF3 vary between Input and Elution lanes due to a TEV protease-mediated cleavage of the TAP tag). We also tested the TAP-tagged eRF1 strain, however, no proteins were recovered – not even the TAP-eRF1 by itself – indicating that this particular fusion allele is not functional. Importantly, the yield of neither of these experiments was affected by RNase A treatment (Figure S6) and no ribosomes were present in the purified complexes (see RPS0A strips in panels A–D) strongly suggesting that the ribosome- and RNA-free complexes of eIF3, HCR1, eRF1, eRF3 and RLI1 do exist in the cytoplasm. More specifically, these experiments show that eIF3 and HCR1 contacts all critical termination players discussed in this study, though we cannot conclude whether all these factors occur in one single super-complex, or whether we are pulling down their partial subcomplexes.

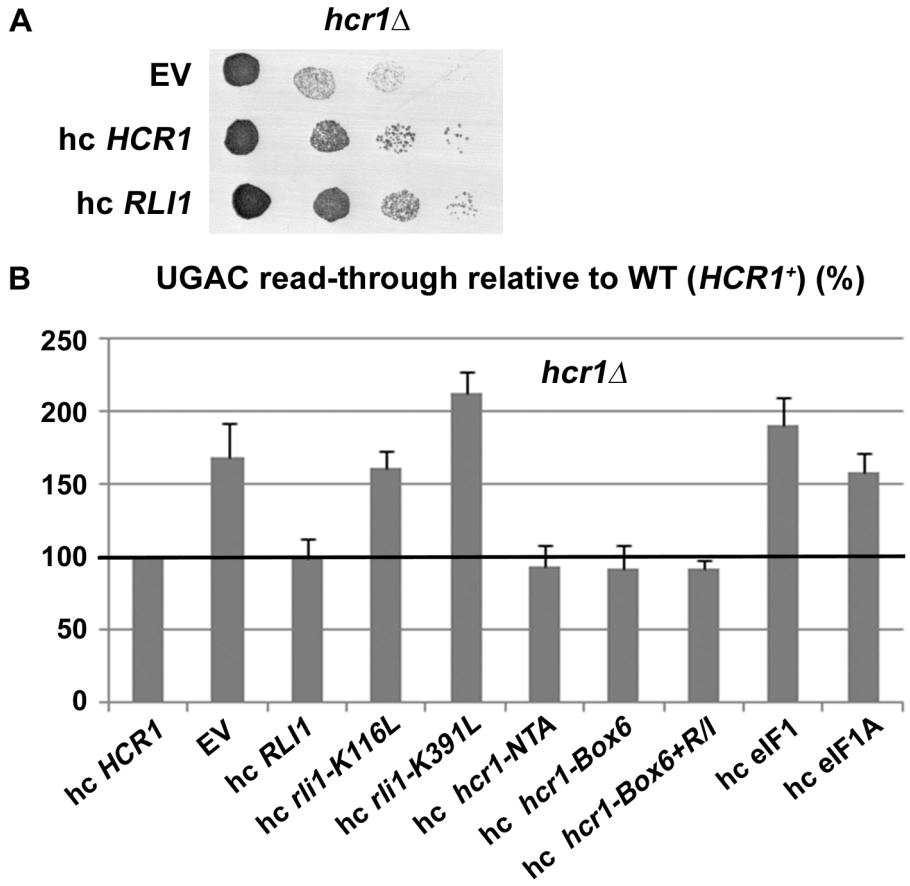

Figure 2. Increased gene dosage of ABCE/RLI1 suppresses the slow growth and read-through defects of *hcr1Δ*. (**A**) The *hcr1Δ* strain was transformed with either empty vector (EV), hc *HCR1* or hc *RLI1*. The resulting transformants were subjected to a growth spot assay at 30°C for 2 days. (**B**) The *hcr1Δ* strain was transformed with hc vectors carrying either wt or mutant *HCR1* and *RLI1* alleles, and *SUI1* (eIF1) and *TIF11* (eIF1A). The resulting transformants were grown in SD and analyzed for stop codon read-through as described in Figure 1. Thus obtained values were normalized to the value obtained with the *hcr1Δ* strain transformed with wt *HCR1*, which was set to 100%.
doi:10.1371/journal.pgen.1003962.g002

The N-M domains of eRF1 directly interact with the N-terminal domain of g/TIF35 and weakly also with i/TIF34 *in vitro*

The fact that eIF3 and HCR1 associate with eRFs *in vivo* and that their mutations affect fidelity of the termination process prompted us to test protein-protein interactions between eIF3 subunits, HCR1 and both eRFs. We fused individual eIF3 subunits and HCR1 to a GST moiety and used these fusions in pull-down assays with *in vitro* synthesized, radiolabeled, well-defined domains of eRF1 and eRF3. As shown in Figure 3E, the N-terminal and Middle (N-M) domains but not the middle and C-terminal (M-C) domains of eRF1 specifically interacted with GST-g/TIF35 and weakly also with GST-i/TIF34, in contrast to GST-HCR1 and a negative control of the GST protein alone. (The N domain of eRF1 carries determinants of the stop codon recognition; the M domain contains the conserved GGQ motif required for peptide release; and the C domain interacts with eRF3.) Interestingly, DOM34/Pelota, the release-like factor closely related in sequence and structure to eRF1, also binds eIF3g in human cell lines [26], albeit in this case *via* Pelota's C-terminal domain. No interactions between eIF3 subunits and eRF3 were observed. g/TIF35 can be divided into the N-terminal Zn-finger and C-terminal RRM domains and our GST pull down experiments revealed that eRF1-NM binds specifically to the N-terminal Zn-finger domain of g/TIF35 (Figure 3F). Hence we propose that eIF3 and eRF1 are in a direct contact *via* two small eIF3 subunits and the NTD of eRF1, which requires further support from the M domain to get fully engaged in these interactions.

eIF3 and HCR1 associate with 80S couples isolated from heavy polysomes

To provide more solid evidence implicating eIF3 and HCR1 in the process of termination *in vivo*, we tested whether or not both factors associate with polysomal 80S ribosomes by separating the formaldehyde cross-linked whole cell extracts (WCEs) on sucrose gradients by high velocity sedimentation into two major polysomal pools; the first containing light polysomes (disomes and trisomes) and the other heavy polysomes (from pentasomes up). These two pools were then treated with RNase I (Invitrogen) to chop polysomal mRNAs into segments containing either initiating 43S-48S PICs or elongating/terminating 80S ribosomes. The second round of sucrose gradient centrifugation (so called resedimentation; [25]) was employed to separate the 43-48S PICs from 80S couples in each polysomal pool into two fractions, which were then subjected to Western blotting. In both pools, the 80S fractions contained more than 50% of total eIF3 in comparison with the 40S fractions (Figure 4A), clearly demonstrating that only the

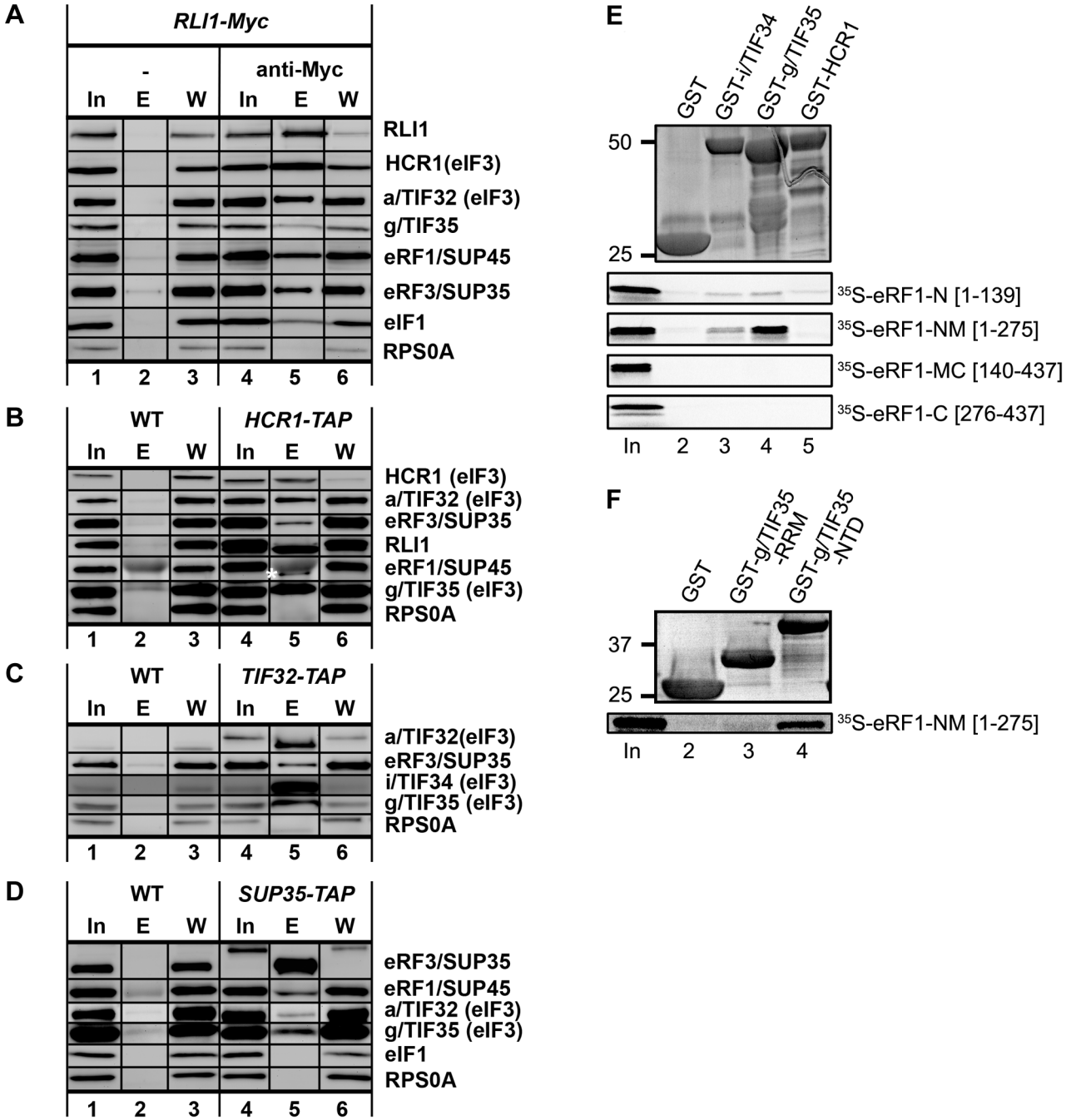

Figure 3. Complexes containing eIF3, HCR1, ABCE1/RLI1 and both eRFs, free of ribosomes and RNA, occur *in vivo*; and the NTD of g/TIF35 and i/TIF34 directly interact with the N and M domains of eRF1. (**A**) WCEs were prepared from YDH353 bearing chromosomal Myc-tagged *RLI1* and immunoprecipitated with or without anti-Myc antibodies. The immune complexes were subjected to Western analysis. In, 5% of input; E, 100% of the elution fraction; W, 5% of the supernatant fraction. Also note that anti-RLI1 and -eRF1 antibodies were raised for the purpose of this study. (**B**) WCEs were prepared from HCHO-treated (1%) cells bearing wt (H2879) or TAP-tagged (H553) chromosomal alleles of *HCR1* and incubated with IgG Sepharose 6 Fast Flow beads. The immune complexes were eluted by boiling in the SDS buffer and subjected to Western analysis. In, 1.5% of input; E, 50% of the elution fraction; W, 1.5% of the supernatant fraction. eRF1 is indicated by an asterisk below the immunoglobulins. (**C**) WCEs from HCHO-treated cells (1%) cells bearing wt (H2879) or TAP-tagged (H555) chromosomal alleles of *TIF32* were processed as in panel B except that the immune complexes were eluted by TEV protease cleavage. In, 1.5% of input; E, 100% of the elution fraction; W, 1.5% of the supernatant fraction. (**D**) WCEs from HCHO-treated cells (1%) cells bearing wt (74D-694) or TAP-tagged (H517) chromosomal alleles of *SUP35* were processed as in panel C. (**E**) Full-length i/TIF34 (lane 3), g/TIF35 (lane 4), and HCR1 (lane 5) fused to GST, and GST alone (lane 2), were tested for binding to ^{35}S-labeled individual domains of eRF1; 10% of input amounts added to each reaction is shown in lane 1 (In). (**F**) The RRM (lane 3) and N-terminal (lane 4) domains of g/TIF35 fused to GST, and GST alone (lane 2), were tested for binding to ^{35}S-labeled NM domains of eRF1; 10% of input amounts added to each reaction is shown in lane 1.

doi:10.1371/journal.pgen.1003962.g003

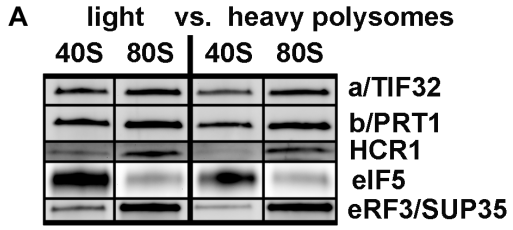

80S/40S ratios of heavy vs. light polysomes

1.8	a/TIF32
2.1	b/PRT1
2.5	j/HCR1
1.1	eIF5
3.3	eRF3

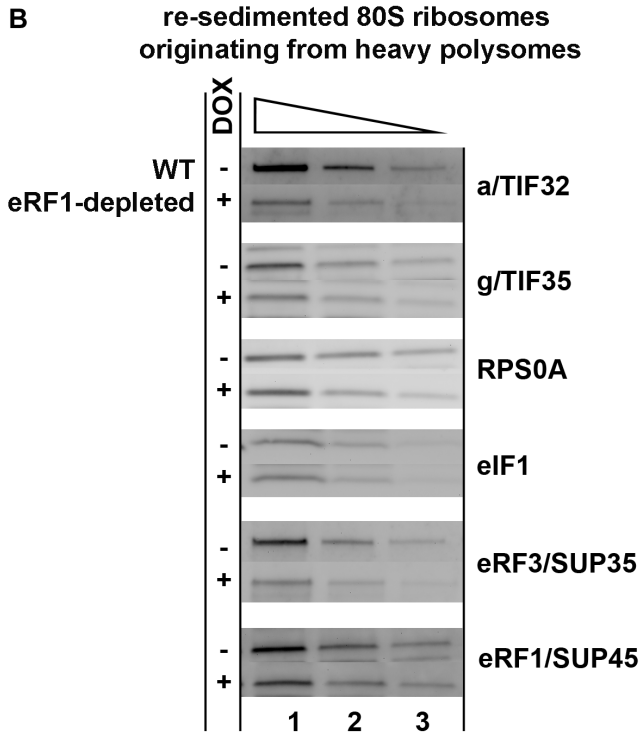

Figure 4. eIF3 associates with 80S couples isolated from heavy polysomes in an eRF1-dependent manner. (**A**) The wt strain (H2819) was grown in SD medium at 30°C to an OD_{600} of ~1 and cross-linked with 0.5% HCHO prior to harvesting. WCEs were prepared, separated on a 5%–45% sucrose gradient by centrifugation at 39,000 rpm for 2.5 h and two collected fractions containing either disomes and trisomes or pentasomes and heavier polysomes were treated with RNase A to separate the initiating PICs from 80S couples on mRNAs and subjected to the sucrose gradient resedimentation protocol [25]. Two fractions containing 43-48S PICs and 80S ribosomes from each polysomal pool were collected and subjected to Western blot analysis; the ratio of the 80S/40S ratios for heavy over light polysomes was calculated and plotted for each factor. This experiment was repeated four times. (**B**) eRF1 depletion reduced association of eRF3 and eIF3 with 80S ribosomes isolated from heavy polysomes. The *Tet::SUP45* cells were grown in SD medium at 30°C in the presence or absence of 1 μg/ml doxycycline for six hours before harvesting, and treated as described in Figure 4A with the exception that only heavy polysomes were collected after the first round of centrifugation, and only the 80S couples were collected after the second round of centrifugation. Thus obtained samples were subsequently subjected to Western blot analysis; this experiment was conducted three times.
doi:10.1371/journal.pgen.1003962.g004

lesser proportion of eIF3 occuring in polysomes is associated with initiation complexes. Strikingly, in case of HCR1, the 80S fractions contained even more, ~90% of this protein from the overall pool. In contrast, the "polysomal" fraction of eIF5, which is known to tightly interact with eIF3 during translation initiation, was predominantly associated with 40S species. These results are thus consistent with a role of eIF3 and HCR1 in other translational phases than just initiation.

In the resedimented light and heavy polysomes different ratios of terminating versus initiating plus elongating ribosomes can be expected based on the following arguments. Under nutrient-rich conditions, the disome/trisome fraction will contain short mRNAs that cannot accommodate more than two/three ribosomes, poorly translated mRNAs, as well as recently transcribed mRNAs, which are not yet in a steady state phase with regards to their ribosome occupancy. Since mRNAs shorter than 60 codons make up only 2% of the yeast transcriptome [27], we expect that a majority of mRNAs in this pool are newly synthetized species with a standard/average mRNA length. Hence we posit that the light polysomal mRNAs contain a smaller proportion of terminating ribosomes than mRNAs isolated from heavy polysomes, since the likelihood of having a stop codon occupied by a terminating ribosome increases with the increasing number of elongating ribosomes per mRNA. In support of this rationale, we observed more than 3-fold increase in the amounts of eRF3 associated with 80S ribosomes isolated from heavy versus light polysomes. By the same token, if eIF3 was involved specifically in translation termination events, we would expect stronger association of eIF3 and HCR1 with 80S couples originating from heavy polysomes. We do indeed observe that the 80S/40S ratio of eIF3 and HCR1 association is 2- and 2.5-fold higher, respectively, for heavy polysomes than for the light ones, in contrast to eIF5 where it remains the same (Figure 4A). These results thus strongly suggest that eIF3 and HCR1 are present at 80S ribosomes during the terminating process.

To further support this conclusion, we employed the *Tet::SUP45* conditional depletion strain. We rationalized that if eIF3 specifically associates with terminating ribosomes, depletion of eRF1 should significantly reduce the presence of eIF3 subunits (as well as the presence of eRF3) in the 80S couples isolated from heavy polysomes. To test this, we formaldehyde cross-linked the *Tet::SUP45* cells grown in the presence or absence of 1 μg/ml doxycycline for six hours before harvesting, resolved the WCEs on sucrose gradients, collected only the fractions containing heavy polysomes, treated these fractions with RNase I and separated the resulting 43-48S PICs and 80S species by the second round of centrifugation (resedimentation). Thus isolated 80S couples from Dox^- versus Dox^+ *Tet::SUP45* cells were loaded in six serial two-fold dilutions to the SDS-PAGE gel and the amounts of RPS0A (as a loading control) and associated eIFs and eRFs were analyzed by quantitative western blotting. Depletion of the key termination factor had to be rapid to avoid disassembly of stalled post-TCs in polysomes as well as secondary defects of dying cells. In our set-up we achieved ~70% depletion of eRF1 and observed no changes in polysome profiles of Dox^- versus Dox^+ *Tet::SUP45* cells (data not shown). As predicted, whereas the 80S-associated amounts of eIF1 remained unchanged (small), the amounts of eRF3 and two eIF3 subunits were significantly reduced (by ~40%) in Dox^+ versus Dox^- *Tet::SUP45* cells (Figure 4B). Note that while the overall levels

of eRF1 were depleted by ~70%, polysome-associated eRF1 was only depleted by ~30%, which is consistent with the quantitatively similar reduction in polysome association observed for eRF3 and eIF3.

Deletion of *hcr1* results in accumulation of eRF3 in heavy polysomes, and the *sup45^{Y410S}* mutant prevents stable association of eRF3 and HCR1 with polyribosomes

In order to examine how the network of interactions between translation initiation and termination factors affects their functions, we investigated the distribution of selected translation factors in wt cells and cells mutated for either of the factors under study using formaldehyde cross-linking of living cells by sucrose density gradients analysis of WCEs [25].

Figures 5A and S7A show a typical distribution of the selected proteins across all gradient fractions obtained from wt WCEs and divided into several separable groups: "Top" (fractions 1–4), "40S" (5–6), "60S" (7–8), "80S+light polysomes" (9–13) and "heavy polysomes" (14–18). For technical reasons, several fractions from individual groups were pooled together to fit all samples on a single SDS-PAGE gel. Whereas eRF3 is clearly enriched in the polysome-containing fractions and practically lacking in the Top fractions, eRF1 is more or less evenly distributed across the entire gradient, and RLI1 predominantly sediments in the Top fractions and partially also in the 40S-containing fractions. Importantly, all strains that we worked with in this study are [psi$^-$] and hence the observed sedimentation of eRF3 into heavier fractions cannot be attributed to SUP35 aggregation. In agreement with the aforementioned analysis, eIF3 (represented by a/TIF32) and HCR1 show a robust enrichment in polysomal fractions, similar to eRF3, whereas eIF5 occurs mainly in the Top and 40S fractions.

As shown in Figures 5B, E and S7A, deletion of *hcr1* significantly shifted the amounts of "initiating" eIF3 from the 40S fractions to the Top, as observed before [20], whereas it had no effect on polysomal distribution of eRF1 and RLI1. However, it led to a statistically significant accumulation of eRF3 in heavy polysomes with a commensurate reduction in lighter fractions (Figures 5B, D and S7A). We interpret the accumulation of eRF3 in heavy polysomes as an increased number of post-TCs bound by eRF3 in a less-productive manner; perhaps with a decreased dissociation rate. Most importantly, overexpression of RLI1, which suppresses both the read-through and Slg$^-$ phenotypes of *hcr1Δ* (Figure 2), partially but significantly restored the eRF3 distribution in polysomes to wt (Figures 5C, D and S7A). The fact that the 40S-binding by the "initiating" eIF3 was not restored (Figures 5C, E and S7A) underscores a specificity of the RLI1 suppressor effect on the HCR1 role in termination versus initiation. One way to explain these observations is that HCR1 may promote the release of eRF3·GDP from the post-TCs upon stop codon recognition and GTP hydrolysis on eRF3, which serves as a prerequisite for the subsequent binding of RLI1 as well as the eRF1-stimulated hydrolysis of the bond between the P-site tRNA and the nascent polypeptide (see our model in Figure 6). Inability to complete this step may lead to a reduced stop codon recognition resulting in an increased read-through, which was observed. Hence the suppression effect of RLI1 on the molecular level could be explained by proposing that increased dosage of RLI1 forces dissociation of eRF3·GDP from the post-TCs by mass action and thus eliminates a need for HCR1.

If our model is correct, one can predict that the polysomal levels of HCR1 could be reduced without any functional defect, if the interaction between eRF1 and eRF3 was impaired. Hence we next analyzed changes in polysomal distribution of factors of interest in the *sup45^{Y410S}* mutant, which disrupts the eRF1–eRF3 interaction [28]. As expected, the *sup45^{Y410S}* mutant significantly shifted the amounts of eRF3 from polysomal to the Top fractions when compared to wt (Figures 7A–C and S7B). Importantly, in accord with our proposed model, a similar, significant change was also observed for HCR1 but not for a/TIF32 and RLI1. We interpret these data by proposing that HCR1 readily dissociates along with eRF3 when eRF3 binding to the post-TCs is weakened by a mutation. This effect could be either direct or indirect/allosteric. The fact that we could not detect any direct binding between HCR1 and eRF3 using conventional *in vitro* protein-protein binding techniques may speak for the latter option; however, it is also possible that HCR1–eRF3 binding does occur but only in the context of the post-TCs.

Genetic interactions between *hcr1Δ*, mutant eIF3 subunits and mutant release factors

To further support our model, we analyzed genetic interactions between the *hcr1* deletion strain and selected mutations in both release factors. The temperature sensitive eRF mutants we used are all known to cause termination defects including stop codon read-through strong enough to suppress the *ade1-14* nonsense allele [29]. They include a *sup35^{N536T}* mutant located in a region near the C-terminus of eRF3 that disrupts termination by an unknown mechanism, a *sup45^{M48I}* mutant that interferes with stop codon decoding [30], and the aforementioned *sup45^{Y410S}* mutant that directly disrupts the eRF1–eRF3 interaction [28].

It could be proposed that if the *sup45^{Y410S}* Ts$^-$ mutant reduced or even eliminated a need for HCR1 functioning in termination, an epistatic interaction should be observed when this mutant is combined with *hcr1Δ*. Consistently, at the permissive temperature the absence of HCR1 further increased read-through of this *sup45* mutant (Figure 8A, 30°C; compare open and grey bars with the black one) and also exacerbated its slow growth (Figure 8B). However, at the higher temperature, where the eRF1:eRF3 interaction is more severely disrupted by the *sup45^{Y410}* mutation [28], as evidenced by its increased termination defect (Figure 8A; compare grey bars between 30 and 34°C), the absence of HCR1 had only a little additional effect on the *sup45^{Y410S}* read-through (Figure 8A, 34°C; black vs. grey bars). Moreover, the *sup45^{Y410S}* mutation also completely eliminated the negative impact of *hcr1Δ* on growth rates at this temperature (Figure 8B). The specificity of this epistatic interaction is further underscored by the fact that neither *sup45^{M48I}* (eRF1) nor *sup35^{N536T}* (eRF3) mutants showed any synthetic effects in the background of the *hcr1* deletion (Figure S7C).

Finally, to obtain further genetic evidence supporting our findings implicating eIF3 in regulation of the termination process, we combined two selected mutations in the a/TIF32 subunit of eIF3 (*Δ8* and *Box17*), both reducing the stop codon read-through in otherwise wt cells (Figure 1), with the *sup35^{N536T}* and *sup45^{Y410S}* mutants. When combined, the double mutants show a stop codon read-through frequency that is clearly reduced compared to either release factor mutant (Figure 8C), demonstrating that the *tif32* mutations partially rescue the read-through phenotype of the latter. In contrast, when we investigated slow growth (Slg$^-$) and temperature sensitive (Ts$^-$) phenotypes, we observed synthetic exacerbation of these phenotypes (Figure 8D). This demonstrates that i) the release factors and the core eIF3 complex have antagonistic functions in the same stage of the termination phase and losses in their functions can thus partially compensate for each other in terms of the stop codon read-through efficiency; and ii) that the degree of stop codon read-through *per se* is not the major source of the fitness defects in these strains. This latter notion is consistent with earlier quantitative trait analyses, which showed that the termination defects are unlinked from growth defects in many eRF1

A *hcr1Δ* + hc *HCR1*

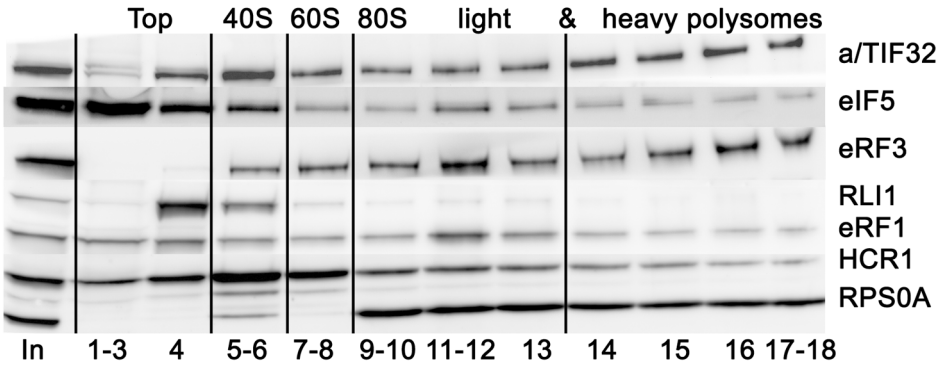

B *hcr1Δ* + EV

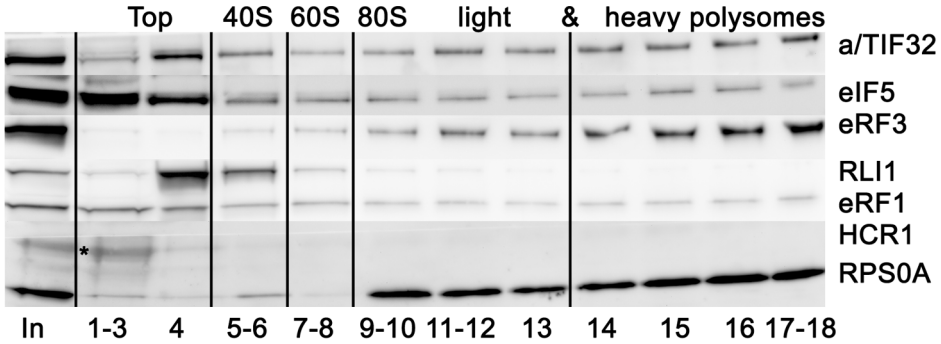

C *hcr1Δ* + hc *RLI1*

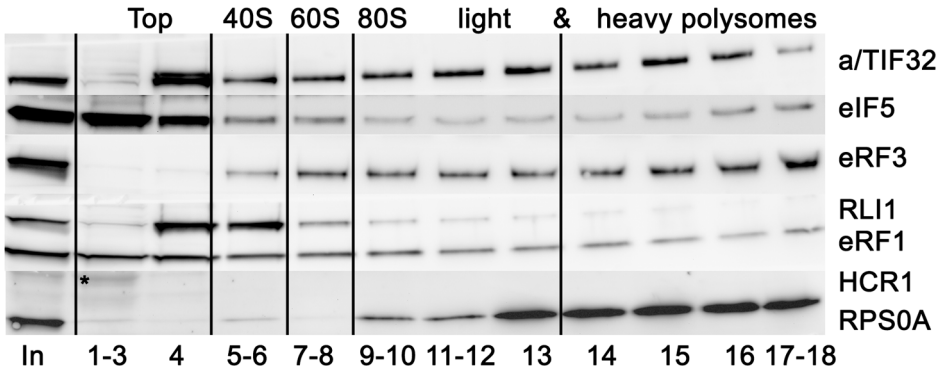

D relative amounts of eRF3 in heavy polysomes / lighter fractions

hcr1Δ + hc *HCR1*	0.469±0.029
hcr1Δ + EV	1.448±0.163 *
hcr1Δ + hc *RLI1*	0.793±0.036 **

*signif. of eRF3 accumulation in heavy polys. in *hcr1*Δ+EV relative to *hcr1*Δ+hc *HCR1* (*P*<0.05)

**signif. of eRF3 redistribution back to lighter fractions in *hcr1*Δ+hc *RLI1* relative to *hcr1*Δ+EV (*P*<0.1)

E relative amounts of a/TIF32 in Top / 40S fractions

hcr1Δ + hc *HCR1*	0.590±0.011
hcr1Δ + EV	2.657±0.375 *
hcr1Δ + hc *RLI1*	1.701±0.218 *

*signif. of a/TIF32 shift from 40S to TOP fractions in *hcr1*Δ+EV or +hc *RLI1* relative to *hcr1*Δ+hc *HCR1* (P<0.05)

Figure 5. Deletion of *hcr1* results in accumulation of eRF3 in heavy polysomes. (**A–C**) The *hcr1Δ* strain (H3675) was transformed with either hc *HCR1* (**A**), empty vector (**B**), or hc *RLI1* (**C**), and the resulting transformants were grown in SD medium at 30°C to an OD_{600} of ~1 and cross-linked with 0.5% HCHO prior to harvesting. WCEs were prepared, separated on a 5%–45% sucrose gradient by centrifugation at 39,000 rpm for 2.5 h and subjected to Western blot analysis. Several fractions corresponding to the Top, 40S, 60S, and 80S plus polysomal species were pooled, as indicated. Asterisk indicates a non-specific band. (**D**) Statistical significance of the eRF3 accumulation in heavy polysomes in the *hcr1* strain and its partial recovery by hc *RLI1*. Amounts of each individual factor in all fractions were quantified by fluorescence imaging. Thus obtained values for the fractions containing heavy polysomes (14–18) as well as all remaining fractions (1–13) were added up for each of these two groups. Values (mean±SE; n = 4) given in the table then represent relative amounts of factors in heavy polysomes divided by the compound value of the rest of the gradient. Changes in the redistribution of factors between the heavy polysomes and lighter fractions in all three strain were analyzed by the student's *t*-test and shown to be statistically significant only for eRF3 as shown in the table. (**E**) Statistical significance of the eIF3 shift from 40S-containing fractions to the top, which is independent of the effect of hc *RLI1* on eRF3. Essential the same as in panel D, except that the values for the Top fractions (1–4) as well as the 40S fractions (5–6) were added up for each of these two groups. Values (mean±SE; n = 4) given in the table then represent relative amounts of factors in the Top divided by the 40S group. Changes in the redistribution of factors between the 40S and Top fractions in *hcr1Δ*+EV or +hc *RLI1* strains vs. wt were analyzed by the student's *t*-test and shown to be statistically significant only for eIF3 as shown in the table.
doi:10.1371/journal.pgen.1003962.g005

mutants [31]. Hence, synthetic exacerbation of growth could be explained by proposing that besides the stop codon recognition step (which is assessed in the dual luciferase assay), also other aspects of termination are impaired in the eRF and eIF3 mutants, which, in combination with the initiation defects of eIF3 mutants, reduce the growth rate as a compound effect.

Discussion

It is becoming increasingly apparent that factors involved in regulating various steps of gene expression may have multiple functions and that this multitasking may integrate transcription, mRNA export, translation and mRNA decay into a delicately regulated higher-order process. For example, translation initiation factor eIF3 links translation initiation to transcription [32], to mRNA export [3] and to the NMD pathway [33,34]. Here we show for the first time that eIF3 and HCR1 critically connects initiation of translation with its termination.

In particular, deletion of *hcr1* increases stop codon read-through, independently of its association with the rest of eIF3, and results in accumulation of eRF3 in heavy polysomes. Increased

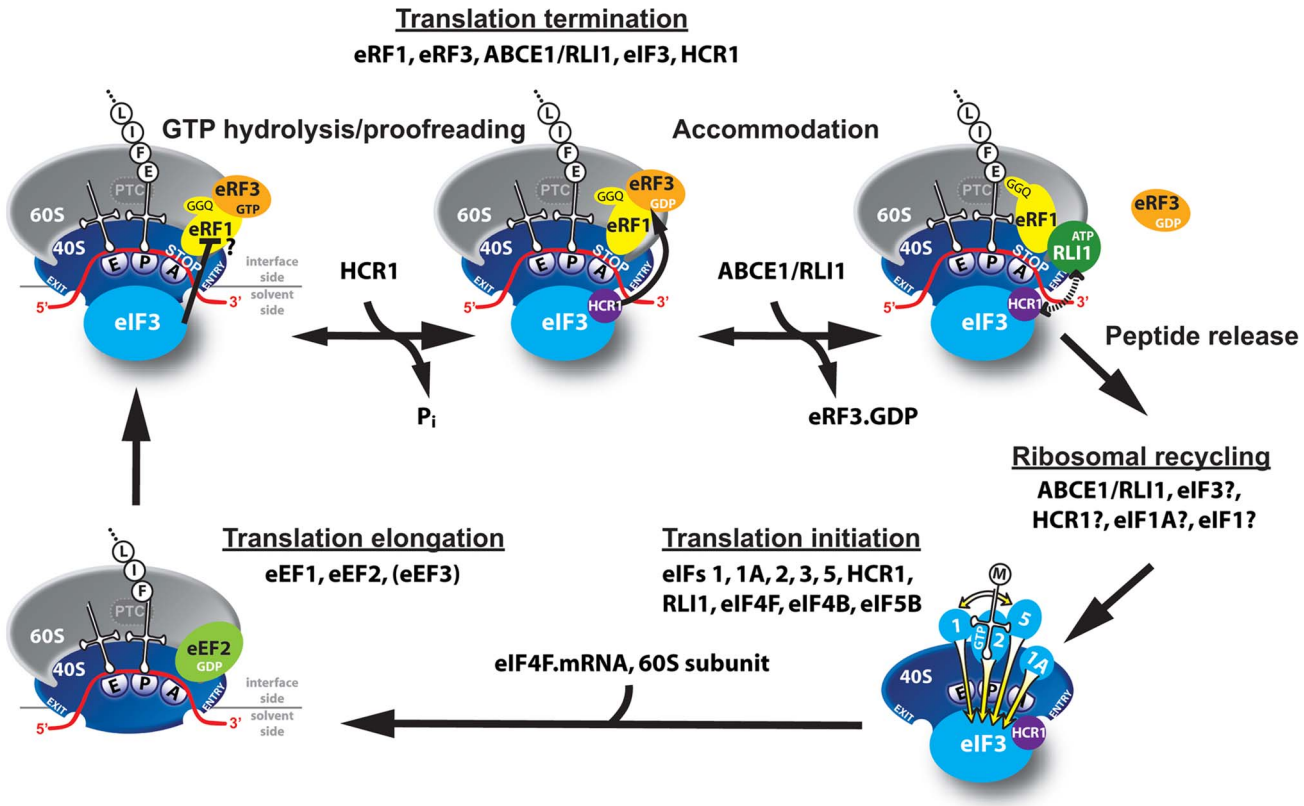

Figure 6. Model of eIF3 and HCR1 involvement in yeast translation termination. Upon stop codon entry into the ribosomal A-site the pre-TC forms, composed of the canonical release factors eRF1 and eRF3·GTP, and eIF3 and HCR1. eRFs and eIF3 may associate with the pre-TC as a pre-formed unit or alone. In the pre-TC, eIF3 interacts with the N domain of eRF1, *via* its two small g/TIF35 and i/TI34 subunits, and modulates, perhaps inhibits its stop codon recognition activity during the proofreading step. Upon stop codon recognition the GTP molecule on eRF3 is hydrolyzed. Subsequently, HCR1 promotes eRF3·GDP ejection to allow the ABCE1/RLI1·ATP recruitment to begin the accommodation phase of termination – the eRF1 GGQ motif is pushed to the peptidyl-transferase center (PTC) – during which HCR1 interacts with ABCE1/RLI1. Subsequently, both factors together with eIF3 participate in ribosomal recycling to enable and promote initiation of the next translational cycle (the elongation step is shown only for illustration purposes).
doi:10.1371/journal.pgen.1003962.g006

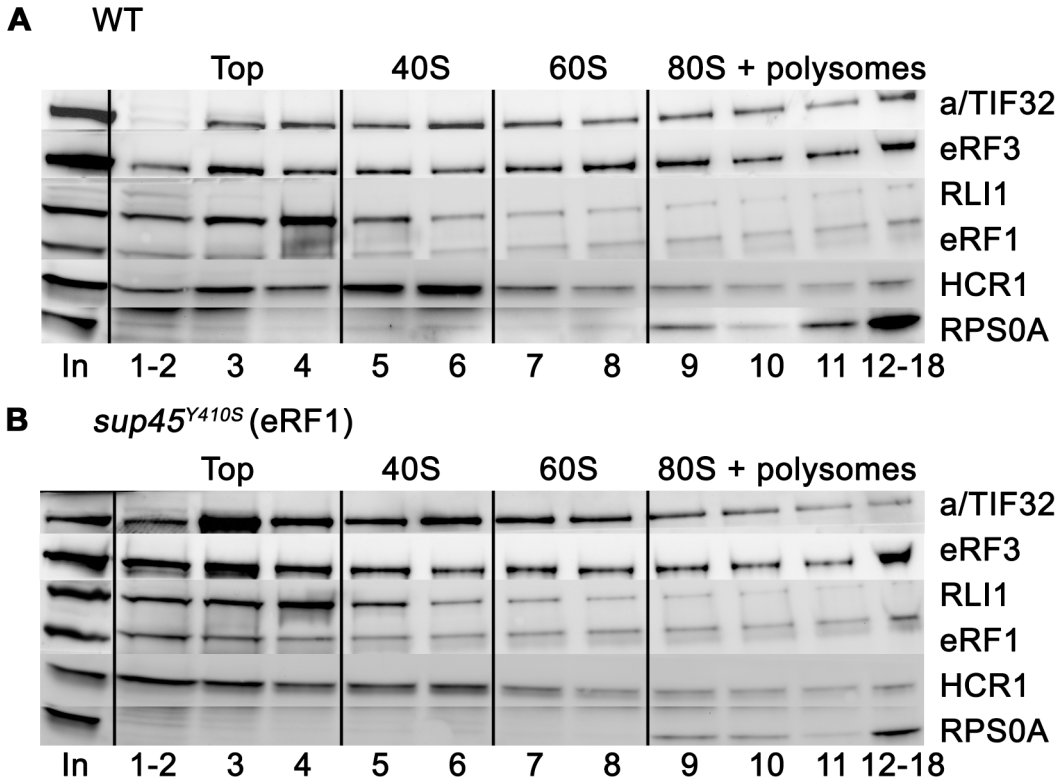

C relative amounts of factors in Top / 80S + polysomes fractions

	WT	*sup45*^{Y410S} (eRF1)
a/TIF32	0.351±0.097	0.507±0.276
eRF3	0.536±0.069	0.837±0.025 *
RLI1	3.887±0.872	5.549±1.595
HCR1	1.135±0.046	1.547±0.019 **

*significance of the shift from 80S/polysomes to Top fractions (P<0.1)

**significance of the shift from 80S/polysomes to Top fractions (P<0.05)

Figure 7. The *sup45*^{Y410S} mutation prevents stable association of eRF3 and HCR1 with polyribosomes. (**A–B**) The *sup45*^{Y410S} mutant and its corresponding wt strain were subjected to HCHO cross-linking (0.5%) and polysomal gradient analysis as described in Figure 5. (**C**) Statistical significance of the reduction of polysomes-associated amounts of eRF3 and HCR1 in *sup45*^{Y410S}. Amounts of each individual factor in all fractions were quantified by fluorescence imaging. Thus obtained values for the Top fractions as well as fractions containing 80S couples and polysomes were added up for each of these two groups. Values (mean±SE; n = 4) given in the table then represent relative amounts of factors in the Top divided by the 80S+polysomes group. Changes in the redistribution of factors between the Top and 80S+polysomes fractions in the *sup45*^{Y410S} mutant vs. wt were analyzed by the student's *t*-test and shown to be statistically significant for HCR1 (P<0.05) and SUP35 (P<0.1).
doi:10.1371/journal.pgen.1003962.g007

dosage of ribosomal recycling factor RLI1 then substitutes for the HCR1 roles in termination (but not in initiation) and in enabling efficient cell growth, together implying that the HCR1 function in termination is more critical for optimal cell proliferation than its function in translation initiation. This is consistent with the fact that yeast HCR1 is only loosely associated with the core eIF3 complex [19] and that it was shown to interact with both sides of the 40S mRNA entry channel on its own [21]. Similarly, its mammalian ortholog also appears to be the most loosely associated subunit of all 13 eIF3 subunits that is, in addition, often missing from the purified 12-subunit complex [35–37]. Moreover, it was also shown to associate with the 40S ribosome completely independently of the rest of eIF3 and promote several translational steps practically on its own (see for example [5,35–40]). Taken together, we suggest considering eIF3j/HCR1 as an independent initiation factor (eIF) that associates and closely co-operates with eIF3 but it is not its integral part. We therefore propose to use the following designations for this old-new eIF: HCR1 for the yeast protein and hHcr1 for its mammalian counterpart.

In contrast to *hcr1Δ*, various mutants of core eIF3 subunits, but not of other initiation factors, decrease stop codon read-through in living cells and show synthetic phenotypes with mutant release factors eRF1 and 3. eIF3 also directly interacts with eRF1 and occurs in complex with eRF1, eRF3 and RLI1 *in vivo*. Since eIF3 and HCR1 were, based on *in vitro* experiments, previously implicated in promoting also the very final step of translation – ribosomal recycling [5], we propose that eIF3 – and to some extend also HCR1 – is one of the very few factors that connects

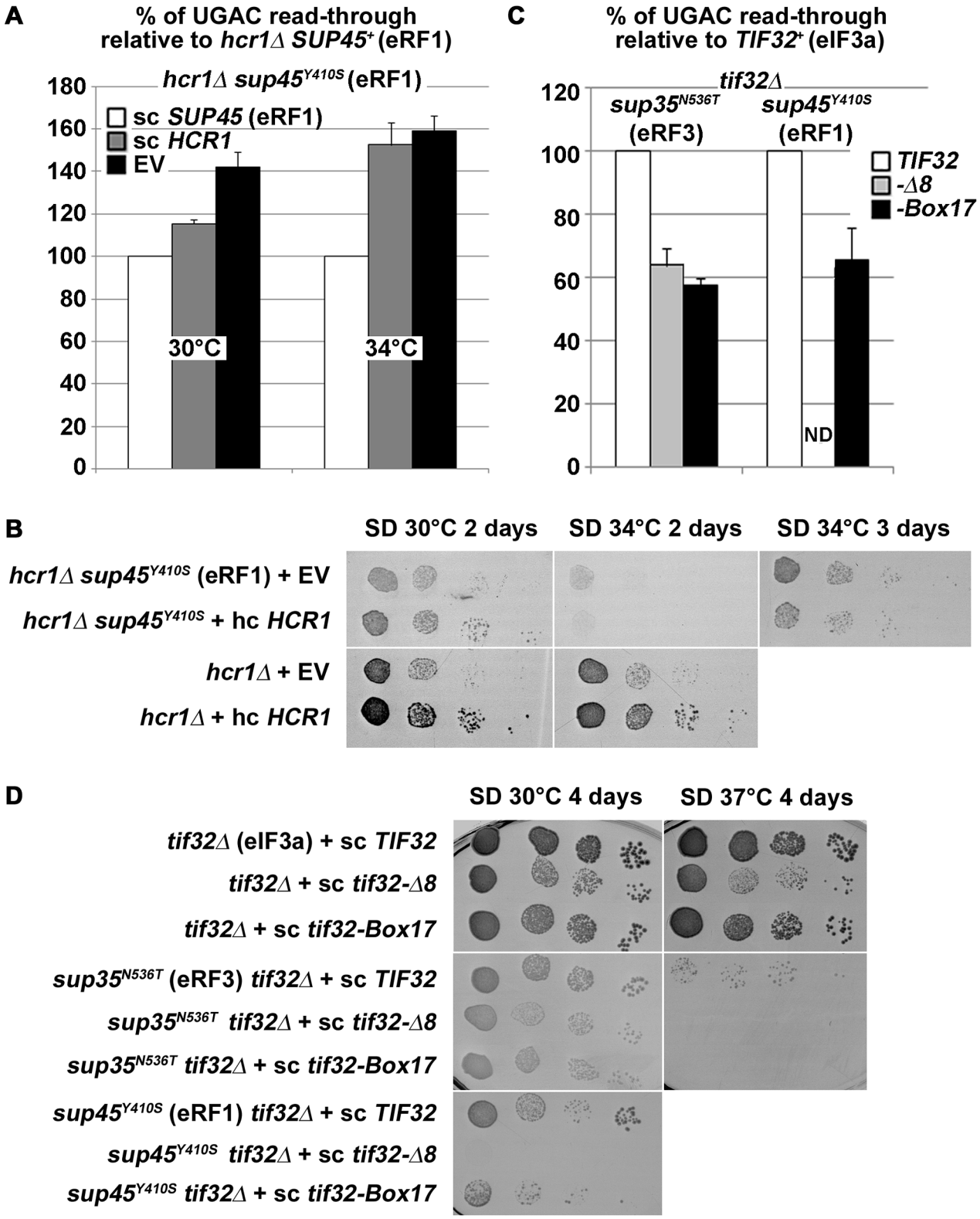

Figure 8. *hcr1Δ* and eIF3 mutants genetically interact with release factor mutants. (**A–B**) The *sup45*^{Y410S} mutation eliminates the negative impact of *hcr1Δ* on (**A**) read-through and (**B**) growth rates. The *hcr1Δ* strain was crossed with the *sup45*^{Y410S} mutant strain and the resulting double mutant was transformed with sc *SUP45*, hc *HCR1*, or empty vector (EV), respectively, and (**A**) processed for stop codon read-through as described in Figure 1 (*hcr1Δ* read-through values were set to 100%) or (**B**) subjected to a growth spot assay at indicated temperatures for 2 or 3 days. (**C–D**) Combining the selected *TIF32* mutants with *sup35*^{N536T} and *sup45*^{Y410S} (**C**) reduces their read-through defects and (**D**) produces synthetic growth phenotypes. The wt and mutant alleles of *TIF32* were introduced into *tif32Δ*, *sup35*^{N536T} *tif32Δ*, and *sup45*^{Y410S} *tif32Δ* strains, respectively, by plasmid shuffling. (**C**) The resulting double mutant strains were grown in SD and processed for the stop codon read-through as described in Figure 1 (the

read-through values of both single eRF mutants were set to 100%), or (**D**) spotted in four serial 10-fold dilutions on SD medium and incubated at indicated temperatures for 4 days. ND; not determined due to severe growth deficiency.
doi:10.1371/journal.pgen.1003962.g008

various processes of mRNA life and integrates them into the ultimate translational output. Taking into account that the translation pathway is highly conserved among low and high eukaryotes, it is highly likely that this connecting role of eIF3 is also conserved.

eIF3 modulates the precision of the stop codon recognition by eRF1

Our observations that 1) eIF3 and eRF3 can be found enriched in 80S fractions isolated from RNase-treated heavy polysomes in an eRF1-dependent manner (Figure 4); 2) that a complex between eIF3, RLI1 and eRFs exists free of RNA and ribosomes in the cytoplasm (Figure 3A–D), and 3) that two small eIF3 subunits g/TIF35 (in particular its NTD) and i/TIF34 directly interact with the N and N-M domains of eRF1 (Figure 3E–F) together suggest that eIF3 does associate with terminating 80S couples and may come to the pre-TC in a pre-formed complex with eRFs. The alternative that they are ejected from post-TCs as a holocomplex upon completion of termination is highly unlikely considering that i) eRF3 must be ejected prior to RLI1 binding [12] and ii) that eIF3 is supposed to participate in the late steps of ribosomal recycling that should be devoid of eRF1 and RLI1 [5,6]. The last scenario would be that eIF3 stays present on the elongating ribosome throughout the entire elongation cycle and promotes recruitment of eRF1·eRF3·GTP to the pre-TCs; there is, however, genetic evidence contradicting this possibility [9].

Our data show that eIF3 mutants specifically decrease stop codon read-through in otherwise wt cells (Figures 1 and S1) and that *tif32* mutations partially compensate for the increased read-through in eRF mutants (Figure 8C). This clearly suggests that wt eIF3 modulates the precision of stop codon recognition by eRF1 in order to fine tune the termination process (see our model in Figure 6). During stop codon decoding, eRF1 was proposed to sit in the ribosomal A-site with a part of its N-domain contacting small ribosomal protein RPS3 and helix (h) 18 of 18S rRNA [41]. Strikingly, g/TIF35 also interacts with RPS3, in addition to RPS20 [42], and as both g/TIF35 and i/TIF34 are tightly bound to the extreme C-terminus of b/PRT1 [43], i/TIF34 is expected to occur nearby g/TIF35. Moreover, the C-terminal domain of a/TIF32 interacts with h16-18 of 18S rRNA [44] and RPS3 as well [22]. Taylor and colleagues further proposed that one of the conformational changes induced by eRF1–eRF3–GMPPNP binding to pre-TCs involves a movement of h16 of 18S rRNA and the N-terminal domain (NTD) of RPS3 toward each other, which results in the establishment of a new head–body connection on the solvent side of the 40S subunit and a constriction of the mRNA entrance. Hence, it is conceivable that eRF1 and eIF3, by contacting the same 40S binding partners, modulate these conformational changes in the termination complex in a way that influences a proper placement of eRF1 in the spatially restricted A-site. This scenario could provide a rational explanation for the antagonistic effect of eIF3 on translation termination.

For interpretation of these data it must be kept in mind that the reporter constructs we use essentially measure stop codon read-through on a premature termination codon. At present, we do not know whether the antagonistic influence of eIF3 on stop-codon read-through is restricted to such sites, or whether it also affects termination on stop codons located nearer to the poly(A) tail. However, our observation that the *sup45*^{Y410S} mutant, which affects stop codon selection by disrupting the eRF1–eRF3 interaction, reduced the polysome-associated amounts of eRF3 and HCR1 (Figure 7) indicates that a delay or imperfection in the decoding of natural stop codons disrupts this ''initiation-termination'' complex, most probably to enable resumption of elongation. Investigation of the precise molecular mechanism of the eIF3 action in termination is a pressing task for our future research.

HCR1 promotes eRF3·GDP ejection from the post-TCs to allow RLI1 binding

In contrast to mutations in core eIF3 subunits, deletion of *hcr1* did not decrease but increased the stop codon read-through (Figure 1). The fact that mutations disrupting the HCR1 contact with eIF3 had no effect on read-through clearly suggests that the HCR1 role in termination is independent of its association with eIF3, as discussed above. Moreover, our findings that *hcr1Δ* results in accumulation of eRF3 in higher polysomal fractions (Figure 5) and that *sup45*^{Y410S} (breaking the eRF1–eRF3 interaction) shifts HCR1 to the Top fractions (Figure 7) led to the model presented in Figure 6. We propose that following stop codon recognition and subsequent GTP hydrolysis on eRF3, HCR1 promotes eRF3·GDP ejection from the post-TCs to allow binding of its interacting partner RLI1 [2], which in turn stimulates polypeptide release – both eRF3 and RLI1 bind to the same site in the post-TC [13]. Inability to complete this step may lead to a reduced stop codon recognition resulting in an increased read-through. In support, eRF1 was shown to associate more firmly with post-TCs in the presence of eRF3 [6], which led the authors to propose that after GTP hydrolysis, eRF3 might not dissociate entirely from ribosomal complexes on its own and its release thus might require a stimulus by an additional factor; in our opinion by the HCR1 protein.

Based on the cryo-EM structures of DOM34:HBS1 (release factor-like proteins closely related in sequence and structure to eRF1:eRF3) on the yeast ribosome showing that the N-terminus of HBS1 extends away from the body of the protein and contacts the mRNA entry site, it was proposed that the N-terminus of eRF3 also occurs in the A-site area [13]. Since HCR1 was shown to occur in this area too [21], it could directly act upon this eRF3 domain to trigger the release of this factor in its GDP form from eRF1-bound post-TCs. In support, the N-terminal extension of *S. pombe* eRF3 was proposed to regulate eRF1 binding to eRF3 in a competitive manner [45]. Interestingly, both the N-terminus of eRF3 as well as the HCR1 protein as a whole are non-essential [45,46], suggesting that they might act simply by shifting the equilibrium towards the loss of affinity between the eRF1 and eRF3·GDP binary complex. If true, the loss-of-function of both of them could be overcome by redundant mechanisms with slower reaction rates. In agreement, hc *RLI1* fully suppressed the read-through effect of *hcr1Δ* in a manner dependent on its intact 4Fe-4S and ABC domains (Figure 2B). We propose that in the *hcr1Δ* cells, RLI1 makes its way to its binding site in the post-TCs by forcing dissociation of eRF3·GDP through mass action and thus eliminates a need for HCR1. These results are consistent with the aforementioned observation that the eRF1 mutation *sup45*^{Y410S}, disrupting the eRF1–eRF3 interaction, shifts the amounts of eRF3 and also that of HCR1 from polysomes to the top of the gradient (Figure 7).

The model proposed in Figure 6 also explains the behavior of genetic interactions observed for the *hcr1* deletion (Figure 8). Failure to eject eRF3·GDP can perceivably have two consequences. First, if

peptidyl hydrolysis by eRF1 fails to be induced because RLI1 cannot bind to it, the eRF1·eRF3·GDP complex can dissociate from the ribosomal A-site, thus necessitating a renewed round of tRNA sampling with an ensuing risk of stop codon decoding by a near-cognate or suppressor tRNA. This is consistent with the increased stop codon read-through we observe experimentally in *hcr1* deletion strains. Second, if peptidyl hydrolysis does take place (*in vitro*, eRF1 clearly has some release factor activity also in the absence of RLI1 [11]), a stalled ribosome complex would be formed in which eRF1 was still bound to eRF3, and in which RLI1 was thus not free to initiate the recycling step. Such stalled complexes would impede ribosome flow on the affected mRNA, reduce corresponding gene expression levels and potentially necessitate degradation by one of the surveillance pathways. If this occurred frequently, it would give rise to fitness defects, as we observe for *hcr1* deletion strains. This is also consistent with the fact that deletion of *hcr1* produces unexpectedly mild polysomal run-off with respect to its growth defect [23]. However, in the presence of eRF1 mutations, which accelerate spontaneous dissociation of eRF3·GDP from eRF1, timely RLI1 binding to eRF1 in the post-TCs would be re-enabled even in the absence of HCR1. This would explain why the $sup45^{Y410S}$ mutation, but not $sup45^{M48I}$ and $sup35^{N536T}$ mutations, eliminated the negative impact of *hcr1Δ* on growth rates at the semipermissive temperature (Figure 8B).

To further support our model, we wished to employ a recently established *in vitro* reconstituted yeast translation system, which has been used previously to monitor both the peptide release and ribosome recycling steps of the translation cycle [12]. HCR1 did not have an appreciable effect on ribosome recycling in this assay (unpublished observations). This is probably not surprising given that ribosome recycling is slow relative to the preceding steps. Thus, accelerating eRF3.GDP dissociation is unlikely to affect the observed rate of recycling. In contrast, the model predicts that the observed rate of peptide release by eRF1, eRF3 and RLI1 may accelerate in the presence of HCR1. Unfortunately, however, the rate of peptide release by eRF1, eRF3 and RLI1 is very rapid, such that further increases in rate (such as those that may occur in the presence of HCR1) are unable to be measured in this system. Since the former two assays are the only *in vitro* assays available to us at the moment and neither of them can either directly or indirectly monitor the rate of eRF3·GDP dissociation from the post-TCs, further efforts will be necessary to fully characterize the role of HCR1 in termination/recycling reactions biochemically.

Upon completion of the termination-specific reactions, eIF3, HCR1 and RLI1 further participate in the ribosomal recycling steps, as proposed by [6], and it is conceivable that all these factors remain bound to the small 40S subunit to promote the next round of initiation (Figure 6). Alternatively, the pre-occupation of the 40S·mRNA complex by the "initiation factors" that would not be recycled could ensure reinitiation on the same mRNA molecule as proposed by the mRNA closed-loop model [47]. An *in vivo* experimental evidence implicating eIF3, HCR1 and other eIFs in the recycling steps is, however, still lacking.

General conclusions

Taken together, we argue that strict mechanistic separation of translation into its individual, mutually independent phases should be reconsidered in the light of "multitasking" of eIF3, HCR1, RLI1 and most likely also eIF1 and eIF1A, for which evidence is presented here and elsewhere. Collectively, these findings suggest that changes in one phase of translation, evoked for example *via* cell signaling pathways, are promptly communicated to and coordinated with changes in the other phases to maintain cellular homeostasis of all ongoing processes. Without a doubt there is much to be learned about how all four phases of translation come together in one balanced system that rapidly and accurately responds to different needs of the cell exposed to constantly changing environmental conditions.

Materials and Methods

Yeast strains and plasmids

The lists and descriptions of plasmids and yeast strains used throughout this study can be found in the Supplemental Information (Tables S2, S3, S4 and Text S1).

Read-through assays

Stop codon read-through assays were performed using a bicistronic reporter construct consisting of a *Renilla* luciferase gene followed by an in-frame firefly luciferase gene. Separating the two genes is either a tetranucleotide termination signal (e.g., UGA C) [plasmids pTH477 (*URA3*) or YEp-R/T-UGAC-L (*LEU2*)] or, for control purposes, a similar sequence containing a sense codon (e.g., CAA C) [plasmids pTH460 (*URA3*) or YEp-R/T-CAAC-L (*LEU2*)]. It is noteworthy that this system avoids possible artifacts associated with changes in the efficiency of translation initiation associated with the function of the NMD machinery [48], because both the *Renilla* and firefly enzymes initiate translation from the same AUG codon. For further details, see [14]. Microtitre-plate based dual luciferase assays and analyses of the resulting data were as described [31]. Samples were processed in quintuplicate, and each experiment was repeated at three times.

Co-immunoprecipitation and affinity tag pull downs

Yeast whole cell extracts (WCEs) were prepared as described previously [49] except that buffer A (30 mM HEPES (pH 8.8), 20 mM KAc, 3 mM magnesium acetate,1 mM dithiothreitol, 1% Nonidet P-40 supplemented with Complete Protease Inhibitor Mix tablets (ROCHE), and protease inhibitors 1 μg/ml aprotinin, 1 μg/ml leupeptin, 1 μg/ml pepstatin and 100 μM phenylmethylsulfonyl fluoride (PMSF)) was used for lysis of the cells, and cell lysates were centrifuged at 3,000 r.p.m. for 10 min at 4°C. The co-immunoprecipitation analysis was performed as described elsewhere [50], using 500 μg of the total protein and 1 μl of mouse anti Myc-Tag IgG (CELL SIGNALING TECHNOLOGY).

Yeast cells expressing the TAP-tagged genes of interest were grown in YPD medium at 30°C to an OD_{600} of ~1 and treated with 1% HCHO prior to harvesting for 60 mins. The WCEs was prepared as described above using buffer B (50 mM Tris-HCl (pH 7.6), 150 mM NaCl, 0.05% Tween 20) with all protease inhibitors in the presence or absence of 0.1 mg/ml RNase A. Samples containing 1 mg of total protein in a final volume of 600 μl were incubated for 2 h at 4°C with 50 μl of 1:1 slurry of IgG Sepharose 6 Fast Flow beads in buffer B. Samples were centrifuged briefly and the supernatants were removed. The collected beads were then washed five times with 1 ml of ice cold buffer B, and incubated either with TEV protease (INVITROGEN) for 30 min at 30°C followed by boiling in the SDS-loading buffer for 5 min at 95°C, or directly boiled the SDS-loading buffer. Corresponding aliquots of input, eluate and wash (supernatant) were analyzed by SDS-PAGE followed by immunoblotting.

Polysomal gradient analysis

The 0.5% formaldehyde (HCHO) cross-linking followed by WCE preparation and fractionation of extracts for analysis of translational complexes were carried out as described previously [25] with the following exceptions. Cycloheximide was added at a

concentration of 0.05 mg/ml 5 minutes before the HCHO treatment, after which the cells were broken by FastPrep Instrument (MP Biomedicals) at the intensity level of 5 in two 20 second cycles. The resulting WCEs were separated on 5–45% sucrose gradients.

Other yeast biochemical methods

GST pull-down experiments with GST fusions and *in vitro*-synthesized [^{35}S]-labeled polypeptides (see Table S3 for vector descriptions) were conducted as follows. Individual GST-fusion proteins were expressed in *E. coli*, immobilized on glutathione-Sepharose beads and incubated with 10 µl of ^{35}S-labeled potential binding partners at 4°C for 2 h. The beads were washed 3 times with 1 ml of phosphate-buffered saline, and bound proteins were separated by SDS-PAGE. Gels were first stained with Gelcode Blue Stain Reagent (Pierce) and then subjected to autoradiography. β-galactosidase assays were conducted as described previously [51].

Preparation of antibodies against RLI1 and SUP45

The GST-RLI1 and GST-SUP45 fusion proteins encoded by pGEX-RLI1, pGEX-SUP45, respectively, were expressed in *E. coli* and purified from the WCE by incubation with Glutathione-Sepharose 4B beads (Pharmacia). The isolated proteins were resolved by SDS-PAGE (4–20% gels), excised from the gel, and washed with 1× PBS. Rabbits were injected with the purified protein and sera containing polyclonal antibodies against RLI1, SUP45, respectively, were obtained commercially by Apronex (Prague, the Czech Republic).

Supporting Information

Figure S1 DaMP alleles of various 43S PIC-associated initiation factors display distinct effects on efficiency of stop codon read-through. Yeast strains containing kanMX4 cassettes integrated into their 3′-UTRs (so-called DaMP alleles) were recovered from the genome-wide collection for these alleles [15]. We were able to recover alleles for all 43S PIC-associated eIFs with the exception of eIF2β, for which no allele was present in the collection. In order to aid interpretation of results, and to assess the efficiency of depletion of the gene in question, we initially measured growth rates of the respective strains (top panel). Since all of the factors studied here are essential, we expected a reduction in growth rate upon significant depletion of any of these factors. We then proceeded to measure stop codon read-through in these strains, using dual luciferase reporters as described in the main text. Of the eIF3 subunits tested, only g/TIF35 is sufficiently depleted to cause a significant growth defect, and this strain shows a significant reduction in stop codon read-through. Moreover, the c/NIP1 DaMP allele also shows a significant reduction in stop codon read-through, even though this protein is not sufficiently depleted to produce a significant growth defect. Together, these results confirm those presented for other eIF3 alleles in the main text. In contrast to the eIF3 subunits, other 43S PIC-associated translation initiation factors do not reduce stop codon read-through upon depletion. Conversely, both eIF2 subunits tested and eIF1A increased read-through when depleted. This demonstrates that the role of eIF3 in translation termination is specific to this factor.
(TIF)

Figure S2 Increased gene dosage of eRFs 1 and 3 reduces stop-codon read-through. Wild type strain H416 was transformed with designated plasmids overexpressing eRFs and the resulting transformants were grown in SD and processed for the stop codon read-through measurements as described in Figure 1.
(TIF)

Figure S3 Increased gene dosage of eEF3 does not suppress the slow growth and read-through defects of *hcr1Δ*. (**A**) The *hcr1Δ* strain (H3675) was transformed with either empty vector, high copy (hc) *HCR1* or hc *YEF3* (eEF3), the resulting transformants were spotted in four serial 10-fold dilutions on SD medium and incubated at 30°C for 2 days. Unlike RLI1, eEF3 (which is also an ABC cassette-containing protein) does not suppress the growth defect of an *hcr1* deletion strain. (**B**) The strains from panel A were grown in SD and processed for the stop codon read-through measurements as described in Figure 1.
(TIF)

Figure S4 Increased gene dosage of HCR1 does not suppress the slow growth and read-through defects of the *Tet::RLI1* strain; intact ATP-binding cassettes and the Fe-S cluster of RLI1 are indispensable for its role in ensuring stop codon selection accuracy. (**A**) The *Tet::RLI1* (Tet-RLI1) and the corresponding wt strain (W303) were transformed with either empty vector or hc *HCR1*, and the resulting transformants were spotted in four serial 10-fold dilutions on SD medium supplemented with 0.25 µg/ml of doxycycline and incubated at 30°C for 2 days. (**B**) The *Tet::RLI1* (Tet-RLI1) strain was transformed with hc vectors carrying wt or mutant *RLI1* alleles, or empty vector or hc *HCR1*. The resulting transformants were grown in SD supplemented with 1 µg/ml of doxycycline (DOX) and processed for the stop codon read-through measurements as described in Figure 1. Obtained values were normalized to the value obtained with the *Tet::RLI1* strain transformed with wt *RLI1*, which was set to 100%.
(TIF)

Figure S5 Increased gene dosage of ABCE1/RLI1 does not suppress the leaky scanning defect of *hcr1Δ*. The *HCR1*$^+$ (H2879) and *hcr1Δ* (H3675) strains were first transformed with either empty vector or hc *RLI1* and subsequently with the *GCN4-lacZ* reporter plasmid plig102-3. The resulting double transformants were grown in SD medium at 30°C to an OD_{600} of ~1. The β-galactosidase activities were measured in the WCEs and expressed in units of nmol of o-nitrophenyl-b-D-galactopyranoside hydrolyzed per min per mg of protein. The plots show mean values and standard deviations obtained from at least 3 independent measurements with three independent transformants. The fold-difference between the *hcr1Δ* versus *HCR1*$^+$ strains with or without hc *RLI1* is indicated.
(TIF)

Figure S6 Complexes containing eIF3, HCR1, ABCE1/RLI1 and both eRFs, free of ribosomes and RNA, occur *in vivo* – the RNase A treatment. (**A**) RNAse A-treated WCEs were prepared from HCHO-treated (1%) cells bearing wt (H2879) or TAP-tagged (H553) chromosomal alleles of *HCR1* and incubated with IgG Sepharose 6 Fast Flow beads. The immune complexes were eluted by boiling in SDS buffer and subjected to Western analysis. In, 1.5% of input; E, 50% of the elution fraction; W, 1.5% of the supernatant fraction. eRF1 is indicated by an asterisk below the immunoglobulins. (**B**) RNAse A-treated WCEs from HCHO-treated cells (1%) cells bearing wt (H2879) or TAP-tagged (H555) chromosomal alleles of *TIF32* were processed as in panel A except that the immune complexes were eluted by the TEV protease cleavage. In, 1.5% of input; E, 100% of the elution fraction; W, 1.5% of the supernatant fraction. (**C**) RNAse A-treated WCEs from HCHO-treated cells (1%) cells bearing wt (74D-694) or TAP-tagged (H517) chromosomal alleles of *SUP35* were processed as in panel B.
(TIF)

Figure S7 (**A**) Deletion of *hcr1* results in accumulation of the polysome-associated eRF3 – factor distributions across gradient fractions as shown in Figure 5. Amounts of each individual factor in the pooled fractions from three independent experiments were quantified by fluorescence imaging, combined, and the percentage representation of the signal corresponding to the Top (1–3 and 4), 40S (5–6), 60S (7–8), and 80S plus polysomal fractions (9 through 18) was calculated and plotted. (**B**) The $sup45^{Y410S}$ mutation prevents stable association of eRF3 and HCR1 with polyribosomes – factor distributions across gradient fractions as shown in Figure 7. Amounts of each individual factor in the pooled fractions from three independent experiments were quantified by fluorescence imaging, combined, and the percentage representation of the signal corresponding to the Top (1–3), 40S (4–5), 60S (6–7), and 80S plus polysomal fractions (8–11) was calculated and plotted. (**C**) The $sup45^{Y410S}$ but not the other mutations in eRFs 1 and 3 eliminate the negative impact of *hcr1Δ* on growth rates. The *hcr1Δ* strain was crossed with the indicated *sup45* and *sup35* mutant strains and the resulting double mutants (PBH104, PBH103 and PBH105) were transformed with either empty vector (EV) or hc vector containing *HCR1* and together with the corresponding *hcr1Δ SUP35 SUP45* "wt" strain (YLVH13) spotted in four serial 10-fold dilutions on SD medium and incubated at indicated temperatures for 2 or 3 days.
(TIF)

Table S1 Mutant alleles used in this study and their associated phenotypes.
(DOCX)

Table S2 Yeast strains used in this study.
(DOCX)

Table S3 Plasmids used in this study.
(DOCX)

Table S4 Primers used in this study.
(DOCX)

Text S1 Supporting Materials and Methods.
(DOCX)

Acknowledgments

We are grateful to Rachel Green, Matthias Hentze and Mick F. Tuite for critical reading of the manuscript. We would like to thank Mick F. Tuite and Nadja Koloteva-Levine (University of Kent, UK) for sharing an unpublished SUP35-TAP strain, and David Bedwell, Susan Liebman, Alan G. Hinnebusch, and Terri Kinzy for strains and plasmids.

Author Contributions

Conceived and designed the experiments: LSV TvdH PB LC SW CJS. Performed the experiments: PB LC SW CJS SG TvdH. Analyzed the data: PB LC SW CJS TvdH LSV. Wrote the paper: LSV TvdH.

References

1. Dong J, Lai R, Nielsen K, Fekete CA, Qiu H, et al. (2004) The essential ATP-binding cassette protein RLI1 functions in translation by promoting preinitiation complex assembly. J Biol Chem 279: 42157–42168.
2. Khoshnevis S, Gross T, Rotte C, Baierlein C, Ficner R, et al. (2010) The iron-sulphur protein RNase L inhibitor functions in translation termination. EMBO Rep 11: 214–219.
3. Bolger TA, Folkmann AW, Tran EJ, Wente SR (2008) The mRNA export factor Gle1 and inositol hexakisphosphate regulate distinct stages of translation. Cell 134: 624–633.
4. Saini P, Eyler DE, Green R, Dever TE (2009) Hypusine-containing protein eIF5A promotes translation elongation. Nature 459: 118–121.
5. Pisarev AV, Hellen CUT, Pestova TV (2007) Recycling of Eukaryotic Posttermination Ribosomal Complexes. Cell 131: 286–299.
6. Pisarev AV, Skabkin MA, Pisareva VP, Skabkina OV, Rakotondrafara AM, et al. (2010) The Role of ABCE1 in Eukaryotic Posttermination Ribosomal Recycling. Mol Cell 37: 196–210.
7. Valášek LS (2012) 'Ribozoomin' – Translation Initiation from the Perspective of the Ribosome-bound Eukaryotic Initiation Factors (eIFs). Curr Protein Pept Sci 13: 305–330.
8. Pöyry TA, Kaminski A, Jackson RJ (2004) What determines whether mammalian ribosomes resume scanning after translation of a short upstream open reading frame? Genes Dev 18: 62–75.
9. Szamecz B, Rutkai E, Cuchalova L, Munzarova V, Herrmannova A, et al. (2008) eIF3a cooperates with sequences 5′ of uORF1 to promote resumption of scanning by post-termination ribosomes for reinitiation on GCN4 mRNA. Genes Dev 22: 2414–2425.
10. Munzarová V, Pánek J, Gunišová S, Dányi I, Szamecz B, et al. (2011) Translation Reinitiation Relies on the Interaction between eIF3a/TIF32 and Progressively Folded cis-Acting mRNA Elements Preceding Short uORFs. PLoS Genet 7: e1002137.
11. Alkalaeva EZ, Pisarev AV, Frolova LY, Kisselev LL, Pestova TV (2006) In vitro reconstitution of eukaryotic translation reveals cooperativity between release factors eRF1 and eRF3. Cell 125: 1125–1136.
12. Shoemaker CJ, Green R (2011) Kinetic analysis reveals the ordered coupling of translation termination and ribosome recycling in yeast. Proc Natl Acad Sci U S A 108: E1392–1398.
13. Becker T, Franckenberg S, Wickles S, Shoemaker CJ, Anger AM, et al. (2012) Structural basis of highly conserved ribosome recycling in eukaryotes and archaea. Nature 482: 501–506.
14. Keeling KM, Lanier J, Du M, Salas-Marco J, Gao L, et al. (2004) Leaky termination at premature stop codons antagonizes nonsense-mediated mRNA decay in S. cerevisiae. RNA 10: 691–703.
15. Schuldiner M, Collins SR, Thompson NJ, Denic V, Bhamidipati A, et al. (2005) Exploration of the function and organization of the yeast early secretory pathway through an epistatic miniarray profile. Cell 123: 507–519.
16. Firczuk H, Kannambath S, Pahle J, Claydon A, Beynon R, et al. (2013) An in vivo control map for the eukaryotic mRNA translation machinery. Mol Syst Biol 9: 635.
17. Barthelme D, Dinkelaker S, Albers SV, Londei P, Ermler U, et al. (2011) Ribosome recycling depends on a mechanistic link between the FeS cluster domain and a conformational switch of the twin-ATPase ABCE1. Proc Natl Acad Sci U S A 108: 3228–3233.
18. Yarunin A, Panse VG, Petfalski E, Dez C, Tollervey D, et al. (2005) Functional link between ribosome formation and biogenesis of ironsulfur proteins. EMBO J 24: 580–588.
19. Valášek L, Phan L, Schoenfeld LW, Valášková V, Hinnebusch AG (2001) Related eIF3 subunits TIF32 and HCR1 interact with an RNA recoginition motif in PRT1 required for eIF3 integrity and ribosome binding. EMBO J 20: 891–904.
20. Nielsen KH, Valášek L, Sykes C, Jivotovskaya A, Hinnebusch AG (2006) Interaction of the RNP1 motif in PRT1 with HCR1 promotes 40S binding of eukaryotic initiation factor 3 in yeast. Mol Cell Biol 26: 2984–2998.
21. ElAntak L, Wagner S, Herrmannová A, Karásková M, Rutkai E, et al. (2010) The indispensable N-terminal half of eIF3j co-operates with its structurally conserved binding partner eIF3b-RRM and eIF1A in stringent AUG selection. J Mol Biol 396: 1097–1116.
22. Chiu W-L, Wagner S, Herrmannová A, Burela L, Zhang F, et al. (2010) The C-Terminal Region of Eukaryotic Translation Initiation Factor 3a (eIF3a) Promotes mRNA Recruitment, Scanning, and, Together with eIF3j and the eIF3b RNA Recognition Motif, Selection of AUG Start Codons. Mol Cell Biol 30: 4415–4434.
23. Valášek L, Hašek J, Nielsen KH, Hinnebusch AG (2001) Dual function of eIF3j/Hcr1p in processing 20 S Pre-rRNA and translation initiation. J Biol Chem 276: 43351–43360.
24. Kovarik P, Hašek J, Valášek L, Ruis H (1998) RPG1: an essential gene of saccharomyces cerevisiae encoding a 110-kDa protein required for passage through the G1 phase. Curr Genet 33: 100–109.
25. Valášek L, Szamecz B, Hinnebusch AG, Nielsen KH (2007) In vivo stabilization of preinitiation complexes by formaldehyde cross-linking. Methods Enzymol 429: 163–183.
26. Burnicka-Turek O, Kata A, Buyandelger B, Ebermann L, Kramann N, et al. (2010) Pelota interacts with HAX1, EIF3G and SRPX and the resulting protein complexes are associated with the actin cytoskeleton. BMC Cell Biol 11: 28.
27. von der Haar T (2008) A quantitative estimation of the global translational activity in logarithmically growing yeast cells. BMC Syst Biol 2: 87.
28. Akhmaloka, Susilowati PE, Subandi, Madayanti F (2008) Mutation at tyrosine in AMLRY (GILRY like) motif of yeast eRF1 on nonsense codons suppression and binding affinity to eRF3. Int J Biol Sci 4: 87–95.
29. Bradley ME, Bagriantsev S, Vishveshwara N, Liebman SW (2003) Guanidine reduces stop codon read-through caused by missense mutations in SUP35 or SUP45. Yeast 20: 625–632.
30. Bertram G, Bell HA, Ritchie DW, Fullerton G, Stansfield I (2000) Terminating eukaryote translation: domain 1 of release factor eRF1 functions in stop codon recognition. Rna 6: 1236–1247.

31. Merritt GH, Naemi WR, Mugnier P, Webb HM, Tuite MF, et al. (2010) Decoding accuracy in eRF1 mutants and its correlation with pleiotropic quantitative traits in yeast. Nucleic Acids Res 38: 5479–5492.
32. Harel-Sharvit L, Eldad N, Haimovich G, Barkai O, Duek L, et al. (2010) RNA polymerase II subunits link transcription and mRNA decay to translation. Cell 143: 552–563.
33. Isken O, Kim YK, Hosoda N, Mayeur GL, Hershey JWB, et al. (2008) Upf1 Phosphorylation Triggers Translational Repression during Nonsense-Mediated mRNA Decay. Cell 133: 314–327.
34. Sha Z, Brill LM, Cabrera R, Kleifeld O, Scheliga JS, et al. (2009) The eIF3 interactome reveals the translasome, a supercomplex linking protein synthesis and degradation machineries. Mol Cell 36: 141–152.
35. Querol-Audi J, Sun C, Vogan JM, Smith MD, Gu Y, et al. (2013) Architecture of human translation initiation factor 3. Structure 21: 920–928.
36. Hashem Y, des Georges A, Dhote V, Langlois R, Liao HY, et al. (2013) Structure of the Mammalian Ribosomal 43S Preinitiation Complex Bound to the Scanning Factor DHX29. Cell 153: 1108–1119.
37. Zhou M, Sandercock AM, Fraser CS, Ridlova G, Stephens E, et al. (2008) Mass spectrometry reveals modularity and a complete subunit interaction map of the eukaryotic translation factor eIF3. Proc Natl Acad Sci USA 105: 18139–18144.
38. Fraser CS, Berry KE, Hershey JW, Doudna JA (2007) 3j is located in the decoding center of the human 40S ribosomal subunit. Mol Cell 26: 811–819.
39. Pisarev AV, Kolupaeva VG, Yusupov MM, Hellen CUT, Pestova TV (2008) Ribosomal position and contacts of mRNA in eukaryotic translation initiation complexes. EMBO J 27: 1609–1621.
40. Masutani M, Sonenberg N, Yokoyama S, Imataka H (2007) Reconstitution reveals the functional core of mammalian eIF3. EMBO J 26: 3373–3383.
41. Taylor D, Unbehaun A, Li W, Das S, Lei J, et al. (2012) Cryo-EM structure of the mammalian eukaryotic release factor eRF1-eRF3-associated termination complex. Proc Natl Acad Sci U S A 109: 18413–18418.
42. Cuchalová L, Kouba T, Herrmannová A, Danyi I, Chiu W-l, et al. (2010) The RNA Recognition Motif of Eukaryotic Translation Initiation Factor 3g (eIF3g) Is Required for Resumption of Scanning of Posttermination Ribosomes for Reinitiation on GCN4 and Together with eIF3i Stimulates Linear Scanning. Mol Cell Biol 30: 4671–4686.
43. Herrmannová A, Daujotyte D, Yang JC, Cuchalová L, Gorrec F, et al. (2012) Structural analysis of an eIF3 subcomplex reveals conserved interactions required for a stable and proper translation pre-Initiation complex assembly. Nucleic Acids Res 40: 2294–2311.
44. Valášek L, Mathew A, Shin BS, Nielsen KH, Szamecz B, et al. (2003) The Yeast eIF3 Subunits TIF32/a and NIP1/c and eIF5 Make Critical Connections with the 40S Ribosome in vivo. Genes Dev 17: 786–799.
45. Kong C, Ito K, Walsh MA, Wada M, Liu Y, et al. (2004) Crystal structure and functional analysis of the eukaryotic class II release factor eRF3 from S. pombe. Mol Cell 14: 233–245.
46. Valášek L, Hašek J, Trachsel H, Imre EM, Ruis H (1999) The *Saccharomyces cerevisiae HCR1* gene encoding a homologue of the p35 subunit of human translation eukaryotic initiation factor 3 (eIF3) is a high copy suppressor of a temperature-sensitive mutation in the Rpg1p subunit of yeast eIF3. J Biol Chem 274: 27567–27572.
47. Tarun SZ, Sachs AB (1996) Association of the yeast poly(A) tail binding protein with translation initiation factor eIF-4G. EMBO J 15: 7168–7177.
48. Muhlrad D, Parker R (1999) Recognition of yeast mRNAs as "nonsense containing" leads to both inhibition of mRNA translation and mRNA degradation: implications for the control of mRNA decapping. Mol Biol Cell 10: 3971–3978.
49. Nielsen KH, Valášek L (2007) In vivo deletion analysis of the architecture of a multi-protein complex of translation initiation factors. Methods Enzymol 431: 15–32.
50. Valášek L, Trachsel H, Hašek J, Ruis H (1998) Rpg1, the *Saccharomyces cerevisiae* homologue of the largest subunit of mammlian translation initiation factor 3, is required for translational activity. J Biol Chem 273: 21253–21260.
51. Grant CM, Hinnebusch AG (1994) Effect of sequence context at stop codons on efficiency of reinitiation in *GCN4* translational control. Mol Cell Biol 14: 606–618.

Supplementary Information

Material and Methods

Construction of yeast strains and plasmids

List of all strains used throughout this study can be found in Table S2.

To generate *TIF32*$^{+}$, *tif32*^{Box17}, *tif32*^{Box6}, *tif32*$^{Box6+17}$ and *tif32*$^{\Delta 8}$ mutant strains (all showing in Figure 1), del'32a9A was transformed with YCp-a/TIF32-His-L, YCp-a/tif32-Box17-His, YCp-a/tif32-Box6-His , YCp-a/tif32-Box6+17-His, and YCp-a/tif32-Δ8-His-L, respectively, and the resident *URA3*-based plasmid carrying wt *TIF32* was evicted on 5-FOA-containing medium.

To generate *PRT1*$^{+}$ and *prt1*^{W647A} mutant strains (Figure 1), YAH06 was transformed with pRS-b/PRT1-HisXS and pRS-b/PRT1-W674A-His, respectively, and the resident *URA3*-based plasmid carrying wt *PRT1* was evicted on 5-FOA-containing medium.

To generate *NIP1*$^{+}$, *nip1*^{Box1} and *nip1*$^{\Delta 60}$ mutant strains (Figure 1), HMJ08 was transformed with YCpNIP1-Myc-L, YCpNIP1-743A752(box1) and YCpNIP1-Δ60-MYC-L, respectively, and the resident *URA3*-based plasmid carrying wt *NIP1* was evicted on 5-FOA-containing medium.

To generate *TIF34*$^{+}$, *tif34*^{Q258R} and *tif34*$^{DD/KK}$ mutant strains (Figure 1), H450 was transformed with YCp-i/TIF34-HA, YCpL-i/tif34-HA-3 (Q258R) and YCp-i/TIF34-D207K-D224K-HA, respectively, and the resident *URA3*-based plasmid carrying wt *TIF34* was evicted on 5-FOA-containing medium.

To generate *TIF35*$^{+}$, *tif35*^{KLF}, *tif35*^{TKMQ}, *tif35*^{RLFT} and *tif35*^{C121R} mutant strains (Figure 1), H464 was transformed with YCp22-g/TIF35-screen, YCp22-g/tif35-KLF, YCp22-g/tif35-TKMQ, YCp22-g/tif35-RLFT and YCp22-g/tif35-C121R, respectively, and the resident *URA3*-based plasmid carrying wt *TIF35* was evicted on 5-FOA-containing medium.

Strains PBH103 [*hcr1Δ sup35*^{N536T}], PBH104 [*hcr1Δ sup45*^{M48I}], and PBH105 [*hcr1Δ sup45*^{Y410S}] were all generated by a genetic cross of YLVH13 with L2334, L2337, and L2521, respectively, selecting for a haploid ascospore showing the Ts^{-} phenotype and being prototrophic for leucine.

PBH106 [*tif32Δ sup45*^{Y410S}] and PBH107 [*tif32Δ sup35*^{N536T}] were generated by a genetic cross of del'32a9B with L2521 and L2334, respectively, selecting for a haploid ascospore showing the Ts^{-} phenotype and being unable to lose the resident *URA3*-based cover plasmid.

TAP-tagging at the chromosomal locus of SUP35 was performed in strain 74D-694 as described [1] producing H517.

List of all plasmids and PCR primers used throughout this study can be found in Tables S3 and S4, respectively.

YEp-R/T-UGAC-L and YEp-R/T-CAAC-L were constructed by inserting the 4567-bp *Alw*NI-*Nsi*I fragment from pTH477 and pTH460, respectively, into YEplac181 digested by AlwNI-NsiI.

YCp-a/tif32-Δ8-His-L was made by inserting the *Bam*HI-*Xba*I digested PCR product obtained with primers SG-TIF32D8bamHI and BS-TIF32D8nheI-R using pRS-eIF3a-Δ8-His-L as a template into *Bam*HI-*Xba*I digested YCp-a/TIF32-His-L.

YCp22-g/TIF35-TKMQ was generated by fusion PCR. The following pairs of primers were used for separate PCR amplifications using YCp22-g/TIF35-screen as template: (1) TIF35 NdeI – MM2r 3gTLKVr; and (2) y3gTKMQ (RNP2) – y3g XhoIr.

The PCR products thus obtained were used in a 1:1 ratio as templates for the third PCR amplification using primers y3g XhoIr and TIF35 NdeI. The resulting PCR product was digested with *Nde*I and *Xho*I and ligated with *Nde*I-XhoI-cleaved YCp22-g/TIF35-screen.

YCp22-g/TIF35-RLFT was generated by fusion PCR. The following pairs of primers were used for separate PCR amplifications using YCp22-g/TIF35-screen as template: (1) TIF35 NdeI – MM1r; and (2) y3gRLFT (RNP1) – y3g XhoIr. The PCR products thus obtained were used in a 1:1 ratio as templates for the third PCR amplification using primers y3g XhoIr and TIF35 NdeI. The resulting PCR product was digested with *Nde*I and *Xho*I and ligated with *Nde*I-XhoI-cleaved YCp22-g/TIF35-screen.

YCp22-g/TIF35-C121R was obtained by random mutagenesis of the template plasmid YCp22-g/TIF35-screen with help of XL1-Red Competent Cells (Stratagene).

YEp-RLI1-L was constructed by inserting the 2887-bp *Spe*I-*Pst*I fragment from PDH177 into YEplac181 digested with *Xba*I-*Pst*I.

YEp-rli1-K116L-L was made by inserting the *Nde*I-*Acc*I digested PCR product obtained with primers PB-RLI1ndeI and PB-RLI1-K116LaccI-R using YEp-RLI1-L as the template into *Nde*I-*Acc*I digested YEp-RLI1-ndeI-L. To create YEp-RLI1-ndeI-L, fusion PCR was employed. The following pairs of primers were used for separate PCR amplifications using YEp-RLI1-L as template: (1) PB-RLI1ndeI – PB-RLI1accI-R; and (2) PB-RLI1ncoI – PB-RLI1ndeI-R. The PCR products thus obtained were used in a 1:1 ratio as templates for the third PCR amplification using primers PB-RLI1ncoI and PB-RLI1accI-R. The resulting PCR product was digested with *Nco*I and *Acc*I and ligated with *Nco*I-*Acc*I-cleaved YEp-RLI1-L.

YEp-rli1-K391L-L was generated by fusion PCR. The following pairs of primers were used for separate PCR amplifications using YEp-RLI1-ndeI-L as template: (1) PB-RLI1ndeI – PB-RLI1-K391L-R; and (2) PB-RLI1-K391L – PB-RLI1termXbaI-R. The PCR products thus obtained were used in a 1:1 ratio as templates for the third PCR amplification using primers PB-RLI1ndeI and PB-RLI1termXbaI-R. The resulting PCR product was digested with *Nde*I and *Xba*I and ligated with *Nde*I-*Xba*I-cleaved YEp-RLI1-ndeI-L.

YEp-rli1-G224D,G225D-L, YEp-rli1-G470D,G471D-L, and YEp-rli1-E493Q-L were made by inserting the *Nde*I-*Xba*I digested PCR product obtained with primers PB-RLI1ndeI and PB-RLI1xbaI-R using PDH184, PDH185, and PDH202 as templates, respectively, into *Nde*I-*Xba*I digested YEp-RLI1-ndeI-L.

YEp-rli1-C25S-L was generated by fusion PCR. The following pairs of primers were used for separate PCR amplifications using YEp-RLI1-ndeI-L as template: (1) PB-RLI1ndeI – PB-RLI1-C25S-R; and (2) PB-RLI1-C25S – PB-RLI1accI-R. The PCR products thus obtained were used in a 1:1 ratio as templates for the third PCR amplification using primers PB-RLI1ndeI and PB-RLI1accI-R. The resulting PCR product was digested with *Nde*I and *Acc*I and ligated with *Nde*I-*Acc*I-cleaved YEp-RLI1-ndeI-L.

YEp-rli1-C61S-L was generated by fusion PCR. The following pairs of primers were used for separate PCR amplifications using YEp-RLI1-ndeI-L as template: (1) PB-RLI1ndeI – PB-RLI1-C61S-R; and (2) PB-RLI1-C61S – PB-RLI1accI-R. The PCR products thus obtained were used in a 1:1 ratio as templates for the third PCR amplification using primers PB-RLI1ndeI and PB-RLI1accI-R. The resulting PCR product was digested with *Nde*I and *Acc*I and ligated with *Nde*I-*Acc*I-cleaved YEp-RLI1-ndeI-L.

To generate YEpSUI1-L, a *Sac*I-*Hind*III fragment from YEpSUI1-U [2] was ligated into *Sac*I-*Hind*III-cleaved YEplac181 [3].

Plasmids used for the generation of *in vitro*-translated eRF1 fragments (pTH339-342) were generated as follows. Fragments of the *SUP45* gene were generated by PCR using yeast genomic DNA as template. The primers used were Sup45_D1f and Sup45_D3r (for eRF1(fl)); Sup45_D1f and Sup45_D1r (for eRF1-N); Sup45_D1f and Sup45_D2r (for eRF1-NM); Sup45_d2f and Sup45_D3r (for eRF1-MC); and Sup45_D3f and Sup45_D3r (for eRF1-C). All primers added *Nco*I and *Not*I sites at the 5'- and 3'-ends of the PCR products, respectively, and also introduced translation start- and stop codons where required. The DNA fragments were then cloned into the yeast two-hybrid binding domain vector pGBK-T7 (Clontech Europe, France), which also contains a T7 transcription start site upstream of the gene's start codon, using *NcoI* and *NotI* sites.

pGEX-RLI1 expression plasmid was constructed by insertion of the corresponding *Sma*I-*Xho*I-digested PCR product amplified from YEp-RLI1-L using the primers PB-RLI1smaI and PB-RLI1xhoI-R into *Sma*I-*Xho*I-digested pGEX-5X-3 [3].

pGEX- g/tif35-NTD expression plasmid was constructed by insertion of the corresponding *Bam*HI-*Xho*I-digested PCR product amplified from YCp22-g/TIF35-screen using the primers pGEX35NTD and pGEX35NTDr into *Bam*HI-*Xho*I-digested pGEX-5X-3 [3].

pGEX- g/tif35-RRM expression plasmid was constructed by insertion of the corresponding *Bam*HI-*Xho*I-digested PCR product amplified from YCp22-g/TIF35-screen using the primers pGEX35RRM and pGEX35RRMr into *Bam*HI-*Xho*I-digested pGEX-5X-3 [3].

YCp22-SUP45-W was made by inserting the *Sph*I-*Sac*I-digested PCR product (2033 bp-long) obtained from genomic DNA using primers PB-SUP45SphI and PB-SUP45SacI-R into the *Sph*I-*Sac*I-cut YCplac22.

References

1. Puig O, Caspary F, Rigaut G, Rutz B, Bouveret E, et al. (2001) The Tandem Affinity Purification (TAP) method: a general procedure of protein complex purification. Methods 24: 218-229.
2. Valášek L, Nielsen KH, Zhang F, Fekete CA, Hinnebusch AG (2004) Interactions of Eukaryotic Translation Initiation Factor 3 (eIF3) Subunit NIP1/c with eIF1 and eIF5 Promote Preinitiation Complex Assembly and Regulate Start Codon Selection. Mol Cell Biol 24: 9437-9455.
3. Gietz RD, Sugino A (1988) New yeast-Escherichia coli shuttle vectors constructed with in vitro mutagenized yeast genes lacking six-base pair restriction sites. Gene 74: 527-534.
4. Schuldiner M, Collins SR, Thompson NJ, Denic V, Bhamidipati A, et al. (2005) Exploration of the function and organization of the yeast early secretory pathway through an epistatic miniarray profile. Cell 123: 507-519.
5. Szamecz B, Rutkai E, Cuchalova L, Munzarova V, Herrmannova A, et al. (2008) eIF3a cooperates with sequences 5' of uORF1 to promote resumption of scanning by post-termination ribosomes for reinitiation on GCN4 mRNA. Genes Dev 22: 2414-2425.

6. Munzarová V, Pánek J, Gunišová S, Dányi I, Szamecz B, et al. (2011) Translation Reinitiation Relies on the Interaction between eIF3a/TIF32 and Progressively Folded cis-Acting mRNA Elements Preceding Short uORFs. PLoS Genet 7: e1002137.
7. Herrmannová A, Daujotyte D, Yang JC, Cuchalová L, Gorrec F, et al. (2012) Structural analysis of an eIF3 subcomplex reveals conserved interactions required for a stable and proper translation pre-Initiation complex assembly. Nucleic Acids Res 40: 2294-2311.
8. Kouba T, Rutkai E, Karasková M, Valášek LS (2012) The eIF3c/NIP1 PCI domain interacts with RNA and RACK1/ASC1 and promotes assembly of the pre-initiation complexes. Nucleic Acids Research 40: 2683-2699.
9. Cuchalová L, Kouba T, Herrmannová A, Danyi I, Chiu W-l, et al. (2010) The RNA Recognition Motif of Eukaryotic Translation Initiation Factor 3g (eIF3g) Is Required for Resumption of Scanning of Posttermination Ribosomes for Reinitiation on GCN4 and Together with eIF3i Stimulates Linear Scanning. Mol Cell Biol 30: 4671-4686.
10. Valášek L, Hašek J, Trachsel H, Imre EM, Ruis H (1999) The *Saccharomyces cerevisiae HCRI* gene encoding a homologue of the p35 subunit of human translation eukaryotic initiation factor 3 (eIF3) is a high copy suppressor of a temperature-sensitive mutation in the Rpg1p subunit of yeast eIF3. J Biol Chem 274: 27567-27572.
11. Valášek L, Phan L, Schoenfeld LW, Valášková V, Hinnebusch AG (2001) Related eIF3 subunits TIF32 and HCR1 interact with an RNA recoginition motif in PRT1 required for eIF3 integrity and ribosome binding. EMBO J 20: 891-904.
12. ElAntak L, Wagner S, Herrmannová A, Karásková M, Rutkai E, et al. (2010) The indispensable N-terminal half of eIF3j co-operates with its structurally conserved binding partner eIF3b-RRM and eIF1A in stringent AUG selection. J Mol Biol 396: 1097-1116.
13. Chiu W-L, Wagner S, Herrmannová A, Burela L, Zhang F, et al. (2010) The C-Terminal Region of Eukaryotic Translation Initiation Factor 3a (eIF3a) Promotes mRNA Recruitment, Scanning, and, Together with eIF3j and the eIF3b RNA Recognition Motif, Selection of AUG Start Codons. Mol Cell Biol 30: 4415-4434.
14. Kispal G, Sipos K, Lange H, Fekete Z, Bedekovics T, et al. (2005) Biogenesis of cytosolic ribosomes requires the essential iron-sulphur protein Rli1p and mitochondria. EMBO J 24: 589-598.
15. Bradley ME, Bagriantsev S, Vishveshwara N, Liebman SW (2003) Guanidine reduces stop codon read-through caused by missense mutations in SUP35 or SUP45. Yeast 20: 625-632.
16. Bertram G, Bell HA, Ritchie DW, Fullerton G, Stansfield I (2000) Terminating eukaryote translation: domain 1 of release factor eRF1 functions in stop codon recognition. Rna 6: 1236-1247.
17. Akhmaloka, Susilowati PE, Subandi, Madayanti F (2008) Mutation at tyrosine in AMLRY (GILRY like) motif of yeast eRF1 on nonsense codons suppression and binding affinity to eRF3. Int J Biol Sci 4: 87-95.
18. Chernoff YO, Derkach IL, Inge-Vechtomov SG (1993) Multicopy SUP35 gene induces de-novo appearance of psi-like factors in the yeast Saccharomyces cerevisiae. Curr Genet 24: 268-270.

19. Dong J, Lai R, Nielsen K, Fekete CA, Qiu H, et al. (2004) The essential ATP-binding cassette protein RLI1 functions in translation by promoting preinitiation complex assembly. J Biol Chem 279: 42157-42168.
20. Nielsen KH, Valášek L, Sykes C, Jivotovskaya A, Hinnebusch AG (2006) Interaction of the RNP1 motif in PRT1 with HCR1 promotes 40S binding of eukaryotic initiation factor 3 in yeast. Mol Cell Biol 26: 2984-2998.
21. Nielsen KH, Szamecz B, Valasek LJ, A., Shin BS, Hinnebusch AG (2004) Functions of eIF3 downstream of 48S assembly impact AUG recognition and GCN4 translational control. EMBO J 23: 1166-1177.
22. Yen K, Gitsham P, Wishart J, Oliver SG, Zhang N (2003) An improved tetO promoter replacement system for regulating the expression of yeast genes. Yeast 20: 1255-1262.
23. Keeling KM, Lanier J, Du M, Salas-Marco J, Gao L, et al. (2004) Leaky termination at premature stop codons antagonizes nonsense-mediated mRNA decay in S. cerevisiae. RNA 10: 691-703.
24. Olsen DS, Savner EM, Mathew A, Zhang F, Krishnamoorthy T, et al. (2003) Domains of eIF1A that mediate binding to eIF2, eIF3 and eIF5B and promote ternary complex recruitment *in vivo*. EMBO J 22: 193-204.
25. Smith DB, Johnson KS (1988) Single-step purification of polypeptides expressed in Escherichia coli as fusions with glutathione S-transferase. Gene 67: 31-40.
26. Asano K, Phan L, Anderson J, Hinnebusch AG (1998) Complex formation by all five homologues of mammalian translation initiation factor 3 subunits from yeast *Saccharomyces cerevisiae*. J Biol Chem 273: 18573-18585.
27. Grant CM, Miller PF, Hinnebusch AG (1994) Requirements for intercistronic distance and level of eIF-2 activity in reinitiation on GCN4 mRNA varies with the downstream cistron. Mol Cell Biol 14: 2616-2628.
28. Bidou L, Stahl G, Hatin I, Namy O, Rousset JP, et al. (2000) Nonsense-mediated decay mutants do not affect programmed -1 frameshifting. Rna 6: 952-961.

Figures and Figure legends

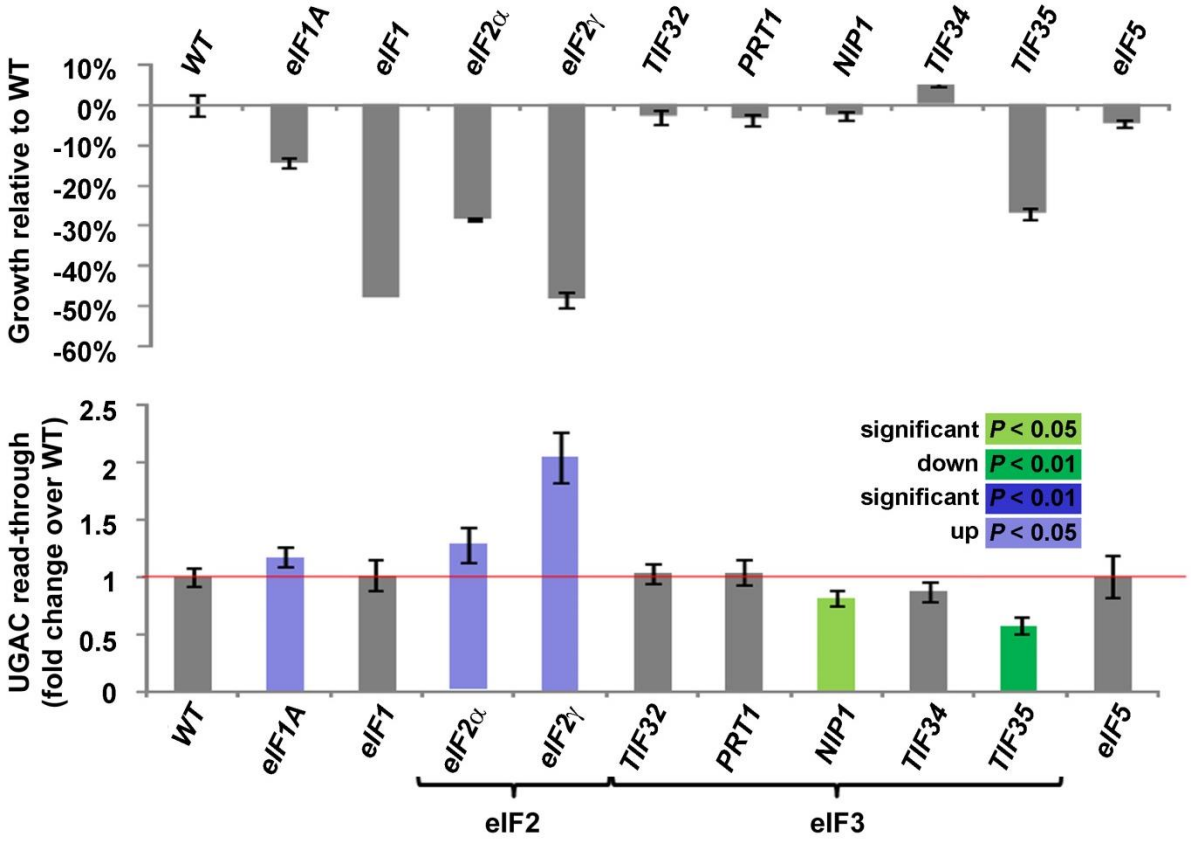

Figure S1. DaMP Alleles of Various 43S PIC-associated Initiation Factors Display Distinct Effects on Efficiency of the Stop Codon Read-through. Yeast strains containing kanMX4 cassettes integrated into their 3'-UTRs (so-called DaMP alleles) were recovered from the genome-wide collection for these alleles [4]. We were able to recover alleles for all 43S PIC-associated eIFs with the exception of eIF2β, for which no allele was present in the collection.

In order to aid interpretation of results, and to assess the efficiency of depletion of the gene in question, we initially measured growth rates of the respective strains (top panel). Since all of the factors studied here are essential, we expected a reduction in growth rate upon significant depletion of any of these factors. We then proceeded to measure stop codon read-through in these strains, using dual luciferase reporters as described in the main text.

Of the eIF3 subunits tested, only g/TIF35 is sufficiently depleted to cause a significant growth defect, and this strain shows a significant reduction in stop codon read-through. Moreover, the c/NIP1 DaMP allele also shows a significant reduction in stop codon read-through, even though this protein is not sufficiently depleted to produce a significant growth defect. Together, these results confirm those presented for other eIF3 alleles in the main text.

In contrast to the eIF3 subunits, other 43S PIC-associated translation initiation factors do not reduce stop codon read-through upon depletion. Conversely, both eIF2 subunits tested and eIF1A increased read-through when depleted. This demonstrates that the role of eIF3 in translation termination is specific to this factor.

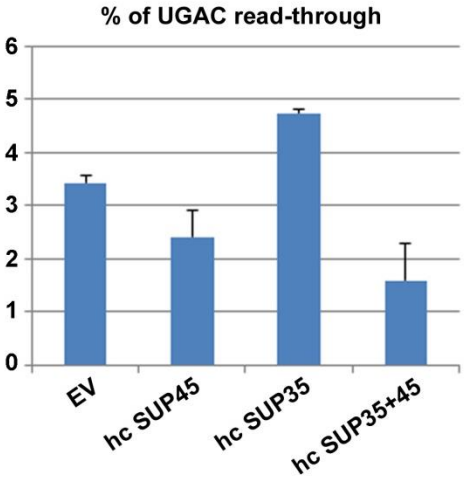

Figure S2. Increased Gene Dosage of eRFs 1 and 3 Reduces Stop-codon Read-through. Wild type strain H416 was transformed with designated plasmids overexpressing eRFs and the resulting transformants were grown in SD and processed for the stop codon read-through measurements as described in Figure 1.

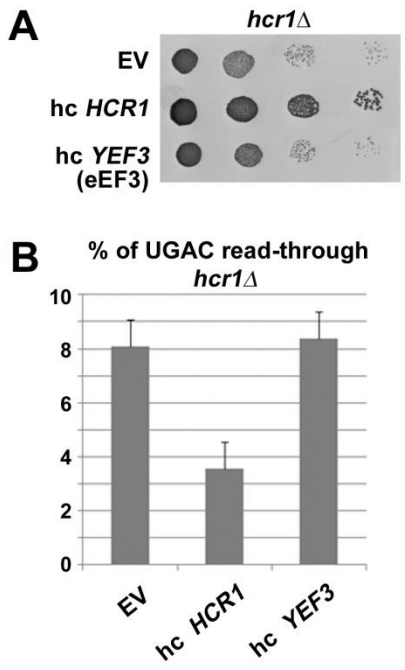

Figure S3. Increased Gene Dosage of eEF3 Does Not Suppress the Slow Growth and Read-through Defects of *hcr1Δ.* (**A**) The *hcr1Δ* strain (H3675) was transformed with either empty vector, high copy (hc) *HCR1* or hc *YEF3* (eEF3), the resulting transformants were spotted in four serial 10-fold dilutions on SD medium and incubated at 30°C for 2 days. Unlike RLI1, eEF3 (which is also an ABC cassette-containing protein) does not suppress the growth defect of an *hcr1* deletion strain.
(**B**) The strains from panel A were grown in SD and processed for the stop codon read-through measurements as described in Figure 1.

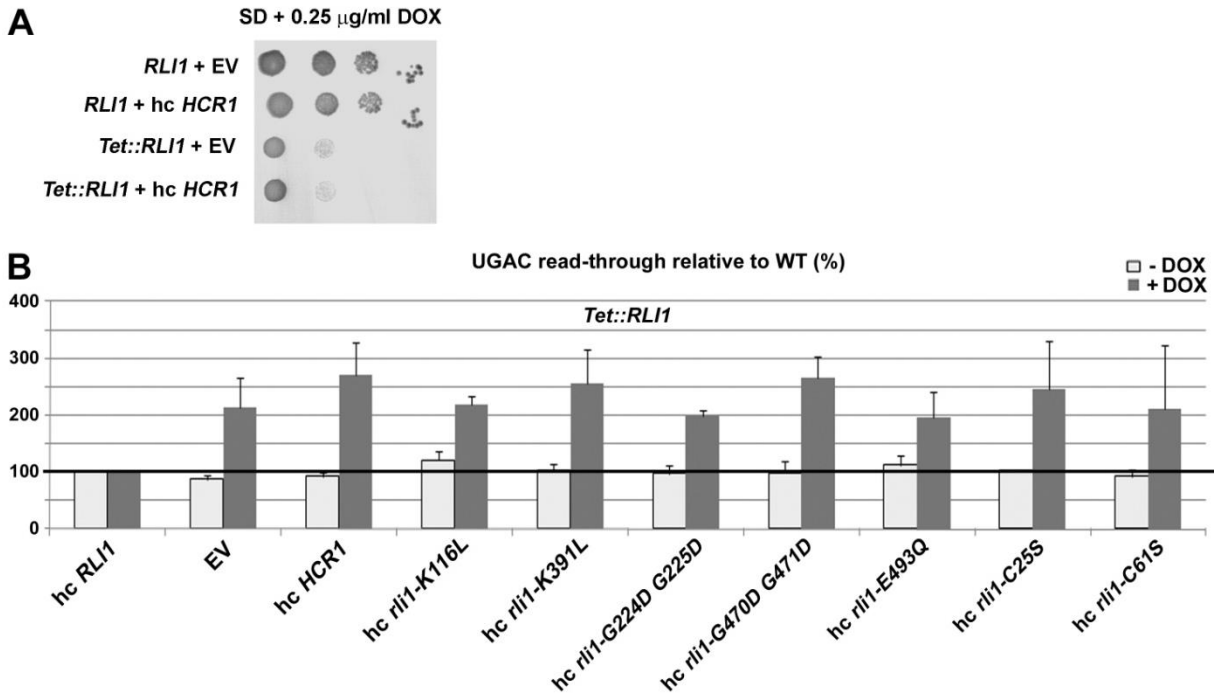

Figure S4. Increased Gene Dosage of *HCR1* Does Not Suppress the Slow Growth and Read-through Defects of the *Tet::RLI1* strain; Intact ATP-Binding Cassettes and the Fe-S Cluster of RLI1 are Indispensable for its Role in Ensuring the Stop Codon Selection Accuracy. (**A**) The *Tet::RLI1* (Tet-RLI1) and the corresponding wt strain (W303) were transformed with either empty vector or hc *HCR1,* and the resulting transformants were spotted in four serial 10-fold dilutions on SD medium supplemented with 0.25 μg/ml of doxycycline and incubated at 30°C for 2 days. (**B**) The *Tet::RLI1* (Tet-RLI1) strain was transformed with hc vectors carrying wt or mutant *RLI1* alleles, or empty vector or hc *HCR1*. The resulting transformants were grown in SD supplemented with 1 μg/ml of doxycycline (DOX) and processed for the stop codon read-through measurements as described in Figure 1. Obtained values were normalized to the value obtained with the *Tet::RLI1* strain transformed with wt *RLI1*, which was set to 100%.

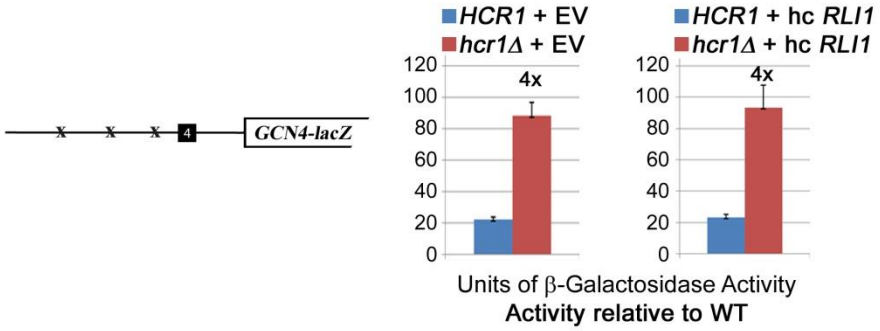

Figure S5. Increased Gene Dosage of ABCE1/RLI1 Does Not Suppress the Leaky Scanning Defect of *hcr1Δ*. The *HCR1*$^+$ (H2879) and *hcr1Δ* (H3675) strains were first transformed with either empty vector or hc *RLI1* and subsequently with the *GCN4-lacZ* reporter plasmid plig102-3. The resulting double transformants were grown in SD medium at 30°C to an OD_{600} of ~ 1. The β-galactosidase activities were measured in the WCEs and expressed in units of nmol of o-nitrophenyl-b-D-galactopyranoside hydrolyzed per min per mg of protein. The plots show mean values and standard deviations obtained from at least 3 independent measurements with three independent transformants. The fold-difference between the *hcr1Δ* versus *HCR1*$^+$ strains with or without hc *RLI1* is indicated.

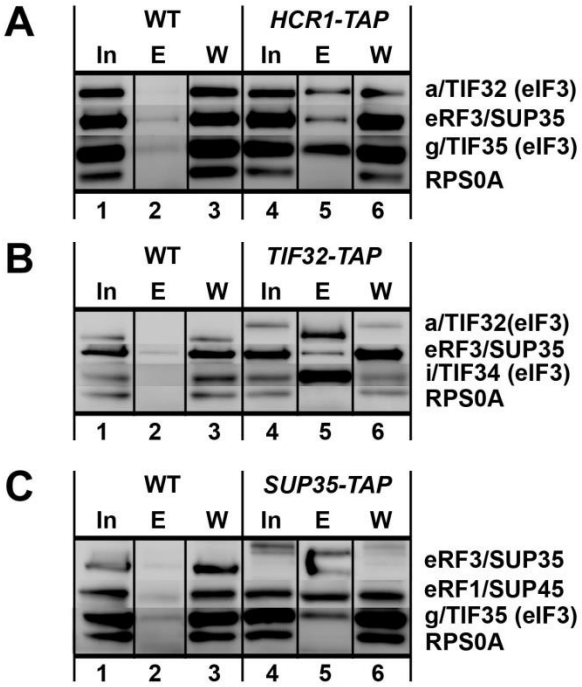

Figure S6. Complexes containing eIF3, HCR1, ABCE1/RLI1 and both eRFs, free of ribosomes and RNA, occur *in vivo* – the RNase A treatment. (**A**) RNAse A-treated WCEs were prepared from HCHO-treated (1%) cells bearing wt (H2879) or TAP-tagged (H553) chromosomal alleles of *HCR1* and incubated with IgG Sepharose 6 Fast Flow beads. The immune complexes were eluted by boiling in the SDS buffer and subjected to Western analysis. In, 1.5% of input; E, 50% of the elution fraction; W, 1.5% of the supernatant fraction. eRF1 is indicated by an asterisk below the immunoglobulins. (**B**) RNAse A-treated WCEs from HCHO-treated cells (1%) cells bearing wt (H2879) or TAP-tagged (H555) chromosomal alleles of *TIF32* were processed as in panel A except that the immune complexes were eluted by the TEV protease cleavage. In, 1.5% of input; E, 100% of the elution fraction; W, 1.5% of the supernatant fraction. (**C**) RNAse A-treated WCEs from HCHO-treated cells (1%) cells bearing wt (74D-694) or TAP-tagged (H517) chromosomal alleles of *SUP35* were processed as in panel B.

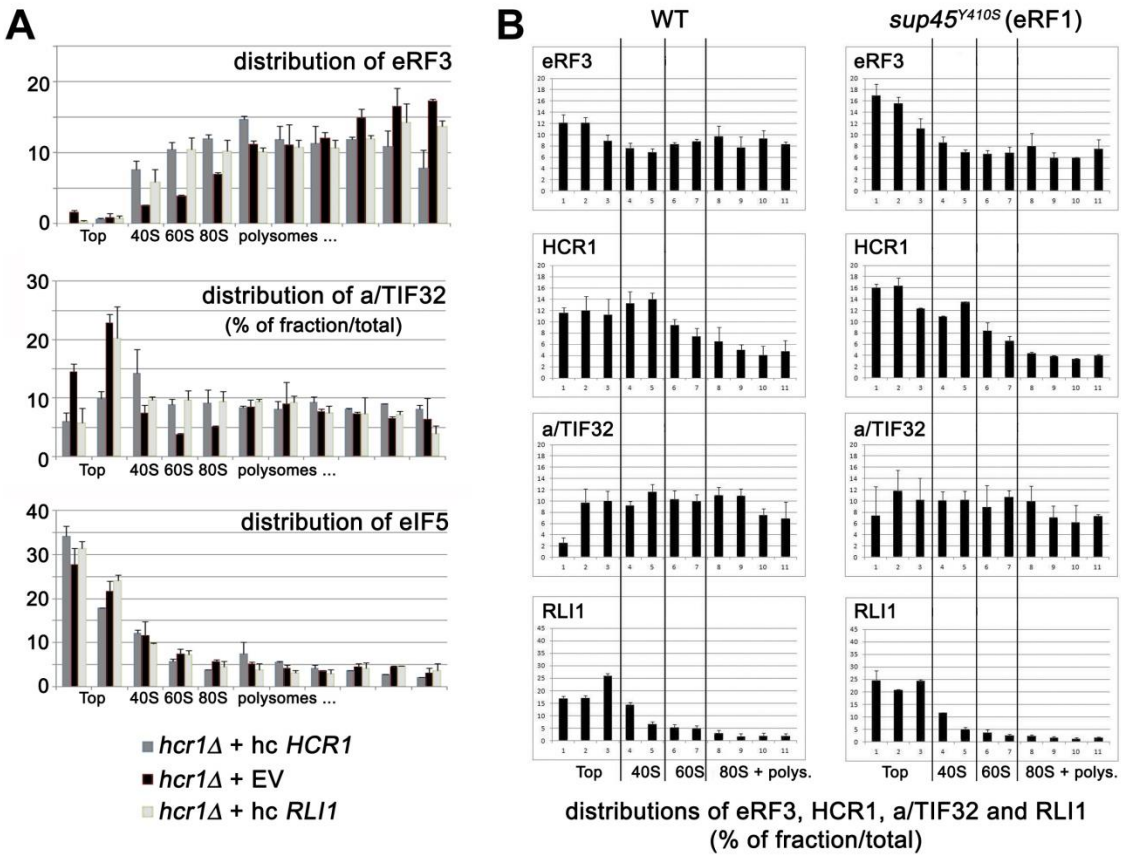

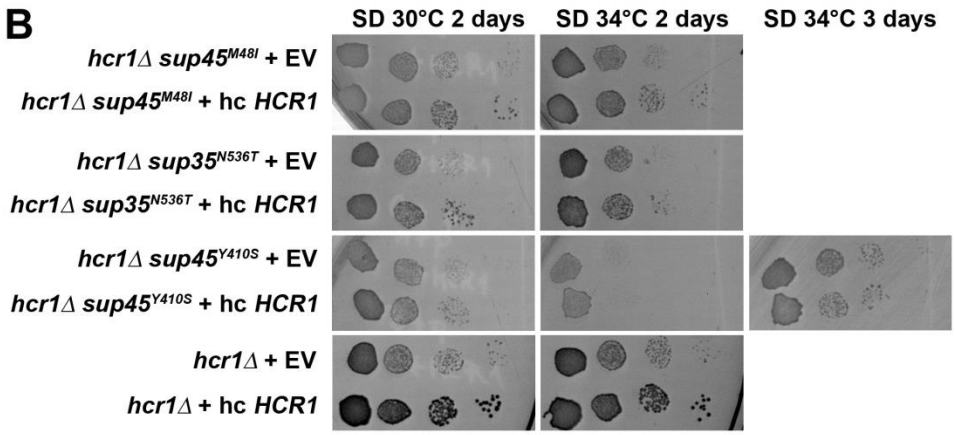

Figure S7. (**A**) Deletion of *hcr1* results in accumulation of the polysome-associated eRF3 – factors distributions across gradient fractions as shown in Figure 5. Amounts of each individual factor in the pooled fractions from three independent experiments were quantified by fluorescence imaging, combined, and the percentage representation of the signal corresponding to the Top (1-3 and 4), 40S (5-6), 60S (7-8), and 80S plus polysomal fractions (9 through 18) was calculated and plotted. (**B**) The *sup45*^{Y410S} mutation prevents stable association of eRF3 and HCR1 with polyribosomes – factors distributions across gradient fractions as shown in Figure 7. Amounts of each individual factor in the pooled fractions from three independent experiments were quantified by fluorescence imaging, combined, and the percentage representation of the signal corresponding to the Top (1 – 3), 40S (4-5), 60S (6-7), and 80S plus polysomal fractions (8-11) was calculated and plotted. (**C**) The

sup45^{Y410S} but not the other mutations in eRFs 1 and 3 eliminate the negative impact of *hcr1Δ* on growth rates. The *hcr1Δ* strain was crossed with the indicated *sup45* and *sup35* mutant strains and the resulting double mutants (PBH104, PBH103 and PBH105) were transformed with either empty vector (EV) or hc vector containing *HCR1* and together with the corresponding *hcr1Δ SUP35 SUP45* "wt" strain (YLVH13) spotted in four serial 10-fold dilutions on SD medium and incubated at indicated temperatures for 2 or 3 days.

Tables

Table S1. Mutant alleles used in this study and their associated phenotypes.

mutant allele	disrupts binding to:	major phenotypes:	references
tif32-Δ8	reduced eIF3 binding to 40S by 40%	Slg-; severe Gcn-; reinitiation defect	[5]
tif32-Box17		Slg-; Gcn-; reinitiation defect	[6]
tif32-Box6		Slg-; Gcn-; reinitiation defect	[6]
tif32-Box6+17		severe Slg-; severe Gcn-; reinitiation defect	[6]
prt1-W674A	diminishes (by >90%) association of i/TIF34 and g/TIF35 with the rest of eIF3/MFC and 40S ribosomes	severe Ts-; Gcn-	[7]
nip1-Box1	reduced amounts of 40S-bound eIF3 and eIF5 *in vivo*	temperature-dependent Slg-	[8]
nip1- Δ60	reduced amounts of 40S-bound eIF3 and eIF5 *in vivo*	Slg-;	[8]
tif34-Q258R		Slg-; reduces the rate of scanning	[9]
tif34-DD/KK	separates eIF3 into the a-b-c and i-g modules; partially destabilizes 48S PICs	severe Ts-; produces a severe leaky scanning phenotype	[7]
tif35-KLF		Ts-; Gcn-; reinitiation defect; reduces processivity of scanning	[9]
tif35-TKMQ		Slg-; severe Gcn-; modest leaky scanning	L.C. and L.S.V. unpublished
tif35-RLFT		Slg-; severe Gcn-	L.C. and L.S.V. unpublished
tif35-C121R		Slg-	L.C. and L.S.V. unpublished
hcr1 Δ	destabilizes the MFC; reduces 40S binding of eIF3	Slg-; reduces the levels of mature 40S ribosome; leaky scanning	[10]; [11]; [12]
hcr1-NTA	eliminates binding of HCR1 to eIF3	leaky scanning	[12]
hcr1-Box6	eliminates binding of		[13]

	HCR1 to eIF3		
hcr1-Box6+R/I	eliminates binding of HCR1 to eIF3	leaky scanning	[13]
rli1-K116L	eliminates binding to HCR1 in Y2H	lethal	[14]
rli1-K391L	eliminates binding to HCR1 in Y2H	lethal	[14]
sup45-M48I		Ts-; nonsense suppression; stop codon decoding defect	[15]; [16]
sup45-Y410S	decrease binding affinity to eRF3	severe Ts-; nonsense suppression	[15]; [17]
sup35-N536T		Ts-; nonsense suppression	[15]

slow growth (Slg^-); temperature sensitivity (Ts^-); prevents translational derepression of *GCN4* expression during amino acid starvation (Gcn^-); multifactor complex (MFC); pre-initiation complex (PIC); yeast two-hybrid (Y2H)

Table S2. Yeast strains used in this study.

Strain	Genotype	Source or reference
del'32a9A[a]	*MAT*a *leu2-3, -112 ura3-52 trp1Δ gcn2Δ a/tif32Δ* (sc *TIF32, URA3*)	[5]
YAH06[a]	*MATa leu2-3,112 ura3-52 trp1Δ prt1::hisG GCN2* (hc *PRT1 URA3*)	[12]
HMJ08[a]	*MATa, trp1 leu2-3,-112 ura3-52 nip1Δ* (sc *NIP1-His URA3*)	[8]
H450[a]	*MAT*a *leu2-3,-112 ura3-52::GCN2 trp1Δ tif34Δ* (hc *TIF34 URA3*))	[9]
H464[a]	*MAT*a *leu2-3,-112 ura3-52::GCN2 trp1Δ tif35Δ* (hc *TIF35 URA3*)	[9]
PBH103	*MATα ade1-14 trp1-289 his3-Δ200 leu2-3,112 ura3-52 sup35-N536T hcr1Δ::LEU2*	this study
PBH104	*MATα ade1-14 trp1-289 his3-Δ200 leu2-3,112 ura3-52 sup45-M48I hcr1Δ::LEU2*	this study
PBH105	*MATa ade1-14 trp1-289 his3-Δ200 leu2-3,112 ura3-52 sup45-Y410S hcr1Δ::LEU2*	this study
YLVH13[b]	*MATα hcr1Δ::LEU2 ade2-1 trp1-1 can1-100 leu2-3 leu2-112 his3-11 his3-15 ura3*	[10]
L2334[c]	*MAT*a *ade1-14 trp1-289 his3-Δ200 leu2-3,112 ura3-52 sup35-N536T*	[15]
L2327[c]	*MAT*a *ade1-14 trp1-289 his3-Δ200 leu2-3,112 ura3-52 sup45-M48I*	[15]
L2521[c]	*MAT*a *ade1-14 trp1-289 his3-Δ200 leu2-3,112 ura3-52 sup45-Y410S*	[15]
74D-694[c]	*MAT*a *ade1-14 trp1-289 his3-Δ200 leu2-3,112 ura3-52*	[18]
PBH106	*MATα trp1-289 his3-Δ200 leu2-3,112 ura3-52 sup45-Y410S a/tif32Δ* (sc *TIF32, URA3*)	this study
PBH107	*MATα ade1-14 trp1-289 his3-Δ200 leu2-3,112 ura3-52 sup35-N536T a/tif32Δ* (sc *TIF32, URA3*)	this study
del'32a9B[a]	*MATα leu2-3, -112 ura3-52 trp1Δ gcn2Δ a/tif32Δ* (sc *TIF32, URA3*)	[5]
YDH353	*MATa his3Δ1 leu2Δ0 ura3Δ0 met15Δ0 RLI1-MYC::HIS3*	[19]
H553[d]	*MATa his3Δ1 leu2Δ0 met15Δ0 ura3Δ0 HCR1-TAP*	Thermo Scientific
H555[d]	*MATa his3Δ1 leu2Δ0 met15Δ0 ura3Δ0 TIF32-TAP*	Thermo Scientific
H517[c]	*MATa ade1-14 trp1-289 his3-Δ200 leu2-3,112 ura3-52 SUP35::TAP-HIS3*	this study
H3675[a]	*MATa PRT1 leu2-3, 112 ura3-52 hcr1Δ*	[20]
H2879[a]	*MATa PRT1 leu2-3, 112 ura3-52*	[21]
W303[b]	*MATa ade2 can1-100 his3-11 his3-15 leu2-3 leu2-112 trp1-1 ura3-1*	A. Hopper
Tet-RLI1[b]	*MATα ade2 can1-100 his3-11 his3-15*	[14]

	leu2-3 leu2-112 trp1-1 ura3-1 Tet::RLI1	
CML476-SUP45	*MATa ura3-52 leu2Δ1 his3Δ200 GAL2 CMVp(tetR'-SSN6)::LEU2 trp1::tTA*	[22]

[a-d] Identical superscripts denote isogenic strain backgrounds.

Table S3. Plasmids used in this study.

Plasmid	Description	Source of reference
YEp-HiPV-UGAC-L	high copy HiPV-Renilla-Firefly R/T cassette (stop codon of Renilla is UGA-C; for read-through measurements) in *LEU2* plasmid from YEplac181	this study
YEp-HiPV-CAAC-L	high copy HiPV-Renilla-Firefly R/T cassette (stop codon of Renilla is replaced with CAA-C [coding triplet]; for control read-through measurements) in *LEU2* plasmid from YEplac181	this study
pTH477	high copy PGK-Renilla-Firefly R/T cassette (stop codon of Renilla is UGA-C; for read-through measurements) in *URA3* plasmid from YEplac195	[23]
pTH460	high copy PGK-Renilla-Firefly R/T cassette (stop codon of Renilla is replaced with CAA-C [coding triplet]; for control read-through measurements) in *URA3* plasmid from YEplac195	[23]
YEp-R/T-UGAC-L	high copy PGK-Renilla-Firefly R/T cassette (stop codon of Renilla is UGA-C; for read-through measurements) in *LEU2* plasmid from YEplac181	this study
YEp-R/T-CAAC-L	high copy PGK-Renilla-Firefly R/T cassette (stop codon of Renilla is replaced with CAA-C [coding triplet]; for control read-through measurements) in *LEU2* plasmid from YEplac181	this study
YCp-a/TIF32-His-L	single copy wt *TIF32-His* in *LEU2* plasmid from YCplac111	[6]
YCp-a/tif32-Box17-His	single copy *tif32-Box17-His* in *LEU2* plasmid from YCplac111	[6]
YCp-a/tif32-Box6-His	single copy *tif32-Box6-His* in *LEU2* plasmid from YCplac111	[6]
YCp-a/tif32-Box6+17-His	single copy *tif32-Box6+17-His* in *LEU2* plasmid from YCplac111	[6]
YCp-a/tif32-Δ8-His-L	single copy *tif32-Δ8-His* in *LEU2* plasmid from YCplac111	this study
pRS-b/PRT1-HisXS	low copy wt *PRT1* in *LEU2* plasmid from pRS315	[12]
pRS-b/PRT1-W674A-His	low copy *prt1-W674A* in *LEU2* plasmid from pRS315	[7]
YCpNIP1-Myc-L	single copy wt *NIP1-Myc* in *LEU2*	[8]

	plasmid from YCplac111	
YCpNIP1-743A752(box1)	single copy *NIP1-Myc* containing 10 Ala substitutions between amino acid residues 743 and 752, in *LEU2* plasmid from YCplac111	[8]
YCpNIP1-Δ60-MYC-L	single copy *NIP1-Myc* truncated by 60 amino acid residues, in *LEU2* plasmid from YCplac111	[8]
YCp-i/TIF34-HA	single copy wt *TIF34-HA* in *LEU2* plasmid from YCplac111	[9]
YCpL-i/tif34-HA-3 (Q258R)	single copy *tif34-HA-Q258R* in *LEU2* plasmid from YCplac111	[9]
YCp-i/TIF34-D207K-D224K-HA	single copy *TIF34-HA* containing D207K and D224K mutations in *LEU2* plasmid from YCplac111	[7]
YCp22-g/TIF35-screen	single copy wt *TIF35-His* in *TRP1* plasmid from YCplac22	[9]
YCp22-g/TIF35-KLF	single copy *TIF35-KLF-His* in*TRP1* plasmid from YCplac22	[9]
YCp22-g/TIF35-TKMQ	single copy *TIF35-TKMQ-His* in *TRP1* plasmid from YCplac22	this study
YCp22-g/TIF35-RLFT	single copy *TIF35-RLFT-His* in *TRP1* plasmid from YCplac22	this study
YCp22-g/TIF35-C121R	single copy *TIF35-C121R-His* in *TRP1* plasmid from YCplac22	this study
YEplac181	high copy cloning vector, *LEU2*	[3]
YEplac195	high copy cloning vector, *URA3*	[3]
YEpLVHCR1	high copy wt *HCR1* in *LEU2* plasmid from YEplac181	[10]
YEp-HCR1-DS-U	high copy *HCR1* coding region flanked by *Bam*HI and *Nco*I sites, respectively, in *URA* plasmid from YEplac195	[12]
YEp-RLI1-L	high copy wt *RLI1* in *LEU2* plasmid from YEplac181	this study
YEp-hcr1-NTD	high copy *hcr1-NTD* in *LEU2* plasmid from YEplac181	[12]
YEp-hcr1-CTD	high copy *hcr1-CTD* in *LEU2* plasmid from YEplac181	[12]
YEp-hcr1-NTA1	high copy *hcr1-NTA1* in *LEU2* plasmid from YEplac181	[12]
YEp-hcr1-box6	high copy *hcr1-Box6* in *LEU2* plasmid from YEplac181	[13]
YEp-hcr1-box6-R215I	high copy *hcr1-Box6-R215I* in *LEU2* plasmid from YEplac181	[13]
PDH177	single copy wt *RLI1* in *URA3* plasmid from YCplac33	[19]
YEp-rli1-K116L-L	high copy *rli1-K116L* in *LEU2* plasmid	this study

	from YEplac181	
YEp-RLI1-ndeI-L	high copy wt *RLI1* in *LEU2* plasmid from YEplac181	this study
YEp-rli1-K391L-L	high copy *rli1-K391L* in *LEU2* plasmid from YEplac181	this study
YEp-rli1-G224D,G225D-L	high copy *rli1-G224D,G225D* in *LEU2* plasmid from YEplac181	this study
YEp-rli1-G470D,G471D-L	high copy *rli1-G470D,G471D* in *LEU2* plasmid from YEplac181	this study
YEp-rli1-E493Q-L	high copy *rli1-E493Q* in *LEU2* plasmid from YEplac181	this study
PDH184	single copy P_{GAL}-UBI-M-FH-rli1-G224D,G225D plasmid from YCplac111	[19]
PDH185	single copy P_{GAL}-UBI-M-FH-rli1-G470D,G471D plasmid from YCplac111	[19]
PDH202	low copy *rli1-E493Q-myc*$_5$ plasmid from pRS315	[19]
YEp-rli1-C25S-L	high copy *rli1-C25S* in *LEU2* plasmid from YEplac181	this study
YEp-rli1-C61S-L	high copy *rli1-C61S* in *LEU2* plasmid from YEplac181	this study
YEpSUI1-U	high copy *SUI1* in *LEU2* plasmid from YEplac181	this study
pDSO166	high copy *TIF11* in *LEU2* plasmid from YEplac181	[24]
pGEX-5X-3	cloning vector for GST fusions	[25]
pGEX- g/TIF34	GST-g/Tif34 fusion plasmid from pGEX-4T-1	[26]
pGEX- g/TIF35	GST-g/Tif35 fusion plasmid from pGEX-5X-3	[26]
pGEX-HCR1	GST-HCR1 fusion plasmid from pGEX-5X-3	[11]
pTH338	T7 promoter plasmid containing a full length SUP45 gene	this study
pTH339	T7 promoter plasmid containing the SUP45 N-domain	this study
pTH340	T7 promoter plasmid containing the SUP45 N- and M-domains	this study
pTH341	T7 promoter plasmid containing the SUP45 M- and C-domains	this study
pTH342	T7 promoter plasmid containing the SUP45 C-domain	this study
TKB668	high copy *YEF3* in *URA3* plasmid from YEPlac195	a gift of T. Kinzy
pGEX-RLI1	GST-RLI1 fusion plasmid from pGEX-5X-3	this study
pGEX-SUP45	GST-SUP45 fusion plasmid from	a gift of A. Hinnebusch

	pGEX-6P-1	
plig102-3	Low copy *URA3* vector with *GCN4* leader point mutations containing uORF4 only at its original position in front of the *GCN4-lacZ* coding region	[27]
YCplac22	single copy cloning vector, *TRP1*	[3]
YCp22-SUP45-W	single copy wt *SUP45* in *TRP1* plasmid from YCplac22	this study
pGEX- g/tif35-NTD	GST-g/tif35-NTD fusion plasmid from pGEX-5X-3	this study
pGEX-g/tif35-RRM	GST-g/tif35-RRM fusion plasmid from pGEX-5X-3	this study
pTH422	high copy wt *SUP45* in *URA3*	this study
pRS426-SUP35	high copy wt *SUP35* in *URA3*	this study
pSP35-45	high copy wt *SUP45 SUP35* in *URA3*	[28]

Table S4. Primers used in this study.

Primer name	Primer sequence (5´to 3´)
SG-TIF32D8bamHI	GCGGATCCATATGAGATTAGCTGAAATG
BS-TIF32D8nheI-R	GGGGCTAGCGGGTCCCTGCCCCCCTTGGCCAATC
TIF35 NdeI	TAACGACCATATGACCATGAA
MM2r 3gTLKVr	ACACATATCATCACGTTCTCT
y3gTKMQ (RNP2)	GACTCTAGAGAACGTGATGATATGTGTgctTTGgcaATTgctgcaGTTAATGAAAATGCCGATGAAAATAGT
y3g XhoIr	GTGCATCTCGAGCTAATGATG
MM1r	TGATTTACCTGTTTCTTTGT
y3gRLFT (RNP1)	GTTAGAAACAAAGAAACAGGTAAATCAgcaGGTgcaGCCgcaGTTgcaTTTTCGAGCGAAGAAGTTGCCGAACAA
PB-RLI1ndeI	AATAACATATGAGTGATAAAAACAGTCGT
PB-RLI1-K116LaccI-R	AATAAGTAGACAGACCAATACCGTTGGTACCGAC
PB-RLI1accI-R	CAAGGCGGTAGACTTAC
PB-RLI1ncoI	GCAAATACCATGGATAG
PB-RLI1ndeI-R	ACGACTGTTTTTATCACTCATATGGGTCTGTCGTGTTTTCTTAAG
PB-RLI1-K391L-R	AGACCGGTACCGTTTTCACCCAT
PB-RLI1-K391L	ATGGGTGAAAACGGTACCGGTCTGACCACTTTGATCAAATTACTA
PB-RLI1termXbaI-R	GGCGTATATCTAGAAATAAACAACC
PB-RLI1xbaI-R	AATAATCTAGATTAAATACCGGTGTTATCCAA
PB-RLI1-C25S	CTAAACGTTCGTGTCCCG
PB-RLI1-C25S-R	CGGGACACGAACGTTTAGACTCTTGACGACACTTTTTTGG
PB-RLI1-C61S	CCGTTAAGAAATGTCCATTTG
PB-RLI1-C61S-R	CAAATGGACATTTCTTAACGGAAATACCACAACCAATAC
Sup45_D1f	CGGGCCATGGAGATGGATAACGAGGTTGAAAAAAA
Sup45_D3r	CGGGCCTGCAGTTAAATGAAATCATAGTCGGAT
Sup45_D1r	CGGGCCTGCAGTTATTGAAGCAATTCCGAAAGAAC
Sup45_D2r	CGGGCCTGCAGTTAATTGGCCAACGCTTCGGC
Sup45_D2f	CGGGCCATGGAGGCTGACGACAAGTTCGGT
Sup45_D3r	CGGGCCTGCAGTTAAATGAAATCATAGTCGGAT
Sup45_D3f	CGGGCCATGGAGGTCAAGTATGTTCAAGAAAAGA
PB-RLI1smaI	AATAACCCGGGTCATGAGTGATAAAAACAGTCGT
PB-RLI1xhoI-R	AATAACTCGAGTTAAATACCGGTGTTATCCAA
PB-SUP45SphI	AATAAGCATGCGCTACATCATTTCCCCCAATAGC
PB-SUP45SacI-R	AATAAGAGCTCCGAGGCTTTTGAAGAGAAACTCTCC
pGEX35NTD	AATAAGGATCCCCATGAGTGAAGTTGCACCAGAG
pGEX35NTDr	AATAACTCGAGctaAGAGTCTCTGTAAGCATCGGA
pGEX35RRM	AATAAGGATCCCCAGAGAACGTGATGATATGTGT
pGEX35RRMr	AATAACTCGAGCTATTCCTTAACCTTAGGTTTGGA

PUBLICATION II

Nucleic Acids Research Advance Access published January 13, 2014

Nucleic Acids Research, 2014, 1–17
doi:10.1093/nar/gkt1369

Structural integrity of the PCI domain of eIF3a/TIF32 is required for mRNA recruitment to the 43S pre-initiation complexes

Sohail Khoshnevis[1], Stanislava Gunišová[2], Vladislava Vlčková[2], Tomáš Kouba[2], Piotr Neumann[1], Petra Beznosková[2], Ralf Ficner[1,*] and Leoš Shivaya Valášek[2,*]

[1]Department of Molecular Structural Biology, Institute for Microbiology and Genetics, George-August University, Goettingen, Germany, 37077 and [2]Laboratory of Regulation of Gene Expression, Institute of Microbiology ASCR, Videnska 1083, 142 20 Prague, the Czech Republic

Received April 19, 2013; Revised December 3, 2013; Accepted December 12, 2013

ABSTRACT

Transfer of genetic information from genes into proteins is mediated by messenger RNA (mRNA) that must be first recruited to ribosomal pre-initiation complexes (PICs) by a mechanism that is still poorly understood. Recent studies showed that besides eIF4F and poly(A)-binding protein, eIF3 also plays a critical role in this process, yet the molecular mechanism of its action is unknown. We showed previously that the PCI domain of the eIF3c/NIP1 subunit of yeast eIF3 is involved in RNA binding. To assess the role of the second PCI domain of eIF3 present in eIF3a/TIF32, we performed its mutational analysis and identified a 10-Ala-substitution (Box37) that severely reduces amounts of model mRNA in the 43–48S PICs *in vivo* as the major, if not the only, detectable defect. Crystal structure analysis of the a/TIF32-PCI domain at 2.65-Å resolution showed that it is required for integrity of the eIF3 core and, similarly to the c/NIP1-PCI, is capable of RNA binding. The putative RNA-binding surface defined by positively charged areas contains two Box37 residues, R363 and K364. Their substitutions with alanines severely impair the mRNA recruitment step *in vivo* suggesting that a/TIF32-PCI represents one of the key domains ensuring stable and efficient mRNA delivery to the PICs.

INTRODUCTION

Protein biosynthesis begins with formation of the 43S pre-initiation complex (PIC) consisting of the small ribosomal subunit, Met-tRNA$_i^{Met}$ [in the form of the ternary complex (TC) together with the eukaryotic initiation factor eIF2 in its GTP form], eIF1A, eIF1, eIF3 and eIF5 [reviewed in (1)]. In the following step, messenger RNA (mRNA) is loaded onto the 43S PIC with help of eIF3, poly(A)-binding protein (PABP) and the eIF4F factors bound to its 5′ 7-methylguanosine cap structure, producing the 48S PIC. Subsequently, usually the first AUG codon in the mRNA's 5′ UTR is recognized as the start site during the successive movement—called scanning—of the 48S PICs downstream from the cap. On AUG recognition, eIF2 in its GDP form is released from the ribosome along with several other eIFs, the 60S subunit joins the 40S•Met-tRNA$_i^{Met}$•mRNA complex in a reaction promoted by eIF5B and the resulting 80S initiation complex is on ejection of the remaining eIFs—with the exception of eIF3 and perhaps also eIF4F (2,3)—prepared for elongation.

In prokaryotes, the mRNA recruitment step is well defined and involves a direct RNA–RNA interaction between the 3′-end of 16S rRNA of the small ribosomal subunit and a specific Shine–Dalgarno sequence located in the 5′-end of mRNAs to allow direct positioning of the AUG start codon into the ribosomal P-site. In contrast, eukaryotic mRNAs do not contain anything like Shine–Dalgarno, initiating AUG is usually tens or even hundreds of nucleotides downstream from the cap and their recruitment to the 43 PICs requires the concerted action of several eIFs. This step, along with the subsequent scanning (base-to-base inspection of the mRNA's 5′ UTR), represents one of the least understood reactions in the entire eukaryotic initiation pathway. In the current textbook view, eIF3, PABP and the eIF4F complex (comprising the molecular scaffold eIF4G, to which the

*To whom correspondence should be addressed. Tel: +420 241 062 288; Fax: +420 241 062 665; Email: valasekl@biomed.cas.cz
Correspondence may also be addressed to Ralf Ficner. Tel: +49 5513 914 072; Fax: +49 5513 914 082; Email: ralf.ficner@biologie.uni-goettingen.de
Present address:
Sohail Khoshnevis, Department of Cancer Biology, The Scripps Research Institute, Jupiter, FL 33458, USA.

The authors wish it to be known that, in their opinion, the first three authors should be regarded as Joint First Authors.

cap-binding protein eIF4E and the DEAD-box RNA helicase eIF4A bind) are proposed to be responsible for mRNA loading to the 43S PICs [reviewed in (1)]. Besides eIF4E and eIF4A, the scaffold eIF4G also interacts with PABP and, in mammals, with eIF3 (4–8). The eIF4G–eIF3 interaction has been long believed to serve as the umbilical cord connecting the eIF4F•mRNA and 43S complexes, thus mediating formation of the 48S PIC, at least in mammals [in budding yeast, where the eIF3-binding domain in eIF4G is not evident, the direct eIF3–eIF4G interaction has never been detected (9)]. However, recent *in vivo* findings suggested that not only in yeast but probably also in mammals the mRNA recruitment step might be a lot less dependent on the direct eIF4G–eIF3 contact than it has been believed so far (10–13). Consistently, recent *in vivo* and *in vitro* studies in yeast indicated that eIF3 plays a more critical role in mRNA recruitment than eIF4G (14,15). Certainly, a more systematic approach is needed to fully understand this critical initiation step that is also known to serve as one of the two major targets for the general translational control [reviewed in (16)]. The first attempt in this direction has been recently made by identifying several mutations occurring in the j/HCR1-like domain (HLD) of the eIF3a/TIF32 subunit that, besides other effects on general initiation steps, also partially affected efficiency of the model mRNA recruitment to 40S ribosomes (17).

Despite the critical importance of the multisubunit eIF3 complex in translation—in addition to the mRNA recruitment, it also promotes the TC recruitment, scanning, AUG recognition and strikingly also translation termination (17–27)—a high-resolution structural picture of both yeast and mammalian eIF3 as whole remains elusive. Only partial either crystal or nuclear magnetic resonance structures were solved for a handful of domains of some of the eIF3 subunits, alongside the low-resolution Cryo-EM structure of the 13-subunit human eIF3 (28,29). In particular, the structures of RNA recognition motif (RRM) of yeast eIF3b/PRT1 subunit (30) as well as its human ortholog alone (31) or bound to the N-terminal peptide of eIF3j/HCR1 (24), the seven-bladed β-propeller of the WD40 eIF3i/TIF34 subunit bound to the extreme C-terminal α-helix of b/PRT1 (25), the RRM of human eIF3g/TIF35 (19) and finally the atypical PCI domain-containing human eIF3k subunit (32) have been determined at atomic resolution so far. The PCI domain is a conserved bipartite domain comprising the helical bundle (HB) and winged-helix (WH) subdomains initially identified as the principal scaffold for the multisubunit 26S proteasome lid, signalosome (CSN) and eIF3 complexes (33). Yeast eIF3 contains two PCI domains, one at the N-terminus of its eIF3a/TIF32 subunit and the other at the C-terminus of eIF3c/NIP1. In fact, the 3D architecture of the eIF3c/NIP1-PCI was recently predicted *in silico* and proposed to fold into a typical bipartite arrangement (34). Most of these partial structures and the latter prediction were incorporated into a structural model of yeast eIF3 shown in Figure 1A. Importantly, the latter report also revealed for the first time that the c/NIP1-PCI domain, this typical protein–protein interacting mediator, is capable of strong binding to RNA. Later, yeast SAC3 and THP1 components of the TREX-2 transcription–export complex, both containing the PCI domain, were shown to have their WH subdomains juxtaposed in a way forming a platform that is also capable of nucleic acid binding (35).

To analyze the function of the N-terminus of a/TIF32 harboring the second PCI domain of yeast eIF3, we undertook a systematic mutagenesis of a large N-terminal segment of a/TIF32 including an N-terminal part of the PCI domain. We show that a 10-alanine substitution of residues 361–370 (designated Box37) markedly affects growth and translation initiation rates at the elevated temperature. Structural investigation of the a/TIF32-PCI domain showed that it consists of two intimately connected subdomains: an N-terminal right-handed helical domain capped by a C-terminal winged helix domain. Furthermore, we provide evidence that specifically the PCI domain of a/TIF32 (i) mediates its binding to the eIF3c/NIP1 subunit of eIF3 and (ii) that the entire N-terminal half of a/TIF32 interacts with RNA, as proposed before (2,37). Interestingly, neither the N-terminal domain nor the PCI domain alone is sufficient for this binding; however, they are both required. In addition to that, we show that α-helix 4 of the HB subdomain, and in particular its two consecutive basic residues R363 and K364, strongly contributes to mRNA recruitment of the model mRNAs to the 43S PICs *in vivo*. Although R363 is also required for stabilization of the HB fold, K364 is fully exposed to the solvent with no structural role. Further analysis of the crystal structure and the *in silico*-generated structure of the helical region preceding this domain revealed the dominance of continuous positively charged areas over the surface of the a/TIF32 N-terminal half, proposing a molecular basis for its role in RNA recruitment. In support, 10-Ala substitutions of these basic patches resulted in lethality. Taken together, because our mutants in Box37 impair the mRNA loading process as the only detectable defect *in vivo*, we propose that one of the key roles of this well-defined domain is, besides building the eIF3 core, to contact mRNAs in a non-specific manner and promote their delivery to and/or stable binding on the small ribosomal subunit. Hence, the a/TIF32-PCI domain is yet another PCI domain demonstrated to be involved in RNA binding.

MATERIALS AND METHODS

Yeast strains, plasmids and biochemical methods

Lists of strains, plasmids and oligonucleotides used in this study (Supplementary Tables S1–S3), details of their construction, as well as description of all well-established biochemical assays used throughout the study can be found in the Supplementary Data that are available at NAR online.

Cloning, expression, purification and crystallization of the a/TIF32$^{276-494}$ domain and crystal structure determination

a/TIF32$^{276-494}$ was cloned into a pGEX6P1 vector, expressed in *Escherichia coli* Rosetta2 (DE3) cells and purified via affinity and size-exclusion chromatography (SEC) (detailed purification schemes of proteins used in

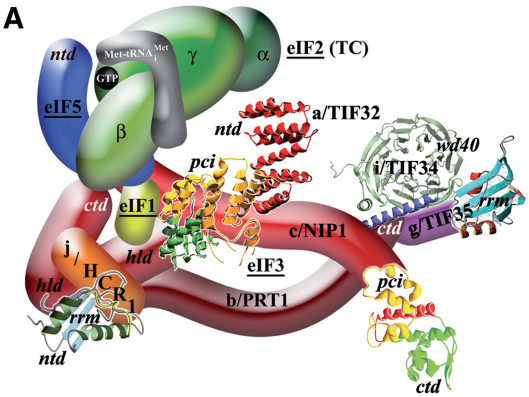

B

mutation	30°C	34°C	37°C	basic residues	description
a/TIF32 - wt	-	-	-		
a/TIF32-BOX20	let	let	let	R194,R195,K196	back RNA track
a/TIF32-BOX24	let	let	let	R235	front RNA track
a/TIF32-BOX27	let	let	let	K268	along the front RNA track below region 2
a/TIF32-BOX29	let	let	let	K288	along the front RNA track below region 2
a/TIF32-BOX31	let	let	let	K304,K305,K308	basic region 2
a/TIF32-BOX34	-	+	+++		long loop
a/TIF32-BOX35	let	let	let	R350	basic region 1
a/TIF32-BOX37	-	+	+++++	R363,K364	basic region 3
a/TIF32-BOX38	let	let	let		not involved in RNA binding surface

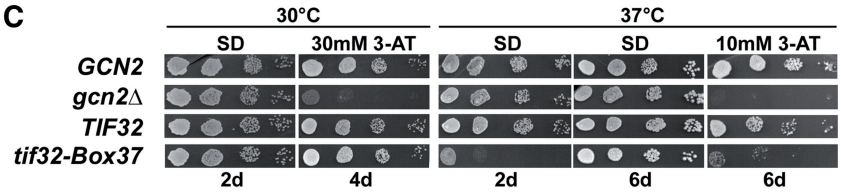

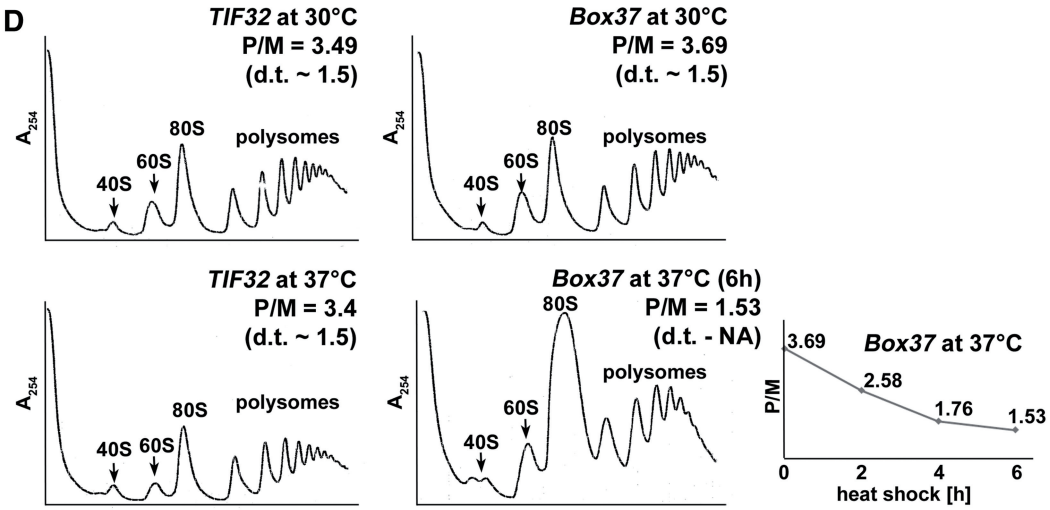

Figure 1. The 10-Ala *Box37* substitution of α-helix 4 of the HB subdomain in the a/TIF32-PCI domain reduces the translation initiation rates at the restrictive temperature. (**A**) A 3D model of eIF3 and its associated eIFs in the MFC [adapted from (25)]. *ntd*, N-terminal domain; *ctd*, C-terminal domain; *hld*, HCR1-like domain; *rrm*, RNA recognition motif; *pci*, PCI domain; TC, ternary complex. The nuclear magnetic resonance structure of the interaction between the RRM of human eIF3b (green and light blue) and the N-terminal peptide of human eIF3j (yellow) (24), the nuclear magnetic resonance structure of the C-terminal RRM of human eIF3g (19), the X-ray structure of the yeast i/TIF34–b/PRT1-CTD complex (green versus blue) (25), the X-ray structure of the a/TIF32-PCI (yellow and green) and structural prediction of the N-terminal domain of a/TIF32 (red) (both this study) and the 3D homology model of the c/NIP1-CTD (34) were used to replace the original schematic representations of the

(continued)

this study are provided in Supplementary Methods). Crystals were grown at 4°C in sitting drop vapor diffusion plates by mixing 0.8 µl of crystallization solution [100 mM HEPES, pH 7, 12% (w/v) PEG 2000, 80 mM $MnCl_2$] and 1.2 µl of protein solution (at a concentration of 6 mg/ml in the gel filtration buffer). Crystals were cryoprotected by soaking in reservoir solution supplemented with increasing concentration of PEG400 to 40% (w/v) and flash frozen in liquid nitrogen before data collection.

X-ray diffraction images were collected at 100 K at beamline 14.1 [BESSY, Berlin, Germany; (37)] equipped with a MAR Mosaic 225 mm CCD detector (Norderstedt, Germany). The oscillation images were indexed, integrated and merged using the XDS package (38,39) to the final resolution of 2.65 Å for the native and to 2.79, 2.81 and 2.97 Å for Se-Met derivative crystal (peak, inflection and remote data sets, respectively). The crystal structure of a/TIF32 was solved by means of single wavelength anomalous dispersion SAD using the Se-Met data set at the peak wavelength in SHARP/autoSHARP (40). Within autoSHARP, the heavy atom search was performed by SHELXD (41) and resulted in localizing four heavy atom positions that were further refined using SHARP followed by density modification in Solomon (42) and automatic model building in Arp/wARP (43). Structure determination and refinement procedure are discussed in detail in Supplementary Methods.

RNA-binding assay

RNA-binding studies were performed in 1× recon buffer (44). Two micromolars of *DAD4* RNA (see Supplementary Methods for transcription procedure) was mixed with 10 µM a/TIF32^{FL}, a/TIF32$^{1-494}$, a/TIF32$^{276-494}$, GST-a/TIF32$^{1-276}$ and GST in a total volume of 10 µl. After a 30-min incubation on ice, samples were mixed with native loading dye and applied to a 0.8% agarose gel supplemented with GelRed (Biotium). Electrophoresis was performed at 90 V for 30 min on ice using pre-cooled 1 × Tris acetate + ethylenediaminetetraacetic acid running buffer. The gel was subsequently exposed to ultraviolet-light to visualize nucleic acids.

Binding of the a/TIF32$^{276-494}$ domain to c/NIP1 by analytical SEC

Interaction studies were performed on an analytical Superdex 200 (10/300) column (GE Healthcare) in a buffer containing 150 mM KCl, 10 mM Hepes, pH 7.5, and 5% glycerol. Fifty micrograms of c/NIP1 (0.5 nmol), b/PRT1 (0.5 nmol) or a/TIF32$^{276-494}$ (2 nmol) in the total volume of 500 µl was loaded on the column separately or after being incubated together for 30 min.

Isothermal titration calorimetry

c/NIP1 and a/TIF32$^{276-494}$ were extensively dialyzed against ITC buffer (150 mM KCl, 10 mM Hepes, pH 7.5, 5% glycerol) and concentrated to 10 and 100 µM, respectively. The experiment was performed on a VP-ITC calorimeter (Microcal, USA). Twenty microliter aliquots of a/TIF32$^{276-494}$ were injected into the cell containing c/NIP1 every 40 s, during which the titration peak returned to the base line. Separately, seven injections of the same concentration of a/TIF32$^{276-494}$ into the buffers were performed under the same conditions to determine the heat of dilution. The titration data were analyzed using the ORIGIN software to calculate the thermodynamics parameters.

RESULTS

A specific 10-alanine substitution (*Box37*) in the a/TIF32-PCI domain results in temperature sensitivity and reduces translation initiation rates

Domain prediction programs detect two PCI domains in the yeast eIF3 complex. The first one, located at the C-terminus of c/NIP1, was previously implicated in RNA binding as the first PCI domain known to do so (34). Here we sought to investigate the role of the second PCI domain of eIF3 occurring in the N-terminal half of a/TIF32. We have recently demonstrated that the proteolytic digestion of a/TIF32 generates a fragment harboring its first 494 residues (45) suggesting that the entire a/TIF32 N-terminal half, including the PCI domain, is folded into a higher order structure. Earlier we also showed that the a/TIF32 region corresponding to amino acid (aa) residues 201 through 400, encompassing a part of the a/TIF32-PCI domain, interacts with the small ribosomal protein RPS0A (46) situated on the solvent-exposed side near the 40S mRNA exit channel (47).

To show whether the a/TIF32-PCI domain is involved in RPS0A binding and to identify specific residues that mediate this contact, we introduced Ala substitutions in consecutive blocks of 10 residues between amino acids 191 and 400 (dubbed Boxes 20–40) and tested them for growth phenotypes, first in a yeast strain containing a/

Figure 1. Continued
corresponding molecules. (**B**) Summary of the phenotypic analysis of Ala substitutions in consecutive blocks of 10 residues between amino acids 191 and 400 (dubbed Boxes 20–40). The indicated mutant alleles were introduced into the H477 strain containing a/TIF32 under control of *MET3* promoter and tested for growth in the presence of methionine. Alleles showing the Ts$^-$ or Slg$^-$ or lethal (Let) phenotypes are listed; the ± scoring system defines the wt as '–' and no growth as 5+. (**C**) The *tif32-Box37* mutation imparts the Ts$^-$ and Gcn$^-$ phenotypes. YBS52 (*GCN2 a/tif32Δ*) was transformed with YCplac111-based plasmids carrying either *a/TIF32* wt or *a/tif32-Box37* mutant alleles, and the resident YCpTIF32-His-U plasmid was evicted on 5-FOA. The resulting strains, together with isogenic strains H2880 (*GCN2 a/TIF32*; row 1) and H2881 (*gcn2Δ a/TIF32*; row 2) transformed with empty YCplac111 vector, were then spotted in four serial dilutions on SD or SD containing 10- or 30-mM 3-AT and incubated at 30°C or 37°C for up to 6 days. (**D**) The *tif32-Box37* mutation reduces the translation initiation rates at the restrictive temperature. Polysome profiles of *TIF32* wt and *tif32-Box37* mutant strains described in section B were recorded from cells cultured in YPD medium at 30°C or heat shocked at 37°C for indicated time points and subsequently treated with cycloheximide before harvesting. Whole-cell extracts were separated by velocity sedimentation through a 5–45% sucrose gradient centrifugation at 39 000 rpm for 2.5 h. The gradients were collected and scanned at 254 nm to visualize the ribosomal species. Positions of 40S, 60S and 80S species are indicated by arrows, and polysome to monosome (P/M) ratios and doubling times (d.t.) are given above the profiles. The plot indicates P/M ratios collected at various time points of heat shock.

TIF32 under control of *MET3* promoter. Several of these Ala substitutions led to lethal phenotypes (Figure 1B; see also below) in accord with our earlier observation that deletion of the first 350 residues of a/TIF32 is deleterious (18). One of these substitutions, Box37 (residues 361–370), produced strong temperature-sensitive (Ts^-) and Gcn^- phenotypes (Figure 1C), which we could analyze further for its primary defect—the Gcn^- (general control non-derepressible) phenotype indicates an impairment of the *GCN4* induction (see below). (Box34 [residues 331–340] also showed the Ts^- phenotype; however, as it was rather mild, we did not pursue this mutant any further). Careful inspection of polysome profiles carried out at the non-permissive temperature at three time points following the temperature up-shift clearly suggests that the *Box37* mutation specifically affects translation initiation rates as the run-off 80S couples accumulate at the expense of heavy polysomes, which is displayed by ~2.2-fold decrease in the polysome to monosome (P/M) ratio (Figure 1D).

Next we examined the potential effect of *Box37* on the direct interaction of the 201–400 subdomain of a/TIF32 with RPS0A in an *in vitro* binding assay as well as on the integrity of native eIF3 with eIFs 1, 2 and 5 into the ribosome-free multifactor complex (MFC) *in vivo*. Neither was found dramatically affected by this mutation (data not shown) suggesting that *Box37* did not markedly affect the mutant protein fold, if at all (see also 'Discussion' section), and also that it is not the critical anchor point between the a/TIF32-NTD and RPS0A. Despite that we still asked whether this mutation may interfere—perhaps in some indirect way—with the initial assembly of eIFs on the 40S ribosomes. Toward this end, we analyzed the distribution of selected initiation factors in *Box37* cells grown at 30°C and subsequently subjected to heat shock at 37°C for 6 h using formaldehyde cross-linking of living cells followed by high velocity sedimentation of whole-cell extracts (WCE) in sucrose density gradients (48). No reduction in the 40S-associated amounts of selected eIF3 subunits as well as eIF2 and eIF5 was observed in heat-shocked cells (Figure 2B). On the contrary, when normalizing to the levels of 40S species, we detected ~1.5-fold accumulation of the latter eIFs in heat-shocked cells compared with cells grown at the permissive temperature. Wild-type (wt) cells showed rather decreased, but definitely not increased, amounts of eIFs in 40S fractions on heat shock (Figure 2A). This suggests that the rate-limiting step that is impaired in *Box37* follows the 43S PIC assembly.

The *tif32-Box37* mutation imparts severe Gcn^- phenotype that is not caused by post-assembly defects in the initiation pathway

To examine what step is affected by *Box37*, we used the translational control mechanism of *GCN4*, which depends on four short upstream open reading frame (uORFs) found in its mRNA leader and has been adapted to serve as an experimental tool for monitoring various translational steps [reviewed in (49)]. The expression of *GCN4*, a transcriptional activator of many biosynthetic genes, is delicately regulated in a nutrient-dependent manner by the GCN2 kinase. Under nutrient-replete conditions, the kinase is inactive and the *GCN4* expression is repressed. On amino acid starvation, GCN2 becomes activated and derepresses *GCN4* synthesis by reducing the steady-state levels of the TC. Mutants defective in the TC formation and/or its recruitment to the 40S subunit mimic starvation conditions and constitutively derepress *GCN4* even under nutrient-replete conditions, producing the Gcd^- phenotype. Conversely, mutants that fail to derepress *GCN4* under starvation conditions provoke the Gcn^- phenotype, which typically signals defects in the steps following assembly of 43–48S PICs, such as processivity of scanning, AUG recognition or subunit joining.

The fact that *Box37* displayed the severe Gcn^- phenotype at the restrictive temperature (Figure 1C), which is characterized by a failure to grow in the presence of an inhibitor of histidine biosynthetic genes—3-aminotriazole (3-AT), prompted us to use a battery of *GCN4-lacZ* reporter constructs with specific modifications in the *GCN4* mRNA leader. These have been successfully used in the past to reveal malfunctioning in scanning processivity, scanning rates, stringency of AUG selection or in subunit joining (2,17,19,20,24,25,50). First, we tested the wt *GCN4-lacZ* reporter plasmid to verify the true nature of the Gcn^- phenotype in *Box37* cells and found that the degree of *GCN4-lacZ* induction was ~4-fold reduced in mutant (showing rather low ~2-fold induction) versus wt (showing standard ~8-fold induction) cells. This clearly indicates that the inability to compete with 3-AT on plates is a direct consequence of an insufficient *GCN4* derepression in response to 3-AT. Surprisingly, detailed analysis of all potential post-assembly defects described above did not reveal any clearly distinguishable defects; we only noticed that most of the constructs showed generally reduced β-galactosidase activities in mutant *versus* wt strains. Taking this into consideration, plus the fact that yeast eIF3 has been recently implicated in serving as one of the major factors ensuring stable mRNA binding to 40S ribosomes (14,15,17), low levels of wt *GCN4-lacZ* induction could be explained by a failure to recruit or stably accommodate mRNAs on the 43S PICs to form the 48S PICs poised for scanning. Interestingly, a similar phenotype was only recently reported for the eIF4G mutant *tif4632-7R* (51). In fact, this particular defect could also explain increased amounts of eIFs on 40S ribosomes that we observed in heat-shocked mutant cells (Figure 2B), as an increased number of 40S species bound only by the initial set of factors promoting the Met-$tRNA_i^{Met}$ recruitment would be expected to accumulate in such defective cells. In further support, the '40S' peak in polysome profiles recorded with heat-shocked *Box37* cells is divided into two equally large sub-peaks, whereas only one dominant peak (the heavier one) occurs in wt cells (Figure 1D). In our previous work (9), we proposed that the lighter sub-peak corresponds to 'naked' 40S ribosomes combined with the 43S PICs and the heavier one to the 48S PICs. Hence, occurrence of two 40S sub-peaks in the heat-shocked mutant cells could be explained by slower conversion of 43S PICs into 48S PICs due to impaired mRNA recruitment (see below). To shed light on the molecular mechanism by which a/TIF32-PCI domain

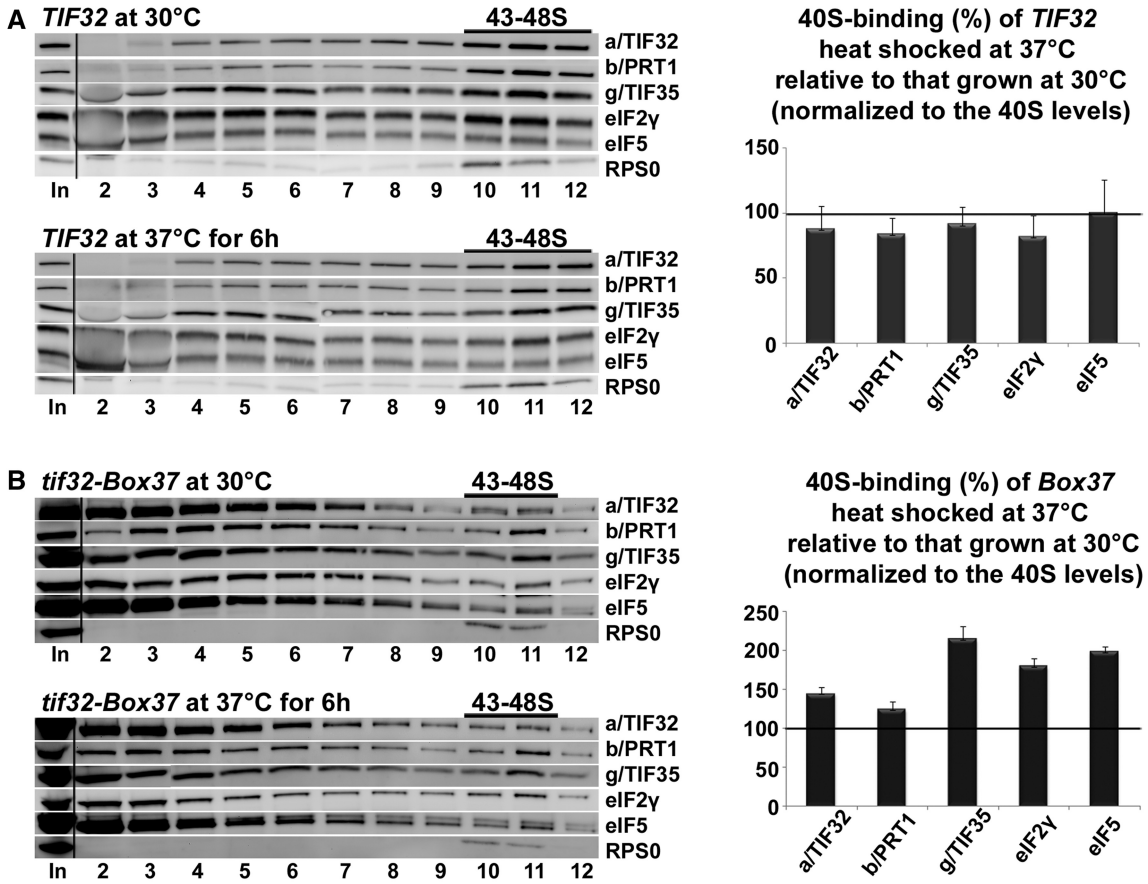

Figure 2. The *tif32-Box37* substitution results in accumulation of the 43S PICs. The *tif32-Box37* mutant strain (**B**) and its corresponding wt (**A**) described in Figure 1C were grown in YPD medium at 30°C or heat shocked at 37°C for 6 h and cross-linked with 2% HCHO before harvesting. Whole-cell extracts were prepared, separated on a 7.5–30% sucrose gradient by centrifugation at 41 000 rpm for 5 h and 5% of each fraction was loaded on the gel and subjected to western blot analysis. 'In' shows 5% input. Proportions of the 40S-bound proteins relative to the amount of 40S subunits were calculated using Quantity One software (BioRad) from at least three independent experiments. The resulting values obtained with cells grown at 30°C were set to 100% and those obtained with heat-shocked cells were expressed as percentages of the 30°C-grown cells in the histogram on the right (SDs are given).

would facilitate the recruitment of mRNA to the ribosome, we set forth to determine its 3D structure at atomic resolution.

Purification, crystallization and structure determination of the a/TIF32 PCI domain

The N-terminal region of a/TIF32 was previously identified as a stable protein domain (45). As mentioned previously, this region is predicted to harbor a PCI domain preceded by several α-helices. PCI domains are made up of two subdomains: N-terminal helical repeats followed by a C-terminal-winged helix motif. While the C-terminal winged helix motif can be fairly accurately predicted, the prediction of the exact length of the N-terminal subdomain of a/TIF32 turned out to be difficult. Because we did not obtain crystals of the entire N-terminal domain of a/TIF32, we systematically removed helices from the N-terminus, keeping the C-terminus at residue 494. However, most of the constructs led to insoluble proteins. The most soluble fragment was obtained by removing the first 275 residues (Supplementary Figure S1). This fragment was crystallized in a solution containing 100 mM HEPES, pH 7, 12% PEG 2000 (w/v), 80 mM $MnCl_2$. Crystals grew at 4°C to the maximum size in 1 week. Cryoprotection was achieved by soaking crystals in several drops containing the crystallization solution and increasing concentration of PEG400. Sudden increase of the PEG400 concentration caused cracks in the crystal and had a severe effect on the diffraction quality. The crystal structure of a/TIF32$^{276\text{-}494}$ was solved by single wavelength anomalous dispersion using a selenomethionine (SeMet) derivative and refined to the final resolution of 2.65 Å. The asymmetric unit (AU) is composed of two molecules of a/TIF32$^{276-494}$, which corresponds to a solvent content of 45%. Although the first molecule in the AU (chain A in the pdb file) is almost complete, the second molecule is only partially defined in the electron density map. The crystallographic statistics for data processing and refinement are presented in Table 1.

Crystal structure analysis

The crystal structure of a/TIF32$^{276–494}$ consists of two intimately connected subdomains; an N-terminal right-handed helical bundle capped by a C-terminal winged

Table 1. Data collection, phasing and refinement statistics

	Native	Peak	Inflection	High remote	Low remote
Data collection					
Wavelength (Å)	0.933400	0.979540	0.979690	0.977260	0.982450
Resolution (Å)	50.00–2.65 (2.75–2.65)	50.00–2.79 (2.89–2.79)	50.00–2.81 (2.91–2.81)	50.00–2.97 (3.07–2.97)	50.00–2.97 (3.07–2.97)
Space group	I 2_1 3	I 2_1 3	I 2_1 3	I 2_1 3	I 2_1 3
Cell parameters:					
a = b = c (Å)	137.137	137.63	137.99	138.06	137.75
α = β = γ = 90 (°)					
R_{merge} (%)	5.9 (78.0)	10.4 (83.4)	10.8 (88.7)	8.8 (60.2)	10.2 (71.7)
$I/\delta I$	17.76 (1.83)	21.44 (2.16)	21.7 (2.0)	23.21 (2.77)	21.36 (2.53)
$CC_{(1/2)}$ (%)	99.9 (66.2)				
Completeness (%)	99.5 (99.8)	99.6 (96.5)	99.7 (97.3)	99.9 (100)	99.8 (99.9)
Redundancy	3.67 (3.71)	4.41 (3.48)	4.44 (3.58)	4.93 (4.92)	3.89 (3.88)
Anomalous correlation		56 (11)	35 (7)	35 (4)	16 (11)
Mean anomalous difference (SigAno)		1.724 (0.849)	1.285 (0.794)	1.269 (0.806)	0.997 (0.845)
Refinement					
Resolution (Å)	48.48–2.65 (2.75–2.65)				
Number of reflections	12 582				
R_{work}/R_{free} (%)	24.89/28.61				
Number of atoms					
Protein	3037				
B-factors (Å^2					
Protein	118.70				
Entity nr. 1/2	81.5/168.8				
R.m.s deviations					
Bond lengths (Å)	0.006				
Bond angles (°)	1.26				
PDB code	4K51				

The $CC_{1/2}$ is the correlation coefficient between two randomly selected half data sets as described in (52).

helix (WH) domain (Figure 3A). The helical bundle (HB) is composed of three pairs of antiparallel helices with structural resemblance to tetratricopeptide repeats (TPR). Helices 3 and 4 are connected via a long loop and a short helix. Residues 342–344 of this loop are poorly visible in the electron density and therefore likely to be flexible. Interestingly, residues 337–362, which form the loop and the helix connecting helices 3 and 4, are not present in the structure of any of the known PCI domains. The winged helix sub-domain shows the canonical α-β-α-α-β-β topology with an N-terminal elongated helix, which is kinked at the beginning. The structure of the WH subdomain is well conserved among known PCI structures. The orientation of the WH relative to the HB is held by several hydrogen bonds and van der Waals interactions between helix 7 (the first helix of WH) and different helices from HB. Most notably, R431 of helix 7, E392 of helix 5 and R363 of helix 4 are tightly linked by hydrogen bonds locking these three helices in place (Figure 3B). R363 and the adjacent K364 together with R431 contribute to a positively charged surface on the concave face of the protein, proposing a function for this region in mRNA recruitment (see below). Y420 and L424 of helix 7 make van der Waals interactions with the side chain of L330 of helix 3. Y420 makes a hydrogen bond with H299 of helix 2, which also interacts with S331 of helix 3. Interestingly, all these residues are highly conserved among eukaryotes, suggesting that maintaining the relative orientation of WH and HB might have a functional relevance (Supplementary Figure S2).

In fact, a/TIF32 is one of the most conserved core eIF3 subunits among eukaryotes. Interestingly, the highest degree of conservation is observed in its N-terminal region, including the PCI domain (Supplementary Figure S2). The majority of the conserved residues were found to be in the hydrophobic core of a/TIF32$^{276–494}$, pointing to their importance in the folding of this domain. We mapped the highly conserved residues on the surface of a/TIF32$^{276-494}$ using ConSurf server (53). Although no region with particularly high degree of conservation was found throughout the surface, scattered regions of high conservation were found to be surrounded by less conserved residues mainly at the concave surface of the protein (Figure 4A).

Comparison of the a/TIF32 PCI domain with other known PCI structures

Comparison of the structure of a/TIF32$^{276–494}$ with PCI domains from RPN6 [proteasomal protein, PDB code 3TXN, (54)], CSN7 [COP9-signalosome subunit, PDB code 3CHM, (55)], eIF3k (eIF3 subunit, PDB code 1RZ4, (56)], SAC3 and THP1 [TREX-2 components, PDB code 3T5V, (35)] reveals high degree of structural similarity despite little sequence conservation (Figure 4B). The highest structural conservation is observed for the C-terminal WH subdomain, whereas the N-terminal HB is more divergent. In all these structures, HB sub-domains show an overall right-handed superhelical arrangement of α-helices with characteristics

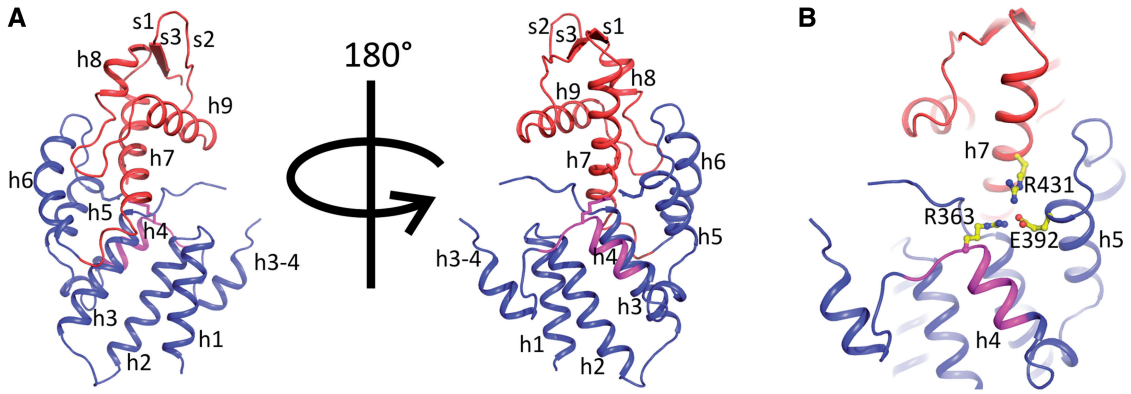

Figure 3. The overall structure of the PCI domain of a/TIF32. (**A**) Cartoon representation of a/TIF32$^{276–494}$ crystal structure. The helical bundle and the winged helix motif are colored blue and red, respectively. Box37 (residues 361–370) within helix 4 is shown in magenta. α-helices and β-strands are denoted as h and s, respectively. (**B**) Interactions between HB and WH sub-domains. HB and WH are held together via hydrogen bonding between helices 4, 5 and 7 (h4, h5 and h7). Residues involved in these interactions are R363 (h4), E392 (h5) and R431 (h7) and are presented as sticks.

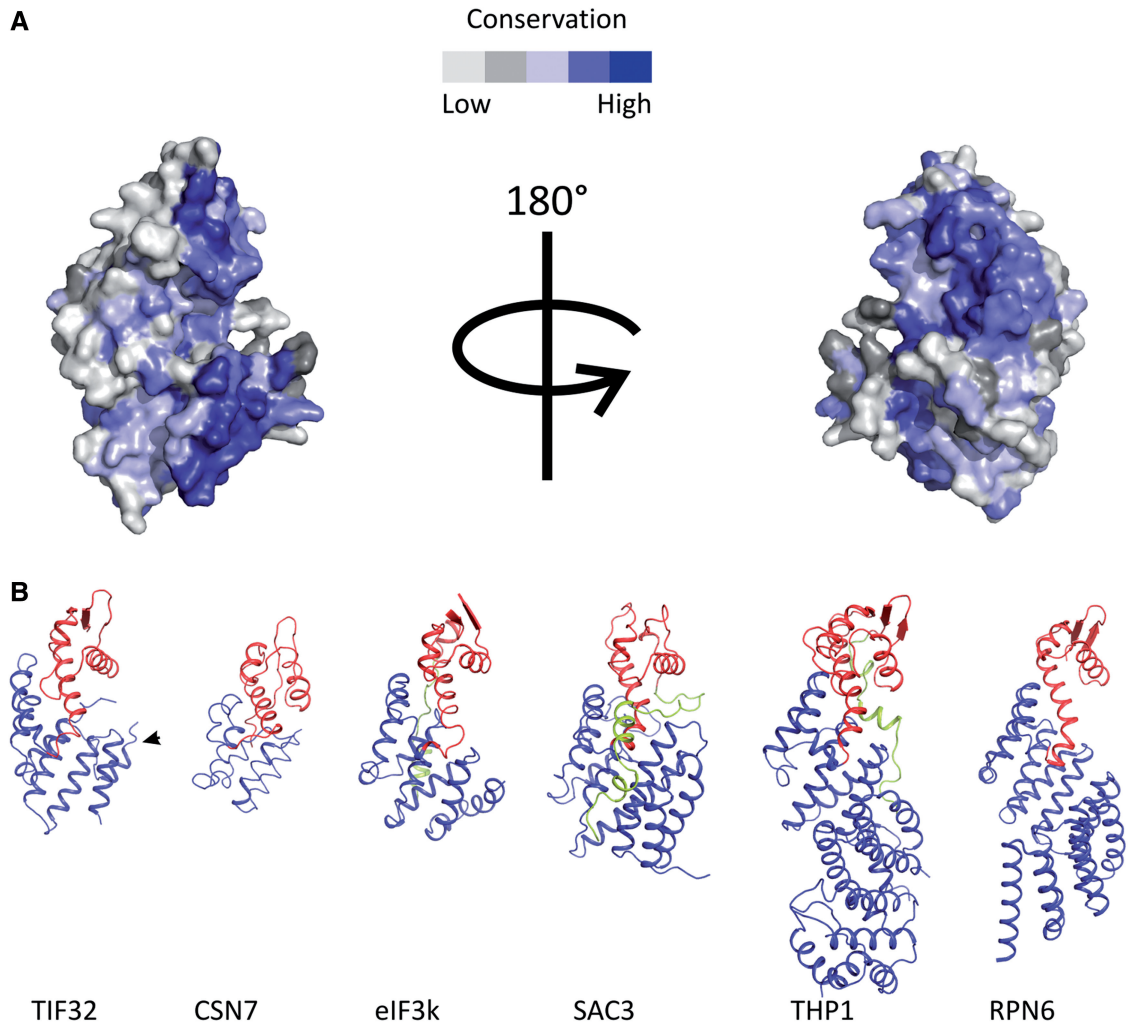

Figure 4. Conserved residues of a/TIF32 and comparison of the 3D structures of different PCI domains. (**A**) Conserved residues of a/TIF32. Surface representation of the conservation of residues among a/TIF32 from different organisms was performed using ConSurf server. (**B**) Comparison of the 3D structures of different PCI domains. In all structures, the HB and WH sub-domains are depicted in blue and red, respectively. C-terminal extensions of the WH, if present, are colored green. In the a/TIF32 PCI domain, the extra helix 3–4 is marked by an arrow.

of both HEAT [**H**untingtin, elongation factor 3 (**E**F3), protein phosphatase 2A (PP2**A**) and the yeast kinase **T**OR1] and TPR helical repeats. While eIF3k has 11 helices, which form 3 HEAT repeats, and CNS7 consists of 6 helices forming a pair of HEAT repeats, one of which resembles an ARM motif, RPN6 and THP1 structures have longer N-terminal extensions of TPR-like repeats. RPN6 contains five pairs of TPR-like repeats forming a twisted solenoid arrangement, whereas Thp1 forms a straighter arrangement that is capped by a helical bundle at the N-terminus formed by four α-helices [for a review see (57)]. Our a/TIF32 structure consists of six helices with a superhelical arrangement. An extra helix connecting helices 3 and 4 is a novel feature of a/TIF32 compared with the other PCI domains. This region is relatively conserved among eIF3a from different eukaryotes.

The PCI domain of a/TIF32 directly mediates its binding to c/NIP1

PCI domains are known to be protein interaction sites (33). a/TIF32, the largest subunit of yeast eIF3, has been implicated in building the core of eIF3 by interacting with c/NIP1 and b/PRT1, two other large eIF3 subunits (18,58). We had previously purified a stable complex between a/TIF32$^{1–494}$ and c/NIP1$^{244–812}$ (45). To find out whether the PCI domain of a/TIF32 (276–494) *per se* mediates this binding, we performed analytical SEC with purified c/NIP1 and a/TIF32$^{276–494}$. While each of the proteins elutes as a single peak from the column, the mixture of two proteins results in two peaks, with one having the same retention volume as a/TIF32$^{276–494}$ alone (as it was used in excess over c/NIP1 to promote complex formation) and the other one shifting toward the smaller volumes compared with c/NIP1 indicating the formation of a complex (Figure 5A). To dissect the thermodynamics of this binding, we performed isothermal titration calorimetry (ITC) using a/TIF32$^{276–494}$ and c/NIP1. The results indicated the formation of a complex with the stoichiometric ratio of nearly 1 (0.944), the dissociation constant (K_d) of 158 nM and a relatively large enthalpy change of −10.23 kcal/mol (Figure 5B). As expected (59), no binding was detected between b/PRT1 and a/TIF32$^{276–494}$ as judged by no change in the retention volumes of the mixture of the two proteins on analytical SEC compared with those of each protein alone (Figure 5C). Hence, the binding of a/TIF32 to b/PRT1 is most likely mediated via the C-terminal part of a/TIF32, as we recently also showed by *in vitro* reconstitution experiments (45).

RNA-binding properties of the a/TIF32-PCI domain

Winged helix motives are well-known nucleic acid binding modules (60). It is therefore likely, but not necessarily self-evident, for a given PCI domain to modulate an interaction with nucleic acids. As mentioned previously, there are two PCI domains in yeast eIF3; one in the N-terminal region of a/TIF32 under study here and the other one in the C-terminal region of c/NIP1, which was recently implicated in RNA binding as the first PCI domain ever found to do so (34). To test whether the a/TIF32-PCI domain is also capable of binding to RNA, we performed electrophoretic mobility shift assay with different fragments of a/TIF32 and *DAD4* mRNA, which is one of the smallest naturally occurring mRNAs in yeast. A stretch of 30 adenosine nucleotides was added to the 3′-end of the mRNA during transcription to mimic the polyA tail of the mRNA. While full-length and the entire N-terminal domain (1–494) of a/TIF32 bound to the mRNA, a/TIF32$^{276–494}$ failed to interact with the mRNA (Figure 5D). This may suggest an RNA-binding activity for the N-terminal region of a/TIF32 before residue 276. To check this, a/TIF32$^{1–276}$ was purified as a GST-fusion protein and tested for binding to *DAD4* mRNA. However, this fragment also failed to bind to the mRNA. This can be explained in several ways; GST-a/TIF32$^{1–276}$ is not properly folded, or the mRNA-binding site is masked by the GST or the RNA-binding site at the N-terminal region of a/TIF32 is distributed over a wide range of residues, both before and after residue 276. It has to be acknowledged here that the concentrations of RNA and protein used in this assay are relatively high and as such might produce non-specific RNA–protein interactions. However, this is of a minor concern as (i) only the entire N-terminal fragment of a/TIF32$^{1–494}$ and not its N- and C-terminal halves interacted with RNA in our assay and (ii) a protein implicated in mRNA recruitment to ribosomes like a/TIF32 is expected to have general non-specific RNA-binding properties.

The *tif32-Box37* mutation specifically diminishes mRNA recruitment to the 43S PICs *in vivo*

With several lines of experimental evidence and predictions from the 3D structure all pointing at the importance of the PCI domain for mRNA recruitment, we next decided to examine the effects of *Box37* on the 48S PIC assembly. To do that, we measured the amounts of three model mRNAs associated with native 48S PICs in whole-cell extracts of formaldehyde (HCHO) cross-linked cells that were resolved on sucrose gradients as described above according to (17). One of the model mRNAs—*RPL41A*—was successfully used in the latter and other studies, and the use of the other two—*DAD4* and *SME1*—was established here to provide broad specificity of our analysis. We specifically chose these mRNAs because they are rather short and thus minimize the 'contamination' effects of large mRNAs assembled into mRNPs that often run in heavy sucrose fractions like ribosomal species (17) and could lead to serious misinterpretations of the mRNA recruitment data. In addition, these experiments were conducted using isogenic strains lacking one of the genes encoding the 60S protein RPL11 (*RPL11B*), as the reduced level of 60S subunits resulting in a reduced rate of subunit joining increases the concentration of 48S PICs in *rpl11BΔ* cells (14). This is a necessary arrangement that increases the peak of mRNAs associated with the 48S PICs relative to the free mRNPs and significantly

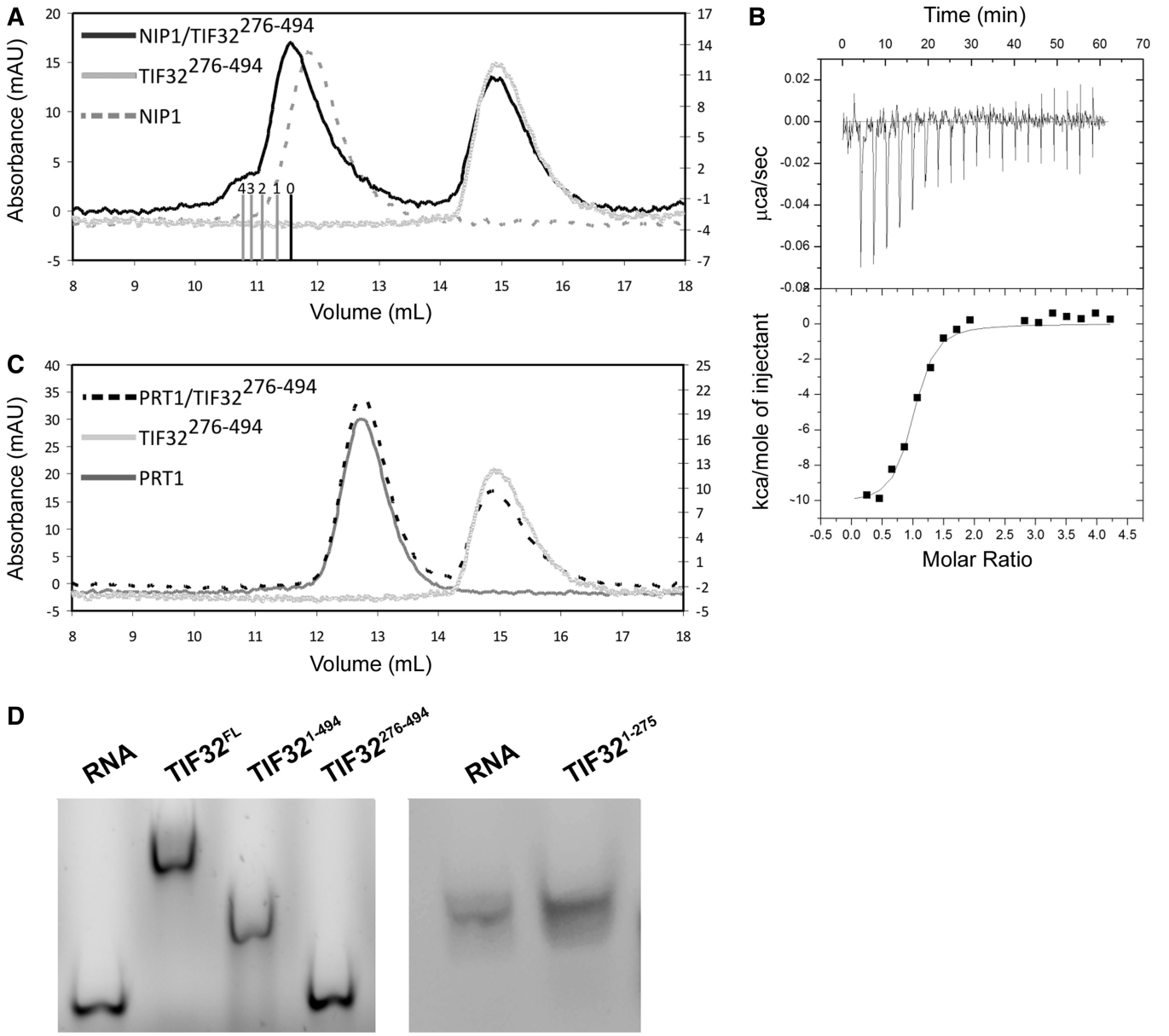

Figure 5. Protein and RNA-binding properties of a/TIF32$^{276\text{-}494}$. (**A**) Interaction of a/TIF32$^{276–494}$ with other major components of eIF3. SEC chromatogram of a/TIF32$^{276–494}$ interaction with c/NIP1. The shift to the smaller volume in the case of the mixture of two proteins indicates a complex formation. Bars indicate different ratios of a/TIF32$^{276–494}$ to c/NIP1, with 0 being only c/NIP1 and 4 being four molecules of a/TIF32$^{276–494}$ bound to c/NIP1. The small peak at 10.8 ml after mixing a/TIF32$^{276–494}$ and c/NIP1 is most probably an artifact of SEC due to incubation of the complex at room temperature for 30 min. (**B**) Isothermal calorimetric titration of c/NIP1 with a/TIF32$^{276–494}$. The upper panel shows raw data of heat effect (in mcal s^{-1}). The lower panel shows the fitted binding isotherms. The data points were obtained by integration of heat signals plotted against the molar ratio of a/TIF32$^{276–494}$ to c/NIP1 in the reaction cell. The solid line represents a calculated curve using the best fit parameters obtained by a non-linear least squares fit. (**C**) The mixture of a/TIF32$^{276–494}$ and b/PRT1 behaves the same as the sum of both proteins individually. (**D**) RNA binding activity of different regions of a/TIF32. Both full-length and the entire N-terminal domain of a/TIF32 bind to RNA. In contrast, a/TIF32$^{276–494}$ or a/TIF32$^{1–276}$ does not disturb the electrophoretic mobility of the mRNA.

facilitates quantification of the 48S-bound species (17). Using real-time quantitative reverse transcription-polymerase chain reaction to assay the three reporter mRNAs and 18S rRNA in 12–13 collected fractions, we found that heat-shocked *Box37* significantly shifts distribution of all three mRNAs from 40S-containing fractions toward the top, indicating a substantial underutilized pool of free mRNPs (Figure 6A, B, and D, and Supplementary Figure S3). Relative amounts of all three mRNAs in PICs of mutant versus wt cells are shown in the corresponding Tables in Figure 6E and Supplementary Figure S3. This experiment was repeated several times with similar results. Taken together, we propose that the *tif32-Box37* 10-Ala substitution primarily impairs the assembly or stability of the 48S PICs. In other words, the α-helix 4 of the HB subdomain encompassing residues 361 through 370 markedly contributes to the stable mRNA recruitment to 43S PICs *in vivo*.

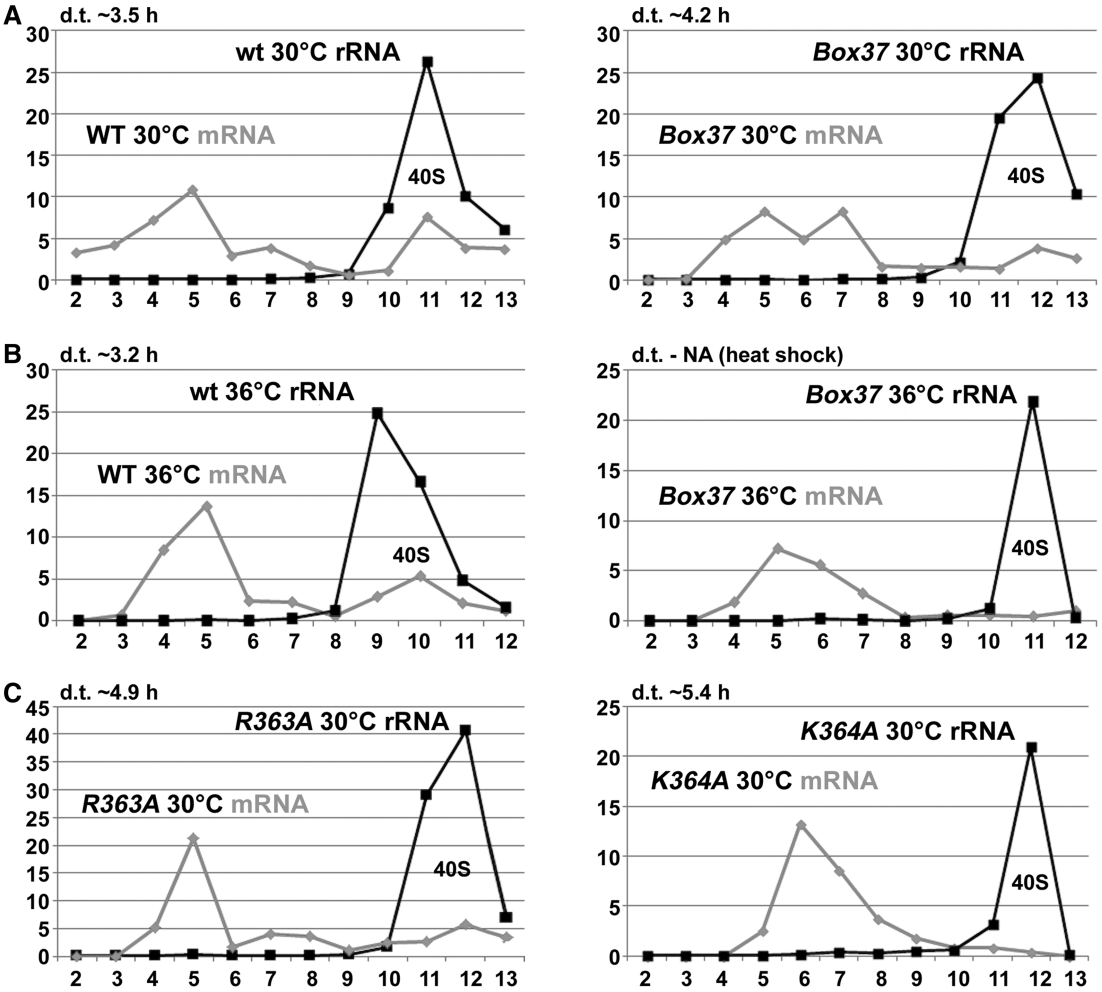

D

	DISTRIBUTION ACROSS the GRADIENTS			
	30°C		36°C	
	the amount (%) corresponding to *RPL41A* mRNA in:			
	free RNPs	PICs	free RNPs	PICs
WT	**68.3** ± 5.5	**31.7** ± 5.5	**74.9** ± 4.6	**25.1** ± 4.6
Box37	**84.2** ± 4.1	**15.8** ± 4.1	**91.2** ± 0.6	**8.8** ± 0.6
R363A	**82.3** ± 6.4	**17.7** ± 6.4	**ND**	**ND**
K364A	**89.8** ± 1.9	**10.1** ± 1.9	**ND**	**ND**

E

RELATIVE AMOUNT of *RPL41A* mRNA in PICs in MUTANT vs. WT CELLS			p-value	
	30°C	36°C	30°C	36°C
WT	**1**	**1**		
Box37	**0.5**	**0.35**	0.008	0.004
R363A	**0.56**	**ND**	0.014	
K364A	**0.32**	**ND**	0.002	

Figure 6. The *tif32-Box37*, *-R363A* and *-K364A* substitutions eliminate mRNA association with 43S PICs *in vivo*. (**A–C**) The isogenic *rpl11bΔ* strains carrying indicated *TIF32* mutations were cultured, cross-linked and separated as described in Figure 2. Total RNA was extracted from each of 12–13 fractions, and the amounts of 18S rRNA and *RPL41A* mRNA were measured by real-time quantitative polymerase chain reaction. The amounts of mRNA and 18S rRNA were calculated as $2^{-Ct} \times 10^{-7}$ and $2^{-Ct} \times 10^{-4}$, respectively. (**D** and **E**) The distribution of *RPL41A* mRNA across all fractions and its relative amounts in mutants versus wt in 18S rRNA containing fractions were calculated. Student's *t* test (*P*-value) indicated that the value for each mutant differed significantly from that for the wt.

Solvent-exposed K364 of the a/TIF32-PIC domain promotes mRNA recruitment

As mentioned previously, two N-terminal residues of the α-helix 4 of the HB subdomain (mutated in *Box37*) are R363 and K364. Whereas R363 is certainly required for stabilization of the HB fold (Figure 3B), K364 is fully exposed to the solvent with no structural role. However, both residues are part of the apparent continuous surface rich in basic residues with a fair probability to interact with RNA (region 3 in Figure 7B). Because the Ala-substitution of Box37 dramatically reduced the *RPL41A* mRNA amounts in the 40S-containing fractions *in vivo* (Figure 6A and B), it was tempting to speculate that these two residues actually mediate the mRNA transfer onto the 43 PICs. To address this question, we substituted both residues with alanine and examined the effects of these individual substitutions on *RPL41A* mRNA association with PICs *in vivo* as described above. As shown in Figure 6C–E and Supplementary Figure S4, both single substitutions decreased growth rates (by ~2-fold) already at 30°C and, most importantly, markedly reduced the *RPL41A* mRNA amounts associated with the PICs. These observations thus strongly suggest that both residues play an important role in the ability of the PCI domain of a/TIF32 to stimulate formation of the 48S PICs. Interestingly, of the two, *K364A* had a stronger effect on mRNA recruitment (the relative amounts of *RPL41A* mRNA in PICs are reduced by ~70%) as well as on the growth rates than *R363A* (showing ~45% reduction in the relative amounts of *RPL41A*, the effect of which was comparable with the effect of *Box37*; see 'Discussion' section for further details). Taken together, we propose that one of the key roles of the a/TIF32-PCI domain is, besides building the eIF3 core, to contact mRNAs in a non-specific manner and promote their delivery to and/or stable binding on the small ribosomal subunit.

Structural basis for the RNA binding of the a/TIF32-PCI domain

Secondary structure prediction suggests the dominance of helical repeats in the N-terminal region of a/TIF32, preceding the crystallized fragment. The sequence-based structure prediction using Phyre2 (62) suggests that the N-terminal HB probably extends further than six helices similar to the extended twisted character of THP1 and RPN6 (see above). Therefore, we built a chimeric molecule *in silico* from the predicted domain (residues 1–275) and the crystallized fragment (residues 276–494, Figure 7A). The relative orientation of the two domains was confirmed by performing protein–protein docking using HEX software (Supplementary Figure S5) (63). Analysis of the surface charge distribution of the predicted piece of the structure shows the dominance of positively charged patches, which form two continuous surfaces on the front and back of this N-terminal region of a/TIF32 implying a possible role in RNA binding (Figure 7B, left and right, respectively). Even though the crystallized fragment does not show an accumulation of charge density that would be comparable with a/TIF32$^{1–276}$, the

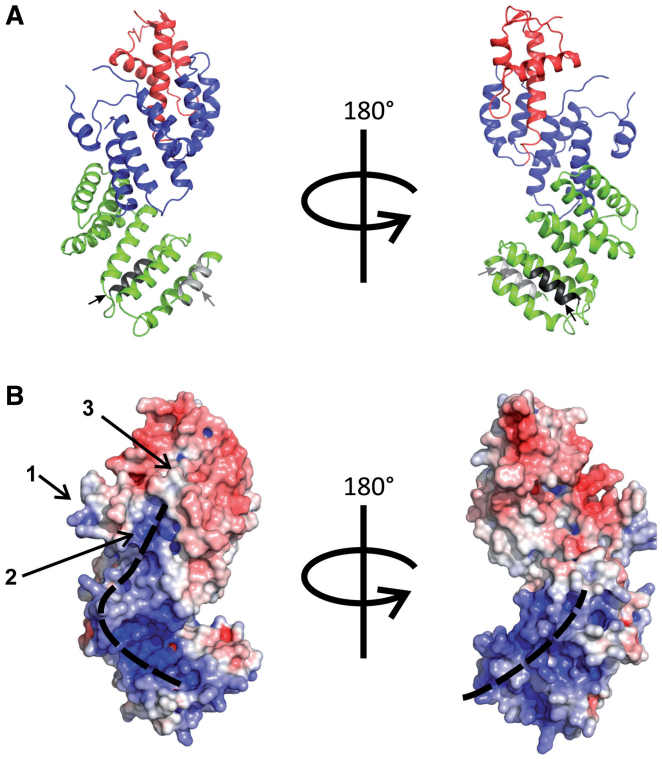

Figure 7. A proposed model of the entire a/TIF32-NTD. The crystal structure (residues 276–494) was extended by a homology-based prediction of residues 1–275. (**A**) The ribbon representation of the chimeric molecule. The WH and HB sub-domains of the crystal structure and the predicted helical extension are depicted in red, blue and green, respectively. Within the predicted region, Box6 (residues 51–60) and Box17 (residues 161–170) (see the text for details) are shown in light and dark gray, respectively, and are further marked by arrows of the same color. (**B**) Surface charge distribution of the chimeric molecule as calculated by APBS (61) plugin in PyMol (The PyMOL Molecular Graphics System, Version 1.0r1 Schrödinger, LLC.) shows the dominance of the basic side chains over the surface of the N-terminal helical extension (the predicted model). Two major patches of positive charges on opposite sides of the molecule are marked. Three major positive patches on the surface of the crystal structure are shown (left; 1, 2 and 3; the latter is created by the juxtaposition of residues R363, K364 and R431—see the text for details), which collectively form a basic area that aligns with the continuous basic patch on the front side of the N-terminal extension.

short α-helix connecting helices 3 and 4 of the PCI domain harbors several positively charged side chains, rendering it relatively basic (region 1, Figure 7B). Adjacent to this region is another patch of positive charge density on the concaved side of the structure made by K304, K305 and K308 of helix 2 (region 2, Figure 7B), followed by the last, only modestly basic region created by the juxtaposition of residues R363, K364 and R431 at the site where the HB joins the WH (region 3, Figure 7B). Together, these three regions constitute an overall basic area, which is, to some extent, aligned with the continuous positive charges on the surface of the modeled N-terminal fragment. Note that the first two of the latter residues from region 3 were experimentally implicated in promoting the mRNA loading to the 43S PICs *in vivo* (Figure 6). Moreover, 10-Ala substitutions of Box20 (the back RNA track of the NTD containing R194, R195 and K196), Box24 (the front RNA

track containing R235), Box27 and Box29 (along the front RNA track below region 2 containing K268 and K288, respectively), Box31 (region 2 containing K304, K305 and K308) and Box35 (region 1 containing R350) produced lethal phenotypes (summarized in Figure 1B), indicating that they might be critical for mRNA recruitment. Although we cannot rule out a lot simpler explanation for the observed lethality—a defect in protein folding—the fact that no other Box mutants (with the only exception of Box38), including those in the PCI domain, were deleterious may speak in favor of a defect in RNA binding. Taken altogether, it is tempting to speculate that both the N-terminal and PCI domains of a/TIF32 promote mRNA recruitment in a co-operative manner, with the a/TIF32$^{1–276}$ part probably making a bigger contribution to the overall binding. This is, in fact, consistent with our observations that neither the crystallized PCI fragment alone nor the N-terminal domain of a/TIF32 displayed any RNA-binding activity in solution, whereas the entire N-terminal half of a/TIF32 encompassing both of these domains did bind to the transcribed mRNA *in vitro* (Figure 5D).

DISCUSSION

We reported previously that depletion of the entire eIF3 complex from cells impaired model *RPL41A* mRNA recruitment *in vivo* (14) and, furthermore, yeast eIF3 was later demonstrated to play a direct role in 43S PIC binding to capped, native mRNA *in vitro*, being even more critical than eIF4F and eIF4B (15). In this study, we showed that Ala substitutions in the α-helix 4 of the HB subdomain of the N-terminal PIC domain of a/TIF32, the crystal structure of which was solved at 2.65-Å resolution, robustly reduce the recruitment of three model mRNAs to the 43S PICs *in vivo* as the only detectable defect. Thus, these findings strongly suggest that this region of the a/TIF32-PCI significantly contributes to the formation of 48S PICs. In addition, our observation that several 10-Ala substitutions specifically mapping onto the mutually interconnected basic patches that we predicted to constitute the a/TIF32-NTD surface (Figure 7B; one of the patches includes the HB α helix 4) result in lethality further supports the idea that the entire N-terminal half of a/TIF32 is significantly involved in mRNA loading onto the 43S PICs, although we cannot rule out the protein folding effects. Importantly, in our recent study (17), substitutions in the KERR motif in the HLD located at the C-terminal half of the a/TIF32 were also shown to impair 40S-binding of model mRNA to the 43S PICs. However, in contrast to the PCI substitutions characterized here, the HLD substitutions also produced phenotypes indicating reduced efficiency of scanning and AUG recognition. Hence, to our knowledge, this is the first report implicating a specific domain of an initiation factor solely in this key role *in vivo*.

Actually, the additional post-assembly phenotypes associated with the HLD versus PCI substitutions can be most likely attributed to the fact that the CTD of a/TIF32 interacts *in vitro* with an 18S rRNA segment containing h16–h18 (64) and with RPS2 and RPS3 (17), all occurring nearby the mRNA entry pore on the solvent side of the 40S subunit (47) (Figure 8). It is believed that RPS3 plays a key role in opening and closing of the mRNA entry channel latch, stabilizing the closed position by interacting with h34 but interacting with h16 on the solvent side of the 40S subunit to promote the open-latch conformation (65). These latch movements are believed to play a critical role for the initial mRNA loading onto the 43S PICs and/or during the subsequent start codon selection process (65,66). Based on that, we naturally proposed that the a/TIF32-CTD can, by interacting with RPS3, h16 or h18, modulate the mRNA entry channel latch as a way of influencing the transition from open to closed PIC conformations during mRNA loading and scanning for AUG recognition (17). In support, hydroxyl radical cleavage mapping of mammalian eIF3 in the 48S PICs also suggested that proportions of its eIF3a and eIF3d subunits interact with h16 (67). Ribosomal location of the a/TIF32-PCI domain can be, on the other hand, predicted from the well-established interaction between RPS0A and the a/TIF32 segment spanning residues 201–400 (2,46,64). Incidentally, a significant contributor to this binding is the C-terminal tail of RPS0A, which is highly acidic (46), indicating an ionic character of its interaction with the basic a/TIF32-NTD. Consistently, a subunit of rabbit eIF3 was only recently predicted to contact RPS1 and 26 that are both situated next to RPS0 (29). Importantly, RPS0A occurs near the mRNA exit not the entry pore (Figure 8); i.e. relatively far from the 'latch feature' that thus should not be affected by the PCI mutations. In agreement, no phenotypes indicating dramatic post-assembly defects were observed using the *GCN4* translational mechanism as a genetic tool.

In detail, we found two basic residues (R363 and K364) located at the beginning of helix 4, which together with R431 of helix 7 constitute a positively charged patch on the surface of a/TIF32-PCI domain (Figure 7B, region 3). To test whether the mRNA recruitment defect observed for the Ala substitution of the entire helix 4 (in Box37) originates from the perturbation of this basic surface, each of these Box37 residues was mutated to Ala. Both *R363A* and *K364A* mutations did impair the recruitment of *RPL41A* mRNA to the 43S PICs *in vivo*, with the latter displaying a more pronounced defect than *Box37* and *R363A* (Figure 6). Attempts to purify the N-terminal half of a/TIF32 harboring *Box37*, *R363A* or *R363A K364A* mutations to examine the effects of helix 4 mutations on the *in vitro* RNA-binding property of the a/TIF32-NTD yielded poorly expressed and/or largely insoluble proteins in the bacterial expression strains that we used. Poor expression and insolubility could be attributed to problems in the folding of the a/TIF32-PCI domain, as R363 plays an important role in bringing helices 4, 5 and 7 together and maintaining the proper relative orientation of the WH and HB subdomains (Figure 3B). However, the folding problem in the context of the entire a/TIF32 would be most likely only minor provided that *Box37* dramatically affects neither the integrity of eIF3 nor the assembly of the MFC *in vivo*. Nevertheless, it is still possible that some minor misfolding stands behind the

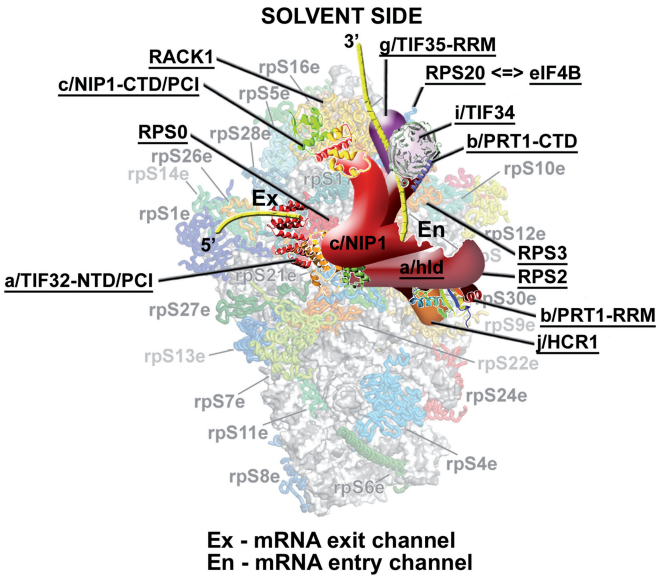

Figure 8. A model of eIF3 on the 40S ribosome spanning the mRNA exit and entry channels. The crystal structure of the 40S subunit is shown from the solvent side with ribosomal proteins shown as cartoons in individual colors; rRNA is shown as gray surface [adapted from (47)]. A hypothetical location of *Saccharomyces cerevisiae* eIF3 on the back side of the 40S subunit is based on the published interactions between RACK1 and the c/NIP1-CTD/PCI (34); RPS0 and the a/TIF32-NTD/PCI (2,46,64); RPS2 and j/HCR1 (24); RPS2 and 3 and the a/TIF32-CTD (17); helices 16-18 of 18S rRNA and the a/TIF32-CTD (64); and RPS3 and 20 and g/TIF35 (19). The extreme N- and C-terminal domains of c/NIP1 and a/TIF32, respectively, are predicted to interact with the interface side of the 40S subunit (64), as hinted. The recently published interaction between RPS20 and eIF4B is indicated by a double-headed arrow (69). Positions of all eIF3 subunits as well as RACK1, RPS0, 2, 3 and 20 are highlighted in bold. Schematic representations of i/TIF34 bound to the b/PRT1-CTD, the b/PRT1-RRM, the a/TIF32-NTD/PCI and the c/NIP1-CTD/PCI were replaced with the X-ray structures (25,30) or the 3D structural model (34), respectively. The yellow lines represent mRNA.

observed differences in the degree of impairment of mRNA recruitment in *Box37* and *R363A* versus *K364A* mutants. It could perhaps indirectly affect some step preceding mRNA binding that would thus become rate-limiting and specifically reduce the net effect on the mRNA recruitment impairment in *Box37* and *R363A* mutants. In contrast to R363, K364 is fully exposed to the solvent and therefore less critical for the folding of the a/TIF32-PCI domain, if at all. Consistently, its Ala substitution produced a soluble protein that, however, did not show any significant effect in our *in vitro* RNA-binding assay (data not shown). The ostensible paradox that *K364A* resulted in severe impairment of mRNA recruitment *in vivo* but did not affect the a/TIF32-NTD RNA binding *in vitro* could be explained by proposing that either our RNA-binding assay is not sensitive enough to detect the impact of *K364A* on the a/TIF32 ability to directly interact with mRNAs, or that the undisputable contribution of K364 to mRNA recruitment is indirect. In the latter case, it could be exerted in co-operation with other mRNA binding and recruitment-promoting eIFs, such as those associated with eIF4G, which most probably also bind to the solvent-exposed side of the 48S PICs as eIF3 does, at least based on their predicted locations [reviewed in (1)]. For example, this region of a/TIF32 could contact 18S rRNA (rather than mRNA) in such a way that it is not required to anchor eIF3 to the ribosome but to make 40S-bound eIF3 to adopt an 'RNA-recruitment-competent' conformation to enable stable binding of incoming mRNA-bound eIF4F complex to start scanning.

Along these lines, the ribosomal position of yeast eIF4B—a factor previously implicated in promoting ribosomal scanning by stimulating the helicase activity of eIF4A and by holding on to the single-stranded regions created by eIF4A (68)—has been only recently mapped. It was shown to interact *in vitro* with RPS20 (69) that is situated on the 40S head right above the mRNA entry pore (47) (Figure 8); its head-location around RPS20 was also corroborated by hydroxyl radical probing. The tight 40S-binding of eIF4B was then demonstrated to play a critical role in its novel unexpected role in promoting mRNA recruitment to 43S PICs. Interestingly, eIF4B interacts with g/TIF35 (70), earlier implicated in promoting processivity of scanning through stable secondary structures (19), and g/TIF35 in turn interacts with RPS20 and also RPS3 (19). Recently, we proposed that the scaffold b/PRT1 subunit serves to connect two eIF3 modules at each of its termini: (i) a/TIF32-HLD-CTD–j/HCR1 at the N-terminal RRM and (ii) i/TIF34–g/TIF35 at the extreme C-terminal α-helix, both of which surround the mRNA entry pore working together to fine-tune scanning and the AUG selection process (25) (Figure 8). Hence, it is tempting to speculate that although these two modules co-operate with eIF4B (via its contacts with g/TIF35 and RPS20) and possibly also with eIF4A in stimulating mRNA recruitment and promoting scanning for AUG, the a/TIF32-PCI co-operates with eIF4G—since time immemorial implicated in bridging the 40S–mRNA contact—to ensure mRNA loading onto the 43S PIC as their primary role. In fact, recent mutational analysis of yeast eIF4G showed that two of its functionally important RNA-binding elements, RNA2 and RNA3, do not critically contribute to formation of the eIF4G–PABP mRNPs suggesting that they could contribute to the function of eIF4G in recruitment of the 43S PIC to mRNAs (71), perhaps hand in hand with the a/TIF32-PCI and other factors. Even though the interaction between eIF3 and eIF4G has never been shown in yeast, in contrast to mammals (6,72), it does not mean that it cannot be established directly in the PIC or that eIF4G and a/TIF32-PCI could not work together without actually being bound to each other. In fact, earlier findings showing that several eIF3 subunits can directly interact with mRNA (2,19,34,67,73,74) may suggest that incoming mRNA is 'grabbed by many hands'—some more, some less contributory—that could be physically and spatially independent of each other; however, collectively they would ensure proper and timely mRNA delivery to the mRNA-binding channel of the 40S ribosomes. Alternatively, as proposed before, the eIF3–eIF4G contact could be bridged by eIF5, which simultaneously interacts with eIF4G and with the extreme NTD of the c/NIP1 subunit of eIF3 (9,26). However, given the fact

that eIF5 is most likely situated on the interface side of the 40S (75), whereas eIF4G is expected to occur on its solvent-exposed side [see (1) for the current view of factor's occupancy on the 40S subunit], this possibility seems unlikely. Furthermore, the stimulatory function of eIF5 on mRNA recruitment to the PIC was not observed in a reconstituted yeast system (15) and a mutation in the eIF5-CTD that disrupts its interaction with eIF4G impaired 43S binding to mRNA only *in vitro* (9). Hence, the eIF5 contribution to this important initiation step, if any, awaits further examination. Without a doubt, detailed structural information about interactions of eIF3 subunits with the 40S ribosome, mRNA and other eIFs including eIF4B and eIF4G will be essential in deciphering molecular details of their critical roles in 43S attachment to mRNA.

Finally, we previously identified two N-terminal mutations in *tif32-Box6* and *17*, which produce the severe Gcn$^-$ phenotype in an additive manner by disturbing the ability of 40S ribosomes to resume scanning after translating uORF1 to reinitiate on *GCN4* (36). Here we predict that they are both located close to two basic patches on the surface of the modeled N-terminal domain of a/TIF32 (Figure 7A). This supports our earlier proposal that both Boxes specifically contact reinitiation-promoting elements (RPEs) occurring in the 5′ UTR of uORF1 in the *GCN4* mRNA leader to stabilize the 40S subunit on uORF1 post-termination to resume scanning for efficient reinitiation downstream. Furthermore, it also indicates that in addition to this specific role, both segments may also non-specifically contact all cellular mRNAs and thus contribute to their recruitment to the 43S PICs.

ACCESSION NUMBERS

The atomic coordinates have been deposited in the Protein Data Bank, www.rcsb.org (PDB ID code 4K51).

SUPPLEMENTARY DATA

Supplementary Data are available at NAR Online.

ACKNOWLEDGEMENTS

The authors are thankful to Béla Szamecz and István Danyi for help with cloning, to the laboratory of Petr Svoboda from IMG ASCR in Prague for their help with qPCR experiments and to all members of our laboratories for insightful discussions. The authors also thank Helmholtz-Zentrum Berlin (HZB, Germany) for the allocation of synchrotron radiation beamtime and for financial support.

FUNDING

The Wellcome Trust [090812/Z/09/Z to L.S.V.]; Czech Science Foundation [305/10/0335 to L.S.V.]. Funding for open access charge: Wellcome Trust.

Conflict of interest statement. None declared.

REFERENCES

1. Valášek,L.S. (2012) 'Ribozoomin' – Translation initiation from the perspective of the ribosome-bound Eukaryotic Initiation Factors (eIFs). *Curr. Protein Pept. Sci.*, **13**, 305–330.
2. Szamecz,B., Rutkai,E., Cuchalova,L., Munzarova,V., Herrmannova,A., Nielsen,K.H., Burela,L., Hinnebusch,A.G. and Valášek,L. (2008) eIF3a cooperates with sequences 5′ of uORF1 to promote resumption of scanning by post-termination ribosomes for reinitiation on GCN4 mRNA. *Genes Dev.*, **22**, 2414–2425.
3. Pöyry,T.A., Kaminski,A. and Jackson,R.J. (2004) What determines whether mammalian ribosomes resume scanning after translation of a short upstream open reading frame? *Genes Dev.*, **18**, 62–75.
4. Imataka,H., Gradi,A. and Sonenberg,N. (1998) A newly identified N-terminal amino acid sequence of human eIF4G binds poly (A)-binding protein and functions in poly(A)-dependent translation. *EMBO J.*, **17**, 7480–7489.
5. Imataka,H. and Sonenberg,N. (1997) Human eukaryotic translation initiation factor 4G (eIF4G) possesses two separate and independent binding sites for eIF4A. *Mol. Cell. Biol.*, **17**, 6940–6947.
6. Korneeva,N.L., Lamphear,B.J., Hennigan,F.L. and Rhoads,R.E. (2000) Mutually cooperative binding of eukaryotic translation initiation factor (eIF) 3 and eIF4A to human eIF4G-1. *J. Biol. Chem.*, **275**, 41369–41376.
7. Lamphear,B.J., Kirchweger,R., Skern,T. and Rhoads,R.E. (1995) Mapping of functional domains in eukaryotic protein synthesis initiation factor 4G (eIF4G) with picornaviral proteases. *J. Biol. Chem.*, **270**, 21975–21983.
8. Morino,S., Imataka,H., Svitkin,Y.V., Pestova,T.V. and Sonenberg,N. (2000) Eukaryotic translation initiation factor 4E (eIF4E) binding site and the middle one-third of eIF4GI constitute the core domain for cap-dependent translation, and the C-terminal one-third functions as a modulatory region. *Mol. Cell. Biol.*, **20**, 468–477.
9. Asano,K., Shalev,A., Phan,L., Nielsen,K., Clayton,J., Valášek,L., Donahue,T.F. and Hinnebusch,A.G. (2001) Multiple roles for the carboxyl terminal domain of eIF5 in translation initiation complex assembly and GTPase activation. *EMBO J.*, **20**, 2326–2337.
10. Hinton,T.M., Coldwell,M.J., Carpenter,G.A., Morley,S.J. and Pain,V.M. (2007) Functional analysis of individual binding activities of the scaffold protein eIF4G. *J. Biol. Chem.*, **282**, 1695–1708.
11. Ramirez-Valle,F., Braunstein,S., Zavadil,J., Formenti,S.C. and Schneider,R.J. (2008) eIF4GI links nutrient sensing by mTOR to cell proliferation and inhibition of autophagy. *J. Cell Biol.*, **181**, 293–307.
12. Park,E.H., Zhang,F., Warringer,J., Sunnerhagen,P. and Hinnebusch,A.G. (2011) Depletion of eIF4G from yeast cells narrows the range of translational efficiencies genome-wide. *BMC Genomics*, **12**, 68.
13. Clarkson,B.K., Gilbert,W.V. and Doudna,J.A. (2010) Functional overlap between eIF4G isoforms in *Saccharomyces cerevisiae*. *PLoS One*, **5**, e9114.
14. Jivotovskaya,A., Valášek,L., Hinnebusch,A.G. and Nielsen,K.H. (2006) Eukaryotic translation initiation factor 3 (eIF3) and eIF2 can promote mRNA binding to 40S subunits independently of eIF4G in yeast. *Mol. Cell. Biol.*, **26**, 1355–1372.
15. Mitchell,S.F., Walker,S.E., Algire,M.A., Park,E.-H., Hinnebusch,A.G. and Lorsch,J.R. (2010) The 5′-7-methylguanosine cap on eukaryotic mRNAs serves both to stimulate canonical translation initiation and to block an alternative pathway. *Mol. Cell*, **39**, 950–962.
16. Sonenberg,N. and Hinnebusch,A.G. (2009) Regulation of translation initiation in eukaryotes: mechanisms and biological targets. *Cell*, **136**, 731–745.
17. Chiu,W.-L., Wagner,S., Herrmannová,A., Burela,L., Zhang,F., Saini,A.K., Valášek,L. and Hinnebusch,A.G. (2010) The C-terminal region of eukaryotic translation initiation factor 3a (eIF3a) promotes mRNA recruitment, scanning, and, together with eIF3j and the eIF3b RNA recognition motif, selection of AUG start codons. *Mol. Cell. Biol.*, **30**, 4415–4434.

18. Valášek,L., Nielsen,K.H. and Hinnebusch,A.G. (2002) Direct eIF2-eIF3 contact in the multifactor complex is important for translation initiation *in vivo*. *EMBO J.*, **21**, 5886–5898.
19. Cuchalová,L., Kouba,T., Herrmannová,A., Danyi,I., Chiu,W.-l. and Valášek,L. (2010) The RNA recognition motif of eukaryotic translation initiation factor 3g (eIF3g) is required for resumption of scanning of posttermination ribosomes for reinitiation on GCN4 and together with eIF3i stimulates linear scanning. *Mol. Cell. Biol.*, **30**, 4671–4686.
20. Nielsen,K.H., Szamecz,B., Valasek,L.J., Jivotovskaya,A., Shin,B.S. and Hinnebusch,A.G. (2004) Functions of eIF3 downstream of 48S assembly impact AUG recognition and GCN4 translational control. *EMBO J.*, **23**, 1166–1177.
21. Valášek,L., Nielsen,K.H., Zhang,F., Fekete,C.A. and Hinnebusch,A.G. (2004) Interactions of eukaryotic translation initiation factor 3 (eIF3) subunit NIP1/c with eIF1 and eIF5 promote preinitiation complex assembly and regulate start codon selection. *Mol. Cell. Biol.*, **24**, 9437–9455.
22. Kovarik,P., Hašek,J., Valášek,L. and Ruis,H. (1998) RPG1: an essential gene of *saccharomyces cerevisiae* encoding a 110-kDa protein required for passage through the G1 phase. *Curr. Genet.*, **33**, 100–109.
23. Nielsen,K.H., Valášek,L., Sykes,C., Jivotovskaya,A. and Hinnebusch,A.G. (2006) Interaction of the RNP1 motif in PRT1 with HCR1 promotes 40S binding of eukaryotic initiation factor 3 in yeast. *Mol. Cell. Biol.*, **26**, 2984–2998.
24. ElAntak,L., Wagner,S., Herrmannová,A., Karásková,M., Rutkai,E., Lukavsky,P.J. and Valášek,L. (2010) The indispensable N-terminal half of eIF3j co-operates with its structurally conserved binding partner eIF3b-RRM and eIF1A in stringent AUG selection. *J. Mol. Biol.*, **396**, 1097–1116.
25. Herrmannová,A., Daujotyte,D., Yang,J.C., Cuchalová,L., Gorrec,F., Wagner,S., Danyi,I., Lukavsky,P.J. and Valášek,L.S. (2012) Structural analysis of an eIF3 subcomplex reveals conserved interactions required for a stable and proper translation pre-Initiation complex assembly. *Nucleic Acids Res.*, **40**, 2294–2311.
26. Karaskova,M., Gunisova,S., Herrmannova,A., Wagner,S., Munzarova,V. and Valasek,L.S. (2012) Functional characterization of the role of the N-terminal domain of the c/Nip1 subunit of eukaryotic initiation factor 3 (eIF3) in AUG recognition. *J. Biol. Chem.*, **287**, 28420–28434.
27. Beznosková,P., Cuchalová,L., Wagner,S., Shoemaker,C.J., Gunišová,S., Von der Haar,T. and Valášek,L.S. (2013) Translation initiation factors eIF3 and HCR1 control translation termination and stop codon read-through in yeast cells. *PLoS Genet.*, **9**, e1003962.
28. Querol-Audi,J., Sun,C., Vogan,J.M., Smith,M.D., Gu,Y., Cate,J.H. and Nogales,E. (2013) Architecture of human translation initiation factor 3. *Structure*, **21**, 920–928.
29. Hashem,Y., des Georges,A., Dhote,V., Langlois,R., Liao,H.Y., Grassucci,R.A., Hellen,C.U., Pestova,T.V. and Frank,J. (2013) Structure of the mammalian ribosomal 43S preinitiation complex bound to the scanning factor DHX29. *Cell*, **153**, 1108–1119.
30. Khoshnevis,S., Neumann,P. and Ficner,R. (2010) Crystal structure of the RNA recognition motif of yeast translation initiation factor eIF3b reveals differences to human eIF3b. *PLoS One*, **5**, e12784.
31. ElAntak,L., Tzakos,A.G., Locker,N. and Lukavsky,P.J. (2007) Structure of eIF3b RNA recognition motif and its interaction with eIF3j: structural insights into the recruitment of eIF3b to the 40 S ribosomal subunit. *J. Biol. Chem.*, **282**, 8165–8174.
32. Wei,Z., Xue,Y., Xu,H. and Gong,W. (2006) Crystal structure of the C-terminal domain of *S.cerevisiae* eIF5. *J. Mol. Biol.*, **359**, 1–9.
33. Pick,E., Hofmann,K. and Glickman,M.H. (2009) PCI complexes: beyond the proteasome, CSN, and eIF3 troika. *Mol. Cell*, **35**, 260–264.
34. Kouba,T., Rutkai,E., Karasková,M. and Valášek,L.S. (2012) The eIF3c/NIP1 PCI domain interacts with RNA and RACK1/ASC1 and promotes assembly of the pre-initiation complexes. *Nucleic Acids Res.*, **40**, 2683–2699.
35. Ellisdon,A.M., Dimitrova,L., Hurt,E. and Stewart,M. (2012) Structural basis for the assembly and nucleic acid binding of the TREX-2 transcription-export complex. *Nat. Struct. Mol. Biol.*, **19**, 328–336.
36. Munzarová,V., Pánek,J., Gunišová,S., Dányi,I., Szamecz,B. and Valášek,L.S. (2011) Translation reinitiation relies on the interaction between eIF3a/TIF32 and progressively folded cis-acting mRNA elements preceding short uORFs. *PLoS Genet.*, **7**, e1002137.
37. Mueller,U., Darowski,N., Fuchs,M.R., Forster,R., Hellmig,M., Paithankar,K.S., Puhringer,S., Steffien,M., Zocher,G. and Weiss,M.S. (2012) Facilities for macromolecular crystallography at the Helmholtz-Zentrum Berlin. *J. Synchrotron Radiat.*, **19**, 442–449.
38. Kabsch,W. (2010) Integration, scaling, space-group assignment and post-refinement. *Acta Crystallogr. D Biol. Crystallogr.*, **66**, 133–144.
39. Kabsch,W. (2010) Xds. *Acta Crystallogr. D Biol. Crystallogr.*, **66**, 125–132.
40. Vonrhein,C., Blanc,E., Roversi,P. and Bricogne,G. (2007) Automated structure solution with autoSHARP. *Methods Mol. Biol.*, **364**, 215–230.
41. Sheldrick,G.M. (2010) Experimental phasing with SHELXC/D/E: combining chain tracing with density modification. *Acta Crystallogr. D Biol. Crystallogr.*, **66**, 479–485.
42. Abrahams,J.P. and Leslie,A.G. (1996) Methods used in the structure determination of bovine mitochondrial F1 ATPase. *Acta Crystallogr. D Biol. Crystallogr.*, **52**, 30–42.
43. Langer,G., Cohen,S.X., Lamzin,V.S. and Perrakis,A. (2008) Automated macromolecular model building for X-ray crystallography using ARP/wARP version 7. *Nat. Protoc.*, **3**, 1171–1179.
44. Acker,M.G., Kolitz,S.E., Mitchell,S.F., Nanda,J.S. and Lorsch,J.R. (2007) *Methods in Enzymology*, Vol. 430. Academic Press, pp. 111–145.
45. Khoshnevis,S., Hauer,F., Milon,P., Stark,H. and Ficner,R. (2012) Novel insights into the architecture and protein interaction network of yeast eIF3. *RNA*, **18**, 2306–2319.
46. Kouba,T., Danyi,I., Gunišová,S., Munzarová,V., Vlčková,V., Cuchalová,L., Neueder,A., Milkereit,P. and Valášek,L.S. (2012) Small ribosomal protein RPS0 stimulates translation initiation by mediating 40S-binding of eIF3 via its direct contact with the eIF3a/TIF32 subunit. *PLoS One*, **7**, e40464.
47. Rabl,J., Leibundgut,M., Ataide,S.F., Haag,A. and Ban,N. (2011) Crystal structure of the eukaryotic 40S ribosomal subunit in complex with initiation factor 1. *Science*, **331**, 730–736.
48. Valášek,L., Szamecz,B., Hinnebusch,A.G. and Nielsen,K.H. (2007) *In vivo* stabilization of preinitiation complexes by formaldehyde cross-linking. *Methods Enzymol.*, **429**, 163–183.
49. Hinnebusch,A.G. (2005) Translational regulation of GCN4 and the general amino acid control of yeast. *Annu. Rev. Microbiol.*, **59**, 407–450.
50. Fekete,C.A., Mitchell,S.F., Cherkasova,V.A., Applefield,D., Algire,M.A., Maag,D., Saini,A.K., Lorsch,J.R. and Hinnebusch,A.G. (2007) N- and C-terminal residues of eIF1A have opposing effects on the fidelity of start codon selection. *EMBO J.*, **26**, 1602–1614.
51. Singh,C.R., Watanabe,R., Chowdhury,W., Hiraishi,H., Murai,M.J., Yamamoto,Y., Miles,D., Ikeda,Y., Asano,M. and Asano,K. (2012) Sequential eukaryotic translation initiation factor 5 (eIF5) binding to the charged disordered segments of eIF4G and eIF2beta stabilizes the 48S preinitiation complex and promotes its shift to the initiation mode. *Mol. Cell. Biol.*, **32**, 3978–3989.
52. Karplus,P.A. and Diederichs,K. (2012) Linking crystallographic model and data quality. *Science*, **336**, 1030–1033.
53. Ashkenazy,H., Penn,O., Doron-Faigenboim,A., Cohen,O., Cannarozzi,G., Zomer,O. and Pupko,T. (2012) FastML: a web server for probabilistic reconstruction of ancestral sequences. *Nucleic Acids Res.*, **40**, W580–W584.
54. Pathare,G.R., Nagy,I., Bohn,S., Unverdorben,P., Hubert,A., Korner,R., Nickell,S., Lasker,K., Sali,A., Tamura,T. *et al.* (2012) The proteasomal subunit Rpn6 is a molecular clamp holding the core and regulatory subcomplexes together. *Proc. Natl Acad. Sci. USA*, **109**, 149–154.

55. Dessau,M., Halimi,Y., Erez,T., Chomsky-Hecht,O., Chamovitz,D.A. and Hirsch,J.A. (2008) The *Arabidopsis* COP9 signalosome subunit 7 is a model PCI domain protein with subdomains involved in COP9 signalosome assembly. *Plant Cell*, **20**, 2815–2834.
56. Wei,Z., Zhang,P., Zhou,Z., Cheng,Z., Wan,M. and Gong,W. (2004) Crystal structure of human eIF3k, the first structure of eIF3 subunits. *J. Biol. Chem.*, **279**, 34983–34990.
57. Ellisdon,A.M. and Stewart,M. (2012) Structural biology of the PCI-protein fold. *Bioarchitecture*, **2**.
58. Asano,K., Phan,L., Anderson,J. and Hinnebusch,A.G. (1998) Complex formation by all five homologues of mammalian translation initiation factor 3 subunits from yeast *Saccharomyces cerevisiae*. *J. Biol. Chem.*, **273**, 18573–18585.
59. Valášek,L., Phan,L., Schoenfeld,L.W., Valášková,V. and Hinnebusch,A.G. (2001) Related eIF3 subunits TIF32 and HCR1 interact with an RNA recoginition motif in PRT1 required for eIF3 integrity and ribosome binding. *EMBO J.*, **20**, 891–904.
60. Gajiwala,K.S. and Burley,S.K. (2000) Winged helix proteins. *Curr. Opin. Struct. Biol.*, **10**, 110–116.
61. Baker,N.A., Sept,D., Joseph,S., Holst,M.J. and McCammon,J.A. (2001) Electrostatics of nanosystems: application to microtubules and the ribosome. *Proc. Natl Acad. Sci. USA*, **98**, 10037–10041.
62. Kelley,L.A. and Sternberg,M.J.E. (2009) Protein structure prediction on the Web: a case study using the Phyre server. *Nat. Protoc.*, **4**, 363–371.
63. Ritchie,D.W., Kozakov,D. and Vajda,S. (2008) Accelerating and focusing protein-protein docking correlations using multi-dimensional rotational FFT generating functions. *Bioinformatics*, **24**, 1865–1873.
64. Valášek,L., Mathew,A., Shin,B.S., Nielsen,K.H., Szamecz,B. and Hinnebusch,A.G. (2003) The yeast eIF3 subunits TIF32/a and NIP1/c and eIF5 make critical connections with the 40S ribosome *in vivo*. *Genes Dev.*, **17**, 786–799.
65. Passmore,L.A., Schmeing,T.M., Maag,D., Applefield,D.J., Acker,M.G., Algire,M.A., Lorsch,J.R. and Ramakrishnan,V. (2007) The eukaryotic translation initiation factors eIF1 and eIF1A induce an open conformation of the 40S ribosome. *Mol. Cell*, **26**, 41–50.
66. Lomakin,I.B. and Steitz,T.A. (2013) The initiation of mammalian protein synthesis and mRNA scanning mechanism. *Nature*, **500**, 307–311.
67. Pisarev,A.V., Kolupaeva,V.G., Yusupov,M.M., Hellen,C.U.T. and Pestova,T.V. (2008) Ribosomal position and contacts of mRNA in eukaryotic translation initiation complexes. *EMBO J.*, **27**, 1609–1621.
68. Rogers,G.W. Jr, Richter,N.J., Lima,W.F. and Merrick,W.C. (2001) Modulation of the helicase activity of eIF4A by eIF4B, eIF4H, and eIF4F. *J. Biol. Chem.*, **276**, 30914–30922.
69. Walker,S.E., Zhou,F., Mitchell,S.F., Larson,V.S., Valasek,L., Hinnebusch,A.G. and Lorsch,J.R. (2013) Yeast eIF4B binds to the head of the 40S ribosomal subunit and promotes mRNA recruitment through its N-terminal and internal repeat domains. *RNA*, **19**, 191–207.
70. Vornlocher,H.P., Hanachi,P., Ribeiro,S. and Hershey,J.W.B. (1999) a 110-kilodalton subunit of translation initiation factor eIF3 and an associated 135-kilodalton protein are encoded by the *Saccharomyces cerevisiae* TIF32 and TIF31 genes. *J. Biol. Chem.*, **274**, 16802–16812.
71. Park,E.-H., Walker,S.E., Lee,J.M., Rothenburg,S., Lorsch,J.R. and Hinnebusch,A.G. (2010) Multiple elements in the eIF4G1 N-terminus promote assembly of eIF4G1[bull]PABP mRNPs *in vivo*. *EMBO J.*, **30**, 302–316.
72. LeFebvre,A.K., Korneeva,N.L., Trutschl,M., Cvek,U., Duzan,R.D., Bradley,C.A., Hershey,J.W. and Rhoads,R. (2006) Translation initiation factor eIF4G-1 binds to eIF3 through the eIF3e subunit. *J. Biol. Chem.*, **281**, 22917–22932.
73. Asano,K., Kinzy,T.G., Merrick,W.C. and Hershey,J.W.B. (1997) Conservation and diversity of eukaryotic translation initiation factor eIF3. *J. Biol. Chem.*, **272**, 1101–1109.
74. Block,K.L., Vornlocher,H.P. and Hershey,J.W.B. (1998) Characterization of cDNAs encoding the p44 and p35 subunits of human translation initiation factor eIF3. *J. Biol. Chem.*, **273**, 31901–31908.
75. Luna,R.E., Arthanari,H., Hiraishi,H., Nanda,J., Martin-Marcos,P., Markus,M.A., Akabayov,B., Milbradt,A.G., Luna,L.E., Seo,H.C. *et al.* (2012) The C-terminal domain of eukaryotic initiation factor 5 promotes start codon recognition by its dynamic interplay with eIF1 and eIF2beta. *Cell Rep.*, **1**, 689–702.

PUBLICATION III

Nucleic Acids Research Advance Access published April 29, 2015

doi: 10.1093/nar/gkv421

Translation initiation factor eIF3 promotes programmed stop codon readthrough

Petra Beznosková[1,2], Susan Wagner[1], Myrte Esmeralda Jansen[1], Tobias von der Haar[3] and Leoš Shivaya Valášek[1,*]

[1]Laboratory of Regulation of Gene Expression, Institute of Microbiology ASCR, Videnska 1083, Prague 142 20, the Czech Republic, [2]Faculty of Science, Charles University, Vinicna 5, Prague 128 44, the Czech Republic and [3]School of Biosciences, University of Kent, Kent CT2 7NJ, UK

Received March 17, 2015; Revised April 16, 2015; Accepted April 18, 2015

ABSTRACT

Programmed stop codon readthrough is a post-transcription regulatory mechanism specifically increasing proteome diversity by creating a pool of C-terminally extended proteins. During this process, the stop codon is decoded as a sense codon by a near-cognate tRNA, which programs the ribosome to continue elongation. The efficiency of competition for the stop codon between release factors (eRFs) and near-cognate tRNAs is largely dependent on its nucleotide context; however, the molecular mechanism underlying this process is unknown. Here, we show that it is the translation initiation (not termination) factor, namely eIF3, which critically promotes programmed readthrough on all three stop codons. In order to do so, eIF3 must associate with pre-termination complexes where it interferes with the eRF1 decoding of the third/wobble position of the stop codon set in the unfavorable termination context, thus allowing incorporation of near-cognate tRNAs with a mismatch at the same position. We clearly demonstrate that efficient readthrough is enabled by near-cognate tRNAs with a mismatch only at the third/wobble position. Importantly, the eIF3 role in programmed readthrough is conserved between yeast and humans.

INTRODUCTION

Terminating protein synthesis at the appropriate stop codon is as important as initiating at the proper start codon. During canonical termination the stop codon is decoded by the release factor 1 (eRF1) that enters the A-site of the 80S ribosome in complex with the GTP-binding protein eRF3 (reviewed in (1)). In eukaryotes, eRF1 recognizes all three stop codons (UAA, UAG and UGA) with high precision. However, in some specific cases, not all stop codons signal the proper end of translation, which can thus continue beyond to the next stop codon. Generally speaking, translation termination can be viewed as a competition between stop codon recognition by release factors and stop codon decoding by near-cognate tRNAs. This competition differs genome-wide in its efficiency. The efficiency can be influenced by the identity of the stop codon (2–4), the nucleotide context of the stop codon (5–7), the identity of the last two amino acids incorporated into the polypeptide chain (8), the identity of the P-site tRNA (9) and the presence of stimulatory elements downstream from the stop codon (10–12). All these features increase the odds of the stop codon being decoded by a near-cognate, natural suppressor tRNA rather than by eRF1, resulting in the process termed stop codon readthrough. This allows production of C-terminally extended polypeptides with new or at least modified biological roles compared to their shorter, original versions. The mechanism whereby near-cognate tRNAs outcompete conventional stop codon recognition by eRF1 is not yet known, nor is which protein factors, if any, might be functionally important for stop codon readthrough.

In recent years several groups have proposed that the stop codon readthrough mechanism is specifically regulated by cis-acting RNA elements downstream of the first stop codon that may exist to generate proteome diversity in response to changing environmental conditions. The rapidly growing list of cellular genes under the control of this 'programmed stop codon readthrough' mechanism, the typical, long standing example of which is from the tobacco mosaic virus (TMV) genome (11), strongly suggests that programmed stop codon readthrough is an important contributor to general translational control in all kingdoms of life (for review; see (13–16)). A recent ribosome profiling study detected many readthrough events occurring at biologically relevant levels in budding yeast, fruit fly and human data sets, suggesting that this mechanism is highly conserved (17).

We recently reported that, besides the well-known eukaryotic release factors eRF1 and eRF3, translation termi-

*To whom correspondence should be addressed. Tel: +420 241 062 288; Fax: +420 241 062 665; Email: valasekl@biomed.cas.cz

nation is also regulated by the initiation factor eIF3 and the eIF3-associated protein HCR1, at least in yeast (18). eIF3 is a large multi-subunit protein complex that orchestrates numerous initiation steps in close cooperation with other eIFs (for review see (19,20)) and has been shown to interact with the solvent-exposed side of the 40S ribosomal subunit covering both mRNA entry and exit channels (21–27). We have demonstrated that besides the small ribosomal subunit, eIF3 also associates with the 80S termination complex in an eRF1-dependent manner and, by a yet to be elucidated mechanism, controls stop codon readthrough as several eIF3 mutations decrease its relative efficiency *in vivo*, showing antagonistic effects with mutations in both eRFs (18).

In this study we present data strongly suggesting that eIF3 is a crucial factor promoting programmed stop codon readthrough and describe the molecular mechanism of its action. eIF3, upon binding to programmed pre-termination complexes; i.e. pre-termination complexes on stop codons in unfavorable termination contexts, interferes with decoding of the third stop codon position and thus shifts the equilibrium toward stop codon readthrough by near-cognate tRNAs. As a result, it allows near-cognate tRNAs with a mismatch at the third position to decode the stop codon as a sense codon and continue with polypeptide synthesis. We show that eIF3 acts specifically on genes containing the aforementioned stimulatory elements downstream from the stop codon that are known to promote programmed stop codon readthrough and that this eIF3 function is evolutionary conserved.

MATERIALS AND METHODS

Yeast strains and plasmids

The lists and descriptions of plasmids and yeast strains used throughout this study (summarized in Supplementary Tables S1–S3) can be found in the Supplementary Data.

Stop codon readthrough assays

The majority of stop codon readthrough assays in this study were performed using a standard bicistronic reporter construct (Figure 1A) bearing a *Renilla* luciferase gene followed by an in-frame firefly luciferase gene. Separating the two genes is either a tetranucleotide termination signal (UGAC) or, for control purposes, the CAA sense codon followed by cytosine. In indicated cases the termination signal and/or the following nucleotide context was modified. It is noteworthy that this system avoids possible artifacts associated with changes in the efficiency of translation initiation associated with the the nonsense mediated decay (NMD) pathway (28), because both *Renilla* and firefly enzymes initiate translation from the same AUG codon. For further details please see (29). The experiments and data analysis were carried out according to the microtiter plate-based dual luciferase protocol developed by (30) and commercially distributed by Promega. The samples were processed in quintuplicates and each experiment was repeated at least three times.

Stop codon readthrough measurements with newly developed dual luciferase constructs driven by the HiPV IRES (Figure 1B) were performed essential the same as described above except that the transformed cells were not directly grown in microtiter plates but in Erlenmeyer flasks in 25 ml of the SD media to OD–0.6. The whole cell extracts (WCEs) were prepared in 1× phosphate buffered saline (PBS) supplemented with 1% Triton X-100 using FastPrep Instrument (MP Biomedicals) at the intensity level of 5 in one 40 seconds long cycle. The 10-fold diluted WCEs were then subjected to the aforementioned microtiter plate-based protocol according to the vendor's instruction.

Stop codon readthrough assays in HeLa cells were performed as follows. Cells were grown in 24-well plates in Dulbecco's modified eagle's medium (DMEM) (Sigma; catalog no. D6429) supplemented with 10% fetal bovine serum (FBS) (Sigma; catalog no. F7524). Twenty-four hours after seeding, the cells were transfected with ON-TARGETplus small interfering RNA (siRNA) cocktail systems from Dharmacon/Thermo Scientific (human eIF3a, catalog no. L-019534-00; human eIF3g, catalog no. L-019533-00; nontargeting siRNA, catalog no. D-001810-10) at concentration of 5nM. INTERFERin (Polyplus; catalog no. 409) was used as a transfection reagent and transfections were carried out according to the vendor's instructions (3 μl/well). After 24 h the media was changed. Transfection of the readthrough reporter plasmids was carried out 48 h after the siRNA transfection using TurboFect (Thermo Scientific; catalog no. R0531), according to the vendor's instructions (500 ng of plasmid DNA and 1 μl of Turbofect per each well) in triplicates. One day after this second transfection, the cells were washed in 1× PBS and lysed directly on plate with 1xGlo lysis buffer (Promega; catalog no. E266A). Equal amounts of each lysate were then transferred into two white flat-bottom 96-well plates. One plate was treated with the Bright-Glo Luciferase Assay System (Promega; catalog no. E2620) to measure the firefly luciferase signal according to the vendor's instructions. The other plate was treated with the Renilla-Glo Assay System (Promega; catalog no. E2720/50). Subsequently, the ratio of the firefly to renilla luciferase signal was calculated for each reporter (bearing either UAG or CAG). The actual readthrough value (in%) was obtained as the ratio of the normalized UAG value to the normalized CAG value. This experiment was repeated three times.

Polysomal gradient analysis

The 0.5% formaldehyde (HCHO) cross-linking followed by WCE preparation and fractionation of WCEs for analysis of translational complexes were carried out as described previously (18,31) with the following exceptions. Cycloheximide was added at a concentration of 0.05 mg/ml 5 min before the HCHO treatment, after which the cells were instantly broken by the FastPrep Instrument (MP Biomedicals) at the intensity level of 5 in two consecutive 20 s cycles. The resulting WCEs were separated on 5–45% sucrose gradients.

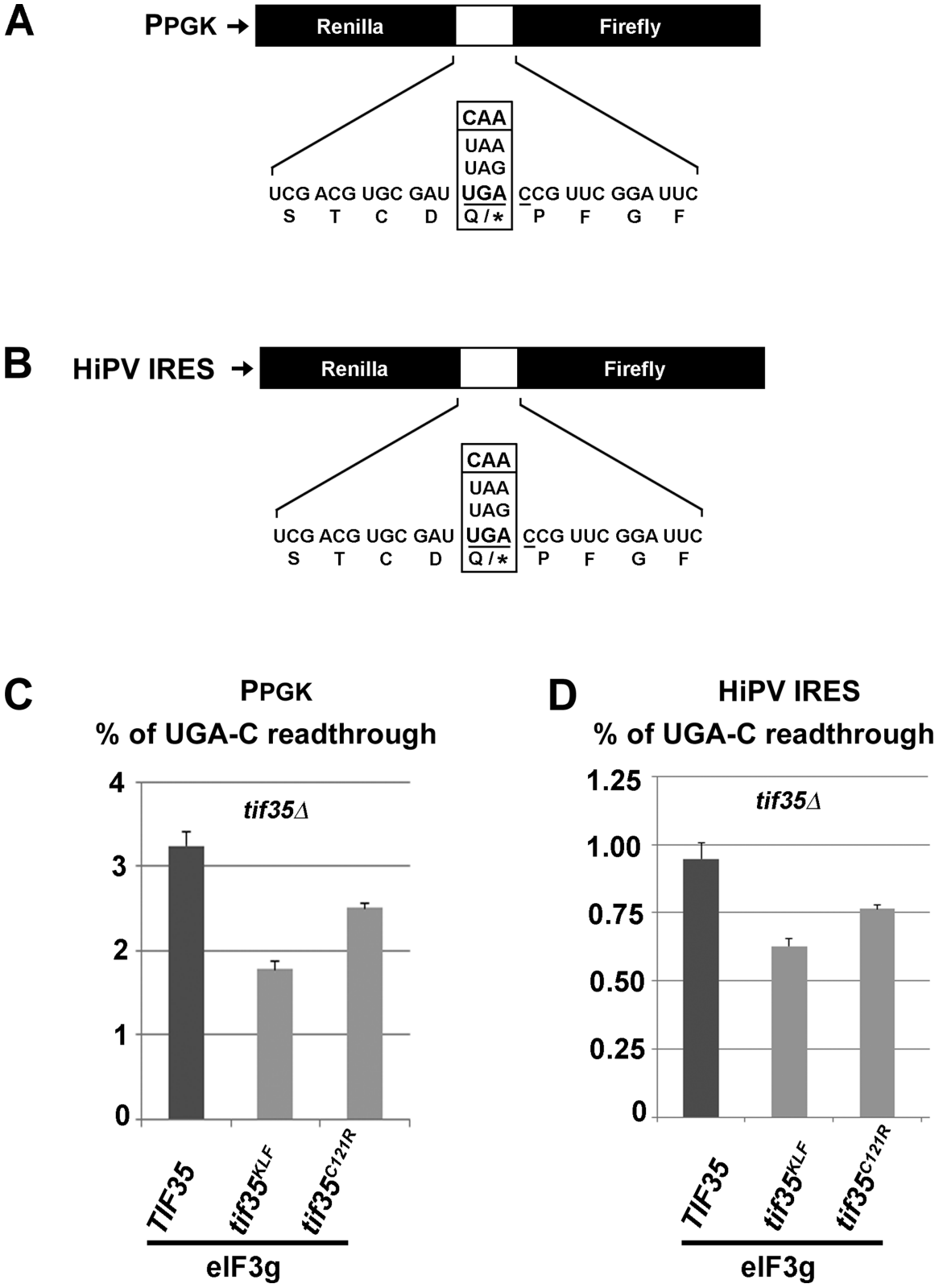

Figure 1. Readthrough measurements using the standard dual luciferase assay are not sensitive to defects in translation initiation. (**A**) Schematics of the standard dual luciferase readthrough reporter constructs with variable stop codons (or a CAA coding codon) under the P_{PGK} promoter adapted from (29). (**B**) Schematics of the modified dual luciferase readthrough reporter constructs containing the HiPV IRES in their 5′ UTRs. (**C**) eIF3 mutations affect stop codon readthrough independently of their initiation phenotypes. The *TIF35* wt, *tif35-KLF* and *tif35-C121R* mutant alleles were introduced into the H464 strain by plasmid shuffling. The resulting transformants were grown in SD and processed for stop codon readthrough measurements using standard dual luciferase readthrough reporter constructs schematically illustrated in panel A as described in Materials and Methods. (**D**) Same as in panel C except that modified dual luciferase reporter constructs YEp-HiPV-UGAC-L and YEp-HiPV-CAAC-L, schematically illustrated in panel B, were employed.

RESULTS

Readthrough measurements using the standard dual luciferase assay are not sensitive to defects in translation initiation

A standard way to measure the efficiency of stop codon readthrough is by dual-luciferase reporter assays specifically designed to be independent of mRNA level changes (29). In this reporter system, two genes encoding luciferases are separated by an in frame stop codon or by the CAA coding triplet as a reference (Figure 1A). To increase the sensitivity of this assay, the UGA stop codon with the C at the fourth position (UGA-C), which is known to allow relatively high levels of readthrough, is typically used (5). Using this approach, we previously demonstrated that eIF3 controls translation termination and stop codon readthrough; mutations in the core subunits of eIF3 decrease the relative efficiency of readthrough with this pre-sensitized construct (18). However, this reporter system is, by definition, dependent on the canonical initiation event on the first luciferase gene. In order to investigate whether the involvement of eIF3 in termination is fully independent of its role in initiation, we replaced the 5′ UTR of the first luciferase gene in our reporters with the cricket paralysis virus IRES-like HiPV IRES (Figure 1B). This IRES allows initiation of translation in the absence of any initiation factors (32–34) and, importantly, was shown to initiate translation also in the yeast *Saccharomyces cerevisiae*. We then employed these first-canonical-initiation-event-independent constructs to re-examine the readthrough efficiency of our eIF3 mutants and observed similar effects when compared to the standard reporter; stop codon readthrough is sensitive to eIF3 mutants in both cases (Figure 1C and D; $P < 0.05$ for both measurements of both mutants). These results not only completely rule out any impact of the initiation phenotypes of our eIF3 mutants on their termination phenotypes, but also fully justify the use of these standard readthrough reporters for subsequent analysis of the role of eIF3 in termination and stop codon readthrough.

eIF3 promotes stop codon readthrough but only on stop codons in an unfavorable termination context

Previous studies of readthrough implicated the nucleotide context surrounding the stop codon in modulating readthrough rates in various systems (3,5–7). Since eIF3 controls stop codon readthrough, we asked whether or not its action is also dependent on the stop codon nucleotide context. Because termination efficiency is particularly sensitive to the nucleotide immediately following the stop codon (5,6), we employed bicistronic reporters (kindly provided by D. Bedwell) bearing the in-frame UGA stop codon between both luciferases containing all possible combinations of the 'stop' tetranucleotide; i.e. UGA-C with the most efficient readthrough (5), UGA-A, -G or –U (Figure 2). Firstly, we observed that the impact of the fourth nucleotide on the relative termination efficiency of the UGA-N tetranucleotide was gradual in the following sequence: C > A > G > U (from the least to the most efficient termination) (Figure 2). Secondly, the effect of *tif35-KLF* on readthrough also turned out to be gradual and, in addition, in perfect accord with the C > A > G > U sequence of impact. The greatest difference in termination efficiency between wild-type (wt) and mutant *TIF35* was seen with UGA-C (∼1.5-fold in *SUP35* genetic background), followed by the UGA-A tetranucleotide etc. (Figure 2; *SUP35*). The differences seen in UGA-G and -U were not statistically significant; see also below. These findings thus indicate that wt eIF3 increases readthrough but preferentially on stop codons in unfavorable termination contexts—readthrough values change from the lowest in UGA-U *tif35-KLF* (0.035) to the highest in UGA-C *TIF35* (0.217; i.e. 6.2-fold), with UGA-C *tif35-KLF* reaching only 0.142 (4.1-fold). In other words, readthrough sensitive eIF3 mutations prevent full propagation of stop codon readthrough that the wt eIF3 complex is normally capable of—in the context-dependent manner—by a molecular mechanism elucidated below.

To corroborate these results in a pre-sensitized genetic background with higher basal levels of readthrough, we performed the same type of experiment in the *sup35-N536T* mutant, which increases readthrough by up to ∼9-fold, and observed essentially the same effects (Figure 2; *sup35-N536T*). The differences between *TIF35* wt and mutant cells detected in UGA-G and –U cases remained statistically insignificant, even though the individual readthrough values measured with these constructs are much higher than those in *SUP35* wt cells, practically as high as those seen with UGA-C and UGA-A in *SUP35* wt cells (Figure 2; compare *SUP35* and *sup35-N536T*). This suggests that the observed effects of wt eIF3 are dependent on the identity of the fourth nucleotide (C or A) and not simply on the absolute level of readthrough.

eIF3 stimulation of stop codon readthrough is dependent on its association with pre-termination 80S complexes *in vivo*

We showed previously that eIF3 core subunits associate with 80S couples isolated from heavy polysomes and that this association is dependent on the presence of termination factors eRF1 and eRF3, implying that these eIF3-bound 80S species most probably represent the pre-termination 80S complexes (pre-TCs) (18). To investigate how eIF3 mutations prevent its participation in stop codon readthrough, we first asked whether or not eIF3 mutations interfere with its ability to associate with the pre-TCs.

To do that, we selected three mutants of the a/TIF32 subunit of eIF3 and analyzed the amounts of factors bound to the 80S couples isolated from heavy polysomes using the resedimentation protocol described previously (18,31). Briefly, WCEs derived from formaldehyde cross-linked cells were resolved on sucrose gradients after high velocity centrifugation. The higher polysomal fractions were collected, treated with RNase I and the resulting 43S–48S pre-initiation complexes and 80S species were separated in a second round of centrifugation (resedimentation). Isolated 80S couples were loaded in six serial two-fold dilutions onto sodium dodecyl sulphate-polyacrylamide gel electrophoresis and the amounts of the small ribosomal protein uS2/RPS0A (as a loading control) and 80S-associated factors were analyzed by quantitative western blotting. As can be seen in Figure 3A and B, mutations *tif32-Δ8* and

	SUP35				sup35-N536T			
	UGA-C	UGA-A	UGA-G	UGA-U	UGA-C	UGA-A	UGA-G	UGA-U
TIF35	0.217±0.009 **100%**	0.096±0.003 **100%**	0.071±0.002 **100%**	0.039±0.002 **100%**	1.957±0.073 **100%**	0.432±0.029 **100%**	0.363±0.022 **100%**	0.124±0.001 **100%**
tif35-KLF	0.142±0.008 **65% ***	0.074±0.002 **76%***	0.062±0.004 **87%**	0.035±0.002 **91%**	1.121±0.031 **57%***	0.299±0.016 **69%***	0.256±0.044 **71%**	0.097±0.010 **78%**

% readthrough normalized to *TIF35*
*** significant difference ($P < 0.01$)**

Figure 2. Wild-type eIF3 promotes stop codon readthrough but only on stop codons in the unfavorable termination context. The *TIF35* wt and *tif35-KLF* mutant alleles were introduced into the PBH140 (*tif35Δ SUP35*) and PBH134 (*tif35Δ sup35-N536T*) strains by plasmid shuffling. The resulting transformants were grown in SD and processed for stop codon readthrough measurements as described in Materials and Methods. Percentages of readthrough of *tif35-KLF* given in the table were calculated from measured values (mean ± SE; $n = 6$) normalized to *TIF35* wt. Changes in readthrough levels were analyzed by the student's *t*-test and shown to be statistically significant only for those values marked with the asterisk ($P < 0.01$).

tif32-Box17, two mutant eIF3 complexes that fail to fully promote readthrough (18), displayed statistically significant enrichment of the eRF1 (*SUP45*) and eRF3 (*SUP35*) signal in heavy polysomes compared to the wt control. In addition to that, in the case of the stronger *tif32-Δ8* mutant, there is a visible reduction (by ∼60%; Figure 3B) in the amounts of selected eIF3 subunits bound to pre-TCs in comparison to wt. Similar results were also obtained for another strong terminating mutant (*tif35-KLF*) in the g/TIF35 subunit of eIF3 (Figure 3C). Together these results suggest that heavy polysomes in these three specific mutants contain a significantly higher proportion of terminating ribosomes lacking eIF3. Importantly, initiation and elongation factors eIF1 and eEF1A, respectively, neither of which imparts any termination phenotype when down-regulated (18), showed no significant alterations (Figure 3A and B; residual amounts of eIF1 occurring in the 80S samples most probably reflect the existence of an eIF1-containing 'eIF3-translasome' complex proposed to associate with elongating 80S ribosomes (35)—we used it as a specificity control). These observations further underscore our conclusion that the observed termination efficiency changes specifically arise from eIF3 association with the pre-TCs and not with initiating or elongating ribosomes. Furthermore, our observation that the amount of ribosome-associated eEF1A remains unchanged also indicates that eIF3 mutants do not impact the elongation phase. Taken together with the fact that the *tif32-Box6* mutant—which does not affect translation termination (18)—did not produce any significant difference in factor occupancy in the pre-TCs (Figure 3A and B), these results suggest that the presence of eIF3 within the pre-TCs is an important requirement for its stimulatory role in stop codon readthrough.

eIF3 is one of the major players in programmed stop codon readthrough

As aforementioned, UGA-C belongs to a group of tetranucleotides that are under-represented in genomes and that allow relatively inefficient termination (5) (Figure 2). Another sequence-specific feature implicated in permitting even less efficient termination than UGA-C; i.e. promoting much higher readthrough, is the hexanucleotide CAR-NBA consensus sequence immediately following the stop codon (10). This 'readthrough element' is exploited by several viral and cellular genes to extend their C-termini in a specific regulatory mechanism referred to as 'programmed stop codon readthrough' (13–15).

To explore whether the ability of eIF3 to promote readthrough specifically on poor-context stop codons is important also for this specific 'programmed' regulatory mechanism, we replaced the hexanucleotide sequence immediately following the stop codon of our UGA-C standard reporter with several pre-selected hexanucleotide sequences. In particular, UGA-CCG-UUC from our elevated-readthrough-promoting reporter (Figure 1A), which we took as a positive control, was exchanged for UGA-AUA-AAU or UGA-AAC-GGU, representing the hexanucleotides taken from the *SUP45* and *ADE1* termination sequences, respectively. These were deliberately chosen as a negative control because of their highly efficient termination. In the next three replacements we used termination hexanucleotides from genes known to undergo programmed stop codon readthrough, the strongest of which is the CAA-UUA hexanucleotide of the TMV (11). Among cellular genes from the *S. cerevisiae* genome, we picked *BSC4* (CAA-CUA) and *PDE2* (CAA-GAA). The hexanucleotide of *BSC4* is very similar in sequence to the TMV hexanucleotide and, consistent with this, it was classified as one of the genes with the highest level of stop codon bypass efficiency (36). In the case of *PDE2*, its hexanucleotide was directly implicated in affecting its biological role via increased readthrough (37). As can be seen in Figure 4, all three modified reporters containing the CAR-NBA or CAR-NNA consensus sequences produced robust readthrough, the efficiency of which is strictly dependent on intact eIF3 bound to pre-TCs (compare *TIF35* wt versus mutant datasets). In contrast, the inefficient readthrough observed for both negative controls is practically wt eIF3-independent. These results suggest that eIF3 is one of the major players in programmed stop codon readthrough.

A

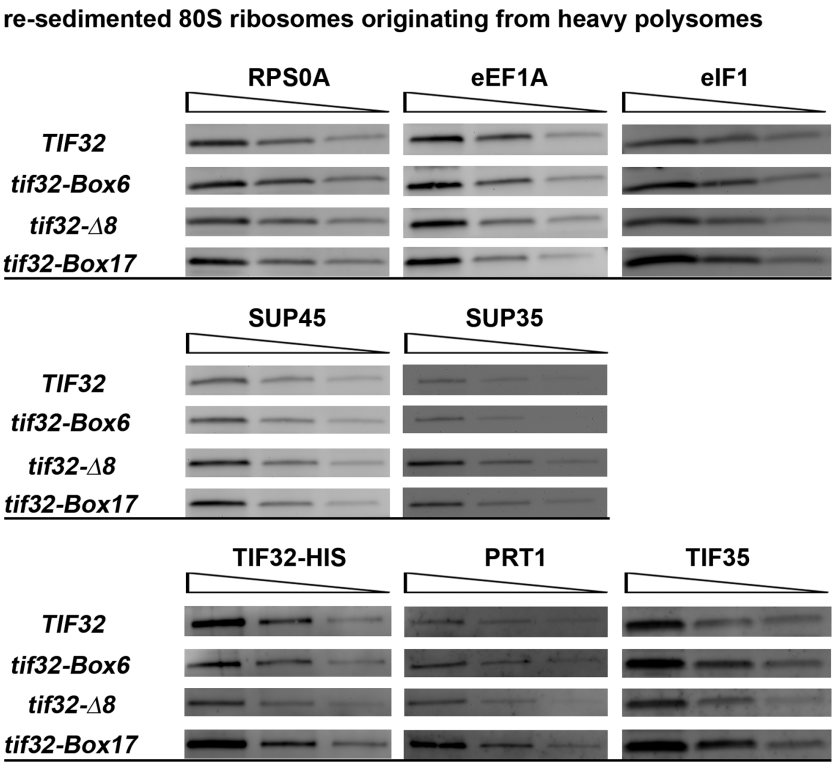

B

relative amounts (in %) of selected factors associated with re-sedimented 80S ribosomes in mutant vs. *TIF32* wt cells

	RPS0A	eEF1A	eIF1	SUP45	SUP35	TIF32-HIS
tif32-Box6	109 ± 11.31	106 ± 18.38	89.5 ± 2.12	103 ± 19.8	125 ± 7.07	83.45 ± 24.68
tif32-Δ8	104.45 ± 6.43	88.3 ± 12.3	97.5 ± 0.71	134.5 ± 13.44	367.5 ± 31.82 *	36.75 ± 11.53 *
tif32-Box17	106 ± 8.49	96.5 ± 12.02	96 ± 1.41	143 ± 7.07 *	285.5 ± 6.36 **	98.25 ± 7.99

* significant difference ($P < 0.05$)
** significant difference ($P < 0.01$)

C

relative amounts (in %) of selected factors associated with re-sedimented 80S ribosomes in mutant vs. *TIF35* wt cells

	RPS0A	eIF1	SUP45	SUP35	TIF32
tif35-KLF	97.85 ± 2.76	100.25 ± 4.74	128.7 ± 4.1 *	165.15 ± 18.4 **	58.85 ± 7.99 *

* significant difference ($P < 0.05$)
** significant difference ($P < 0.1$)

Figure 3. eIF3 stimulation of stop codon readthrough is dependent on its association with pre-termination 80S complexes *in vivo.* (**A**) Changes in amounts of translation factors associated with the pre-TCs in cells bearing *TIF32* mutations *in vivo*. Plasmid-born mutant alleles of *TIF32* (*tif32-Box6*, *tif32-Δ8* and *tif32-Box17*) and its corresponding wild-type (*TIF32*) were introduced into YBS52 strain by plasmid shuffling. The resulting transformants were grown in SD medium at 30°C to an OD_{600} of ∼1 and cross-linked with 0.5% HCHO prior to harvesting. WCEs were prepared, separated on a 5–45% sucrose gradient by centrifugation at 39 000 rpm for 2.5 h and heavier polysome fractions were collected and treated with RNase I to separate the pre-initiation complexes (PICs) from 80S couples on actively translated mRNAs. Thus treated samples were subjected to the second sucrose gradient centrifugation according to the resedimentation protocol described before and 80S couples—predominantly containing termination complexes (18)—were collected, loaded in six two-fold dilutions onto the SDS-PAGE gel and processed for western blot analysis with antibodies raised against factors shown above the strips. Three representative dilutions for each factor are shown. (**B**) Quantification of selected factors from at least three independent experiments shown in Figure 3A with corresponding *P*-values, where applicable. Western blot signals from each of the six two-fold dilutions obtained with individual anti-bodies were quantified by NIH ImageJ and plotted against their corresponding loadings. Individual slopes (representing relative amount of each factor in mutant cells) calculated from the linear regression of resulting plots were normalized to the slope obtained with the *TIF32* wt strain, which was set to 100%. (**C**) Changes in amounts of translation factors associated with the pre-TCs in cells bearing the *tif35-KLF* mutation *in vivo*. Quantification of selected factors from at least three independent experiments carried out as described in panel A with the exception that *tif35-KLF* and its corresponding *TIF35* wt were introduced into the H464 strain by plasmid shuffling.

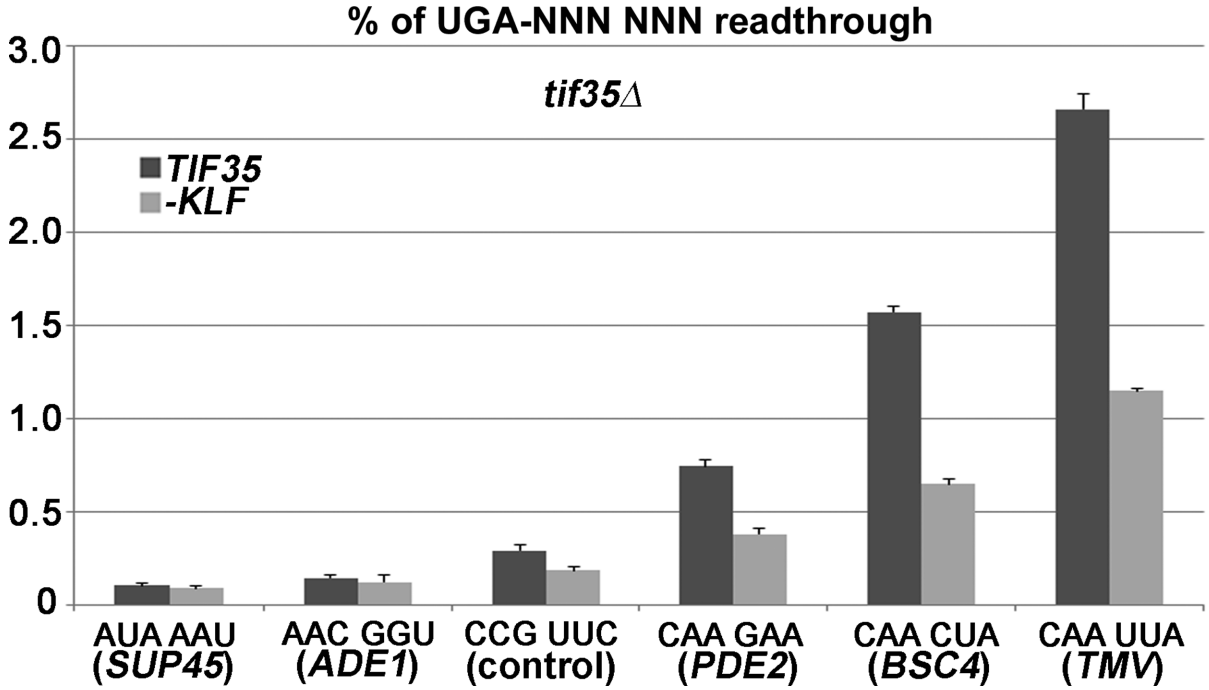

Figure 4. eIF3 is one of the major players in programmed stop codon readthrough. The PBH140 derivatives bearing *TIF35* wt and *tif35-KLF* mutant alleles (generated as described in Figure 2) were grown and processed for stop codon readthrough measurements as described in Materials and Methods, except that besides our standard ('control') pTH477 readthrough construct (shown in Figure 1A), five derivatives with variable hexanucleotide sequence immediately following the stop codon were also employed: PBB85 (for *SUP45*), PBB83 (for *ADE1*), PBB84 (for *PDE2*), PBB80 (for *BSC4*) and PBB82 (for *TMV*).

Wild-type eIF3 promotes incorporation of aminoacyl-tRNAs with a mismatch at the third position of the stop codon

Next we wished to uncover the molecular mechanism by which eIF3 promotes programmed stop codon readthrough. Considering that readthrough occurs when the stop codon is decoded by near-cognate tRNAs (i.e. tRNAs that can base-pair with two of the three stop codon bases) (16), we first explored which aminoacyl-tRNAs get incorporated during programmed stop codon readthrough. We did so by measuring readthrough using programmed reporters in cells individually overexpressing selected near-cognate tRNAs versus control empty vectors. We expected that overexpression of a near-cognate tRNA that successfully decodes the corresponding programmed stop codon will increase readthrough levels significantly more in *TIF35* wt cells than in *tif35-KLF* mutant cells, which are seriously compromised in promoting programmed stop codon readthrough (Figure 4). In particular, we tested (i) all known near-cognate tRNAs that form Watson–Crick base pairs with the first 2 nt of the UGA stop codon [tW(CCA) and tC(GCA)] as well as of both UAA and UAG stop codons [tY(GUA)]; (ii) both existing near-cognate tRNAs that form Watson–Crick base pairs with the second and third positions of the UGA stop codon [tR(UCU) and tG(UCC)]; (iii) a mutated tyrosine tRNA [tY*(UCA)] unable to base pair with the second position of the UAA stop codon only; and (iv) several non-cognate tRNAs that form Watson–Crick base pairs only with the first position of either UAA [tW(CCA)] or UAG [tY*(UCA) and tW(CCA)] stop codons chosen as negative controls. As can be seen in Figure 5, wt eIF3 promotes readthrough of the UGA stop codon by incorporation of tryptophan [tW(CCA)] or cysteine [tC(GCA)] tRNAs (Figure 5A) with a mismatch at the third position, and also of the UAA and UAG stop codons by incorporation of the tyrosine [tY(GUA)] tRNA with the same mismatch (Figure 5B and Supplementary Figure S1). In contrast, overexpression of near-cognate or non-cognate tRNAs with a single mismatch either at the first or second positions, respectively, did not significantly increase readthrough in eIF3 wt cells (Figure 5B and C), similarly to overexpression of our control, non-cognate tRNAs base-paring only with the first stop codon nucleotide (Figure 5B and Supplementary Figure S1). These results suggest that wt eIF3 specifically promotes incorporation of near-cognate tRNAs with a mismatch at the third (wobble) position of a given programmed stop codon. In addition, these results also imply that the effect of eIF3 on programmed stop codon readthrough is not limited to the UGA stop codon alone, as it promotes readthrough on all three stop codons and to the same degree, provided that they are set in a readthrough-permissive context.

Wild-type eIF3 interferes with decoding of the third (wobble) position of programmed stop codons

Taking into account that wt eIF3 promotes read-though by only those near-cognate tRNAs with a mismatch at the third (wobble) position of the programmed stop codon, we wondered whether it may play a more direct role in decoding of the third position *per se*. We overexpressed tY*(UCA), a tyrosine-coding tRNA in which the anti-

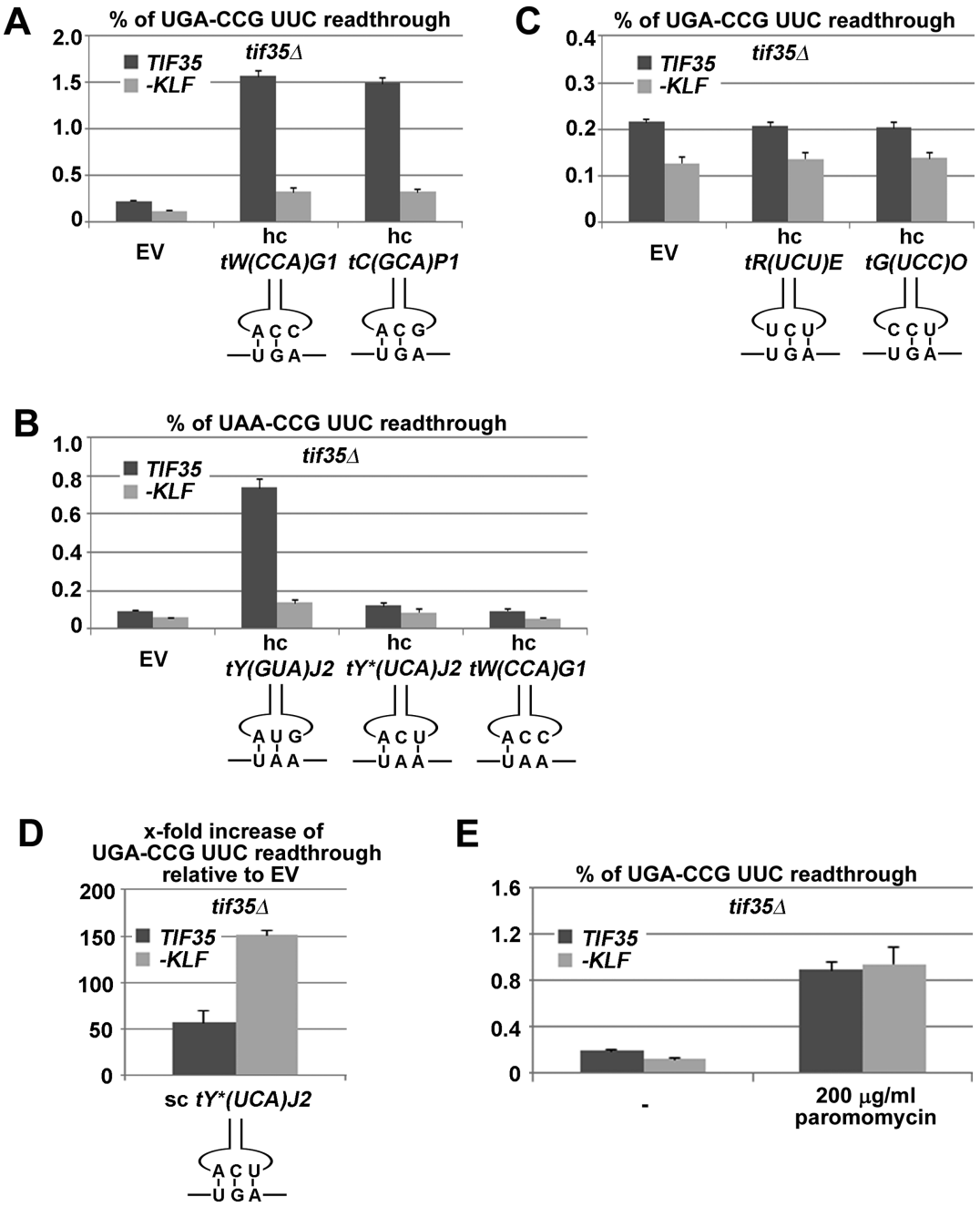

Figure 5. eIF3 interferes with decoding of the third position of the stop codon allowing incorporation of near-cognate tRNAs with the mismatch at the same position. (**A**) eIF3 promotes incorporation of both existing near-cognate tRNAs with a mismatch at the third position of the UGA stop codon. The PBH140 derivatives bearing *TIF35* wt and *tif35-KLF* mutant alleles (generated as described in Figure 2) were transformed with either empty vector (EV), high copy (hc) tW(CCA)G1 or hc tC(GCA)P1 and the resulting transformants were grown and processed for stop codon readthrough measurements as described in Materials and Methods. (**B**) eIF3 enhances incorporation of the near-cognate tRNA also at the UAA stop codon with a mismatch at the third position [tY(GUA)J2—encoding tyrosine] but not with a mismatch at the second position [tY*(UCA)J2] or non-cognate [tW(CCA)G1—encoding tryptophan]. The PBH140 derivatives bearing *TIF35* wt and *tif35-KLF* mutant alleles (generated as described in Figure 2) were transformed with empty vector (EV), hc tY(GUA)J2, hc tY*(UCA)J2 or hc tW(CCA)G1 and subsequently also with the readthrough construct YEp-R/T-UAAC-L and the resulting transformants were grown and processed for stop codon readthrough measurements as described in Materials and Methods. (**C**) eIF3 does not affect incorporation of both existing near-cognate tRNAs with a mismatch at the first position of the UGA stop codon. The PBH140 derivatives bearing *TIF35* wt and *tif35-KLF* mutant alleles (generated as described in Figure 2) were transformed with either empty vector (EV), hc tR(UCU)E or hc tG(UCC)O and the resulting transformants were grown and processed for stop codon readthrough measurements as described in Experimental Procedures. (**D**) eIF3 impedes stop codon decoding by fully cognate tRNA. The PBH140 derivatives bearing *TIF35* wt and *tif35-KLF* mutant alleles (generated as described in Figure 2) were transformed with either empty vector (EV) or a single copy (sc) plasmid carrying tY*(UCA)J2 and the resulting transformants were grown and processed for stop codon readthrough measurements as described in Materials and Methods. (**E**) Paromomycin nullifies the effect of wt eIF3 on programmed stop codon readthrough. The PBH140 derivatives bearing *TIF35* wt and *tif35-KLF* mutant alleles (generated as described in Figure 2) were grown in SD without or with 200μg/ml paromomycin for 6 h and processed for stop codon readthrough measurements as described in Materials and Methods.

codon has been mutated to the cognate of UGA, assuming that if eIF3 specifically causes mis-decoding at the wobble position (which would be beneficial for incorporation of the above defined near-cognate tRNAs), the UGA stop codon suppressing impact of this artificial cognate tRNA would be more pronounced in *TIF35* mutant versus wt cells. Indeed, overexpressing tY*(UCA) results in a ∼150-fold increase in UGA readthrough in *tif35-KLF* mutant cells compared to a ∼50-fold increase in eIF3 wt cells (Figure 5D). Together these results imply that wt eIF3 does generally impair decoding of the third (wobble) position of a stop codon. Thus it is highly likely that it directly interferes with the stop codon recognition process by the eRF1.eRF3.GTP complex, as we recently proposed (18). This particular effect of eIF3 would play only a negligible role during the canonical termination event (Figure 4); however, it would become critical in programmed stop codon readthrough as a necessary prerequisite for the subsequent incorporation of near-cognate tRNAs with the mismatch at the wobble position (see our model below).

The miscoding agent paromomycin, disabling ribosomal discrimination against near-cognate tRNAs, nullifies the effect of wt eIF3 on programmed stop codon readthrough

The aminoglycoside antibiotic paromomycin is a widely used drug for termination studies as it has been shown that its presence within the pre-TCs causes displacement of the A1493 phosphate group relaxing the A-site codon decoding pocket. As a result, paromomycin changes the deformation of the near-cognate codon-anticodon helix, after which the ribosome does not actively sense the correct Watson–Crick base-pairing geometry and thus does not discriminate against near-cognate tRNAs (38). Because wt eIF3 was proposed to act similarly on poor-context stop codons, we re-examined the efficiency of UGA-C readthrough in *TIF35* wt versus mutant cells in the presence of 200 μg/ml paromomycin. Consistent with previous results, we observed increased readthrough efficiency in the presence of paromomycin (Figure 5E). In addition, no difference in the efficiency of readthrough promoted by either wt or mutant g/TIF35 was observed in the presence of paromomycin, perhaps because the magnitude of the paromomycin effect masks that of eIF3 or because eIF3 no longer promotes readthrough if the decoding center is perturbed.

The role of eIF3 in stop codon readthrough is conserved between yeast and humans

Because programmed stop codon readthrough has been shown to play a critical role in regulating gene expression in several organisms such as plant viruses, yeast, fruit flies, and mammals, and because the number of genes apparently under the control of this regulatory mechanism continues to increase (see for example the most recent genome-wide high-throughput screen (17)), we wished to investigate whether the role of eIF3 in programmed stop codon readthrough is evolutionarily conserved. To do that, we individually knocked down the a (eIF3a$^{K.D.}$—homolog of yeast *TIF32*) and g (eIF3g$^{K.D.}$—homolog of yeast *TIF35*) subunits of human eIF3 in HeLa cells using the ON-TARGETplus SMART pool siRNA system

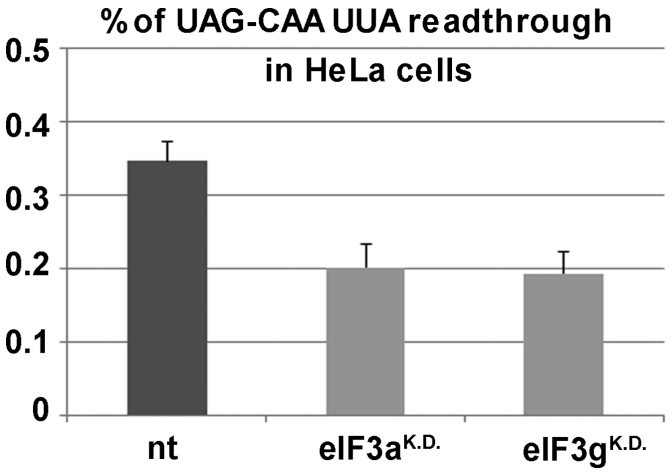

Figure 6. Human eIF3 promotes stop codon readthrough. HeLa cells were transfected with siRNA against the eIF3a and eIF3g subunits (eIF3a$^{K.D.}$ and eIF3g$^{K.D.}$) or non-targeting siRNA (nt) as control. Two days later, the siRNA-treated cells were further transfected with the bicistronic firefly/*renilla* luciferase readthrough reporters (40). Both luciferases are separated by a stop (UAG) or sense codon (CAG) followed—in both cases—by a highly readthrough permissive sequence (CAAUUA) from TMV (41). The UAG-C readthrough is displayed as % of the signal obtained with the sense codon reporter; standard deviations are given.

(Dharmacon/Thermo Scientific) following the previously established protocol (39). On the second day after the transfection of these specific siRNAs and a control non-targeting siRNA (nt), the cells were further transfected with human dual-luciferase reporter plasmids containing the highly permissive TMV CAA-UAA hexanucleotide sequence immediately following the stop codon to boost the sensitivity of this assay (40,41). As can be seen in Figure 6, downregulation of both human eIF3 subunits resulted in a significant decrease of the efficiency of readthrough, to a similar degree as that previously observed with mutations in orthologous eIF3 subunits in yeast (18) (Figure 1C). This finding suggests that the role of eIF3 in termination, and in particular in stop codon readthrough, has been conserved throughout evolution.

DISCUSSION

The proteomic diversity achieved in all kingdoms of life, by various regulatory mechanisms, is extraordinary. Growing evidence suggests that stop codon readthrough is one mechanism whereby cells expand the functional repertoire of proteins beyond an apparently limited genetic script (17,37,42–44). For example, a C-terminal isoform of the endothelial growth factor A (VEGFA) generated by programmed readthrough has been shown to exhibit anti-angiogenic activity in contrast to the pro-angiogenic activity of the original protein (42); efficient programmed readthrough occuring at the UGA-CU termination hexanucleotide of two normally cytosolic enzymes was shown to target these new protein C-terminal isoforms into peroxisomes in both fungi and animals (44). Despite the growing importance of this paradigm, our mechanistic knowledge of how pre-termination ribosomes recognize a programmed stop codon

for readthrough and how the readthrough event occurs on the molecular level is still rather poor.

Here, we demonstrate that the *bona fide* translation initiation factor eIF3, recently implicated in controlling translation termination besides its critical initiation roles (18), is one of the major trans-acting factors in programmed stop codon readthrough in yeast and perhaps also in mammals (Figure 6). In particular, we show that the presence of eIF3 in pre-TC complexes increases readthrough on stop codons in unfavorable termination contexts in a manner that is independent of its role during initiation (Figures 1–3). More importantly, eIF3 is critically required for efficient readthrough on three mRNAs previously demonstrated to be under the control of the programmed stop codon readthrough pathway (Figure 4). More detailed analysis of the codon specificity of eIF3-mediated stop codon readthrough suggests that eIF3 promotes the incorporation of near-cognate tRNAs with mismatches at the third (wobble) position, perhaps via an interaction with the decoding center of the ribosome.

Our previous experiments strongly suggested that the association of eIF3 with pre-TCs is strictly dependent on eRF1 (18). Thus it seems likely that eIF3 is generally present at any termination event regardless of its canonical or programmed readthrough predisposition, although we cannot rule out that it may preferentially associate with the readthrough programmed pre-TC by recognizing their unique structural features.

During canonical termination (Figure 7A), when the stop codon in the termination favorable context appears in the ribosomal A-site, eRF1, in complex with eRF3.GTP, enters the A-site triggering major conformational rearrangements of the pre-TC, particularly at and around the mRNA entry channel (45–47). During these ribosome-specific re-arrangements, the N-terminal domain (NTD) of eRF1 itself undergoes an important conformational change, which plays a critical role in the two-step model of stop codon selection (sampling), as recently proposed by (48). In the first step, the first and second nucleotides of the stop codon are recognized by specific residues of the eRF1-NTD (Figure 7A, 'sampling—step i.'), followed by its rearrangement during the second step, which permits decoding of the third nucleotide. It has been proposed that—as a result of this re-arrangement—the second stop codon nucleotide is contacted by different amino acid residues of the eRF1-NTD than during the first step; the third nucleotide is most probably recognized directly by the ribosome, highly likely in close cooperation with eRF1 (Figure 7A, 'sampling—step ii.'). (An alternative option is that the ribosome recognizes the second nucleotide and the third is read by eRF1 – for simplicity, our model in Figure 7 depicts only the former option.) As a result, eRF1 stably accommodates in the A-site triggering GTP hydrolysis on eRF3, followed by downstream termination/recycling events. The presumed presence of eIF3 in the pre-TCs with stop codons in a favorable termination context would have only a negligible, if any, impact on termination efficiency (Figure 4).

During programmed readthrough (Figure 7B), the stop codon occurs in an unfavorable termination context that promotes stop codon readthrough. One example of this is the CAR-NBA hexanucleotide immediately following the stop codon. The effect of this and other, functionally similar sequences varies. They can for example base-pair with 18S rRNA to stabilize and/or specifically rearrange the pre-TC, such as in the CAR-NBA case (10). Alternatively, they can recruit trans-acting factors proposed to interact with translating ribosomes in a way that prevents eRF1 binding to the stop codon as in the very recently reported case of vascular endothelial growth factor A (VEGFA) mRNA (42). Because a part of the eIF3 body projects into the vicinity of the mRNA entry channel and several of its subunits interact with RNA (reviewed in (19), see also (24,27,49–50)), it is conceivable that eIF3 could directly interact with these sequences and perhaps even mediate their effects in promoting programmed readthrough; however, there is no experimental evidence for that yet. In light of our results, we propose that during or after the first step of the two-step recognition mechanism, which would happen uninfluenced by eIF3 (single mismatches at the first or second stop codon positions showed no genetic interaction with eIF3 whatsoever—Figure 5B and C), eIF3 alters the decoding property of the third stop codon nucleotide. It could do this either directly, as it was proposed to reach the A-site via its a/TIF32 and c/NIP1 subunits (50,51) and interact with the N-M domain of eRF1 via its g/TIF35 subunit (18) or allosterically by binding to constituents of the decoding pocket such as the small ribosomal protein uS5/RPS2. Indeed, uS5/RPS2 was shown to interact with the C-terminus of a/TIF32 (25) and, remarkably, act as an omnipotent suppressor of all three stop codons while bearing the *SUP44* mutation (52). Either way, as a result, proper decoding of the third stop codon position by the ribosome and/or eRF1 would be impaired, as indicated in Figure 5D, resulting in premature rejection of the eRF1.eRF3.GTP complex from pre-TCs. Subsequently, the eIF3-mediated altered property of the third position would invite near-cognate tRNAs with a mismatch at this very position (tyrosine tRNA for UAA or UAG and tryptophan and cysteine tRNAs for UGA) to incorporate into the A-site and allow elongation to continue to the next stop codon downstream (Figure 5A and B). This is consistent with the fact that paromomycin, which makes the pre-TCs incapable of discriminating against near-cognate tRNAs and thus dramatically increases readthrough, prevented eIF3 from further increasing readthrough over its mutant showing genetic epistasis (Figure 5E). Taken together, we propose that eIF3 disables proper decoding of the third stop codon position by the ribosome co-operating with the 'cognate' eRF1 and at the same time promotes wobble miscoding by near-cognate tRNAs to occasionally win the battle over the stop codon predisposed for programmed readthrough.

Programmed stop codon readthrough has recently emerged as an important contributor to proteomic diversity and has also been implicated in the replication of several pathogenic RNA virus families and thus represents an appealing target for antiviral therapies (53–56). Programmed stop codon readthrough has also been proposed as a potential treatment for hereditary diseases caused by premature termination codons (PTCs), many of which occur in unfavorable termination contexts (for review see (57)). PTCs produce truncated proteins that are non-functional or even toxic and targeted, mRNA-specific increase in readthrough

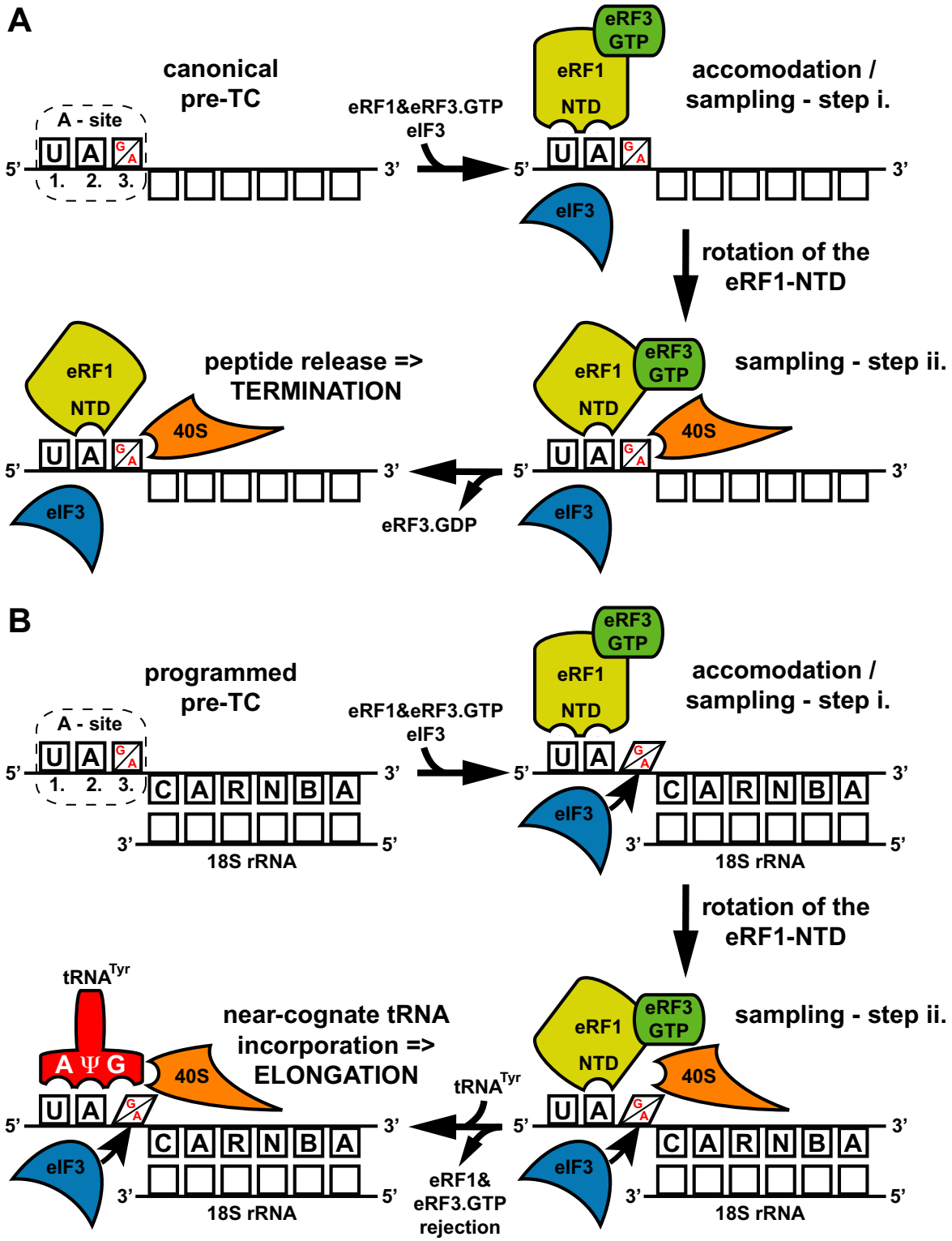

Figure 7. Model: translation initiation factor eIF3 promotes programmed stop codon readthrough. (**A**) Canonical termination; stop codon in the termination favorable context appears in the A-site (only UAG and UAA stop codons are indicated for illustration purposes; UGA works by the same mechanism), eRF1 in complex with eRF3.GTP binds to it and samples the codon in a two-step process including conformational re-arrangements of the eRF1-NTD. During the second step the ribosome by itself co-participates in this accommodation phase that ultimately leads to GTP hydrolysis on eRF3, polypeptide release and ribosomal recycling (see text for further details). (**B**) Programmed stop codon readthrough; stop codon occurs in the unfavorable termination context bearing specific consensus sequences like CAR-NBA in its 3′ UTR—in this particular case proposed to base-pair with 18S rRNA. The eIF3 presence in the pre-TC—perhaps in co-operation with these sequences—alters the decoding property of the nucleotide at the third stop codon position. This prevents its proper decoding during the second sampling step and subsequently, after the eRF1-eRF3.GTP complex rejection, allows incorporation of near-cognate tRNAs with the mismatch at the third position to read through the stop codon and continue with elongation.

could restore the functionality of the affected genes and thus cure the disease, provided that the exact molecular mechanism is known and can be purposefully exploited. Here, we reveal that the translation initiation factor eIF3 plays a crucial role in programmed stop codon readthrough and suggest a detailed molecular model for its role. Our results thus open new avenues of inquiry for understanding this important biological event also with respect to human health.

SUPPLEMENTARY DATA

Supplementary Data are available at NAR Online.

ACKNOWLEDGEMENT

We are grateful to David Bedwell, Terri Kinzy and Matthew Cockman for timely gifts of materials and Colin E. Aitken for critical reading of the manuscript.

FUNDING

Wellcome Trust [090812/B/09/Z]; Czech Science Foundation [GA14-05394S to L.S.V.]; Charles University in Prague, project GA UK [762513 to P.B.]. Funding for open charge: Czech Science Foundation [GA14-05394S].
Conflict of interest statement. None declared.

REFERENCES

1. Jackson,R.J., Hellen,C.U. and Pestova,T.V. (2012) Termination and post-termination events in eukaryotic translation. *Adv. Protein Chem. Struct. Biol.*, **86**, 45–93.
2. Robinson,D.N. and Cooley,L. (1997) Examination of the function of two kelch proteins generated by stop codon suppression. *Development*, **124**, 1405–1417.
3. Chao,A.T., Dierick,H.A., Addy,T.M. and Bejsovec,A. (2003) Mutations in eukaryotic release factors 1 and 3 act as general nonsense suppressors in Drosophila. *Genetics*, **165**, 601–612.
4. Napthine,S., Yek,C., Powell,M.L., Brown,T.D. and Brierley,I. (2012) Characterization of the stop codon readthrough signal of Colorado tick fever virus segment 9 RNA. *RNA*, **18**, 241–252.
5. Bonetti,B., Fu,L., Moon,J. and Bedwell,D.M. (1995) The efficiency of translation termination is determined by a synergistic interplay between upstream and downstream sequences in Saccharomyces cerevisiae. *J. Mol. Biol.*, **251**, 334–345.
6. McCaughan,K.K., Brown,C.M., Dalphin,M.E., Berry,M.J. and Tate,W.P. (1995) Translational termination efficiency in mammals is influenced by the base following the stop codon. *Proc. Natl. Acad. Sci. U.S.A.*, **92**, 5431–5435.
7. Cassan,M. and Rousset,J.P. (2001) UAG readthrough in mammalian cells: effect of upstream and downstream stop codon contexts reveal different signals. *BMC Mol. Biol.*, **2**, 3.
8. Janzen,D.M., Frolova,L. and Geballe,A.P. (2002) Inhibition of translation termination mediated by an interaction of eukaryotic release factor 1 with a nascent peptidyl-tRNA. *Mol. Cell. Biol.*, **22**, 8562–8570.
9. Mottagui-Tabar,S., Tuite,M.F. and Isaksson,L.A. (1998) The influence of 5′ codon context on translation termination in Saccharomyces cerevisiae. *Eur. J. Biochem.*, **257**, 249–254.
10. Namy,O., Hatin,I. and Rousset,J.P. (2001) Impact of the six nucleotides downstream of the stop codon on translation termination. *EMBO Rep.*, **2**, 787–793.
11. Skuzeski,J.M., Nichols,L.M., Gesteland,R.F. and Atkins,J.F. (1991) The signal for a leaky UAG stop codon in several plant viruses includes the two downstream codons. *J. Mol. Biol.*, **218**, 365–373.
12. Harrell,L., Melcher,U. and Atkins,J.F. (2002) Predominance of six different hexanucleotide recoding signals 3′ of read-through stop codons. *Nucleic Acids Res.*, **30**, 2011–2017.
13. Namy,O., Rousset,J.P., Napthine,S. and Brierley,I. (2004) Reprogrammed genetic decoding in cellular gene expression. *Mol. Cell*, **13**, 157–168.
14. Dreher,T.W. and Miller,W.A. (2006) Translational control in positive strand RNA plant viruses. *Virology*, **344**, 185–197.
15. von der Haar,T. and Tuite,M.F. (2007) Regulated translational bypass of stop codons in yeast. *Trends Microbiol.*, **15**, 78–86.
16. Bidou,L., Rousset,J.P. and Namy,O. (2010) Translational errors: from yeast to new therapeutic targets. *FEMS Yeast Res.*, **10**, 1070–1082.
17. Dunn,J.G., Foo,C.K., Belletier,N.G., Gavis,E.R. and Weissman,J.S. (2013) Ribosome profiling reveals pervasive and regulated stop codon readthrough in Drosophila melanogaster. *Elife*, **2**, e01179.
18. Beznosková,P., Cuchalová,L., Wagner,S., Shoemaker,C.J., Gunišová,S., Von der Haar,T. and Valášek,L.S. (2013) Translation initiation factors eIF3 and HCR1 control translation termination and stop codon read-through in yeast cells. *PLoS Genet.*, **9**, e1003962.
19. Valášek,L.S. (2012) 'Ribozoomin'—translation Initiation from the perspective of the ribosome-bound eukaryotic initiation factors (eIFs). *Curr. Protein Pept. Sci.*, **13**, 305–330.
20. Hinnebusch,A.G. (2014) The scanning mechanism of eukaryotic translation initiation. *Annu. Rev. Biochem.*, **83**, 779–812.
21. Valášek,L., Mathew,A., Shin,B.S., Nielsen,K.H., Szamecz,B. and Hinnebusch,A.G. (2003) The yeast eIF3 subunits TIF32/a and NIP1/c and eIF5 make critical connections with the 40S ribosome in vivo. *Genes Dev*, **17**, 786–799.
22. Cuchalová,L., Kouba,T., Herrmannová,A., Danyi,I., Chiu,W.-l. and Valášek,L. (2010) The RNA recognition motif of eukaryotic translation initiation factor 3g (eIF3g) is required for resumption of scanning of posttermination ribosomes for reinitiation on GCN4 and together with eIF3i stimulates linear scanning. *Mol. Cell. Biol.*, **30**, 4671–4686.
23. Herrmannová,A., Daujotyte,D., Yang,J.C., Cuchalová,L., Gorrec,F., Wagner,S., Danyi,I., Lukavsky,P.J. and Valášek,L.S. (2012) Structural analysis of an eIF3 subcomplex reveals conserved interactions required for a stable and proper translation pre-Initiation complex assembly. *Nucleic Acids Res.*, **40**, 2294–2311.
24. Hashem,Y., des Georges,A., Dhote,V., Langlois,R., Liao,H.Y., Grassucci,R.A., Hellen,C.U., Pestova,T.V. and Frank,J. (2013) Structure of the mammalian ribosomal 43S preinitiation complex bound to the scanning factor DHX29. *Cell*, **153**, 1108–1119.
25. Chiu,W.-L., Wagner,S., Herrmannová,A., Burela,L., Zhang,F., Saini,A.K., Valášek,L. and Hinnebusch,A.G. (2010) The C-terminal region of eukaryotic translation initiation factor 3a (eIF3a) promotes mRNA recruitment, scanning, and, together with eif3j and the eif3b rna recognition motif, selection of AUG start codons. *Mol. Cell. Biol.*, **30**, 4415–4434.
26. Kouba,T., Rutkai,E., Karasková,M. and Valášek,L.S. (2012) The eIF3c/NIP1 PCI domain interacts with RNA and RACK1/ASC1 and promotes assembly of the pre-initiation complexes. *Nucleic Acids Res.*, **40**, 2683–2699.
27. Erzberger,J.P., Stengel,F., Pellarin,R., Zhang,S., Schaefer,T., Aylett,C.H., Cimermancic,P., Boehringer,D., Sali,A., Aebersold,R. *et al.* (2014) Molecular architecture of the 40SeIF1eIF3 translation initiation complex. *Cell*, **158**, 1123–1135.
28. Muhlrad,D. and Parker,R. (1999) Recognition of yeast mRNAs as 'nonsense containing' leads to both inhibition of mRNA translation and mRNA degradation: implications for the control of mRNA decapping. *Mol. Biol. Cell*, **10**, 3971–3978.
29. Keeling,K.M., Lanier,J., Du,M., Salas-Marco,J., Gao,L., Kaenjak-Angeletti,A. and Bedwell,D.M. (2004) Leaky termination at premature stop codons antagonizes nonsense-mediated mRNA decay in S. cerevisiae. *RNA*, **10**, 691–703.
30. Merritt,G.H., Naemi,W.R., Mugnier,P., Webb,H.M., Tuite,M.F. and von der Haar,T. (2010) Decoding accuracy in eRF1 mutants and its correlation with pleiotropic quantitative traits in yeast. *Nucleic Acids Res.*, **38**, 5479–5492.
31. Valášek,L., Szamecz,B., Hinnebusch,A.G. and Nielsen,K.H. (2007) In vivo stabilization of preinitiation complexes by formaldehyde cross-linking. *Methods Enzymol.*, **429**, 163–183.
32. Wilson,J.E., Pestova,T.V., Hellen,C.U. and Sarnow,P. (2000) Initiation of protein synthesis from the A site of the ribosome. *Cell*, **102**, 511–520.

33. Chu,D., Barnes,D.J. and von der Haar,T. (2011) The role of tRNA and ribosome competition in coupling the expression of different mRNAs in Saccharomyces cerevisiae. *Nucleic Acids Res.*, **39**, 6705–6714.
34. Hertz,M.I. and Thompson,S.R. (2011) In vivo functional analysis of the Dicistroviridae intergenic region internal ribosome entry sites. *Nucleic Acids Res.*, **39**, 7276–7288.
35. Sha,Z., Brill,L.M., Cabrera,R., Kleifeld,O., Scheliga,J.S., Glickman,M.H., Chang,E.C. and Wolf,D.A. (2009) The eIF3 interactome reveals the translasome, a supercomplex linking protein synthesis and degradation machineries. *Mol. Cell*, **36**, 141–152.
36. Namy,O., Duchateau-Nguyen,G., Hatin,I., Hermann-Le Denmat,S., Termier,M. and Rousset,J.P. (2003) Identification of stop codon readthrough genes in Saccharomyces cerevisiae. *Nucleic Acids Res.*, **31**, 2289–2296.
37. Namy,O., Duchateau-Nguyen,G. and Rousset,J.P. (2002) Translational readthrough of the PDE2 stop codon modulates cAMP levels in Saccharomyces cerevisiae. *Mol. Microbiol.*, **43**, 641–652.
38. Bidou,L., Allamand,V., Rousset,J.P. and Namy,O. (2012) Sense from nonsense: therapies for premature stop codon diseases. *Trends Mol. Med.*, **18**, 679–688.
39. Wagner,S., Herrmannova,A., Malik,R., Peclinovska,L. and Valasek,L.S. (2014) Functional and biochemical characterization of human eukaryotic translation initiation factor 3 in living cells. *Mol. Cell. Biol.*, **34**, 3041–3052.
40. Grentzmann,G., Kelly,P.J., Laalami,S., Shuda,M., Firpo,M.A., Cenatiempo,Y. and Kaji,A. (1998) Release factor RF-3 GTPase activity acts in disassembly of the ribosome termination complex. *RNA*, **4**, 973–983.
41. Feng,T., Yamamoto,A., Wilkins,S.E., Sokolova,E., Yates,L.A., Munzel,M., Singh,P., Hopkinson,R.J., Fischer,R., Cockman,M.E. *et al.* (2014) Optimal translational termination requires C4 lysyl hydroxylation of eRF1. *Mol. Cell*, **53**, 645–654.
42. Eswarappa,S.M., Potdar,A.A., Koch,W.J., Fan,Y., Vasu,K., Lindner,D., Willard,B., Graham,L.M., DiCorleto,P.E. and Fox,P.L. (2014) Programmed translational readthrough generates antiangiogenic VEGF-Ax. *Cell*, **157**, 1605–1618.
43. Yamaguchi,Y., Hayashi,A., Campagnoni,C.W., Kimura,A., Inuzuka,T. and Baba,H. (2012) L-MPZ, a novel isoform of myelin P0, is produced by stop codon readthrough. *J. Biol. Chem.*, **287**, 17765–17776.
44. Stiebler,A.C., Freitag,J., Schink,K.O., Stehlik,T., Tillmann,B.A., Ast,J. and Bolker,M. (2014) Ribosomal readthrough at a short UGA stop codon context triggers dual localization of metabolic enzymes in fungi and animals. *PLoS Genet.*, **10**, e1004685.
45. Taylor,D., Unbehaun,A., Li,W., Das,S., Lei,J., Liao,H.Y., Grassucci,R.A., Pestova,T.V. and Frank,J. (2012) Cryo-EM structure of the mammalian eukaryotic release factor eRF1-eRF3-associated termination complex. *Proc. Natl. Acad. Sci. U.S.A.*, **109**, 18413–18418.
46. Alkalaeva,E.Z., Pisarev,A.V., Frolova,L.Y., Kisselev,L.L. and Pestova,T.V. (2006) In vitro reconstitution of eukaryotic translation reveals cooperativity between release factors eRF1 and eRF3. *Cell*, **125**, 1125–1136.
47. Preis,A., Heuer,A., Barrio-Garcia,C., Hauser,A., Eyler,D.E., Berninghausen,O., Green,R., Becker,T. and Beckmann,R. (2014) Cryoelectron microscopic structures of eukaryotic translation termination complexes containing eRF1-eRF3 or eRF1-ABCE1. *Cell Rep.*, **8**, 59–65.
48. Kryuchkova,P., Grishin,A., Eliseev,B., Karyagina,A., Frolova,L. and Alkalaeva,E. (2013) Two-step model of stop codon recognition by eukaryotic release factor eRF1. *Nucleic Acids Res.*, **41**, 4573–4586.
49. Szamecz,B., Rutkai,E., Cuchalova,L., Munzarova,V., Herrmannova,A., Nielsen,K.H., Burela,L., Hinnebusch,A.G. and Valášek,L. (2008) eIF3a cooperates with sequences 5′ of uORF1 to promote resumption of scanning by post-termination ribosomes for reinitiation on GCN4 mRNA. *Genes Dev.*, **22**, 2414–2425.
50. Munzarová,V., Pánek,J., Gunišová,S., Dányi,I., Szamecz,B. and Valášek,L.S. (2011) Translation reinitiation relies on the interaction between eIF3a/TIF32 and progressively folded cis-acting mRNA elements preceding short uORFs. *PLoS Genet.*, **7**, e1002137.
51. Karaskova,M., Gunisova,S., Herrmannova,A., Wagner,S., Munzarova,V. and Valasek,L.S. (2012) Functional characterization of the role of the N-terminal domain of the c/Nip1 subunit of eukaryotic initiation factor 3 (eIF3) in AUG recognition. *J. Biol. Chem.*, **287**, 28420–28434.
52. Synetos,D., Frantziou,C.P. and Alksne,L.E. (1996) Mutations in yeast ribosomal proteins S28 and S4 affect the accuracy of translation and alter the sensitivity of the ribosome to paromomycin. *Biochim. Biophys. Acta*, **1309**, 156–166.
53. Houck-Loomis,B., Durney,M.A., Salguero,C., Shankar,N., Nagle,J.M., Goff,S.P. and D'Souza,V.M. (2011) An equilibrium-dependent retroviral mRNA switch regulates translational recoding. *Nature*, **480**, 561–564.
54. Firth,A.E. and Brierley,I. (2012) Non-canonical translation in RNA viruses. *J. Gen. Virol.*, **93**, 1385–1409.
55. Hartmann,K. (2012) Clinical aspects of feline retroviruses: a review. *Viruses*, **4**, 2684–2710.
56. Mohd Jaafar,F., Attoui,H., De Micco,P. and De Lamballerie,X. (2004) Termination and read-through proteins encoded by genome segment 9 of Colorado tick fever virus. *J. Gen. Virol.*, **85**, 2237–2244.
57. Keeling,K.M., Xue,X., Gunn,G. and Bedwell,D.M. (2014) Therapeutics based on stop codon readthrough. *Annu. Rev. Genomics Hum. Genet.*, **15**, 371–394.

SUPPLEMENTAL INFORMATION

EXPERIMENTAL PROCEDURES

Construction of yeast strains and plasmids

List of all strains used throughout this study can be found in Table S1.

To create PBH140 and PBH134 strains; 74D-694 and L2334, respectively, were first transformed with YCp11-TIF35-MET to cover for the deletion of *TIF35* that was made in the next step by introducing the *Bam*HI-*Aat*I 5.2kb fragment carrying the *tif35Δ::hisG-URA3-hisG* integration cassette from pΔtif35#9. The Uracil auxotrophy was regained by growing the cells on SD plates containing 5-fluoro-orotic acid (5-FOA). The resulting strain was subsequently transformed with YEp-TIF35-U and the Leucine auxotrophy was regained by growing the cells in liquid media containing Leucine and selecting for those that lost the YCp11-TIF35-MET plasmid on SD +/- Leucine plates producing PBH140 and PBH134.

List of all plasmids and PCR primers used throughout this study can be found in Tables S2 and S3, respectively.

pTH779 was created as follows. Nucleotides 6210-6505 of the viral genome, comprising the translational start at nucleotide 6473, were amplified from a cDNA clone of the viral RNA (Nakashima et al., 1999) using primers HiPV_Bam_5 and HiPV_FLuc_3. Firefly luciferase DNA was amplified from plasmid pTH650 (Chu et al., 2011) using primers Ff_5 and Ff_Sal_3. These sequences were then recombined using overlap extension PCR, by using the two PCR products as templates in a second round PCR reaction with primers HiPV_Bam_5 and Ff_Sal_3. This generates an in-frame fusion of the first 11 codons of the HiPV capsid protein, an XbaI restriction site, and firefly luciferase from codon 2. The recombination product was cloned as a BamHI/SalI fragment into pTH645 (Chu et al., 2011) to give pTH779.

YEp-HiPV-UGAC-L and YEp-HiPV-CAAC-L were constructed by three consecutive cloning steps. First, the 1959-pb *Xma*I-*Pst*I fragment from pTH779 was inserted into *Xma*I-*Pst*I digested YEp181. Next, the *Sph*I-*Alw*NI digested PCR product obtained with primers PBRFtermF and NIP1-AlwNI using pTH477 as a template was inserted into *Sph*I-*Alw*NI digested vector from previous step. Last, the *Not*I-*Pst*I digested PCR products obtained by PBRFpstI and PBRFNotI primers using pTH477 or YEp-R/T-CAAC-L as templates were inserted into *Not*I-*Pst*I digested vector from previous step resulting in YEp-HiPV-UGAC-L and YEp-HiPV-CAAC-L, respectively.

YEp-R/T-UAAC-L and YEp-R/T-UAGC-L were constructed by inserting the 4567-bp *Alw*NI-*Nsi*I fragment from pTH461 and pTH469, respectively, into YEplac181 digested by *Alw*NI-*Nsi*I.

PBB75, PBB76 and PBB77 were constructed by inserting the 4567-bp *Alw*NI-*Nsi*I fragment from pDB712, pDB714 and pDB716, respectively, into YEplac181 digested by *Alw*NI-*Nsi*I.

PBB80 was created by inserting the *Sal*I-*Not*I digested PCR product obtained with primers BSC4 and PBRFNotI using pTH477 as template into *Sal*I-*Not*I digested pTH477.

PBB82 was created by inserting the *Sal*I-*Not*I digested PCR product obtained with primers TMV and PBRFNotI using pTH477 as template into *Sal*I-*Not*I digested pTH477.

PBB83 was created by inserting the *Sal*I-*Not*I digested PCR product obtained with primers ADE1 and PBRFNotI using pTH477 as template into *Sal*I-*Not*I digested pTH477.

PBB84 was created by inserting the *Sal*I-*Not*I digested PCR product obtained with primers PDE2 and PBRFNotI using pTH477 as template into *Sal*I-*Not*I digested pTH477.

PBB85 was created by inserting the *Sal*I-*Not*I digested PCR product obtained with primers SUP45 and PBRFNotI using pTH477 as template into *Sal*I-*Not*I digested pTH477.

pTH335 was created by inserting the *BamHI-XhoI* digested PCR product obtained with primers tW_f and tW_r using genomic DNA obtained from yeast strain BY4741as template into *BamHI-XhoI* digested pRS426

pTH638 and pTH640 were created by inserting the *BamHI-HindIII* digested PCR products obtained with primers SUP4_f and SUP4_r using genomic DNA obtained from yeast strain BY4741 (for pTH638) or suppressor strain MT422/1c (for pTH640) as template into *BamHI-HindIII* digested pRS316.

PBB90 and PBB91 were constructed by inserting the 235-bp *Bam*HI-*Kpn*I fragment from pTH638 and pTH640, respectively, into pTH335 digested by *Bam*HI-*Kpn*I.

PBB97 was created by inserting the *BamHI-XhoI* digested PCR product obtained with primers PB94 and PB95 using genomic DNA obtained from yeast strain H464 as template into *BamHI-XhoI* digested pTH335.

PBB99 was created by inserting the *BamHI-XhoI* digested PCR product obtained with primers PB98 and PB99 using genomic DNA obtained from yeast strain H464 as template into *BamHI-XhoI* digested pTH335.

PBB100 was created by inserting the *BamHI-XhoI* digested PCR product obtained with primers PB100 and PB101 using genomic DNA obtained from yeast strain H464 as template into *BamHI-XhoI* digested pTH335.

Table S1. Yeast strains used in this study.

Strain	Genotype	Source or reference
YBS52 [a]	*MAT*a *leu2-3, -112 ura3-52 trp1Δ gcn2Δ tif32Δ URA3::GCN2 ura3* (Ycp-a/TIF32-His-U)	(Munzarová et al., 2011)
H464[a]	*MAT*a *leu2-3,-112 ura3-52::GCN2 trp1Δ tif35Δ* (hc *TIF35 URA3*)	(Cuchalová et al., 2010)
PBH140[b]	*MAT*a *ade1-14 trp1-289 his3-Δ200 leu2-3,112 ura3-52 tif35Δ* (YCp22-g/TIF35-screen)	this study
PBH134[b]	*MAT*a *ade1-14 trp1-289 his3-Δ200 leu2-3,112 ura3-52 tif35Δ sup35-N536T* (YCp22-g/TIF35-screen)	this study
74D-694[b]	*MAT*a *ade1-14 trp1-289 his3-Δ200 leu2-3,112 ura3-52*	(Chernoff et al., 1993)
L2334[b]	*MAT*a *ade1-14 trp1-289 his3-Δ200 leu2-3,112 ura3-52 sup35-N536T*	(Bradley et al., 2003)
BY4741	*MATa his3Δ0 leu2Δ0 met15Δ0 ura3Δ0*	(Brachmann et al., 1998)
MT422/1c	*ade2-1 his5-2 can1-100 ura3-1 leu2-3,122 lys1-1 met8-1 SUP4-o*	(Kurjan et al., 1980)

Table S2. Plasmids used in this study.

Plasmid	Description	Source of reference
pTH779	low copy HiPV-Firefly in *URA3* plasmid from pRS316	this study
YEp-HiPV-UGAC-L	high copy HiPV-Renilla-Firefly R/T cassette (stop codon of Renilla is UGA-C; for read-through measurements) in *LEU2* plasmid from YEplac181	this study
YEp-HiPV-CAAC-L	high copy HiPV-Renilla-Firefly R/T cassette (stop codon of Renilla is replaced with CAA-C [coding triplet]; for control read-through measurements) in *LEU2* plasmid from YEplac181	this study
YCp-a/TIF32-His-L	single copy wt *TIF32-His* in *LEU2* plasmid from YCplac111	(Munzarová et al., 2011)
YCp-a/tif32-Box17-His	single copy *tif32-Box17-His* in *LEU2* plasmid from YCplac111	(Munzarová et al., 2011)
YCp-a/tif32-Box6-His	single copy *tif32-Box6-His* in *LEU2* plasmid from YCplac111	(Munzarová et al., 2011)
YCp-a/tif32-Δ8-His-L	single copy *tif32-Δ8-His* in *LEU2* plasmid from YCplac111	Beznoskova et al 2013
YCp22-g/TIF35-screen	single copy wt *TIF35-His* in *TRP1* plasmid from YCplac22	(Cuchalová et al., 2010)
YCp22-g/TIF35-KLF	single copy *TIF35-KLF-His* in*TRP1* plasmid from YCplac22	(Cuchalová et al., 2010)
YCp22-g/TIF35-C121R	single copy *TIF35-C121R-His* in *TRP1* plasmid from YCplac22	(Beznosková et al., 2013)
YEp-R/T-UGAC-L	high copy PGK-Renilla-Firefly R/T cassette (stop codon of Renilla is UGA-C; for read-through measurements) in *LEU2* plasmid from YEplac181	(Beznosková et al., 2013)
YEp-R/T-CAAC-L	high copy PGK-Renilla-Firefly R/T cassette (stop codon of Renilla is replaced with CAA-C [coding triplet]; for control read-through measurements) in *LEU2* plasmid from YEplac181	(Beznosková et al., 2013)
YEplac181	high copy cloning vector, *LEU2*	(Gietz and Sugino, 1988)
YEplac195	high copy cloning vector, *URA3*	(Gietz and Sugino, 1988)
pSP35-45	high copy wt *SUP45 SUP35* in *URA3*	(Bidou et al., 2000)
pTH335	high copy *URA3* vector (pRS426) containing genomic DNA surrounding the tW(CCA)G1 gene	this study
pTH461	high copy PGK-Renilla-Firefly R/T	(Keeling et al., 2004)

	cassette (stop codon of Renilla is UAA-C; for read-through measurements) in *URA3* plasmid from YEplac195	
pTH469	high copy PGK-Renilla-Firefly R/T cassette (stop codon of Renilla is UAG-C; for read-through measurements) in *URA3* plasmid from YEplac195	(Keeling et al., 2004)
YEp-R/T-UAAC-L	high copy PGK-Renilla-Firefly R/T cassette (stop codon of Renilla is UAA-C; for read-through measurements) in *LEU2* plasmid from YEplac181	this study
YEp-R/T-UAGC-L	high copy PGK-Renilla-Firefly R/T cassette (stop codon of Renilla is UAG-C; for read-through measurements) in *LEU2* plasmid from YEplac181	this study
pTH638	centromeric *URA3* vector (pRS316) containing the tY(GUA)J2 wild-type gene (=*SUP4*)	this study
pTH640	centromeric *URA3* vector (pRS316) containing an opal suppressor mutant of tY(GUA)J2 gene	this study
PBB90	high copy *URA3* vector (pRS426) containg the tY(GUA)J2 wild-type gene (=*SUP4*)	this study
PBB91	high copy *URA3* vector (pRS426) containing an opal suppressor mutant of tY(GUA)J2 gene	this study
PBB97	high copy *tC(GCA)P1* in *URA2* plasmid from pRS426	this study
PBB99	high copy *tR(UCU)E* in *URA2* plasmid from pRS426	this study
PBB100	high copy *tG(UCC)O* in *URA2* plasmid from pRS426	this study
pDB712	high copy PGK-Renilla-Firefly R/T cassette (stop codon of Renilla is UGA-A; for read-through measurements) in *URA3* plasmid from YEplac195	(Keeling et al., 2004)
pDB714	high copy PGK-Renilla-Firefly R/T cassette (stop codon of Renilla is UGA-G; for read-through measurements) in *URA3* plasmid from YEplac195	(Keeling et al., 2004)
pDB716	high copy PGK-Renilla-Firefly R/T cassette (stop codon of Renilla is UGA-U; for read-through	(Keeling et al., 2004)

	measurements) in *URA3* plasmid from YEplac195	
PBB75	high copy PGK-Renilla-Firefly R/T cassette (stop codon of Renilla is UGA-A; for read-through measurements) in *LEU2* plasmid from YEplac181	this study
PBB76	high copy PGK-Renilla-Firefly R/T cassette (stop codon of Renilla is UGA-G; for read-through measurements) in *LEU2* plasmid from YEplac181	this study
PBB77	high copy PGK-Renilla-Firefly R/T cassette (stop codon of Renilla is UGA-U; for read-through measurements) in *LEU2* plasmid from YEplac181	this study
pTH477	high copy PGK-Renilla-Firefly R/T cassette (stop codon of Renilla is UGA-CCGUUC; for read-through measurements) in *URA3* plasmid from YEplac195	(Keeling et al., 2004)
PBB80	high copy PGK-Renilla-Firefly R/T cassette (stop codon of Renilla is UGA-CAACUA; for read-through measurements) in *URA3* plasmid from YEplac195	this study
PBB82	high copy PGK-Renilla-Firefly R/T cassette (stop codon of Renilla is UGA-CAAUUA; for read-through measurements) in *URA3* plasmid from YEplac195	this study
PBB83	high copy PGK-Renilla-Firefly R/T cassette (stop codon of Renilla is UGA-AACGGU; for read-through measurements) in *URA3* plasmid from YEplac195	this study
PBB84	high copy PGK-Renilla-Firefly R/T cassette (stop codon of Renilla is UGA-CAAGAA; for read-through measurements) in *URA3* plasmid from YEplac195	this study
PBB85	high copy PGK-Renilla-Firefly R/T cassette (stop codon of Renilla is UGA-AUAAAU; for read-through measurements) in *URA3* plasmid from YEplac195	this study
YCp11-TIF35-MET	single copy *TIF35* under *MET3* promoter, *LEU2* plasmid from Ycplac11	(Cuchalová et al., 2010)

pΔtif35#9	the *TIF35* deletion construct with the *hisG-URA3-hisG* cassette inserted in between the 5‘ and 3‘ UTRs of *TIF35*	(Cuchalová et al., 2010)
YEp-TIF35-U	high copy wt *TIF35* in *LEU2* plasmid from YEplac352	(Asano et al., 1998)

Table S3. Primers used in this study.

Primer name	**Primer sequence (5´to 3´)**
HiPV_Bam_5	GCGCGGGATCCAAACATTGTGCGAAGCTTCTTGGCTC
HiPV_FLuc_3	CCTTTCTTTATGTTTTTGGCGTCTTCCTGCAGATTTGTATTGTTATTATTATT
Ff_5	GAAGACGCCAAAAACATAAAGAAAGG
Ff_Sal_3	GGGGGGGTCGACTTACAATTTGGACTTTCCGCCCTTC
PBRFtermF	AATAAGCATGCGCGGCCGCAAGCTTTTCGTGGCCGAGG
NIP1-AlwNI	CTGTTACCAGTGGCTGCTGCC
PBRFpstI	AATAACTGCAGACTTCGAAAGTTTATGATCCA
PBRFNotI	CTCGAAGCGGCCGCTCTAGAATTACAC
BSC4	CAAATGTCGACGTGCGATTGACAACTAGGATCCTTCAACTTCCCTGAGCTCG
TIF32	CAAATGTCGACGTGCGATTGACAGACAGGATCCTTCAACTTCCCTGAGCTCG
TMV	CAAATGTCGACGTGCGATTGACAATTAGGATCCTTCAACTTCCCTGAGCTCG
ADE1	CAAATGTCGACGTGCGATTGAAACGGTGGATCCTTCAACTTCCCTGAGCTCG
PDE2	CAAATGTCGACGTGCGATTGACAAGAAGGATCCTTCAACTTCCCTGAGCTCG
SUP45	CAAATGTCGACGTGCGATTGAATAAATGGATCCTTCAACTTCCCTGAGCTCG
tW_f	GCGCGCCTCGAGATTTTTTACATTTGTTCTATCAGTTAGT
tW_r	CGCGCGGGATCCTATAAAAAGAACATATTCATACGGGC
SUP4_f	CCCCCGGATCCTTCAATTGTATATGTGTTATGTAGTATAC
SUP4_r	CCCCCAAGCTTTTTCAACTTGCAAGTCTGGGAAGTG
PB94	AATAACTCGAGTTGCGTGGATAAGTGTTATTATTCTATTGCC
PB95	AATAAGGATCCAAAGCCGTACAGGCGAACGTATATAATTAAAATTC
PB98	AATAACTCGAGTAACACGTTAATATGGTGGAGTCAGCTGAG
PB99	AATAAGGATCCTAATCTGCCGTATGTTCTGGTATTTACTGGTTAGG
PB100	AATAACTCGAGTAATGTTATAGTGATTGAGATCAGTTTCACC
PB101	AATAAGGATCCGGTTATTTCACGTCCCGGAGGAAAAAAAGTTTG

REFERENCES

Asano, K., Phan, L., Anderson, J., and Hinnebusch, A.G. (1998). Complex formation by all five homologues of mammalian translation initiation factor 3 subunits from yeast *Saccharomyces cerevisiae*. J Biol Chem *273*, 18573-18585.

Beznosková, P., Cuchalová, L., Wagner, S., Shoemaker, C.J., Gunišová, S., Von der Haar, T., and Valášek, L.S. (2013). Translation initiation factors eIF3 and HCR1 control translation termination and stop codon read-through in yeast cells. PLoS Genet *9*, e1003962.

Bidou, L., Stahl, G., Hatin, I., Namy, O., Rousset, J.P., and Farabaugh, P.J. (2000). Nonsense-mediated decay mutants do not affect programmed -1 frameshifting. Rna *6*, 952-961.

Bradley, M.E., Bagriantsev, S., Vishveshwara, N., and Liebman, S.W. (2003). Guanidine reduces stop codon read-through caused by missense mutations in SUP35 or SUP45. Yeast *20*, 625-632.

Brachmann, C.B., Davies, A., Cost, G.J., Caputo, E., Li, J., Hieter, P., and Boeke, J.D. (1998). Designer deletion strains derived from Saccharomyces cerevisiae S288C: a useful set of strains and plasmids for PCR-mediated gene disruption and other applications. Yeast *14*, 115-132.

Cuchalová, L., Kouba, T., Herrmannová, A., Danyi, I., Chiu, W.-l., and Valášek, L. (2010). The RNA Recognition Motif of Eukaryotic Translation Initiation Factor 3g (eIF3g) Is Required for Resumption of Scanning of Posttermination Ribosomes for Reinitiation on GCN4 and Together with eIF3i Stimulates Linear Scanning. Mol Cell Biol *30*, 4671-4686.

Gietz, R.D., and Sugino, A. (1988). New yeast-Escherichia coli shuttle vectors constructed with in vitro mutagenized yeast genes lacking six-base pair restriction sites. Gene *74*, 527-534.

Chernoff, Y.O., Derkach, I.L., and Inge-Vechtomov, S.G. (1993). Multicopy SUP35 gene induces de-novo appearance of psi-like factors in the yeast Saccharomyces cerevisiae. Curr Genet *24*, 268-270.

Chu, D., Barnes, D.J., and von der Haar, T. (2011). The role of tRNA and ribosome competition in coupling the expression of different mRNAs in Saccharomyces cerevisiae. Nucleic Acids Res *39*, 6705-6714.

Keeling, K.M., Lanier, J., Du, M., Salas-Marco, J., Gao, L., Kaenjak-Angeletti, A., and Bedwell, D.M. (2004). Leaky termination at premature stop codons antagonizes nonsense-mediated mRNA decay in S. cerevisiae. RNA *10*, 691-703.

Kurjan, J., Hall, B.D., Gillam, S., and Smith, M. (1980). Mutations at the yeast SUP4 tRNATyr locus: DNA sequence changes in mutants lacking suppressor activity. Cell *20*, 701-709.

Munzarová, V., Pánek, J., Gunišová, S., Dányi, I., Szamecz, B., and Valášek, L.S. (2011). Translation Reinitiation Relies on the Interaction between eIF3a/TIF32 and Progressively Folded cis-Acting mRNA Elements Preceding Short uORFs. PLoS Genet *7*, e1002137.

Nakashima, N., Sasaki, J., and Toriyama, S. (1999). Determining the nucleotide sequence and capsid-coding region of himetobi P virus: a member of a novel group of RNA viruses that infect insects. Archives of virology *144*, 2051-2058.

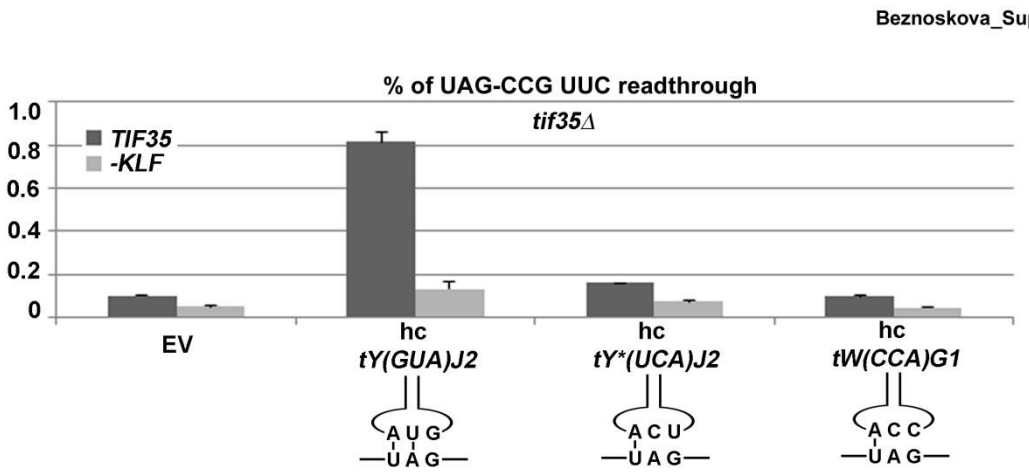

Figure S1. eIF3 promotes incorporation of aminoacyl-tRNAs with a mismatch at the 3rd position only of all three stop codons

eIF3 enhances incorporation of the near-cognate tRNA also at the UAG stop codon with a mismatch at the 3rd position [tY(GUA)J2 – encoding tyrosine] but not with non-cognate tY*(UCA)J2 or tW(CCA)G1. The PBH140 derivatives bearing *TIF35* wt and *tif35-KLF* mutant alleles (generated as described in Figure 2) were transformed with empty vector (EV), hc tY(GUA)J2, hc tY*(UCA)J2 or hc tW(CCA)G1, and subsequently also with the readthrough construct YEp-R/T-UAGC-L, and the resulting transformants were grown and processed for stop codon readthrough measurements as described in Experimental Procedures.

PUBLICATION IV

Rules of UGA-N decoding by near-cognate tRNAs and analysis of readthrough on short uORFs in yeast

PETRA BEZNOSKOVÁ,[1,2] STANISLAVA GUNIŠOVÁ,[1] and LEOŠ SHIVAYA VALÁŠEK[1]

[1]Laboratory of Regulation of Gene Expression, Institute of Microbiology ASCR, 142 20 Prague, Czech Republic
[2]Faculty of Science, Charles University in Prague, 128 43 Prague, Czech Republic

ABSTRACT

The molecular mechanism of stop codon recognition by the release factor eRF1 in complex with eRF3 has been described in great detail; however, our understanding of what determines the difference in termination efficiencies among various stop codon tetranucleotides and how near-cognate (nc) tRNAs recode stop codons during programmed readthrough in *Saccharomyces cerevisiae* is still poor. Here, we show that UGA-C as the only tetranucleotide of all four possible combinations dramatically exacerbated the readthrough phenotype of the stop codon recognition-deficient mutants in eRF1. Since the same is true also for UAA-C and UAG-C, we propose that the exceptionally high readthrough levels that all three stop codons display when followed by cytosine are partially caused by the compromised sampling ability of eRF1, which specifically senses cytosine at the +4 position. The difference in termination efficiencies among the remaining three UGA-N tetranucleotides is then given by their varying preferences for nc-tRNAs. In particular, UGA-A allows increased incorporation of Trp-tRNA whereas UGA-G and UGA-C favor Cys-tRNA. Our findings thus expand the repertoire of general decoding rules by showing that the +4 base determines the preferred selection of nc-tRNAs and, in the case of cytosine, it also genetically interacts with eRF1. Finally, using an example of the *GCN4* translational control governed by four short uORFs, we also show how the evolution of this mechanism dealt with undesirable readthrough on those uORFs that serve as the key translation reinitiation promoting features of the *GCN4* regulation, as both of these otherwise counteracting activities, readthrough versus reinitiation, are mediated by eIF3.

Keywords: programmed stop codon readthrough; termination; eRF1; tetranucleotide; GCN4; uORF

INTRODUCTION

The accuracy of translation of genetic information from genes into proteins that occurs on the ribosome is highly dependent on the precise decoding of the genetic code, which is contained in individual mRNAs. The sequence of nucleotide triplets in the right open reading frame determines the sequence of amino acid residues in the corresponding polypeptide and, with a few exceptions, such as for example, ambiguous decoding of the same codon by two different sense tRNAs or various types of programmed frameshifting (Dinman 2012), this basic rule is relatively strictly observed; translation has a misincorporation rate of 10^{-3} to 10^{-4} (Zaher and Green 2009). Nearly the same applies to recognition of all three stop codons by the release factor eRF1 that enters the A-site of the 80S ribosome in complex with the GTP-binding protein eRF3 (for review, see Jackson et al. 2012; von der Haar and Valasek 2014). There are some specific cases, however, when a stop codon does not signal the proper end of translation, which can thus continue beyond to the next stop codon. This phenomenon is called stop codon readthrough or nonsense suppression and occurs when a near-cognate aminoacyl-tRNA (nc-tRNA) or a suppressor tRNA is incorporated at a given stop codon (Dabrowski et al. 2015). It can be "spontaneous" and thus relatively infrequent (the order of spontaneous stop codon leakiness is UGA > UAG > UAA); or it can be programmed to C-terminally extend the protein of interest as a response to, for example, specific environmental changes demanding an alteration of the corresponding protein's properties (for more details, see Dinman 2012). Stop codon readthrough can also occur at a premature termination codon (PTC) within the coding region of a given gene, which is desirable because it can prevent the action of a nonsense-mediated decay (NMD) pathway by ensuring the synthesis of a full-length protein (Keeling et al. 2014). In fact, there are many diseases caused by PTCs that often occur in the termination nonfavorable context, making them good substrates for drug-stimulated programmed readthrough (Linde and Kerem 2008).

Corresponding author: valasekl@biomed.cas.cz

Article published online ahead of print. Article and publication date are at http://www.rnajournal.org/cgi/doi/10.1261/rna.054452.115. Freely available online through the *RNA* Open Access option.

Mainly from this point of view this topic is of high importance also for medical reasons (Lee and Dougherty 2012).

Taking all this into account, it is important to investigate which nc-tRNAs can decode individual stop codons and under what circumstances. Namy's group has only recently made great progress in this direction by experimentally demonstrating in vivo that tyrosine or glutamine preferentially incorporates at UAA (with similar frequencies), tyrosine predominantly inserts at UAG, and tryptophan or cysteine at UGA (Blanchet et al. 2014). Lysine and arginine were also shown to incorporate at UAA/UAG and UGA stop codons, respectively, and glutamine at UAG, but at very low rates. Soon after that, Jacobson's group extended these findings by a comprehensive in vivo analysis of termination readthrough from a PTC under different readthrough-inducing conditions (Roy et al. 2015). Their work identified exactly the same amino acid residues that are being inserted during readthrough, only with the predominant frequencies of incorporation for glutamine and not for tyrosine at UAG. However, what determines which of the amino acid residues that are specific for each stop codon incorporates at a given stop codon at a given frequency is not known. It was previously demonstrated that the identity of a nucleotide immediately following any stop codon (the +4 nucleotide) fine-tunes its termination efficiency; i.e., determines its permissiveness for readthrough (for an overview, see Dabrowski et al. 2015). For example, efficiency of readthrough on UGA determined by the +4 nucleotide identity follows this order of tetranucleotides: UGA-C > UGA-A > UGA-G > UGA-U (Beznosková et al. 2015). In fact, C at the +4 position is the strongest readthrough inducer among all four bases at all three stop codons (Dabrowski et al. 2015). Hence it is possible that in addition to the stop codon, it is also the +4 base that influences which nc-tRNA gets preferentially accepted by the A-site during readthrough.

We recently showed that one of the key translation initiation factors—eIF3—interacts with pretermination complexes (pre-TCs) and controls translation termination and readthrough (Beznosková et al. 2013). In particular, it interferes with the eRF1 ability to recognize the third/wobble position of any programmed stop codon leading to the rejection of the eRF1–eRF3.GTP complex from pre-TCs. At the same time, eIF3 promotes incorporation of nc-tRNAs with a mismatch at the same position and thus represents one of the key players in programmed stop codon readthrough (Beznosková et al. 2015). For UGA there are two nc-tRNAs with the mismatch at the third/wobble position, Trp- and Cys-tRNAs. The third and last nc-tRNA with the wobble mismatch, Tyr-tRNA, is shared by the UAA and UAG stop codons. Incorporation of all of these three nc-tRNAs is promoted by eIF3 and, in fact, we provided evidence that efficient readthrough at UGA is enabled exclusively by the former two nc-tRNAs with the mismatch at the third/wobble position (Beznosková et al. 2015). This does not seem to apply to the other two stop codons, however, because other studies based on different approaches that were mentioned above showed that in addition to Tyr-tRNA, UAA and UAG can be also recoded by Gln- and Lys-tRNAs; i.e., nc-tRNAs with the mismatch at the first position (Blanchet et al. 2014; Roy et al. 2015). The UGA stop codon has two nc-tRNAs with the first position mismatch, Gly- and Arg-tRNA, the latter of which was also suggested to insert at the A-site with low frequencies by these authors; however, it did not do so in our hands (Beznosková et al. 2015).

An interesting aspect of the specific role of eIF3 in promoting readthrough is that it may actually interfere with another peculiar role of eIF3 in promoting translation reinitiation (REI) (Valášek 2012). REI is a gene-specific mechanism of translational control exerted by some short upstream ORFs (uORFs) to fine-tune the expression of the main ORF. It requires the small ribosomal subunit to remain associated with mRNA even after termination on these so called REI-permissive uORFs in order to resume scanning on the same mRNA molecule until the 40S ribosome reinitiates at the next AUG. eIF3 was shown to play a critical role in this process by making contacts with both the 40S subunit as well as sequences upstream of REI-permissive uORFs to stabilize their mutual interaction (Szamecz et al. 2008; Munzarová et al. 2011; Gunišová and Valášek 2014). Hence both processes—readthrough and REI—are dependent on the physical presence of eIF3 in termination complexes, yet from the regulatory point of view they act against each other. In other words, increased readthrough will prevent REI. Since to our knowledge virtually nothing is known about readthrough on short uORFs, it would be of interest to investigate the mutual functional relationship of readthrough and REI during termination on uORFs that are set in regulatory networks relying on high levels of REI. This is the case of, for example, the *GCN4* mRNA (Gunišová and Valášek 2014), where the integrated regulatory output provided by its four short uORFs could be largely influenced by increased readthrough.

Here, we specifically focused on the leakiest stop codon of all three (UGA) that, when featuring as a PTC, responds relatively unpredictably to various types of anti-PTC treatment (Linde and Kerem 2008; Lee and Dougherty 2012). Our genetic experiments suggest that the key determinant of the highest readthrough levels displayed specifically by the UGA-C tetranucleotide (Bonetti et al. 1995; Beznosková et al. 2015) is the impaired ability of eRF1 to unambiguously recognize the stop codon when it is followed by the cytosine base. Importantly, this "cytosine-specific termination effect" has a general character because it is manifested also on the UAA and UAG stop codons. In addition, we also show that the identity of the +4 base determines the preference of nc-tRNAs for a given UGA-N tetranucleotide. And last but not least, we shed light on readthrough on short uORFs at which the eIF3-promoted REI activity meets but does not collide with the eIF3-promoted, potentially antagonistic, programmed readthrough. Hence we bring new insights into ribosomal decoding rules and translational control that can be

used for better qualitative predictions of medically relevant nonsense suppressions.

RESULTS

Cytosine immediately following any stop codon specifically interferes with the eRF1 decoding in vivo

It has been shown by us and others that the nucleotide immediately following the stop codon largely determines the efficiency of readthrough, with cytosine allowing significantly the highest readthrough levels of all four bases regardless of the nature of the stop codon (Bonetti et al. 1995). However, this effect has never been explained. While this manuscript was under preparation, Ramakrishnan's group showed that guanine at the +4 position after any stop codon is pulled into the A-site and stabilized by stacking interaction with G626 of 18S rRNA (Brown et al. 2015). The authors proposed that this stacking would be more stable for purines, explaining the statistical bias at the +4 position in eukaryotes. However, from all four possibilities, only one, G at the +4 position, features in their structures with different stop codons, and, more importantly, the order of the termination leakiness (stop codon readthrough) determined by the +4 base is C > A > G > U. This means that both supposedly best terminating purines are right in between two pyrimidines, one of which terminates worse but the other even better. Hence, this novel observation still does not fully explain the differences in termination efficiency originating from the identity of the nucleotide following the stop codon.

We thus asked whether it could be caused by some specific decoding properties of the release factor eRF1 (encoded by *SUP45*) that might somehow sense the identity of the +4 nucleotide and perhaps interfere with or specifically accommodate its stacking interaction with 18S rRNA G626. To address this question, we first analyzed UGA as the most readthrough permissive stop codon and used two temperature-sensitive mutants of eRF1 that were shown to increase stop codon readthrough in the past. In particular, we used a *sup45-M48I* mutant that interferes with stop codon decoding (Bertram et al. 2000) and a *sup45-Y410S* mutant that directly disrupts the eRF1–eRF3 interaction (Akhmaloka et al. 2008). As shown before, the efficiency of readthrough in wild-type cells with respect to the nature of the +4 nucleotide followed this order: C > A > G > U (Beznosková et al. 2015), and both eRF1 mutants expectedly increased readthrough for all four bases at the +4 position compared to wild-type (Fig. 1A). However, whereas neither of the eRF1 mutants showed any genetic interaction with A, G and U at the +4 position (the fold increase of readthrough normalized to UGA-U was comparable to that seen in *SUP45* wild-type suggesting that none of these three nucleotides interferes with the stop codon decoding by eRF1), the presence of cytosine produced a robust additive phenotype with both mutants (Fig. 1B). Importantly, essentially the same results were obtained when we subsequently examined two remaining stop codons, UAA and UAG, set in all four possible tetranucleotide combinations (Fig. 1C,D). Hence, we propose that this additive effect

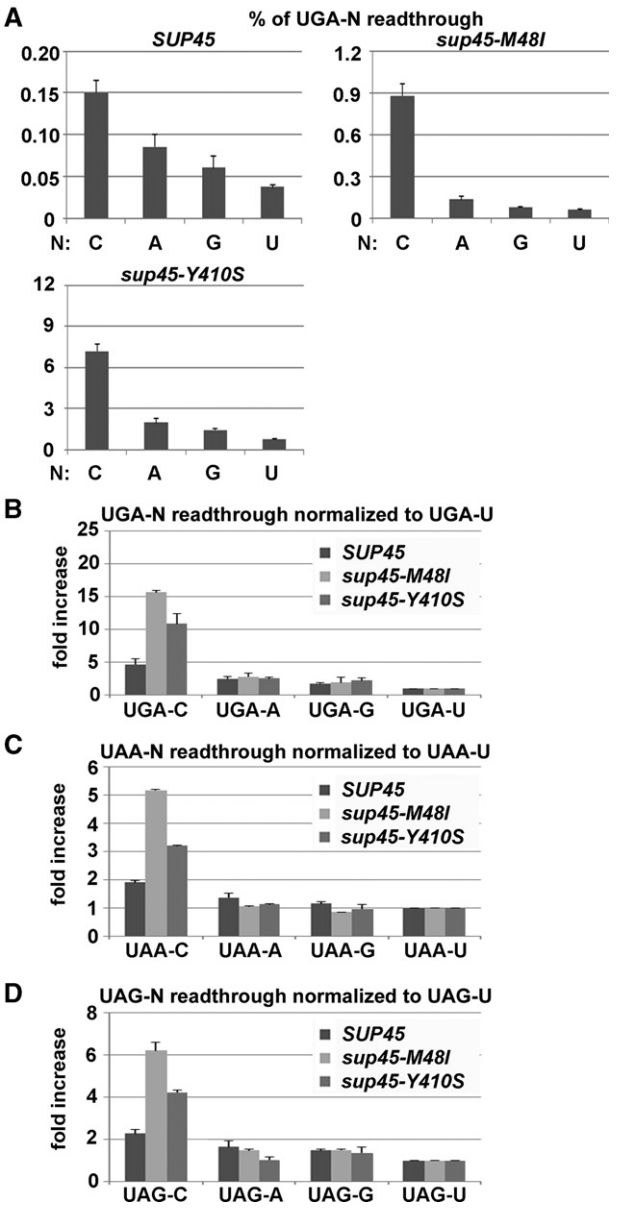

FIGURE 1. Cytosine immediately following any stop codon interferes with the eRF1 decoding in vivo. (*A*) Stop codon readthrough measured at all four UGA-N termination tetranucleotides in wt cells (*SUP45*) and two eRF1 mutants (sup45-M48I and sup45-Y410S). The 74D-694, L2327, and L2521 strains were grown in SD and processed for stop codon readthrough measurements using standard dual luciferase readthrough reporter constructs YEp-R/T-CAAC-L; YEp-R/T-UGAC-L; PBB75; PBB76; and PBB77, as described in Materials and Methods. Readthrough values are represented as mean ± SD from quintuplicates ($n = 5$) and each experiment was repeated at least three times. (*B*) Normalization of readthrough measurements from panel *A*; values measured for UGA-U of each of the four strains were set to one. (*C*) Same as in panel *A*, except that all four UAA-N termination tetranucleotides were examined. (*D*) Same as in panel *A*, except that all four UAG-N termination tetranucleotides were examined.

originates from the compromised ability of eRF1 to properly recognize any stop codon when it is followed specifically by the cytosine base, which would explain why cytosine at +4 position promotes the highest readthrough levels of all four bases regardless of the nature of the stop codon (Bonetti et al. 1995).

UGA-A and UGA-G tetranucleotides are preferentially read through by tryptophan and cysteine nc-tRNAs, respectively

Since cytosine was the only nucleotide at the +4 position displaying the additive effect with eRF1 mutants, we next asked what determines the differences in termination efficiency among the remaining UGA-A, -G, and -U tetranucleotides. We hypothesized that the identity of the +4 nucleotide could influence the stop codon decoding ability of nc-tRNAs that compete for the A-site occupancy with eRF1. If true, overexpression of a nc-tRNA that preferentially incorporates at a given tetranucleotide will increase the fold change of readthrough at this specific tetranucleotide more dramatically than an overexpressed nc-tRNA that is not preferred by this tetranucleotide. Since we focused this study on UGA and in our previous work we demonstrated that efficient readthrough at UGA is enabled exclusively by nc-tRNAs with a mismatch at the third, wobble position (Beznosková et al. 2015), we aimed our attention at tryptophan [tW(CCA)G1] and cysteine [tC(GCA)P1] tRNAs (Fig. 2A), overexpressed them individually in *TIF35* wild-type versus *tif35-KLF* mutant strains (*TIF35* encodes the g subunit of yeast eIF3), and measured the luciferase activities on all four UGA-N tetranucleotides. Note that the *tif35-KLF* mutant is defective in promoting programmed stop codon readthrough and thus the difference between *TIF35* wild type and this mutant indicates the degree of programmed readthrough (Beznosková et al. 2015).

Overexpression of Trp-tRNA increased the overall readthrough efficiency with all four tetranucleotides and this effect was in all cases dependent on intact eIF3 (Fig. 2B, compare fold differences between *TIF35* wt versus mutant cells). The lowest increase (by approximately threefold) was seen with UGA-U and with UGA-G, which suggests that these two tetranucleotides incorporate this particular nc-tRNA with the same low preference. The UGA-C tetranucleotide displayed an intermediate increase (by approximately sixfold); i.e., twice above the UGA-U and -G levels. We ascribe this effect to the specific interaction between UGA-C and eRF1 mentioned above, which allows the highest fold change of readthrough (by approximately twofold) among all four tetranucleotides under physiological conditions (Fig. 1A). The highest, strongly eIF3-dependent increase of readthrough (by approximately ninefold) was upon Trp-tRNA overexpression observed with the UGA-A tetranucleotide, which is with respect to the basal readthrough efficiency otherwise comparable to UGA-G (Fig. 1A). These results thus suggest that tW(CCA)G1 has a lot higher preference for recognition of the A-containing tetranucleotide over the other three, and that the difference in the basal readthrough efficiency on UGA-G or -U is not caused by better incorporation of Trp-tRNA.

Overexpression of Cys-tRNA showed essentially the same "low preference" increase of readthrough (by threefold) as Trp-tRNA with UGA-U and, this time, with UGA-A instead of the UGA-G tetranucleotide (Fig. 2C). UGA-G conversely displayed an increase in readthrough levels by approximately sixfold and UGA-C by ~12-fold. Note that the 12-fold increase with UGA-C cannot solely account for the readthrough increasing effect of the C_4–eRF1 specific interaction and hence we propose that Cys-tRNA preferentially recognizes the C- and G-containing tetranucleotides. Unfortunately, our approach does not allow the dissection of the degree of specific contribution of the C_4–eRF1 interaction versus the

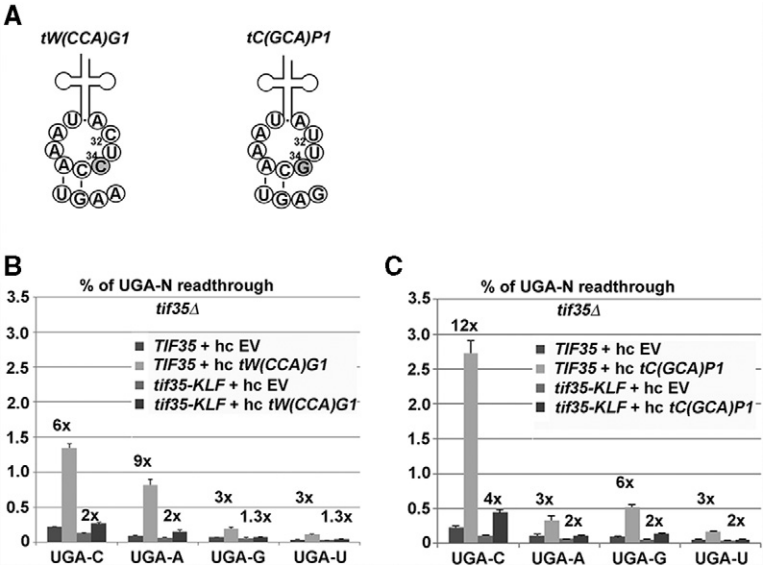

FIGURE 2. The UGA-A tetranucleotide is preferentially read through by tryptophan nc-tRNA and the UGA-C, and UGA-G tetranucleotides are preferentially read through by cysteine nc-tRNA. (*A*) Schematics of Trp and Cys nc-tRNAs base-paring with the indicated stop codon tetranucleotides. Only the nucleotides of the anticodon loop are shown with the third stop codon base N_{34} (in gray) and N_{32} indicated. (*B*) Effect of the eIF3 presence in pre-TCs on UGA-N readthrough upon increased gene dosage of tryptophan nc-tRNA. The PBH140 derivatives bearing *TIF35* wt and *tif35-KLF* mutant alleles were transformed with either empty vector (EV) or high copy (hc) tW(CCA)G1 and the resulting transformants were grown and processed for stop codon readthrough measurements as described in Figure 1. (*C*) Effect of the eIF3 presence in pre-TCs on UGA-N readthrough upon increased gene dosage of cysteine nc-tRNA. Essentially the same as in *B*, except that hc tC(GCA)P1 was used in place of hc tW(CCA)G1.

Cys-tRNA-driven preference for the UGA-C tetranucleotide in the overall effect. Our observation that Cys-tRNA increased the fold exchange of readthrough at UGA-G only sixfold compared to ninefold for Trp-tRNA at UGA-A is probably due to the fact that Cys-tRNA is a weaker competitor with eRF1 for the UGA stop codon between the two nc-tRNAs, and/or that it is naturally less abundant tRNA in our genetic background than Trp-tRNA. Importantly, all effects were dependent on intact eIF3, as expected.

In contrast, control experiments with arginine [tR(UCU)E] and glycine [tG(UCC)O] tRNAs, which are also near-cognate for UGA but with the mismatch at the first position and, at least in our experimental setup, do not incorporate at UGA even when overexpressed (Beznosková et al. 2015), showed no preference for any tetranucleotide (Supplemental Fig. S1). Notably, Northern blotting revealed that all four nc-tRNAs that were overexpressed in this study show increased levels by ~1.5- through sevenfold, depending on the number of isogenes encoding a corresponding nc-tRNA, with the control Arg and Gly tRNAs displaying ~1.9- and sevenfold increases, respectively (Supplemental Fig. S2). To rule out the "genetic background" effects, we examined two additional genetically unrelated strains and observed consistent tetranucleotide-specific preference of UGA-A for tryptophan and UGA-G for cysteine nc-tRNAs (Supplemental Fig. S3); please note varying fold increases among the tested strains most probably reflecting different endogenous levels of at least these two nc-tRNAs in these backgrounds. Hence we conclude that in contrast to the UGA-U tetranucleotide, UGA-A and UGA-G tetranucleotides are preferentially read through by tryptophan and cysteine nc-tRNAs, respectively, which is the fact that may markedly contribute to the differences in termination efficiency among these three tetranucleotides. Our findings also indicate that the frequency of preferential incorporation of nc-tRNAs at corresponding stop codons or PTCs will most probably vary with varying endogenous levels of individual nc-tRNAs in individual cell types.

Neither the eRF1 decoding ability nor the geometry of the decoding pocket determines the UGA-N tetranucleotide preference for specific nc-tRNAs

To rule out that the observed UGA-N tetranucleotide preference for nc-tRNAs is caused by structural changes that different tetranucleotides may impose on the geometry of the decoding pocket, we measured the effect of overexpression of nc-tRNAs in the presence of 200 μg/mL paromomycin. The miscoding agent paromomycin disables ribosomal discrimination against nc-tRNAs by specific altering of the geometry of the A-site codon decoding pocket, so that eRF1 can no longer actively sense the correct Watson–Crick base-pairing geometry (Bidou et al. 2012). In *TIF35* wild-type cells bearing an empty vector (EV), paromomycin increased readthrough with all four tetranucleotides by a similar fold, as expected (Supplemental Fig. S4). In paromomycin-treated cells overexpressing the Trp-tRNA, however, the highest increase in readthrough compared to cells bearing EV was seen with the UGA-A and the lowest with UGA-G tetranucleotides (Fig. 3A). Conversely, cells overexpressing the Cys-tRNA displayed the highest increase in readthrough—compared to EV—with UGA-G and -C, and the lowest with UGA-A tetranucleotides (Fig. 3B). The fact that the use of paromomycin had practically no effect on the tetranucleotide preference of both nc-tRNAs suggests that it is the specific nature of these tRNAs and not the geometry of the decoding pocket that enables them to selectively sense the nature of the base occurring at the +4 position. To support this suggestion even further, we overexpressed these nc-tRNAs in *sup45-M48I*, which is known to directly impair the stop codon decoding and observed virtually the same effects as in the previous two set-ups (Fig. 4), with the exception of UGA-U that, for some reason, showed increased readthrough in this particular mutant (see also Fig. 1A). In detail, the UGA-A tetranucleotide allowed the highest levels of readthrough with tW(CCA)G1 overexpressed (~4.5-fold), whereas UGA-G (and to a smaller degree also UGA-C) had the same effect with tC(GCA)P1 overexpressed (approximately six- and fourfold). Hence we conclude that the observed UGA-N tetranucleotide preference of nc-tRNAs with a mismatch at the wobble position is highly specific, at least for the termination leakiest UGA stop codon, and most probably reflects some intrinsic tetranucleotide decoding properties of these tRNAs that have not been observed before.

To understand what these properties might be, we compared primary sequences of the anti-codon loop of both tW(CCA)G1 and tC(GCA)P1 and observed the only

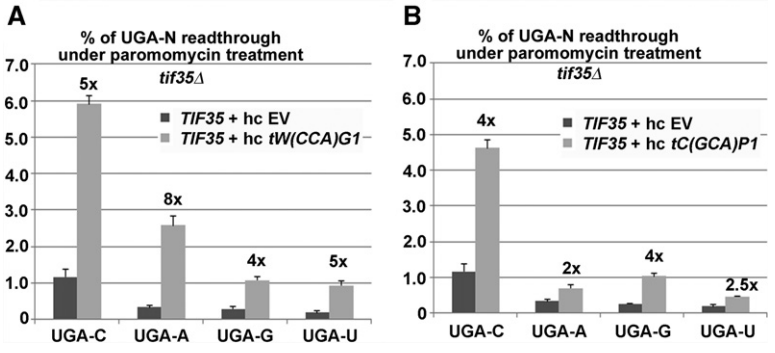

FIGURE 3. Effect of the miscoding agent paromomycin on hc tryptophan or cysteine nc-tRNA incorporation at UGA-N termination tetranucleotides. (*A*) The PBH140 derivative bearing *TIF35* wt was transformed with either empty vector (EV) or hc tW(CCA)G1, and the resulting transformants were grown in SD with 200 μg/mL paromomycin for 6 h and processed for stop codon readthrough measurements as described in Figure 1. (*B*) Essentially the same as in *A*, except that hc tC(GCA)P1 was used in place of hc tW(CCA)G1.

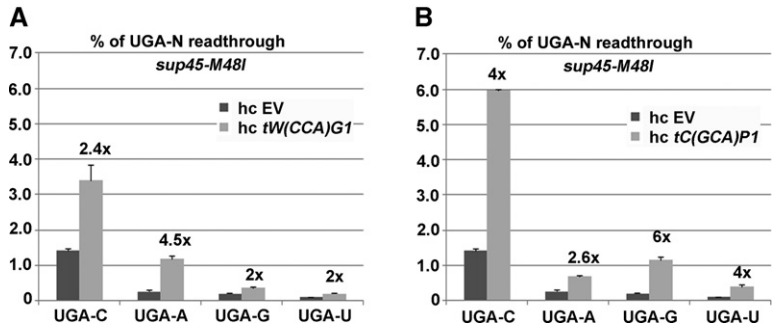

FIGURE 4. Effect of the eRF1 (*sup45-M48I*) mutation with impaired decoding ability on hc tryptophan or cysteine nc-tRNA incorporation at UGA-N termination tetranucleotides. (*A*) The L2327 was transformed with either empty vector (EV) or hc tW(CCA)G1 and the resulting transformants were grown and processed for stop codon readthrough measurements as described in Figure 1. (*B*) Essentially the same as in *A*, except that hc tC(GCA)P1 was used in place of hc tW(CCA)G1.

difference at base 32, indeed with the exception of the anticodon itself (base 34) (Fig. 2A). The tryptophan tW(CCA)G1 tRNA has methylated C (Cm) at position 32, whereas the cysteine tC(GCA)P1 tRNA carries U, which is during maturation modified to become pseudouridine (Pineyro et al. 2014). We hypothesized that by swapping these nucleotides we may possibly change the tetranucleotide preference of these two nc-tRNAs, provided that position 32 plays a critical role in it. However, the C32U replacement rendered the tW(CCA)G1 tRNA inactive in our assay when in high copy (Supplemental Fig. S5). In addition, it produced a modest dominant negative slow growth phenotype (data not shown), suggesting that C32 is critically required for a proper function of this nc-tRNA in general. The U32C replacement of tC(GCA)P1 had virtually no effect on its tetranucleotide preference (Supplemental Fig. S5). Hence the question of what determines the intrinsic ability of nc-tRNAs to sense the nucleotide content of the fourth position remains open.

eIF3-promoted readthrough does not interfere with the eIF3-promoted reinitiation on REI-permissive uORF1 from the *GCN4* mRNA leader

We previously proposed that following elongation, eIF3 associates with any pretermination complex regardless of the character of the stop codon, and its context, however, acts to promote readthrough only when the stop codon is programmed (Beznosková et al. 2015). At the same time, eIF3 was—thanks to its favorable location on the solvent-exposed side of the 40S ribosome (Valášek et al. 2003; Erzberger et al. 2014)—demonstrated to be one of the few initiation factors that is retained on 80S ribosomes translating short upstream ORFs even after subunit joining (Pöyry et al. 2004; Szamecz et al. 2008; Munzarová et al. 2011). More specifically, if the short uORF is not longer than 5–10 codons, eIF3 does not dissociate from the 40S subunit but remains 80S-bound even during elongation until the 80S ribosome reaches the stop codon to become a pre-TC. Some uORFs make use of this specific eIF3 ability and by engaging their 5′ sequences in a specific interaction with the N-terminal domain of the a/TIF32 subunit of eIF3 formed during termination, they prevent the small ribosomal subunit from being recycled. This enables the 40S subunit to subsequently resume scanning downstream until the next AUG has been encountered for translation REI on the same mRNA molecule. The intriguing fact that the eIF3 presence in pre-TCs formed at stop codons of short uORFs can theoretically stimulate readthrough and REI at the same time, but both activities are by their nature antagonistic, prompted us to investigate their prospective mutual interference with the help of the yeast transcriptional activator *GCN4*.

The *GCN4* mRNA leader contains four short uORFs that together constitute a very sophisticated mechanism of translational control in response to numerous stresses, such as, for example, amino acid starvation (Hinnebusch 2005; Valášek 2012). In particular, uORFs 1 and 2 allow highly efficient resumption of scanning and subsequent REI downstream, whereas REI only modestly permissive uORF3 and REI-nonpermissive uORF4 complete the termination process by recycling both ribosomal subunits to prevent *GCN4* derepression under normal growth conditions (Gunišová and Valášek 2014). Under starvation conditions, dramatically decreasing the levels of the Met-tRNA.eIF2.GTP ternary complex (TC), the majority of 40S ribosomes that have resumed scanning past uORFs 1 and 2 will skip uORFs 3 and 4 due to the low TC levels, and eventually rebind the TC on their way from uORF4 to the *GCN4* gene to derepress its expression. Hence, the roles of uORF1 and uORF4 especially are the key for the whole regulatory mechanism, with uORF2 serving only as the uORF1 back-up in the case of increased leaky scanning (Gunišová and Valášek 2014).

A possibility that programmed readthrough further increases the complexity of this regulation has never been considered before. As hinted above, increased readthrough on uORFs 1 and 2 evoked by the presence of eIF3 in pre-TCs could counteract their intrinsically high permissiveness for REI. In other words, if both uORF1 and uORF2 displayed higher rates of readthrough, eIF3 would dissociate from 80S ribosomes elongating past their natural stop codons, and the pre-TCs formed at the next stop codon would thus be fully recycled. This would in turn prevent full derepression of *GCN4* expression under starvation conditions. Increased readthrough on the ultimate uORF4 could, on the other hand, make the whole regulatory system even tighter because the readthrough interference with REI on this specific uORF would further diminish the already low REI activity that uORF4 under nonstarvation conditions allows.

Inspection of the 6-nt-long sequences following stop codons of these four uORFs indicated that the stop codon of one of them (namely uORF4) could be in fact highly programmed (the 6-nt-long "stop codon context" is a critical determinant of programmed readthrough [Namy et al. 2001; von der Haar and Tuite 2007]). Hence we first monitored readthrough efficiency of the UGA stop followed by the 6-nt context corresponding to all four uORFs and to the *GCN4* main ORF. We took the *GCN4* stop codon context as a negative control because it has a readthrough nonpermissive character with basal activity comparable to our negative controls (Beznosková et al. 2015), and because it is a genuine part of this regulatory system. Our standard pTH477 construct with the UGA-C stop codon context, which is known to allow relatively high levels of readthrough (Bonetti et al. 1995), was chosen as a positive control for programmed readthrough. All our measurements were carried out under nonstarvation conditions because the major effect of starvation is the reduction of the TC levels with little to no effect on resumption of scanning efficiencies of all four uORFs per se. Hence we assumed that their readthrough efficiencies would not be largely affected too. Our luciferase assay revealed that uORF4 is indeed subject to programmed readthrough as it displayed the eIF3-dependent ~12-fold higher activity than the *GCN4* stop codon context and approximately twofold higher than our UGA-C control (Fig. 5A). This increase is most likely too high to be explained merely by the presence of cytosine at the +4 position. The contexts of the remaining three uORFs also allowed an increase (by ~2.5-fold) in readthrough compared to *GCN4*, most probably owing to A at the +4 position compared to U in the case of *GCN4*, with mild but still significant dependency on intact eIF3. This modestly programmed character could actually suggest that the presence of eIF3 in pre-TCs specifically in the case of uORF1 might indeed interfere with its eIF3-mediated ability to allow resumption of scanning for REI downstream. It is therefore possible that some mechanism evolved to prevent this undesirable interference between eIF3-mediated readthrough versus resumption of scanning to keep the control of *GCN4* expression as tight as possible. For example, other sequences besides the 3′ adjacent 6-nt-long stop codon context could nullify this effect. Interestingly, the uORF1 coding region and the 3′ sequence immediately following its stop codon were demonstrated in the past to be absolutely essential for its function in REI (Grant and Hinnebusch 1994). To explore the possibility that the uORF1 coding sequence including its stop codon modifies the readthrough effect of its 3′ sequence context, we reexamined the efficiency of readthrough of all four uORFs comprising their genuine stop codons plus six preceding and six following nucleotides. Interestingly, we found that readthrough of the key REI-permissive ORF1 dropped down significantly approaching the minimal readthrough levels obtained with the corresponding *GCN4* sequences surrounding its stop codon (Fig. 5B). In addition, uORF1 readthrough also lost its programmed character de-

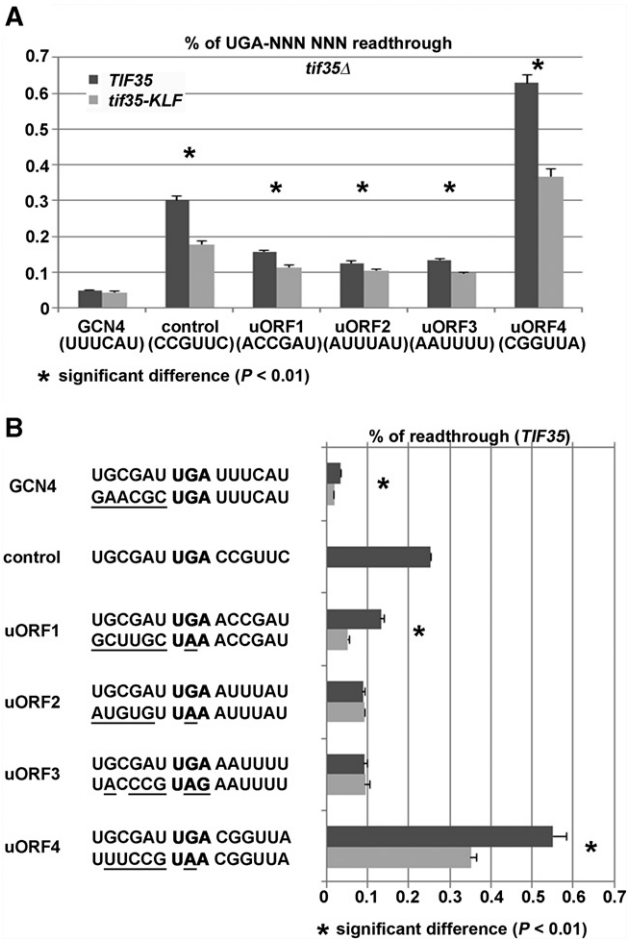

FIGURE 5. eIF3-promoted readthrough does not interfere with the eIF3-promoted REI on REI-permissive uORF1 from the *GCN4* mRNA leader. (*A*) The 6-nt-long context immediately following stop codons of all four uORFs from the *GCN4* mRNA leader allows eIF3-dependent readthrough with varying efficiency. The PBH140 derivatives bearing *TIF35* wt and *tif35-KLF* mutant alleles were grown in SD and processed for stop codon readthrough measurements using standard dual luciferase readthrough reporter constructs pTH460; pTH477; PBB135; PBB136; PBB137; PBB138; and PBB139 as described in Materials and Methods. Changes in the measured readthrough values between *TIF35* and *tif35-KLF* cells were analyzed by the Student's *t*-test (mean ± SD; $n = 6$) and shown to be statistically significant only for those cases marked with the asterisk ($P < 0.01$). (*B*) The 6-nt-long sequence preceding the stop codon of uORF1 nullifies the eIF3-mediated stimulation of stop codon readthrough on this REI-permissive uORF. The PBH140 derivative bearing the *TIF35* wt allele was grown in SD and processed for stop codon readthrough measurements using standard dual luciferase readthrough reporter constructs pTH460; pTH477; PBB135; PBB136; PBB137; PBB138; PBB139; PBB140; PBB141; PBB142; PBB143; and PBB144 as described in Materials and Methods. Changes in the measured readthrough values between selected constructs were analyzed by the Student's *t*-test (mean ± SD; $n = 6$) and shown to be statistically significant only for those cases marked with the asterisk ($P < 0.01$).

fined by the *KLF* mutant (Supplemental Fig. S6). This is remarkable because generally the influence of the 5′-adjacent sequence on the efficiency of readthrough is considered to be more subtle compared to the effect of the 3′-sequence

context (Lee and Dougherty 2012). The other REI-permissive uORF2 that is, however, serving only as the uORF1 back-up showed no significant changes (Fig. 5B). Since both uORF1 and uORF2 terminate at the same UAA stop codon, it is highly likely that the readthrough potential of the uORF1 3′ adjacent sequence was specifically eliminated by its coding sequence and not by the replacement of the programmed UGA stop codon. uORF4 remained programmed as expected (Supplemental Fig. S6), even though its overall readthrough efficiency was reduced, most probably due to the UGA for UAA stop codon replacement (Fig. 5). Here, in contrast to uORF1, the action of the readthrough-promoting eIF3 complex is desirable to keep the uORF4 potential to resume scanning post its translation to a minimum, as proposed above. uORF3 displayed no dramatic change only it lost its programmed character like uORFs 1 and 2 (Fig. 5; Supplemental Fig. S6). Together these results indicate that the key uORF1 naturally evolved to ensure as efficient termination as possible to be able to promote potent REI despite the constant presence of the readthrough-stimulating eIF3 complex. Our data thus point at an interesting phenomenon where two counter-acting regulatory processes exist, both are mediated by the same protein factor, yet their mutual interference is prevented in favor of only one of them.

DISCUSSION

The major goals of our study were to investigate (i) what is the molecular mechanism by which the +4 base influences the readthrough efficiency, (ii) if there is a preference of nc-tRNAs for incorporation into individual stop codons during readthrough, and finally if these two phenomena are interdependent. Despite the fact that several studies suggested that the sequences surrounding the stop codon had no impact on the identity or proportion of amino acids incorporated during the readthrough process (see for example the most recent one by Blanchet et al. 2014), we thought that there were still several hints suggesting the opposite. For example, numerous reports have described that the surrounding nucleotide context had a major effect on termination efficiency (Bonetti et al. 1995; Mottagui-Tabar et al. 1998; Namy et al. 2001). Especially the identity of a nucleotide following the termination codon (position +4) markedly impacts the readthrough permissiveness of all three stop codons by an unknown mechanism (Dabrowski et al. 2015) that could be in principle connected with nc-tRNA preference for a particular stop codon in a specific tetranucleotide context.

Since UGA is the least stringent of all stop codons with respect to termination accuracy and we and others recently showed that there are only two nc-tRNAs (Trp and Cys) that can efficiently incorporate at UGA (Blanchet et al. 2014; Beznosková et al. 2015), we focused our attention on UGA and these two nc-tRNAs with the mismatch at the third position. A very recent study revealed that besides Trp and Cys, also Arg can relatively efficiently incorporate at UGA (Roy et al. 2015); however, Arg-tRNA with the mismatch at the first position does not work as the specific nc-tRNA in our experimental set-up, because it does not incorporate at the UGA stop codon even when overexpressed (Beznosková et al. 2015). Thus we used it as a negative control together with Gly-tRNA, mispairing with UGA also only at the first position. Our detailed analysis of the preference of Trp-tRNA and Cys-tRNA for the UGA stop codon set in all four possible tetranucleotides (UGA-C, -A, -G, and –U) revealed that it is in fact the identity of the +4 base, which is the main determinant of this preference. UGA-U showed the lowest readthrough, as expected, with no preference for any nc-tRNA when overexpressed. UGA-C displayed the highest readthrough, also as expected, with a preference for Cys-tRNA. A strong preference for the Cys-tRNA was also observed with UGA-G, whereas the UGA-A tetranucleotide showed a strong preference for Trp-tRNA (Fig. 2). Considering that other experiments showed a lack of correlation between absolute tRNA abundance and translation elongation rates (Pechmann and Frydman 2013), we should be able to rule out that our nc-tRNA overexpression readthrough data are nonspecifically influenced by changes in elongation rates. In addition, control nc-tRNAs with a mismatch at the first position did not incorporate at UGA at the frequency above the background and expectedly showed no preference for any tetranucleotide whatsoever (Supplemental Figs. S1, S2).

What determines the observed preference of nc-tRNAs for different tetranucleotides on the molecular level remains to be investigated. Our experiments with paromomycin and the eRF1 mutant defective in decoding (Figs. 3, 4) showing little to no impact on the context-specific preference for nc-tRNAs at least rule out the contribution of the altered geometry of the decoding pocket or some noncanonical influence of eRF1. Hence it is very likely that the nc-tRNAs carry by themselves some specific features that markedly contribute to the decoding mechanism by sensing the nature of the base immediately following the stop codon. In theory these features could be represented by unique bases or some tRNA-specific modifications that the individual tRNAs undergo during maturation. In an effort to address this important question, we tested if the major "nc-tRNA preference discriminator" lies in the anticodon loop, in particular in the N_{32} base, but obtained inconclusive results (Supplemental Fig. S5). We also selected all nonessential genes shown to be responsible for differential modification of tryptophan and cysteine tRNAs in the past (Pineyro et al. 2014), and measured readthrough efficiency in the corresponding EUROSCARF deletion mutants. None of these mutants, however, produced any significant effect on the observed context-dependent preference for the Trp and Cys nc-tRNAs (data not shown), though we cannot rule out that we missed some modification(s) or their combination(s) that might be the key in this discriminator effect. Actually, the most obvious feature in which these two tRNAs differ is the anticodon itself, in particular N_{34}—the third position base. It undoubtedly occurs directly

in the decoding site and thus could be involved in some kind of a contact with the neighboring fourth stop codon base of the stop codon, especially in the light of the most recent observations that the stop codon tetranucleotide adopts a stable U-turn-like geometry that pulls the fourth base into the A-site and thus shortens the mRNA (Matheisl et al. 2015). For example, tryptophan's Cm_{34} could have some specific influence during the UGA-A decoding, whereas cysteine's G_{34} during UGA-G decoding (Fig. 2A). Interestingly, recent studies suggested that the position 3 codon–anticodon mispairings could be possible with multiple nonstandard Watson–Crick pairs (A-C > G-G > A-G) (Blanchet et al. 2014; Roy et al. 2015). Hence we speculate that when a nc-tRNA occurs in the A-site with the stop codon tetranucleotide adopting the U-turn, these nonstandard Watson–Crick pairs might form between the fourth stop codon base and the nc-tRNA's N_{34} to drive the observed "nc-tRNA preference." New structural studies with various combinations of stop codons in different contexts bound by corresponding nc-tRNAs are very much needed to resolve this important problem.

The presence of cytosine at the +4 base position shows two effects: (i) the highest readthrough levels of all four bases at this position regardless of the stop codon identity, as shown before (Dabrowski et al. 2015); and (ii) the specific preference for Cys-tRNA in the case of the UGA stop codon. Using two eRF1 mutants with different termination defects, we showed that the first effect could arise from a poorer UGA stop codon recognition by wild-type eRF1, which holds true also for the remaining two stops (Fig. 1). Why it is so we do not know; however, the eRF1 role in this C_4-specific effect is consistent with an earlier suggestion that the most robust readthrough stimulating effect of C_4 could be linked to interactions of mRNA with the translational machinery rather than to interactions of the stop codon with nc-tRNAs (Phillips-Jones et al. 1995). In support, crosslinking experiments demonstrated that the +4 nucleotide in mRNA interacts with eRF1 (Bulygin et al. 2002) and, consistently, the essential K residue from the critical TASNIKS motif in the NTD of eRF1 was in a recent structural study proposed to lie in the proximity of the +4 nucleotide (des Georges et al. 2014). Our results could thus imply that the contact between the K residue and cytosine at the +4 position is qualitatively different from contacts with the other three bases in the same position, which makes it the least stringent base for efficient termination. Alternatively, it is possible that the newly observed stacking interaction between the +4 base and G626 (Brown et al. 2015) could play a specific role in the C_4 effect due to the weakest (i.e., the least stable) stacking of C_4 with G626 of 18S rRNA. On top of this general effect, it appears that Cys-tRNA can specifically sense C_4 when occurring in the context of the UGA stop codon to incorporate more efficiently at this tetranucleotide. This effect is most probably separable from the eRF1 effect; i.e., driven specifically by some intrinsic feature(s) of the Cys-tRNA by itself that remains to be determined experimentally. Sorting out the individual contributions of all possible players in the C_4 effect is especially interesting because this most programmed UGA-C tetranucleotide among all is vastly underrepresented in genomes across the species (McCaughan et al. 1995), which could mean that it is predominantly utilized as a trigger for programmed stop codons.

We also analyzed the readthrough efficiency on short uORFs that are critical for maintaining the tight translational control of a main gene by allowing high rates of translational REI, such as in the case of uORF1 from the mRNA leader of the *GCN4* transcriptional activator (Hinnebusch 2005; Valášek 2012). We revealed that even though the 3′ context of the uORF1 stop codon showed increased rates of readthrough dependent on eIF3, its 5′ context evolved in a way to practically completely eliminate any readthrough whatsoever (Fig. 5). Importantly, this effect was found to be highly specific only for the key uORF1 feature of the whole *GCN4* regulatory network. The last uORF from this network, uORF4, which serves as a barrier in front of the *GCN4* gene allowing negligible REI to prevent *GCN4* expression under normal growth conditions, gained conversely relatively high readthrough efficiency further fortifying its blocking role. Since both readthrough and REI rely on the eIF3 presence in the pre-TC, our results provide an interesting insight into how natural selection prevented one eIF3-promoted mechanism going by its nature against the other eIF3-promoted mechanism to interfere with the overall regulatory process. These results appear to be the exception to the rule that the 5′ adjacent sequences of the stop codon have a much smaller impact on readthrough efficiency compared to the 3′ context sequences (Lee and Dougherty 2012).

Taken together, our findings (i) demonstrate the importance of the +4 base for the preferred incorporation of nc-tRNAs at corresponding stop codons, and (ii) at least partially explain the highest termination leakiness of all three stop codons with cytosine at their +4 position compared to the other three bases. The readthrough phenomenon concerns not only regular stop codons but also nonsense mutations within coding regions; i.e., PTCs. In fact, it was reported that nonsense mutations account for ∼11% of all described gene lesions causing human-inherited disease and ∼20% of disease-associated single-base pair substitutions affecting gene coding regions (Mort et al. 2008). Hence we believe that our findings reported here, as well as the most recent insights by others (Blanchet et al. 2014; Brown et al. 2015; Roy et al. 2015), may potentially help with the design of new drugs or other effectors to specifically promote readthrough on various PTCs to prevent pathological effects of only partially synthetized proteins. The problem with most of the clinical trials is the efficiency of PTC-readthrough therapies, which is unfortunately not always satisfactory mainly due to unexpected discrepancies in response to the currently used drugs, which are in a majority of cases aminoglycosides (Linde and Kerem 2008; Lee and Dougherty 2012). Our experiments

with nc-tRNA's overexpression indicate that changing an intracellular level of a selected endogenous nc-tRNA may in turn change the readthrough specificity of individual tetranucleotides, such as, for example, the case of Cys-tRNA changing the C > A > G > U order of readthrough efficiency to C > G > A > U (Fig. 2B). Taking a look from a different angle, Roy and colleagues recently proposed, but did not experimentally prove, that changing the sequence context and other parameters known to affect readthrough (e.g., the identity of the most 3′ nucleotide to the PTC) will most likely determine the frequency with which an amino acid gets inserted at the PTC (Roy et al. 2015). Hence, it could be proposed that the use of, for example, paromomycin may lead to the observed unexpected variability due to (i) the differing identity of the +4 base following the same type of a PTC, and (ii) differing intracellular levels of endogenous nc-tRNAs among different cell types or organisms. For instance, a paromomycin treatment of the UGA-A PTC in a background with high levels of tryptophan nc-tRNA will have a more potent impact on this PTC suppression than in a background with low tryptophan nc-tRNA levels or when set in the UGA-G context (Fig. 3A). Hence an informed choice of a particular drug that would be best suited to a given PTC mutation of medical interest should include not only the knowledge of the identity of the premature stop codon and its context, but also the knowledge of the intracellular levels of tRNAs that work as near-cognates for the PTC of interest.

MATERIALS AND METHODS

Yeast strains and plasmids

The lists and descriptions of plasmids and yeast strains used throughout this study (summarized in Supplemental Tables S1–S3) can be found in the Supplemental Material.

Stop codon readthrough assays

The majority of stop codon readthrough assays in this study were performed using a standard bicistronic reporter construct bearing a *Renilla* luciferase gene followed by an in-frame firefly luciferase gene. Separating the two genes is either a tetranucleotide termination signal (UGA-C) or, for control purposes, the CAA sense codon followed by cytosine. In indicated cases the termination signal and/or the following nucleotide context was modified. It is noteworthy that this system avoids possible artifacts connected to the changes in the efficiency of translation initiation associated with the NMD pathway (Muhlrad and Parker 1999), because both *Renilla* and firefly enzymes initiate translation from the same AUG codon. For further details, see Keeling et al. (2004). All experiments and data analysis were carried out according to the Microtiter plate-based dual luciferase protocol developed by Merritt et al. (2010) and commercially distributed by Promega. Readthrough values are represented as mean ± SD from quintuplicates ($n = 5$) and each experiment was repeated at least three times.

Northern blot analysis

The Quick RNA miniprep from yeast using glass beads for cell lysis was performed as previously described in Cross and Tinkelenberg (1991). The RNAs were kept in RNase-free water, run on a Criterion Precast Gel 15% TBE-Urea, 1.0 mm (Bio-Rad) and transferred to the 0.45 nylon transfer membrane (Nytran SPC, Whatman). Custom-made 5′ ^{32}P—labeled oligonucleotides were used as probes. Signals were captured in Fuji MS phosphor storage screens, scanned with a Molecular Imager FX (Bio-Rad), and quantified with NIH ImageJ.

SUPPLEMENTAL MATERIAL

Supplemental material is available for this article.

ACKNOWLEDGMENTS

We are grateful to David Bedwell and Sebastian Leidel for material and advice, the Libor Krásný laboratory members, and in particular Michaela Šiková for her help with Northern blotting, Tobias von der Haar for critical reading of the manuscript, and all our laboratory members for fruitful discussions. This research was supported by the Centrum of Excellence of the Czech Science Foundation P305/12/G034, Wellcome Trust grant 090812/B/09/Z (both to L.S.V.), and Charles University in Prague, project GA UK no. 323415 (to P.B.).

Received September 15, 2015; accepted December 10, 2015.

REFERENCES

Akhmaloka, Susilowati PE, Subandi, Madayanti F. 2008. Mutation at tyrosine in AMLRY (GILRY like) motif of yeast eRF1 on nonsense codons suppression and binding affinity to eRF3. *Int J Biol Sci* **4:** 87–95.

Bertram G, Bell HA, Ritchie DW, Fullerton G, Stansfield I. 2000. Terminating eukaryote translation: domain 1 of release factor eRF1 functions in stop codon recognition. *RNA* **6:** 1236–1247.

Beznosková P, Cuchalová L, Wagner S, Shoemaker CJ, Gunišová S, Von der Haar T, Valášek LS. 2013. Translation initiation factors eIF3 and HCR1 control translation termination and stop codon read-through in yeast cells. *PLoS Genet* **9:** e1003962.

Beznosková P, Wagner S, Jansen ME, von der Haar T, Valášek LS. 2015. Translation initiation factor eIF3 promotes programmed stop codon readthrough. *Nucleic Acids Res* **43:** 5099–5111.

Bidou L, Allamand V, Rousset JP, Namy O. 2012. Sense from nonsense: therapies for premature stop codon diseases. *Trends Mol Med* **18:** 679–688.

Blanchet S, Cornu D, Argentini M, Namy O. 2014. New insights into the incorporation of natural suppressor tRNAs at stop codons in *Saccharomyces cerevisiae*. *Nucleic Acids Res* **42:** 10061–10072.

Bonetti B, Fu L, Moon J, Bedwell DM. 1995. The efficiency of translation termination is determined by a synergistic interplay between upstream and downstream sequences in *Saccharomyces cerevisiae*. *J Mol Biol* **251:** 334–345.

Brown A, Shao S, Murray J, Hegde RS, Ramakrishnan V. 2015. Structural basis for stop codon recognition in eukaryotes. *Nature* **524:** 493–496.

Bulygin KN, Repkova MN, Ven'yaminova AG, Graifer DM, Karpova GG, Frolova LY, Kisselev LL. 2002. Positioning of the mRNA stop signal with respect to polypeptide chain release factors and ribosomal proteins in 80S ribosomes. *FEBS Lett* **514:** 96–101.

Cross FR, Tinkelenberg AH. 1991. A potential positive feedback loop controlling CLN1 and CLN2 gene expression at the start of the yeast cell cycle. *Cell* **65:** 875–883.

Dabrowski M, Bukowy-Bieryllo Z, Zietkiewicz E. 2015. Translational readthrough potential of natural termination codons in eucaryotes —the impact of RNA sequence. *RNA Biol* **12:** 950–958.

des Georges A, Hashem Y, Unbehaun A, Grassucci RA, Taylor D, Hellen CU, Pestova TV, Frank J. 2014. Structure of the mammalian ribosomal pre-termination complex associated with eRF1•eRF3•GDPNP. *Nucleic Acids Res* **42:** 3409–3418.

Dinman JD. 2012. Control of gene expression by translational recoding. *Adv Protein Chem Struct Biol* **86:** 129–149.

Erzberger JP, Stengel F, Pellarin R, Zhang S, Schaefer T, Aylett CH, Cimermancic P, Boehringer D, Sali A, Aebersold R, et al. 2014. Molecular architecture of the 40S•eIF1•eIF3 translation initiation complex. *Cell* **158:** 1123–1135.

Grant CM, Hinnebusch AG. 1994. Effect of sequence context at stop codons on efficiency of reinitiation in *GCN4* translational control. *Mol Cell Biol* **14:** 606–618.

Gunišová S, Valášek LS. 2014. Fail-safe mechanism of *GCN4* translational control—uORF2 promotes reinitiation by analogous mechanism to uORF1 and thus secures its key role in *GCN4* expression. *Nucleic Acids Res* **42:** 5880–5893.

Hinnebusch AG. 2005. Translational regulation of GCN4 and the general amino acid control of yeast. *Annu Rev Microbiol* **59:** 407–450.

Jackson RJ, Hellen CU, Pestova TV. 2012. Termination and post-termination events in eukaryotic translation. *Adv Protein Chem Struct Biol* **86:** 45–93.

Keeling KM, Lanier J, Du M, Salas-Marco J, Gao L, Kaenjak-Angeletti A, Bedwell DM. 2004. Leaky termination at premature stop codons antagonizes nonsense-mediated mRNA decay in *S. cerevisiae*. *RNA* **10:** 691–703.

Keeling KM, Xue X, Gunn G, Bedwell DM. 2014. Therapeutics based on stop codon readthrough. *Annu Rev Genomics Hum Genet* **15:** 371–394.

Lee HL, Dougherty JP. 2012. Pharmaceutical therapies to recode nonsense mutations in inherited diseases. *Pharmacol Ther* **136:** 227–266.

Linde L, Kerem B. 2008. Introducing sense into nonsense in treatments of human genetic diseases. *Trends Genet* **24:** 552–563.

Matheisl S, Berninghausen O, Becker T, Beckmann R. 2015. Structure of a human translation termination complex. *Nucleic Acids Res* **43:** 8615–8626.

McCaughan KK, Brown CM, Dalphin ME, Berry MJ, Tate WP. 1995. Translational termination efficiency in mammals is influenced by the base following the stop codon. *Proc Natl Acad Sci* **92:** 5431–5435.

Merritt GH, Naemi WR, Mugnier P, Webb HM, Tuite MF, von der Haar T. 2010. Decoding accuracy in eRF1 mutants and its correlation with pleiotropic quantitative traits in yeast. *Nucleic Acids Res* **38:** 5479–5492.

Mort M, Ivanov D, Cooper DN, Chuzhanova NA. 2008. A meta-analysis of nonsense mutations causing human genetic disease. *Hum Mutat* **29:** 1037–1047.

Mottagui-Tabar S, Tuite MF, Isaksson LA. 1998. The influence of 5′ codon context on translation termination in *Saccharomyces cerevisiae*. *Eur J Biochem* **257:** 249–254.

Muhlrad D, Parker R. 1999. Recognition of yeast mRNAs as "nonsense containing" leads to both inhibition of mRNA translation and mRNA degradation: implications for the control of mRNA decapping. *Mol Biol Cell* **10:** 3971–3978.

Munzarová V, Pánek J, Gunišová S, Dányi I, Szamecz B, Valášek LS. 2011. Translation reinitiation relies on the interaction between eIF3a/TIF32 and progressively folded *cis*-acting mRNA elements preceding short uORFs. *PLoS Genet* **7:** e1002137.

Namy O, Hatin I, Rousset JP. 2001. Impact of the six nucleotides downstream of the stop codon on translation termination. *EMBO Rep* **2:** 787–793.

Pechmann S, Frydman J. 2013. Evolutionary conservation of codon optimality reveals hidden signatures of cotranslational folding. *Nat Struct Mol Biol* **20:** 237–243.

Phillips-Jones MK, Hill LS, Atkinson J, Martin R. 1995. Context effects on misreading and suppression at UAG codons in human cells. *Mol Cell Biol* **15:** 6593–6600.

Pineyro D, Torres AG, de Pouplana LR. 2014. Biogenesis and evolution of functional tRNAs. In *Fungal RNA biology* (ed. Sesma A, von der Haar T), pp. 233–267. Springer International Publishing, Switzerland.

Pöyry TA, Kaminski A, Jackson RJ. 2004. What determines whether mammalian ribosomes resume scanning after translation of a short upstream open reading frame? *Genes Dev* **18:** 62–75.

Roy B, Leszyk JD, Mangus DA, Jacobson A. 2015. Nonsense suppression by near-cognate tRNAs employs alternative base pairing at codon positions 1 and 3. *Proc Natl Acad Sci* **112:** 3038–3043.

Szamecz B, Rutkai E, Cuchalová L, Munzarová V, Herrmannová A, Nielsen KH, Burela L, Hinnebusch AG, Valášek L. 2008. eIF3a cooperates with sequences 5′ of uORF1 to promote resumption of scanning by post-termination ribosomes for reinitiation on GCN4 mRNA. *Genes Dev* **22:** 2414–2425.

Valášek LS. 2012. 'Ribozoomin'—translation initiation from the perspective of the ribosome-bound eukaryotic initiation factors (eIFs). *Curr Protein Pept Sci* **13:** 305–330.

Valášek L, Mathew A, Shin BS, Nielsen KH, Szamecz B, Hinnebusch AG. 2003. The yeast eIF3 subunits TIF32/a, NIP1/c, and eIF5 make critical connections with the 40S ribosome in vivo. *Genes Dev* **17:** 786–799.

von der Haar T, Tuite MF. 2007. Regulated translational bypass of stop codons in yeast. *Trends Microbiol* **15:** 78–86.

von der Haar T, Valasek LS. 2014. *mRNA translation: fungal variations on a eukaryotic theme*. Springer International Publishing, Switzerland.

Zaher HS, Green R. 2009. Fidelity at the molecular level: lessons from protein synthesis. *Cell* **136:** 746–762.

SUPPLEMENTAL INFORMATION

EXPERIMENTAL PROCEDURES

Construction of yeast strains and plasmids

List of all strains used throughout this study can be found in Table S1.

List of all plasmids and PCR primers used throughout this study can be found in Tables S2 and S3, respectively.

Plasmid PBB123 was created using fusion PCR with pTH335 serving as a template and following combinations of primers: (i) PB105/PB108 and (ii) PB106/PB107. Primers PB105 and PB106 were then used in the third reaction with a 1:1 ratio of PCR products from the first and second reactions as templates. The resulting PCR product was digested with *Xho*I and *Bam*HI and inserted into *Xho*I/*Bam*HI cut pTH335.

Plasmid PBB125 was created using fusion PCR with PBB97 serving as a template and following combinations of primers: (i) PB94/PB110 and (ii) PB95/PB109. Primers PB94 and PB95 were then used in the third reaction with a 1:1 ratio of PCR products from the first and second reactions as templates. The resulting PCR product was digested with *Xho*I and *Bam*HI and inserted into *Xho*I/*Bam*HI cut pTH335.

PBB135 was created by inserting the *Sal*I-*Not*I digested PCR product obtained with primers PB115 and PBRFNotI using pTH477 as template into *Sal*I-*Not*I digested pTH477.

PBB136 was created by inserting the *Sal*I-*Not*I digested PCR product obtained with primers PB116 and PBRFNotI using pTH477 as template into *Sal*I-*Not*I digested pTH477.

PBB137 was created by inserting the *Sal*I-*Not*I digested PCR product obtained with primers PB117 and PBRFNotI using pTH477 as template into *Sal*I-*Not*I digested pTH477.

PBB138 was created by inserting the *Sal*I-*Not*I digested PCR product obtained with primers PB118 and PBRFNotI using pTH477 as template into *Sal*I-*Not*I digested pTH477.

PBB139 was created by inserting the *Sal*I-*Not*I digested PCR product obtained with primers PB119 and PBRFNotI using pTH477 as template into *Sal*I-*Not*I digested pTH477.

PBB140 was created by inserting the *Sal*I-*Not*I digested PCR product obtained with primers PB120 and PBRFNotI using pTH477 as template into *Sal*I-*Not*I digested pTH477.

PBB141 was created by inserting the *Sal*I-*Not*I digested PCR product obtained with primers PB121 and PBRFNotI using pTH477 as template into *Sal*I-*Not*I digested pTH477.

PBB142 was created by inserting the *Sal*I-*Not*I digested PCR product obtained with primers PB122 and PBRFNotI using pTH477 as template into *Sal*I-*Not*I digested pTH477.

PBB143 was created by inserting the *Sal*I-*Not*I digested PCR product obtained with primers PB123 and PBRFNotI using pTH477 as template into *Sal*I-*Not*I digested pTH477.

PBB144 was created by inserting the *Sal*I-*Not*I digested PCR product obtained with primers PB124 and PBRFNotI using pTH477 as template into *Sal*I-*Not*I digested pTH477.

Table S1. Yeast strains used in this study.

Strain	Genotype	Source or reference
74D-694[a]	*MAT*a *ade1-14 trp1-289 his3-Δ200 leu2-3,112 ura3-52*	(1)
L2327[a]	*MAT*a *ade1-14 trp1-289 his3-Δ200 leu2-3,112 ura3-52 sup45-M48I*	(2)
L2521[a]	*MAT*a *ade1-14 trp1-289 his3-Δ200 leu2-3,112 ura3-52 sup45-Y410S*	(2)
PBH140[a]	*MAT*a *ade1-14 trp1-289 his3-Δ200 leu2-3,112 ura3-52 tif35Δ* (YCp22-g/TIF35-screen)	(3)
W303-1a	*MATa ade2 can1-100 his3-11 his3-15 leu2-3 leu2-112 trp1-1 ura3-1*	(4)
H2879	*MATa leu2-3 leu2-112 ura3-52 PRT1*	(5)

[a] indicate isogenic strain background

Table S2. Plasmids used in this study.

Plasmid	Description	Source of reference
YCp22-g/TIF35-screen	single copy wt *TIF35-His* in *TRP1* plasmid from YCplac22	(6)
YCp22-g/TIF35-KLF	single copy *tif35KLF-His* in*TRP1* plasmid from YCplac22	(6)
pTH460	high copy PGK-Renilla-Firefly R/T cassette (stop codon of Renilla is CAA-CCGUUC; for read-through measurements) in *URA3* plasmid from YEplac195	(7)
pTH477	high copy PGK-Renilla-Firefly R/T cassette (stop codon of Renilla is UGA-CCGUUC; for read-through measurements) in *URA3* plasmid from YEplac195	(7)
YEp-R/T-UGAC-L	high copy PGK-Renilla-Firefly R/T cassette (stop codon of Renilla is UGA-C; for read-through measurements) in *LEU2* plasmid from YEplac181	(8)
YEp-R/T-CAAC-L	high copy PGK-Renilla-Firefly R/T cassette (stop codon of Renilla is replaced with CAA-C [coding triplet]; for control read-through measurements) in *LEU2* plasmid from YEplac181	(8)
PBB75	high copy PGK-Renilla-Firefly R/T cassette (stop codon of Renilla is UGA-A; for read-through measurements) in *LEU2* plasmid from YEplac181	(3)
PBB76	high copy PGK-Renilla-Firefly R/T cassette (stop codon of Renilla is UGA-G; for read-through measurements) in *LEU2* plasmid from YEplac181	(3)
PBB77	high copy PGK-Renilla-Firefly R/T cassette (stop codon of Renilla is UGA-U; for read-through measurements) in *LEU2* plasmid from YEplac181	(3)
pTH461	high copy PGK-Renilla-Firefly R/T cassette (stop codon of Renilla is UAA-C; for read-through measurements) in *URA3* plasmid from YEplac195	(7)
pTH469	high copy PGK-Renilla-Firefly R/T cassette (stop codon of Renilla is UAG-C; for read-through	(7)

	measurements) in *URA3* plasmid from YEplac195	
pDB689	high copy PGK-Renilla-Firefly R/T cassette (stop codon of Renilla is UAA-A; for read-through measurements) in *URA3* plasmid from YEplac195	D. Bedwell
pDB725	high copy PGK-Renilla-Firefly R/T cassette (stop codon of Renilla is UAA-G; for read-through measurements) in *URA3* plasmid from YEplac195	D. Bedwell
pDB727	high copy PGK-Renilla-Firefly R/T cassette (stop codon of Renilla is UAA-U; for read-through measurements) in *URA3* plasmid from YEplac195	D. Bedwell
pDB730	high copy PGK-Renilla-Firefly R/T cassette (stop codon of Renilla is UAG-A; for read-through measurements) in *URA3* plasmid from YEplac195	D. Bedwell
pDB731	high copy PGK-Renilla-Firefly R/T cassette (stop codon of Renilla is UAG-G; for read-through measurements) in *URA3* plasmid from YEplac195	D. Bedwell
pDB718	high copy PGK-Renilla-Firefly R/T cassette (stop codon of Renilla is UAG-U; for read-through measurements) in *URA3* plasmid from YEplac195	D. Bedwell
YEplac195	high copy cloning vector, *URA3*	(9)
pTH335	high copy *URA3* vector (pRS426) containing genomic DNA surrounding the tW(CCA)G1 gene	(3)
PBB97	high copy *tC(GCA)P1* in *URA3* plasmid from pRS426	(3)
PBB99	high copy *tR(UCU)E* in *URA3* plasmid from pRS426	(3)
PBB100	high copy *tG(UCC)O* in *URA3* plasmid from pRS426	(3)
PBB123	high copy *URA3* vector (pRS426) containing genomic DNA surrounding the tW*(CCA)G1 gene	this study
PBB125	high copy *tC*(GCA)P1* in *URA3* plasmid from pRS426	this study
PBB135	high copy PGK-Renilla-Firefly R/T cassette (stop codon of Renilla is UGA-ACCGAT; for read-through	this study

	measurements) in *URA3* plasmid from YEplac195	
PBB136	high copy PGK-Renilla-Firefly R/T cassette (stop codon of Renilla is UGA-ATTTAT; for read-through measurements) in *URA3* plasmid from YEplac195	this study
PBB137	high copy PGK-Renilla-Firefly R/T cassette (stop codon of Renilla is UGA-AATTTT; for read-through measurements) in *URA3* plasmid from YEplac195	this study
PBB138	high copy PGK-Renilla-Firefly R/T cassette (stop codon of Renilla is UGA-CGGTTA; for read-through measurements) in *URA3* plasmid from YEplac195	this study
PBB139	high copy PGK-Renilla-Firefly R/T cassette (stop codon of Renilla is UGA-TTTCAT; for read-through measurements) in *URA3* plasmid from YEplac195	this study
PBB140	high copy PGK-Renilla-Firefly R/T cassette (stop codon of Renilla is GCTTGC-TAA-ACCGAT; for read-through measurements) in *URA3* plasmid from YEplac195	this study
PBB141	high copy PGK-Renilla-Firefly R/T cassette (stop codon of Renilla is ATGTGT-TAA-ATTTAT; for read-through measurements) in *URA3* plasmid from YEplac195	this study
PBB142	high copy PGK-Renilla-Firefly R/T cassette (stop codon of Renilla is TACCCG-TAG-AATTTT; for read-through measurements) in *URA3* plasmid from YEplac195	this study
PBB143	high copy PGK-Renilla-Firefly R/T cassette (stop codon of Renilla is TTTCCG-TAA-CGGTTA; for read-through measurements) in *URA3* plasmid from YEplac195	this study
PBB144	high copy PGK-Renilla-Firefly R/T cassette (stop codon of Renilla is GAACGC-TGA-TTTCAT; for read-through measurements) in *URA3* plasmid from YEplac195	this study

Table S3. Primers used in this study.

Primer name	Primer sequence (5´to 3´)
PBRFNotI	CTCGAAGCGGCCGCTCTAGAATTACAC
PB94	AATAACTCGAGTTGCGTGGATAAGTGTTATTATTCTATTGCC
PB95	AATAAGGATCCAAAGCCGTACAGGCGAACGTATATAATTAAAATTC
PB105	CCCCCCTCGAGATTTTTTACATTTGTTCTATCAG
PB106	CTAGTGGATCCTATAAAAAGAACATATTCATAC
PB107	CAATGGTAGAGCTTTCGATTCCAATTAAATCTTGG
PB108	CCAAGATTTAATTGGAATCGAAAGCTCTACCATTG
PB109	GTGGTAGCGCAGCAGACTGCAAATCTGTTGGTCCTTAG
PB110	CTAAGGACCAACAGATTTGCAGTCTGCTGCGCTACCAC
PB115	CAAATGTCGACGTGCGATTGAACCGATCCGTTCGGATCCTTCAACTTCCCTGAG
PB116	CAAATGTCGACGTGCGATTGAATTTATCCGTTCGGATCCTTCAACTTCCCTGAG
PB117	CAAATGTCGACGTGCGATTGAAATTTTCCGTTCGGATCCTTCAACTTCCCTGAG
PB118	CAAATGTCGACGTGCGATTGACGGTTACCGTTCGGATCCTTCAACTTCCCTGAG
PB119	CAAATGTCGACGTGCGATTGATTTCATCCGTTCGGATCCTTCAACTTCCCTGAG
PB120	CAAATGTCGACGTGCGATGCTTGCTAAACCGATGGATCCTTCAACTTCCCTGAGCTCG
PB121	CAAATGTCGACGTGCGATATGTGTTAAATTTATGGATCCTTCAACTTCCCTGAGCTCG
PB122	CAAATGTCGACGTGCGATTACCCGTAGAATTTTGGATCCTTCAACTTCCCTGAGCTCG
PB123	CAAATGTCGACGTGCGATTTTCCGTAACGGTTAGGATCCTTCAACTTCCCTGAGCTCG
PB124	CAAATGTCGACGTGCGATGAACGCTGATTTCATGGATCCTTCAACTTCCCTGAGCTCG
tRNA-C	AGCTCGCACTCAGGATCGAAC
tRNA-G	TGAGCGGTACGAGAATCGAACC
tRNA-R	CACTCACGATGGGGGTCGAA
tRNA-W	TGAACCTGCAACCCTTCGATTTGGAGTCGAAAGCTCTACC
5.8S rRNA	GCTGCGTTCTTCATCGATGCGAGAACCAA

REFERENCES

1. Chernoff, Y.O., Derkach, I.L. and Inge-Vechtomov, S.G. (1993) Multicopy SUP35 gene induces de-novo appearance of psi-like factors in the yeast Saccharomyces cerevisiae. *Curr Genet*, **24**, 268-270.
2. Bradley, M.E., Bagriantsev, S., Vishveshwara, N. and Liebman, S.W. (2003) Guanidine reduces stop codon read-through caused by missense mutations in SUP35 or SUP45. *Yeast*, **20**, 625-632.
3. Beznoskova, P., Wagner, S., Jansen, M.E., von der Haar, T. and Valasek, L.S. (2015) Translation initiation factor eIF3 promotes programmed stop codon readthrough. *Nucleic Acids Res*, **43**, 5099-5111.
4. Thomas, B.J. and Rothstein, R. (1989) Elevated recombination rates in transcriptionally active DNA. *Cell*, **56**, 619-630.
5. Nielsen, K.H., Szamecz, B., Valasek, L.J., A., Shin, B.S. and Hinnebusch, A.G. (2004) Functions of eIF3 downstream of 48S assembly impact AUG recognition and GCN4 translational control. *EMBO J.*, **23**, 1166-1177.
6. Cuchalová, L., Kouba, T., Herrmannová, A., Danyi, I., Chiu, W.-l. and Valášek, L. (2010) The RNA Recognition Motif of Eukaryotic Translation Initiation Factor 3g (eIF3g) Is Required for Resumption of Scanning of Posttermination Ribosomes for Reinitiation on GCN4 and Together with eIF3i Stimulates Linear Scanning. *Mol Cell Biol*, **30**, 4671-4686.
7. Keeling, K.M., Lanier, J., Du, M., Salas-Marco, J., Gao, L., Kaenjak-Angeletti, A. and Bedwell, D.M. (2004) Leaky termination at premature stop codons antagonizes nonsense-mediated mRNA decay in S. cerevisiae. *RNA*, **10**, 691-703.
8. Beznosková, P., Cuchalová, L., Wagner, S., Shoemaker, C.J., Gunišová, S., Von der Haar, T. and Valášek, L.S. (2013) Translation initiation factors eIF3 and HCR1 control translation termination and stop codon read-through in yeast cells. *PLoS Genet*, **9**, e1003962.
9. Gietz, R.D. and Sugino, A. (1988) New yeast-Escherichia coli shuttle vectors constructed with in vitro mutagenized yeast genes lacking six-base pair restriction sites. *Gene*, **74**, 527-534.

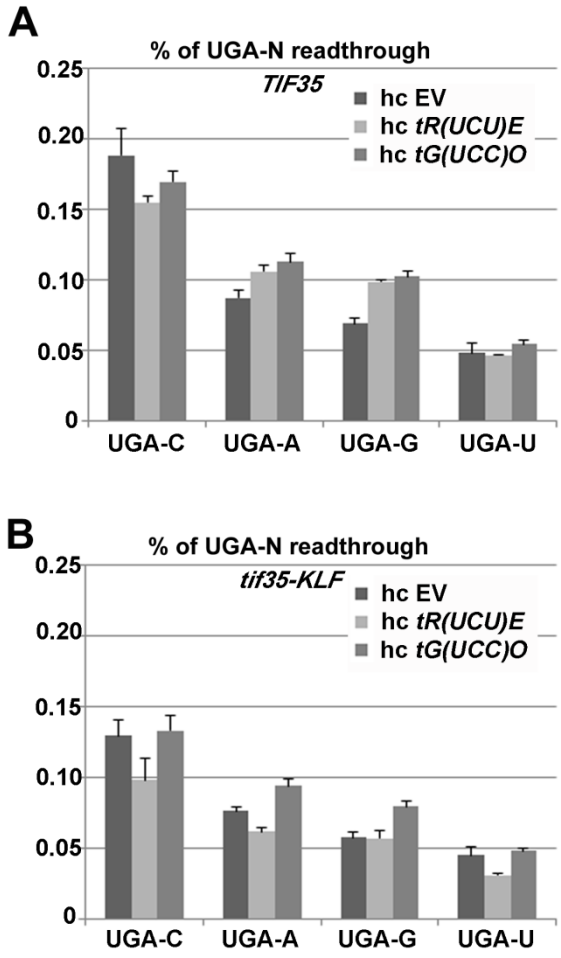

Figure S1. Increased gene dosage of arginine or glycine tRNAs affect readthrough neither in wt (A) nor in mutant *tif35-KLF* (B) cells at any UGA-N tetranucleotide. (**A**) The PBH140 derivative bearing the *TIF35* wt allele was transformed with either empty vector (EV), high copy (hc) tR(UCU)E or hc tG(UCC)O and the resulting transformants were grown and processed for stop codon readthrough measurements as described in Figure 1. (**B**) The PBH140 derivative the bearing *tif35-KLF* mutant allele was transformed with either empty vector (EV), hc tR(UCU)E or hc tG(UCC)O and the resulting transformants were grown and processed for stop codon readthrough measurements as described in Figure 1.

Beznoskova_SuplFig2

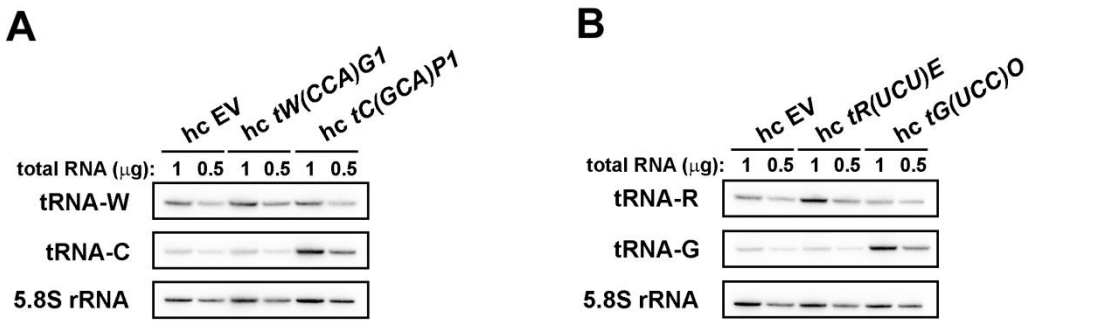

C

	fold increase normalized to 5.8S rRNA
tRNA-W	1.45 ± 0.025
tRNA-C	2.78 ± 0.319
tRNA-R	1.88 ± 0.360
tRNA-G	7.00 ± 0.787

Figure S2. Increased gene dosage of the selected nc-tRNAs increases their cellular levels *in vivo*. (**A**) Total RNAs were extracted from the PBH140 strain bearing a plasmid indicated at the top of each panel and 1 μg or 0.5 μg aliquots were loaded onto the Criterion Precast gels and subjected to Northern blotting with ^{32}P-labelled probes shown to the left. (**B**) Quantification of signals shown in panels A and B. Northern blots were quantified using the NIH ImageJ program and the signals were first normalized to the control 5.8S rRNA. The resulting values obtained with cells bearing an empty plasmid „hc EV“ were then set to 1.00 and those obtained with cells bearing a gene for a given nc-tRNA were expressed relative to the „hc EV“. Standard deviations from three individual experiments are given.

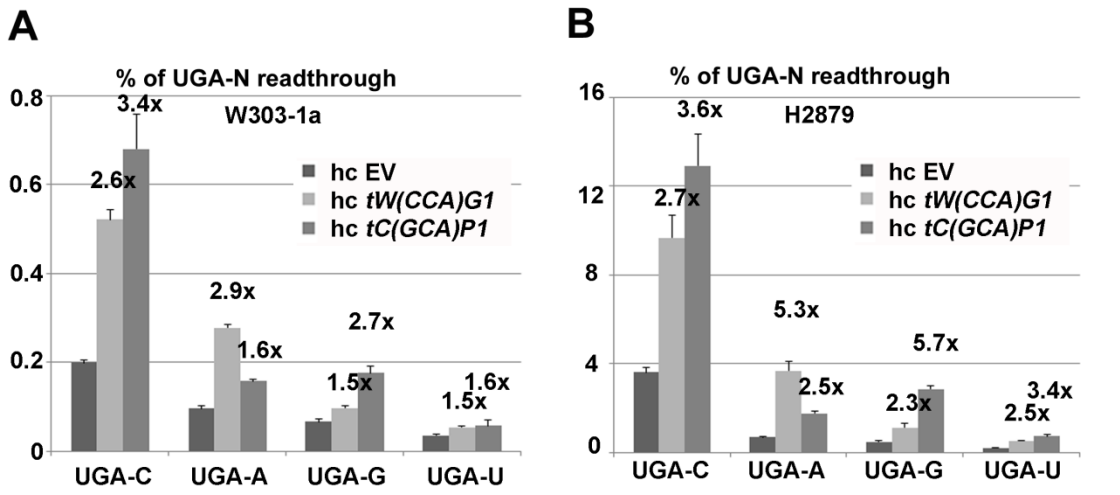

Figure S3. Preferential decoding of UGA-N by tryptophan and cysteine nc-tRNAs in two other genetically unrelated yeast strain backgrounds. Yeast strains W303-1a (**A**) and H2879 (**B**) were transformed with either empty vector (EV), high copy (hc) *tW(CCA)G1* or hc *tC(GCA)P1* and the resulting transformants were grown and processed for stop codon readthrough measurements as described in Figure 1.

% of readthrough (*TIF35*)

	n.t.	paromomycin	
UGA-C	0.217 ± 0.0003	1.168 ± 0.2141	5.4x
UGA-A	0.088 ± 0.0064	0.329 ± 0.0602	3.7x
UGA-G	0.066 ± 0.0029	0.260 ± 0.0102	4.4x
UGA-U	0.032 ± 0.0020	0.182 ± 0 .0429	5.7x

Figure S4. The effect of paromomycin on readthrough at all four UGA tetranucleotides in wild type cells. The PBH140 derivative bearing *TIF35* wt was transformed with empty vector and the resulting transformants were grown in SD without or with 200μg/ml paromomycin for six hours and processed for stop codon readthrough measurements as described in Figure 1; n.t. – non-treated.

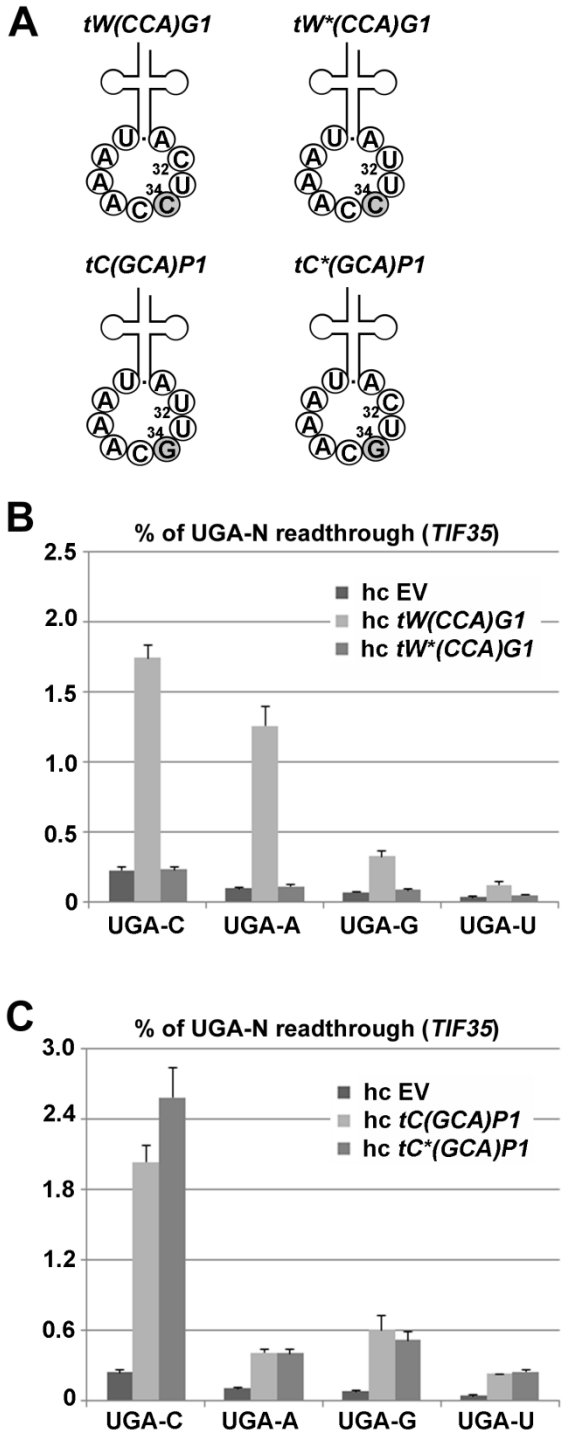

Figure S5. The effect of N_{32} on the nc-tRNA preference for UGA-A or UGA-G tetranucleotides (**A**) Schematics of wt and mutant Trp and Cys nc-tRNAs. Only the nucleotides of the anticodon loop are shown with N_{32} indicated. The only differing base between tryptophan and cysteine tRNA anticodons is highlighted in grey. (**B**) The impact of the C32U substitution in the tryptophan nc-tRNA on its ability to promote readthrough in wt cells. The PBH140 derivative bearing *TIF35* wt was transformed with either empty vector (EV), hc tW(CCA)G1 or mutant hc tW*(CCA)G1 and the resulting transformants were grown in SD and processed for stop codon

readthrough measurements as described in Figure 1. (**C**) The impact of U32C substitution in the cysteine nc-tRNA on its ability to promote readthrough in wt cells. The PBH140 derivative bearing *TIF35* wt was transformed with either empty vector (EV), hc tC(GCA)P1 or mutant hc tC*(GCA)P1 and the resulting transformants were grown in SD and processed for stop codon readthrough measurements as described in Figure 1.

Beznoskova_SuplFig6

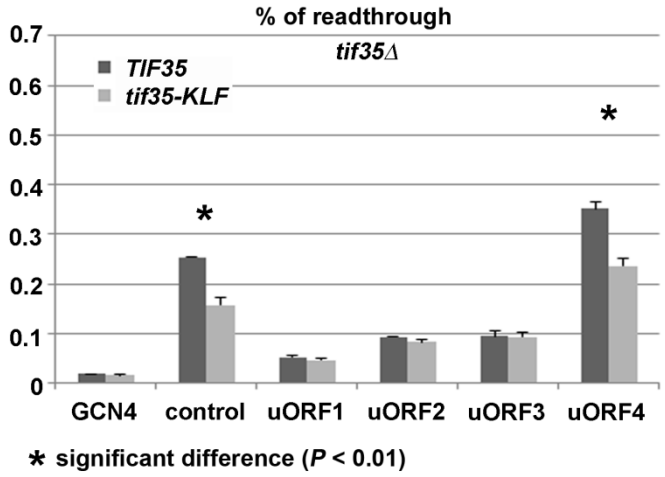

* significant difference ($P < 0.01$)

GCN4	GAACGC **UGA** UUUCAU
control	UGCGAU **UGA** CCGUUC
uORF1	GCUUGC **UAA** ACCGAU
uORF2	AUGUGU **UAA** AUUUAU
uORF3	UACCCG **UAG** AAUUUU
uORF4	UUUCCG **UAA** CGGUUA

Figure S6. The genuine 6 nt-long sequences flanking stop codons of uORF1 – 3 from both sides are not subject to eIF3-dependent readthrough. The PBH140 derivatives bearing *TIF35* wt and *tif35-KLF* mutant alleles were grown in SD and processed for stop codon readthrough measurements using standard dual luciferase readthrough reporter constructs pTH460; pTH477; PBB140; PBB141; PBB142; PBB143 and PBB144 as described in Materials and Methods. Changes in the measured readthrough values between *TIF35* and *tif35-KLF* cells were analyzed by the student´s *t*-test (mean±SE; n=6) and shown to be statistically significant only for those cases marked with the asterisk ($P < 0.01$).

PUBLICATION V

In-depth analysis of *cis*-determinants that either promote or inhibit reinitiation on *GCN4* mRNA after translation of its four short uORFs

STANISLAVA GUNIŠOVÁ, PETRA BEZNOSKOVÁ, MAHABUB PASHA MOHAMMAD, VLADISLAVA VLČKOVÁ, and LEOŠ SHIVAYA VALÁŠEK

Laboratory of Regulation of Gene Expression, Institute of Microbiology AS CR, Prague 142 20, Czech Republic

ABSTRACT

Translational control in eukaryotes is exerted by many means, one of which involves a ribosome translating multiple cistrons per mRNA as in bacteria. It is called reinitiation (REI) and occurs on mRNAs where the main ORF is preceded by a short upstream uORF(s). Some uORFs support efficient REI on downstream cistrons, whereas some others do not. The mRNA of yeast transcriptional activator *GCN4* contains four uORFs of both types that together compose an intriguing regulatory mechanism of its expression responding to nutrients' availability and various stresses. Here we subjected all *GCN4* uORFs to a comprehensive analysis to identify all REI-promoting and inhibiting *cis*-determinants that contribute either autonomously or in synergy to the overall efficiency of REI on *GCN4*. We found that the 3′ sequences of uORFs 1–3 contain a conserved $AU_{1\text{-}2}A/UUAU_2$ motif that promotes REI in position-specific, autonomous fashion such as the REI-promoting elements occurring in 5′ sequences of uORF1 and uORF2. We also identified autonomous and transferable REI-inhibiting elements in the 3′ sequences of uORF2 and uORF3, immediately following their AU-rich motif. Furthermore, we analyzed contributions of coding triplets and terminating stop codon tetranucleotides of *GCN4* uORFs showing a negative correlation between the efficiency of reinitiation and efficiency of translation termination. Together we provide a complex overview of all *cis*-determinants of REI with their effects set in the context of the overall *GCN4* translational control.

Keywords: translational control; reinitiation; uORF; *cis*-regulation; *GCN4*

INTRODUCTION

Translational control of one of yeast's most influential stress-related transcription factors, GCN4, represents undoubtedly the best-studied model of eukaryotic translation reinitiation (REI) (Hinnebusch 2005; Gunišová and Valášek 2014). REI is a gene-specific regulatory mechanism exploiting the presence of short upstream uORFs in mRNA leaders (i.e., 5′ untranslated regions—5′ UTRs) of various genes. The molecular key to this potentially abundant regulation (Davuluri et al. 2000; Iacono et al. 2005; Calvo et al. 2009; Hood et al. 2009; Zhou et al. 2010) is the ability of some of these short uORFs (in yeast up to five codons in length [Vilela et al. 1998; Rajkowitsch et al. 2004; Szamecz et al. 2008], in plants up to 16 [von Arnim et al. 2014], and in mammals up to 30 codons [Kozak 2005]) to retain the 40S ribosomal subunit on the same mRNA molecule even after they have been translated and the large 60S subunit has been recycled by the ribosome recycling factors (for review, see Jackson et al. 2012; Valášek 2012). Such post-termination 40S subunits are then able to resume scanning downstream, and upon acquisition of the new ternary complex (TC), composed of Met-$tRNA_i^{Met}$ and eukaryotic initiation factor eIF2 in its GTP form, they are able to recognize the AUG start codon of the next ORF and reinitiate translation thereon.

Generally speaking, short uORFs in principle impose a functional barrier for sufficient expression of a downstream main ORF. This repressive effect of uORFs can be, however, alleviated under specific conditions, such as various types of stress, in order to boost expression of some regulatory uORF-containing mRNAs that help the cell to cope with sudden environmental changes. It has been shown that the efficiency of REI depends on four main factors: (i) time required for uORF translation, which is determined by the relative length of uORF and the translation elongation rate; (ii) its 5′ and 3′ flanking sequences, which contain specific *cis*-acting features

Corresponding authors: gunisova@biomed.cas.cz, valasekl@biomed.cas.cz

Article published online ahead of print. Article and publication date are at http://www.rnajournal.org/cgi/doi/10.1261/rna.055046.115.

with poorly understood molecular roles; (iii) translation initiation factors (eIFs) involved in the primary initiation event such as the eIF3 and eIF4F complexes, which are believed to remain associated with the ribosome throughout the short elongation as well as termination and recycling phases; and (iv) its distance to the next open reading frame, which determines the likelihood of acquisition of the new TC by the post-termination 40S ribosome that has resumed scanning (Kozak 1987; Dever et al. 1992; Pöyry et al. 2004; Szamecz et al. 2008; Cuchalová et al. 2010; Roy et al. 2010; Munzarová et al. 2011).

The classical REI-dependent mRNA of *GCN4* containing a total of four short uORFs has been studied in great detail for several decades; it has been found to be very sensitive to the TC levels that are changing in response to different nutrient conditions and to rely mainly on the first REI-permissive uORF1 and the last REI-nonpermissive uORF4 (reviewed in Hinnebusch 2005 and recently revised in Gunišová and Valášek 2014). Briefly, the first of the four uORFs is efficiently translated under both nutritional replete and deplete conditions, and after its translation the post-termination 40S subunit remains attached to the mRNA and resumes scanning downstream for REI at the next AUG. In nonstressed cells, where the TC levels are high, nearly all of the rescanning ribosomes can rebind the TC before reaching one of the last two distant uORFs (uORFs 3 and 4), neither of which supports efficient REI. As a result, ribosomes terminating on one of these two uORFs undergo the full ribosomal recycling step, which prevents them from reaching and translating the main *GCN4* ORF (Supplemental Fig. S1).

Under starvation conditions, the GCN2 kinase phosphorylates eIF2, which suspends formation of new TCs in the cytoplasm. Consequently, post-termination 40S ribosomes traveling from the uORF1 stop codon downstream will require more time to rebind the TC to be able to recognize the next AUG start codon. This will allow a large proportion of them to bypass uORF3 and uORF4 and reacquire the TC downstream from uORF4 but still upstream of the *GCN4* start codon (Supplemental Fig. S1). Thus, whereas the global protein synthesis is significantly down-regulated under nutrient deplete conditions, protein expression of the GCN4 transcriptional activator is concurrently induced.

The second REI-permissive uORF, uORF2 with ~80%–90% of the uORF1 REI activity, occurs only 56-nt downstream from uORF1 and serves as a backup of uORF1 to capture all ribosomes that leaky scanned past the uORF1 AUG (Gunišová and Valášek 2014), especially during stress conditions that seem to increase the frequency of leaky scanning in general (Lee et al. 2009; Raveh-Amit et al. 2009; Palam et al. 2011; Sundaram and Grant 2014). This ensures that the maximum capacity of this intriguing regulatory system is met. Similarly, two consecutive uORFs with minimal or no REI-promoting potential occurring further downstream (uORF3 that allows approximately five times less efficient REI than the first two uORFs, but still approximately four times more efficient REI than REI-nonpermissive uORF4) also prevent "leakiness" of this system but during nutrient replete conditions (Gunišová and Valášek 2014). Hence the tightness of *GCN4* translational control is ensured by a fail-safe mechanism that effectively prevents or triggers *GCN4* expression under nutrient replete or deplete conditions, respectively.

The exceptionally high REI potential of uORF1 and uORF2 has been ascribed to (i) their 5′ sequences (Grant et al. 1995) containing several REI-promoting elements (RPEs) that together make up the so-called 5′ enhancer with a specific structural arrangement (Munzarová et al. 2011; Gunišová and Valášek 2014), (ii) the stimulatory role of N-terminal domain (NTD) of the a/TIF32 subunit of the eukaryotic initiation factor eIF3 (Szamecz et al. 2008) that sits near the 40S mRNA exit channel (Valášek et al. 2003; Kouba et al. 2012; Aylett et al. 2015), and, in the case of uORF1, also to (iii) the first 10 nt immediately following the uORF1 stop codon (Grant and Hinnebusch 1994), and (iv) the third coding triplet of uORF1 in combination with its 3′ UTR (Grant and Hinnebusch 1994).

With respect to known molecular functions of these features, some of the RPEs were shown to functionally interact with the a/TIF32-NTD, and this interaction, the exact nature of which still awaits determination, was implicated in stabilizing the post-termination 40S subunits on stop codons of both REI-permissive uORFs in order to facilitate the resumption of scanning downstream (Szamecz et al. 2008; Munzarová et al. 2011; Gunišová and Valášek 2014). The stretch of the first 10 nt past the uORF1 stop codon was owing to its relatively low GC content proposed to allow the 40S subunit to promptly resume scanning, in contrast to the corresponding GC-rich sequence of uORF4, because it would not permit strong base-pairing interactions with the 40S subunit (Grant and Hinnebusch 1994). However, we recently noted that the 3′ sequences of the other two *GCN4* uORFs (2 and 3) have a very similar AU content to uORF1, yet uORF3 permits only poor REI (Munzarová et al. 2011). Hence the idea that it is simply the high AU content of the uORF1 3′ sequence that makes it so robustly REI permissive does not seem to be so unequivocal anymore (Jackson et al. 2012).

With the recent outburst of new findings on the *GCN4* translation control that in some cases clarified and/or extended the earlier observations but in some others led to revised hypotheses, we wished to systematically analyze all potential *cis*-determinants that either promote or inhibit REI on *GCN4* after translation of its uORFs in one complex study. Based on this study we also postulate "reinitiation rules" that can be generalized for any short uORF in yeast (please see the Conclusion section).

RESULTS AND DISCUSSION

Proper functioning of the 3′ sequences immediately following stop codons of *GCN4* uORFs is not determined by their AU content

A considerable difference in the efficiency of resumption of scanning following translation of the REI-permissive

uORF1 vs. REI-nonpermissive uORF4 in the *GCN4* mRNA leader was found to be attributable to the distinct 3′ sequences following the termination codons of these two uORFs. Replacing the sequence of 25-nt downstream from the uORF1 stop codon with the corresponding nucleotides from uORF4 disabled the uORF1-promoted REI on *GCN4* by a great deal (Miller and Hinnebusch 1989). It was originally proposed that this difference is due to a varying AU content of these 3′ sequences, with uORF1 being more AU-rich (the AU content of 25 nt after uORF1 stop codon is 80%) than uORF4 (60%) (Fig. 1A; Grant and Hinnebusch 1994).

In our recent work, however, we noted that the 3′ sequences of the other two uORFs of *GCN4* are similarly AU-rich as the uORF1 3′ sequence by itself; the second REI-permissive uORF2 shows the highest AU content (88%), while the AU content of uORF3 that is only modestly REI-permissive is comparable to that of uORF1 (76%) (Fig. 1A; Munzarová et al. 2011; Gunišová and Valášek 2014). Therefore, if the degree of AU-richness is the sole factor determining the REI-promoting activity of the 3′ sequences in general, at least a part of the REI potential of uORF2 and probably the whole REI potential of uORF3 could be explained by employment of the REI-promoting 3′ sequences of these two uORFs.

To test this possibility, we substituted 25 nt immediately following stop codons of uORF2 and uORF3 with the corresponding sequence of REI-nonpermissive uORF4 in the same way as it was done previously for uORF1. In all our constructs, only the uORF under study was functional while the start codons of the other three uORFs were mutated out. Note that since the uORF4 start codon is separated from the uORF3 stop codon by only 13 nt, the 3′ sequence of the *uORF3-3333* construct contains the mutated out uORF4 start codon (Fig. 1A). This mutation, however, does not change the overall AU content of the uORF3 3′ sequence.

Also note that we divided the sequences constituting and flanking all four uORFs into four segments, A through D, for each uORF (Fig. 1B) according to Munzarová et al. (2011). In short, segment A is 166 bp in length (from position −181 to −16 relative to the uORF1-4 AUG start codons) and corresponds to the 5′ REI-promoting sequences of uORF1 (Szamecz et al. 2008; Munzarová et al. 2011); segment B designated previously as the linker is 15-bp long (−15 to −1); segment C contains coding triplets and the stop codon; and segment D encompasses 25 bp immediately following the stop codon that corresponds to the 3′ REI-promoting sequence of uORF1 (Miller and Hinnebusch 1989; Munzarová et al. 2011; Gunišová and Valášek 2014). Mutual replacements of these segments among all four uORFs that feature in the whole study are always indicated by the sequence of ABCD segments expressed as numbers 1–4, indicating which uORF each particular segment comes from: For example, a hypothetical *uORF1-1234* construct would correspond to segment A from uORF1 followed by B from uORF2, C from uORF3, and D from uORF4, all situated in the uORF1 position.

With respect to the aforementioned substitutions, replacing the 3′ sequence (segment D) of uORF1 with that of uORF4 (*uORF1-1114*) reduced its REI potential down to ∼31% (Fig. 1C), as reported before (Miller and Hinnebusch 1989). Replacing also the segment C along with D of uORF1 with those of uORF4 (*uORF1-1144*) further reduced its REI activity, almost to the basal level corresponding to the activity of REI-nonpermissive uORF4 (*uORF1-4444*), as also observed before (Fig. 1C; Miller and Hinnebusch 1989; Munzarová et al. 2011; Gunišová and Valášek 2014). This illustrates the magnitude of the 3′ sequence contribution to the REI potential of uORF1, as its loss leads to a remarkable impairment (∼69% drop in this experimental setup) of the uORF1 ability to allow resumption of scanning of post-termination ribosomes. Similar replacements of uORF2 and uORF3 in *uORF2-2224* and *uORF3-3334* did not decrease but actually increased REI activities of both uORFs (Fig. 1C). These findings indicate that (i) the REI potential of uORF2 and uORF3 does not depend on their AU-rich 3′ sequences, and thus (ii) the degree of AU content per se does not play the key role in rendering the 3′ sequences active in promoting REI. They also contradict our earlier suggestion that the GC-rich 3′ sequence of uORF4 functions as the REI inhibitor that can suppress the resumption of scanning from any REI-permissive uORF (Gunišová and Valášek 2014). The fact that the presence of the GC-rich segment D of uORF4 allows even more efficient REI on the middle two uORFs, mainly on uORF3, will be explained below.

The 3′ sequences of uORF1 and uORF2 operate autonomously in the position-specific manner

Since uORF1 seems to be the only uORF utilizing the 3′ sequence for its REI-promoting activity, we next asked whether the 3′ sequences of uORF2 and uORF3 with a similar AU content would also work for uORF1. Interestingly, only the presence of the uORF2 3′ sequence (*uORF1-1112*) was able to functionally replace the uORF1 3′ sequence (Fig. 1D). The 3′ sequence of uORF3 (*uORF1-1113*) decreased the uORF1-mediated REI activity by nearly the same margin as the 3′ sequence of uORF4 (*uORF1-1114*), which will also be explained below. The fact that uORF1 can also utilize the 3′ sequence of uORF2 suggested that its function could be position specific. To examine this, we first attempted to activate the REI enhancing potential of the uORF2 3′ sequence by placing the whole uORF2 ABCD block in the position of uORF1 (*uORF1-2222*). As a control, we replaced segment 2D with that of uORF4 in *uORF1-2224*. However, this replacement had nearly the same effect as when uORF2 occurred in its authentic position—its REI activity mildly increased but did not decrease (cf. Supplemental Figs. S1C, S2A), which further illustrates that uORF2 cannot utilize its 3′ sequence to increase its REI potential. Since comparison of ratios of reinitiation vs. initiation rates for uORF1 and uORF2 showed that uORF1 resumes scanning with

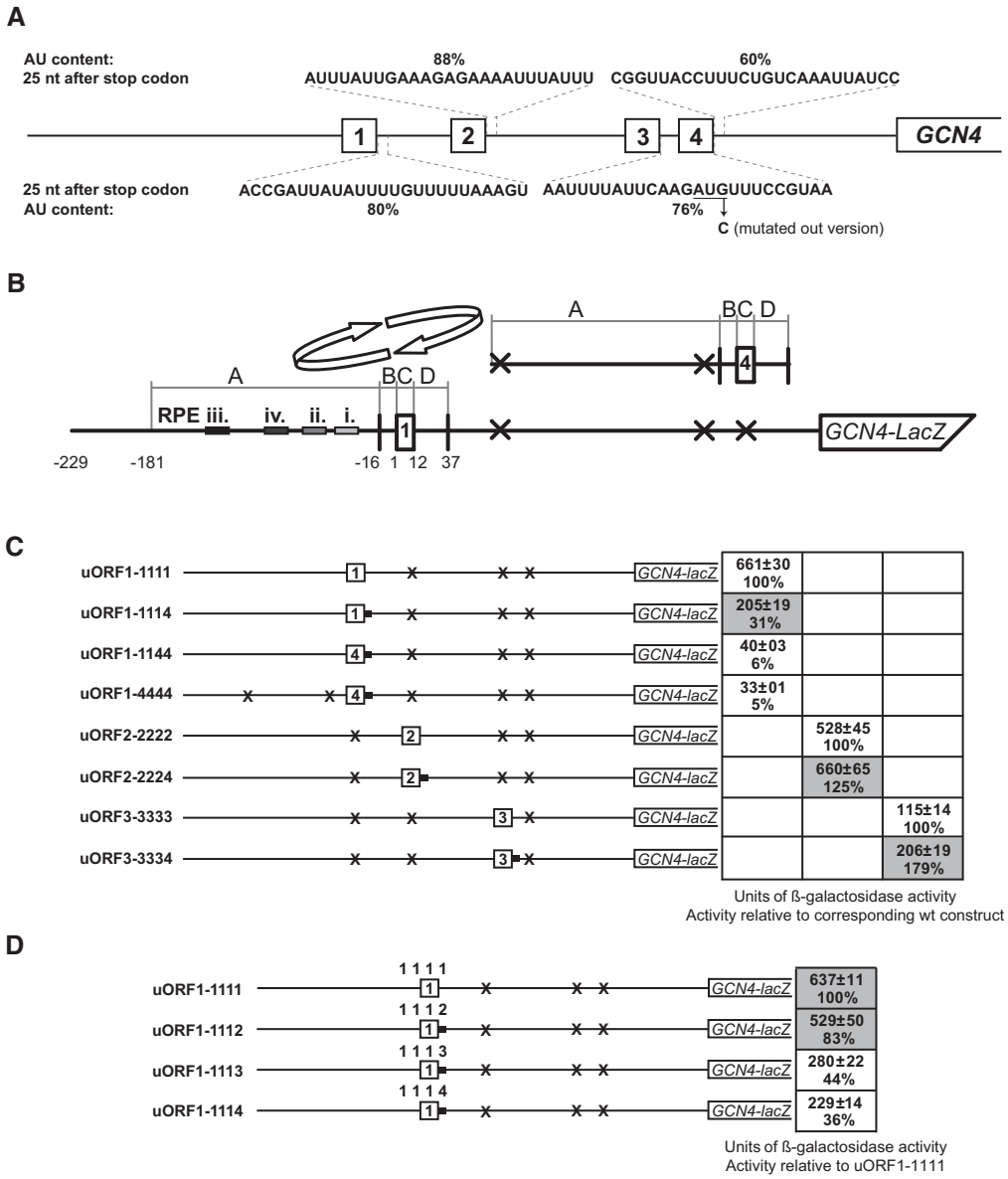

FIGURE 1. uORF1 is the only uORF utilizing its 3′ flanking sequence for its REI-promoting activity. (*A*) Schematic of the *GCN4* leader containing four short uORFs (1–4). The first 25 nt of 3′ flanking sequences (segments D) immediately following stop codon of each uORF are depicted together with the percentage of their AU content. In the uORF3 3′ sequence, the start codon of uORF4 is underlined and arrow indicates G to C substitution used to mutate it out (see text for further details). (*B*) Schematic showing the *GCN4-lacZ* construct containing solitary uORF1, the surrounding sequences of which were divided into four separate segments (A1–D1; see text for further details). Arrows indicate replacements of these segments with the corresponding segments (A4–D4) surrounding uORF4, shown to the *right* of the arrows. Crosses indicate positions of other uORFs in which start codons were mutated out. Gray bars indicate sequence positions of individual uORF1-specific RPEs. Replacements with the corresponding segments surrounding uORF2 and uORF3 that are not depicted were done in the analogous way; adapted from Munzarová et al. (2011). (*C*) Solitary uORFs from the *GCN4* mRNA leader in their authentic positions and their derivatives with their 3′ sequences replaced by the corresponding segment of uORF4 (indicated by the black bar) were introduced into the YSG2 strain. Additional replacements of indicated uORF1 segments by those of uORF4 were also prepared as a control. The resulting transformants were precultured in minimal media overnight, diluted to $OD_{600} \sim 0.35$, and grown for an additional 6 h; the β-galactosidase activities were measured in the WCEs and expressed in units of nmol of *o*-nitrophenyl-β-d-galactopyranoside hydrolyzed/min/mg of protein. The mean values and standard deviations obtained from at least three independent measurements with five independent transformants and activities of the respective constructs relative to their corresponding wt constructs are given in the table. Differences in β-galactosidase activities between *uORF2–2224* and its wt *uORF2-2222* were analyzed by Student's *t*-test and the calculated $P = 0.1335$. (*D*) The 3′ sequence of solitary uORF1 from the *GCN4* mRNA leader in its authentic position was replaced by corresponding segments of the other three uORFs and the resulting constructs were introduced into the YSG2 strain and analyzed as described in panel *C*. Differences in β-galactosidase activities between *uORF1-1112* and its wt *uORF1-1111* were analyzed by Student's *t*-test and the calculated $P = 0.0911$.

~14% higher efficiency than uORF2 (Supplemental Fig. S2B), we propose that it could be in fact the ability of uORF1 to utilize the 3′ sequence expressed in its higher efficiency of resumption of scanning that to a great deal lies behind the small but reproducible difference (from 10% to 20%) in the overall REI efficiency between both uORFs that we routinely observe (Gunišová and Valášek 2014).

Next we tested whether or not the 3′ sequence of uORF1, and as a proof of principle also that of uORF2, can operate from the position of uORF1 regardless of the nature of the preceding three segments. If yes, it would indicate (i) its autonomy and (ii) position specificity. To do that, we moved the whole uORF4 ABCD block into the position of uORF1 (*uORF1-4444*), and replaced segment D with the corresponding segments from the remaining three uORFs (*uORF1-4441*, *uORF1-4442*, and *uORF1-4443*) (Fig. 2A). As a control, we carried out the same D replacements (*uORF4-4441*, *uORF4-4442*, and *uORF4-4443*) also in the authentic position of uORF4 (*uORF4-4444*) (Fig. 2B). Remarkably, uORF1, and to a slightly smaller degree also uORF2 3′ sequences, did increase the REI potential of uORF4 (by approximately twofold), but only when situated in the position of uORF1. The 3′ sequence of uORF3, on the other hand, had the opposite effect on both setups, which is in accord with our findings shown in Figure 1C (see *uORF3-3333* vs. *uORF3-3334*), and we explain it below. Taken together, these results indicate that the REI-promoting 3′ sequence of uORF1, and analogously also that of uORF2, does function autonomously, at least to a certain degree, but its activity is position-restricted. To further support this conclusion, we carried out the D replacements of uORF3 in its authentic position (*uORF3-3333*) and showed that neither uORF1 nor uORF2 3′ sequences (*uORF3-3331* and *uORF3-3332*) had any stimulatory impact on REI allowed by this uORF. Predictably, the authentic 3′ sequence of uORF3 showed the weakest REI activity of all (Supplemental Fig. S3).

What could determine the position specificity for the REI-promoting action of the 3′ sequence of uORF1? In theory it

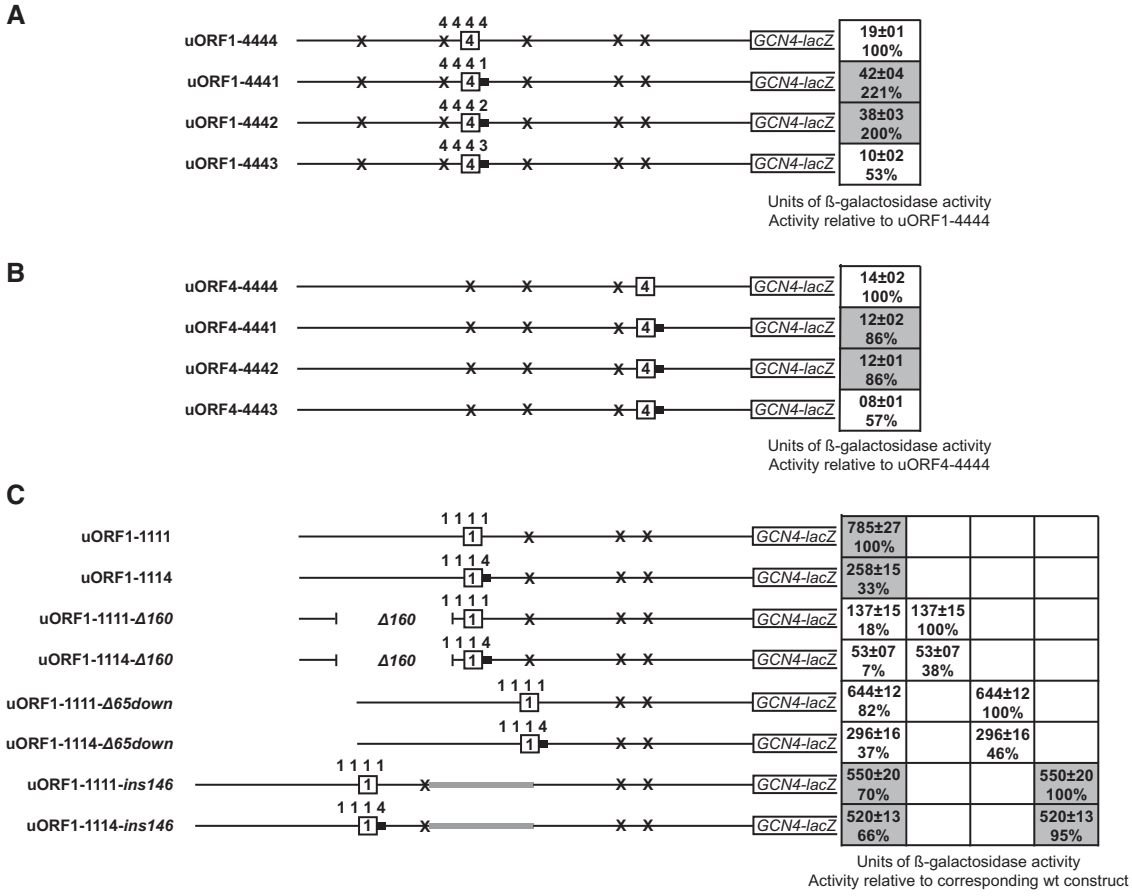

FIGURE 2. Function of the REI-promoting 3′ sequence is position specific. (*A*) The 3′ sequence of solitary uORF4 from the *GCN4* mRNA leader with its authentic flanking sequences (A4–D4) situated in the position of uORF1 was replaced by corresponding segments of the other three uORFs and analyzed as described in Figure 1C. (*B*) Same as in *A* except that the 3′ sequence substitutions were done in the authentic position of uORF4. (*C*) Solitary uORF1 or its derivative containing the 3′ sequence substitution for the corresponding segment of uORF4 situated it the authentic uORF1 position were modified as indicated and analyzed as described in Figure 1C. Differences in β-galactosidase activities between *uORF1-1111-Δ65down*, *uORF1-1111-ins146*, or *uORF1-1114-ins146* and their wt *uORF1-1111* were analyzed by Student's *t*-test and the calculated $P = 0.0014$, 0.0001, or 0.0001, respectively.

could simply be its distance either from the 5′ end of *GCN4* mRNA or from the *GCN4* main gene. To investigate this, we measured (i) the impact of shortening the distance between uORF1 start codon and the 5′ end, or (ii) shortening or (iii) prolonging the distance between the uORF1 3′ sequence and the *GCN4* start codon on the REI potential of wild-type uORF1 using the *1114* versions of all constructs designed for this purpose as a tool (Fig. 2C). We assumed that if any of our manipulations eliminate the REI-promoting activity of the 3′ sequence of uORF1, their replacement with the 3′ sequence of uORF4 would then show genetic epistasis; i.e., would not lead to any further decrease in the REI activity.

Shortening the distance from the 5′ end by the deletion of 160-nt upstream of uORF1 containing all four REI-promoting elements (RPEs) (*uORF1-1111-Δ160*) dramatically decreased the REI potential of uORF1, as expected (Szamecz et al. 2008), but had only marginal, if any, impact on the autonomous activity of the uORF1 3′ sequence (*uORF1-1114-Δ160*) (Fig. 2C, compare 100% vs. 33% and 100% vs. 38%). Hence the distance of the uORF1 3′ sequence from the 5′ end of *GCN4* mRNA does not seem to determine the position-specific phenomenon of the 3′ sequences.

Next we examined the potential importance of the distance of the uORF1 3′ sequence from the *GCN4* ORF. First we deleted 65 nt downstream from the uORF1 segment D, placing uORF1 directly into the uORF2 position (*uORF1-1111-Δ65down)*. This deletion decreased REI on *GCN4* by ∼18% compared to the wild-type *uORF1-1111* construct (Fig. 2C). It can be explained by two effects: (i) impaired function of the 3′ sequence of uORF1 due to its altered position; (ii) shortening the distance that the 40S ribosomes scanning downstream from uORF1 need to reacquire the new ternary complex (TC) in order to become REI-competent, as demonstrated before (Dever et al. 1992). Since the same deletion in the *uORF1-1114-Δ65down* construct reduced REI on *GCN4* to a smaller degree than in the wild-type *uORF1-1114* construct (Fig. 2C, compare 46% to 33%), we believe that the observed drop in the REI activity of *uORF1-1111-Δ65down* is the combination of both aforementioned effects.

In a complementary approach, we prolonged the distance of uORF1 from the *GCN4* start by insertion of 146 nt representing two copies of the previously identified segment S1 downstream from the 3′ sequence of uORF1 (Abastado et al. 1991) (*uORF1-1111-ins146*). Hypothetically, increasing the uORF1–*GCN4* distance should increase the REI on *GCN4*, as the scanning 40S ribosomes would gain even more time (thanks to a longer distance) to reacquire the TC on their way downstream from uORF1. Disruption of a prospective position-specific role of the uORF1 3′ sequence would counteract this effect, producing either no increase of the REI activity on *GCN4* or even a decrease. Replacement of the uORF1 3′ sequence with that of uORF4 should then be epistatic; and this is exactly what we observed (Fig. 2C). The double S1 insertion in the *uORF1-1111-ins146* construct reduced REI on *GCN4* by ∼30% and had virtually the same effect; i.e., the reduction by ∼34% was also seen with the *uORF1-1114-ins146* construct. These observations thus demonstrate that moving the uORF1 3′ sequence further away from the *GCN4* start codon completely abrogates its REI-promoting activity. Taken together, both shortening and lengthening approaches further support our theory that the action of the uORF1 3′ sequence is, within some limited range of tolerance, position-specific.

The question that still remains unanswered is how this feature operates at the molecular level. Taking into account our earlier suggestion that the action of the 3′ sequence of uORF1 is a prerequisite for the action of 5′-based RPEs of uORF1 (Munzarová et al. 2011), we propose the following two options. The RPEs are, in cooperation with eIF3, believed to stabilize the post-termination 40S subunit on the *GCN4* mRNA after the 60S subunit has been recycled in order to facilitate its resumption of scanning. If true, the 3′ sequence of uORF1 that during termination is buried in the mRNA binding channel could, for example, expedite the ribosomal recycling of the large subunit by stabilizing the post-termination 80S ribosomes at the stop codon. It was recently shown that post-termination 80S ribosomes are not stably anchored at the stop codon and can migrate in both directions to codons that are cognate to the P-site deacylated tRNA (Skabkin et al. 2013). Such instability may lead to an undesirable accumulation of nonrecycled aberrant ribosomal complexes in the vicinity of the stop codon, which would indeed dampen the efficiency of REI. With this role, however, it would be hard to reconcile the position specificity of the uORF1 3′ sequence; i.e., its functional requirement to be situated within a defined distance from the *GCN4* start codon.

This requirement brings us to the second option, as it could suggest that the uORF1 3′ sequence interacts with some downstream sequence and/or *trans*-acting factor bound to a downstream sequence. And since it is buried in the terminating 80S ribosome, as hinted above, this prospective interaction could not be formed before completion of the first recycling step involving the 60S subunit dissociation (Pisarev et al. 2007). The purpose of this contact could be to prevent the last recycling step; i.e., dissociation of mRNA from the 40S subunit. Only if this is ensured, the RPEs in co-operation with eIF3 could further strengthen this stabilization effect and enable resumption of scanning of post-termination 40S subunits downstream. Changing the position of the uORF1 3′ sequence with respect to the *GCN4* start site may prevent formation of this interaction, resulting in diminished REI efficiency of uORF1, which we observed.

The 3′ sequences of the first three uORFs contain the conserved, REI-promoting AU-rich motif and at the same time, in the case of uORFs 2 and 3, also inhibitory elements further downstream

The puzzling similarity of the AU-richness of the 3′ sequences of uORF1—3 combined with their differential effects on

GCN4 REI observed in Figure 1D prompted us to inspect the composition of the 3′ sequences of these three uORFs in greater detail. We revealed a potential AU-rich motif ($AU_{1\text{-}2}A/UUAU_2$) specifically occurring within the first 12 nt of segment D of only the first three uORFs (Fig. 3A). To examine whether this motif solely carries the REI-promoting activity of the 3′ sequences of uORFs 1 and 2, and perhaps even of uORF3, we replaced either the first 1–12 nt or the immediately following 13–25 nt of the uORF1 segment D with the corresponding sequences of the other three uORFs and measured the β-galactosidase activities of the resulting constructs. In the case of uORF2, we not only observed that its $AU_{1\text{-}2}A/UUAU_2$ motif-containing 1 through 12 nt sequence behaved as efficiently as the native uORF1 3′ sequence (~102% for *uORF1-1112*$^{1\text{-}12}$), but also that its 13 through 25 nt sequence (*uORF1-1112*$^{13\text{-}25}$) had a modest inhibitory effect on the REI activity of uORF1 (Fig. 3). In the case of uORF3, the first 12 nt containing the AU-rich motif showed only modestly decreased activity compared to the native uORF1 3′ sequence (~79% for *uORF1-1113*$^{1\text{-}12}$), whereas its 13 through 25 nt sequence (*uORF1-1113*$^{13\text{-}25}$) displayed a robust inhibitory effect. Strikingly, this inhibitory effect is dominant over the stimulatory effect of the AU-motif, which perfectly explains why replacing the entire segment D of uORF1 (Fig. 1D) or of uORF4 in the uORF1 position (Fig. 2A) with the same segment of uORF2 or uORF3 reduced the efficiency of REI by varying degree despite their similar AU content. These findings also suggest that the modest dominant inhibitory impact of 13–25 nt of uORF2 3′ sequence (further documented in Fig. 1C; Supplemental Fig. S2A) further contributes to the difference in the overall REI efficiency between uORF1 and uORF2.

Replacing the first 12 nt of the uORF1 segment D with the same uORF4 sequence (*uORF1-1114*$^{1\text{-}12}$) completely eliminated the stimulatory effect of the uORF1 3′ sequence, whereas the replacement of the following 13–25 nt (*uORF1-1114*$^{13\text{-}25}$) had no effect whatsoever (Fig. 3B), clearly suggesting that the 13 through 25 nt segment of uORF4 has no inhibitory effect. This observation explains why the D segment replacement of uORF2 and uORF3 with that of uORF4 increased their overall REI activity (Fig. 1C). Importantly, it was previously suggested that the first 10 (and not 12) nt of

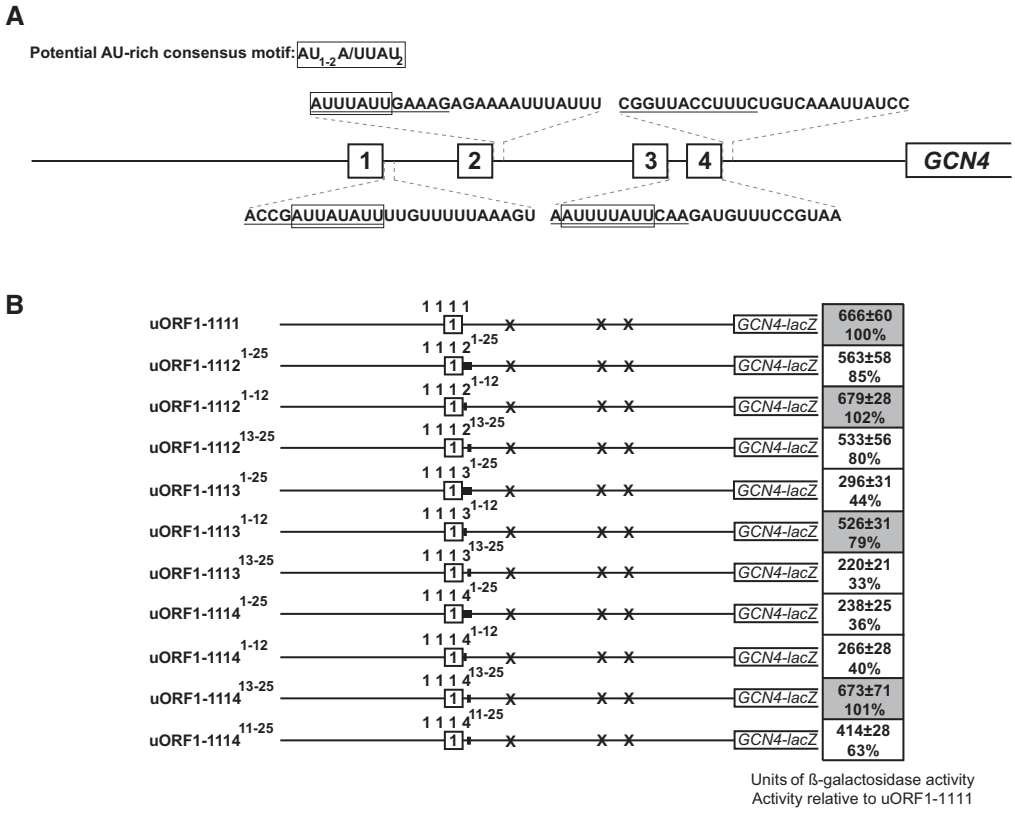

FIGURE 3. The presence of the specific AU-rich motif determines the REI-promoting activity of the 3′ sequence. (*A*) Schematic of the *GCN4* mRNA leader adapted from Figure 1A. The specific AU-rich motif (shown in frame) is present within the first 12 nt of the 3′ sequences of uORF1, 2, and 3; the first 12 nt of the 3′ sequence of each uORF are underlined. (*B*) The "full-length" 3′ sequence (1–25) of solitary uORF1 from the *GCN4* mRNA leader in its authentic position or its parts represented by the first 12 nt (1–12) or second 13 nt (13–25), or 15 nt in the case of uORF4 (11–25), were replaced by corresponding segments of the other three uORFs and analyzed as described in Figure 1C. Differences in β-galactosidase activities between *uORF1-1112*, *uORF1-1112*$^{13\text{-}25}$, *uORF1-1113*$^{1\text{-}12}$, or *uORF1-1114*$^{11\text{-}25}$ and their wt *uORF1-1111* were analyzed by Student's *t*-test and the calculated $P = 0.25$, 0.1469, 0.0722, or 0.0052, respectively.

the 3′ sequence of uORF1 suffice for its full function (Miller and Hinnebusch 1989), which leaves out the last 2 nt from the AU-rich motif. To reconcile these and our observations, we replaced the 11–25 nt of the uORF1 3′ sequence with the corresponding region of uORF4 (*uORF1-1114*$^{11\text{-}25}$) and observed that the REI activity on *GCN4* dropped down to 63%, in contrast to the 13–25 nt replacement showing 100% activity (Fig. 3B). Hence at least in our experimental setup, it is not the first 10 but the first 12 nt that encompass the entire $AU_{1\text{-}2}A/UUAU_2$ motif needed for the full REI potential of the uORF1 3′ sequence.

Taken together, our findings strongly suggest that the specific AU-rich motif occurring within the first 12 nt of segment D of uORF1, uORF2, and uORF3 is solely responsible for the REI-promoting function of the 3′ sequence, provided that it is situated at or near the authentic position of uORF1. As can be seen, however, sequences immediately following this motif also play an important role in this regulatory mechanism as they, at least in the case of uORFs 2 and 3, negatively influence their overall REI potential. Since uORF2 and uORF3 stimulate REI in the AU-rich motif-independent manner (Fig. 1C), and since these inhibitory sequences are transferable also to the ABCD blocks of uORF1 and uORF4, it is conceivable that they also act autonomously and impact a different REI step than that involving the action of the $AU_{1\text{-}2}A/UUAU_2$ motif.

The exact length of uORF1 and uORF2 coding sequences is critical for their maximal REI activity that shows a partially autonomous character

In our effort to systematically assess individual contributions of sequences flanking the REI-permissive uORFs to their REI capacity, we also wished to examine the potential contribution of the uORF1 and uORF2 coding sequences (CDS) per se. Early experiments done in the Hinnebusch laboratory suggested that the last coding triplet, which is represented by TGC coding cysteine for uORF1 and CCG coding proline for uORF4, does somehow contribute to the remarkable difference in the efficiency of REI between these two uORFs (Miller and Hinnebusch 1989; Grant and Hinnebusch 1994). Interestingly, the second REI-permissive uORF, uORF2, also contains a cysteine codon (TGT) as its last sense codon as uORF1, only it is one codon shorter (Fig. 4A). The same kind of similarity for the last sense codon also applies to uORF3 and REI-nonpermissive uORF4, as uORF3, like uORF4, contains the CCG triplet coding proline (Fig. 4A).

In analogy with our previous approach (Fig. 1D), we first replaced the CDS of uORF1 with CDSs of the other three uORFs (*uORF1-1121*, *uORF1-1131*, and *uORF1-1141*). None of them could work in place of uORF1 as efficiently as uORF1 by itself, not even the Cys codon-containing REI-permissive uORF2; the REI activity of these three replacements was reduced by ~51% to 70% (Fig. 4B). This is in agreement with an earlier study where the activity of *uORF1-1141* was measured in the strain deleted for the *GCN4* pathway-specific GCN2 kinase (Miller and Hinnebusch 1989). Hence we propose that not only the character of the last coding triplet but also the exact length of the uORF1 CDS is critical for its function. In support, extending the length of the two-codonal uORF2 by insertion of the uORF1 GCT Ala codon immediately after the uORF2 start codon (*uORF2-2212*) reduced its REI activity by 40% (Fig. 4C). Our findings thus clearly imply that the authentic length of both REI-permissive uORFs has to be maintained for their optimal activity. This could matter, for example, due to the fact that even slight alterations of their length may interfere with proper functioning of their 5′ and/or 3′ sequences.

To find out whether or not the CDSs of uORF1 and uORF2 can at least to some degree stimulate REI independently of their flanking, REI-promoting sequences, we replaced the uORF4 segment C from the uORF4 ABCD block situated either in the position of uORF1 (*uORF1-4444*) (Fig. 4D) or in its authentic position (*uORF4-4444*) (Fig. 4E) with those of uORF1 (*uORF1-4441* and *uORF4-4441*) or uORF2 (*uORF1-4442* and *uORF4-4442*). Regardless of the placement of the uORF4 ABCD block, the presence of CDSs of both REI-permissive uORFs did increase the efficiency of REI by ~26% to 44%. However, since segment C replacements in the uORF1 ABCD block showed >50% decrease in its REI activity (Fig. 4B), it is intuitive that a fully autonomous contribution of CDSs of both REI-permissive uORFs should lead to a larger, approximately twofold increase, which we did not observe. Hence we conclude that both uORFs per se have some inherent ability to promote REI independently of other sequences that is not position-specific, in contrast to the 3′ AU-rich motif. Not surprisingly, however, they also functionally interact with their flanking sequences to maximize their REI potential. Generally speaking, a REI-permissive uORF can be viewed as the complex unit with several independent and/or mutually interdependent contributors with peculiar attributes such as the CDS length.

The CCG triplet coding proline negatively impacts REI efficiency and at least in yeast has a predictable value in this respect

To investigate the causality of the aforementioned occurrence of the Cys triplet as the ultimate coding triplet in REI-permissive uORFs 1 and 2, and of the Pro triplet as the ultimate coding triplet in uORF3 and uORF4, we first inspected the *GCN4* mRNA leaders of closely or distantly related yeast species to *Saccharomyces cerevisiae* (Fig. 5A). With the exception of *Candida glabrata*, there is a clear conserved tendency for all other species to preserve Cys and Pro as the last coding triplets in at least the first and last short uORF, respectively. In the case of *C. glabrata*, the Cys triplet occurs in uORF3 and is followed by long uORF4 that is, owing to its length, by definition strictly REI-nonpermissive (Vilela et al. 1998; Szamecz et al. 2008). Therefore, this regulatory setup simply

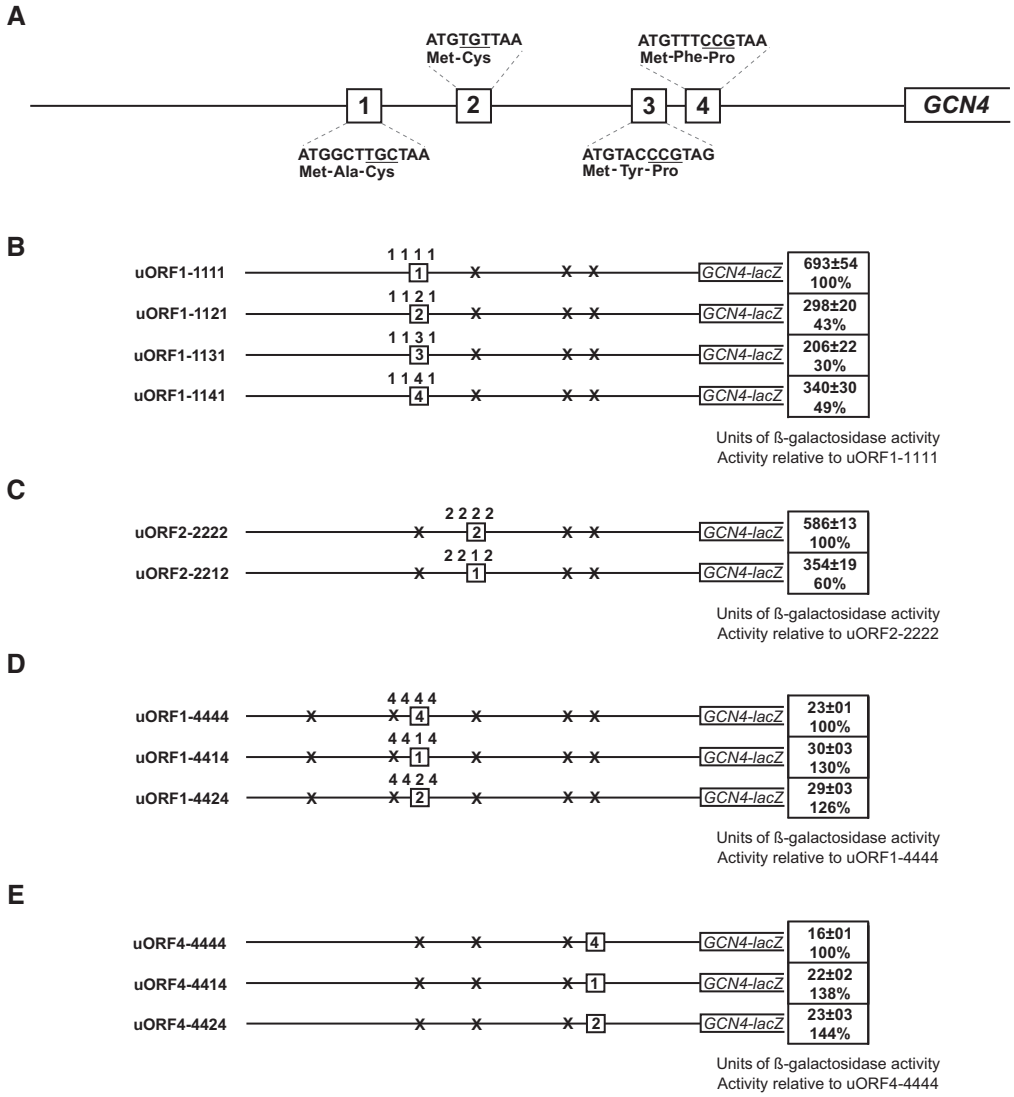

FIGURE 4. Sequence composition and length but not the position of uORF1 and uORF2 CDSs define their REI permissiveness. (*A*) Schematic of the *GCN4* leader containing four short uORFs (1–4). For each uORF, nucleotide as well as amino acid sequences are shown. The triplets of the last sense codon are underlined. (*B*) The CDS (segment C) of solitary uORF1 from the *GCN4* mRNA leader in its authentic position was replaced by corresponding segments of the other three uORFs and analyzed as described in Figure 1C. (*C*) The CDS of solitary uORF2 from the *GCN4* mRNA leader in its authentic position was replaced by corresponding segment of uORF1 and analyzed as described in Figure 1C. (*D*) The CDS of solitary uORF4 from the *GCN4* mRNA leader with its authentic flanking sequences (A4–D4) situated in the position of uORF1 was replaced by corresponding segments of uORF1 and 2 and analyzed as described in Figure 1C. Differences in β-galactosidase activities between *uORF1-4414* or *uORF1-4424* and their wt *uORF1-4444* were analyzed by Student's *t*-test and the calculated $P = 0.0572$ or 0.094, respectively. (*E*) Same as in *D* except that the CDS substitutions were tested in the authentic position of uORF4. Differences in β-galactosidase activities between *uORF4-4414* or *uORF4-4424* and their wt *uORF4-4444* were analyzed by Student's *t*-test and the calculated $P = 0.0275$ or 0.0581, respectively.

does not require featuring Pro as the ultimate coding triplet of the last uORF.

The question is, what stands behind this phenomenon? Is it the Cys/Pro triplet or the identity of these two residues per se? To examine that, we systematically substituted the ultimate coding triplet individually in all four *GCN4* uORFs and measured the resulting REI activities. Recoding the cysteine triplet of uORF1 [*uORF1-1111-Cys (TGT)*] or uORF2 [*uORF2-2222-Cys (TGC)*] showed almost no impact on REI of these uORFs (Fig. 5B,C), which contrasts with the remarkable increase in REI seen when the analogous uORF1 recoding was tested in early days, however, in the artificial setup with the genuine uORF1 3′ sequence replaced with the corresponding 3′ sequence of uORF4 (Grant and Hinnebusch 1994). In fact, our measurements are perfectly consistent with another work by the same group, where the REI activity was measured for the synonymous uORF1 cysteine substitutions under starvation conditions using a minimalistic construct lacking uORF2 and uORF3 and no significant changes were found (Miller and Hinnebusch

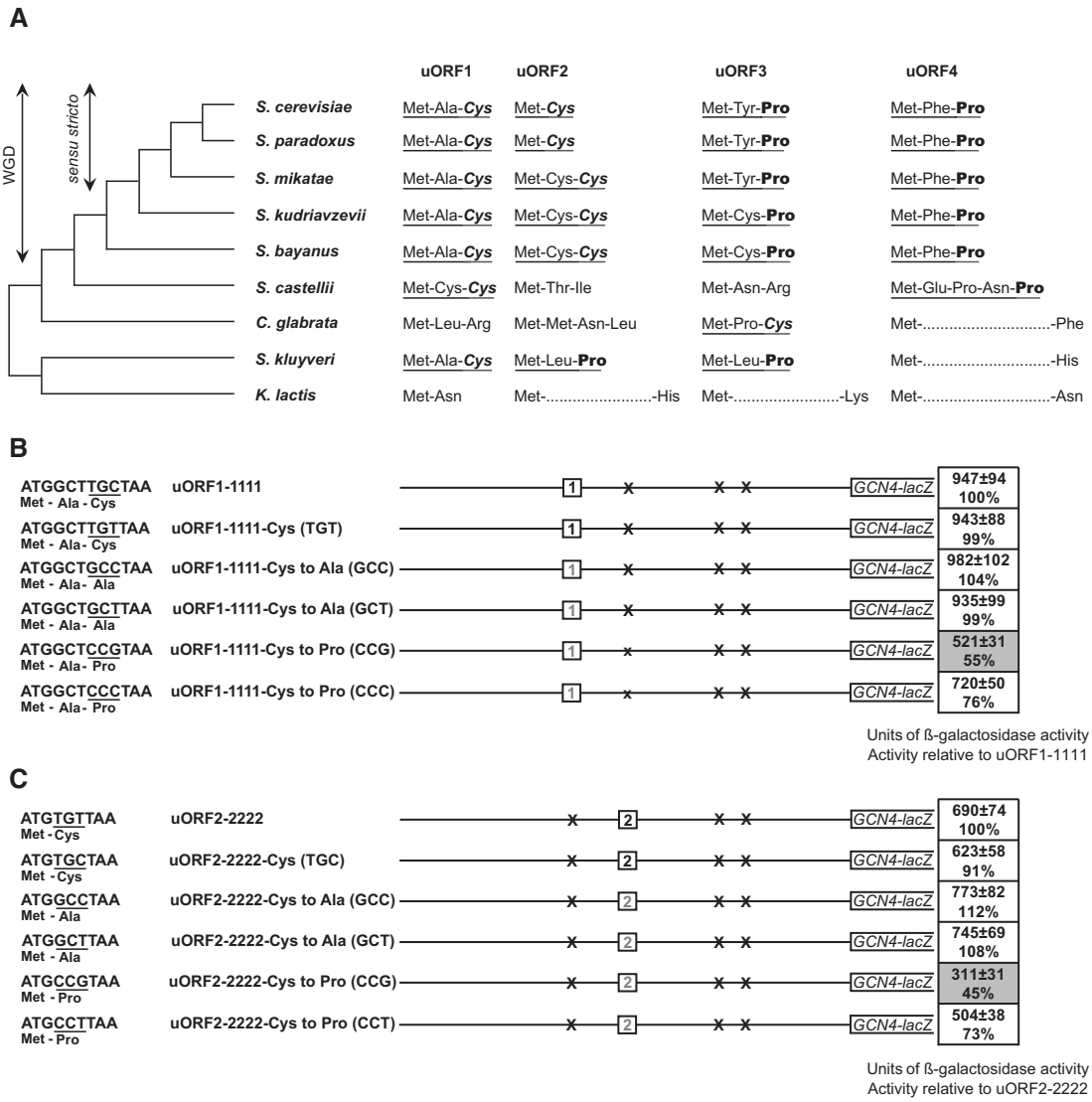

FIGURE 5. Insertion of the CCG triplet as the last sense codon of uORF1 and uORF2 inhibits their REI activity. (*A*) The conservation of Cys and Pro codons in short uORFs from the *GCN4* mRNA leaders of yeast species related to *S. cerevisiae.* The uORFs are presented as identified in Cvijović et al. (2007). uORFs containing Cys (in italics) and Pro (in bold) triplets as their last sense codons are underlined. In longer uORFs, the sequence of their CDSs is represented by a dotted line. WGD, whole-genome duplication. (*B*) The TGC cysteine codon of solitary uORF1 from the *GCN4* mRNA leader in its authentic position was replaced by indicated cysteine, alanine, and proline substitutions and analyzed as described in Figure 1C. Differences in β-galactosidase activities between *uORF1-1111-Cys* to *Pro (CCC)* and its wt *uORF1-1111* were analyzed by Student's *t*-test and the calculated $P = 0.0648$. (*C*) The TGT cysteine codon of solitary uORF2 from the *GCN4* mRNA leader in its authentic position was replaced by indicated cysteine, alanine, and proline substitutions and analyzed as described in Figure 1C. Differences in β-galactosidase activities between *uORF2-2222-Cys* to *Pro (CCT)* and its wt *uORF2-2222* were analyzed by Student's *t*-test and the calculated $P = 0.0554$.

1989). Hence we conclude that both cysteine codons of uORF1 and uORF2 utilizing the same Cys-tRNA are similarly efficient in promoting REI. In addition, our findings further support the idea that it is most probably the length of the CDSs of uORF1 and uORF2 and not the differing Cys triplet that stands behind their inability to replace each other in their authentic environment (Fig. 4B,C).

To examine whether it is the cysteine residue per se that lies behind this phenomenon, we substituted the cysteine codons of uORF1 (TGC) and uORF2 (TGT) with two different alanine codons: (i) GCC [*uORF1-1111-Cys* to *Ala (GCC)* and *uORF2-2222-Cys* to *Ala (GCC)*], and (ii) GCT [*uORF1-1111-Cys* to *Ala (GCT)* and *uORF2-2222-Cys* to *Ala (GCT)*]. Like the cysteine substitutions, neither of the Ala substitutions had any effect on either uORF (Fig. 5B,C). Hence the REI permissiveness of uORF1 and uORF2 CDSs does not exclusively depend on the presence of a cysteine codon as the last coding triplet, as suggested before (Grant and Hinnebusch 1994). It also does not seem to strictly depend on the AU vs. GC content, as proposed by Grant

and Hinnebusch (1994), because the changes that increased or decreased the AU content showed no effect (Fig. 5B,C). This implies that the third codon can most probably tolerate a wide range of codons as long as these do not interfere with the resumption of scanning.

Finally, we substituted Cys codons in both REI-permissive uORFs with the supposedly inhibitory proline CCG triplet from uORFs 3 and 4 [*uORF1-1111-Cys* to *Pro (CCG)* and *uORF2-2222-Cys* to *Pro (CCG)*] as well as with the other two proline triplets; CCC for uORF1 [*uORF1-1111-Cys* to *Pro (CCC)*] and CCT for uORF2 [*uORF2-2222-Cys* to *Pro (CCT)*] (Fig. 5B,C). Whereas the latter CCT and CCC substitutions led to ~24%–27% drop in the REI activity on both uORFs, the CCG triplet produced the most robust ~45%–55% reduction. A similar decrease was also seen when the CCG substitution in uORF2 was made in the construct where the entire uORF2 ABCD block was placed in the position of uORF1 (data not shown). These findings correspond well with our uORF1 segment C replacement data (Fig. 4B), where introduction of the corresponding uORF4 segment in *uORF1-1141* also reduced the REI efficiency by ~51%. This suggests that at least for uORF1 the entire negative effect could be solely attributable to the presence of the last coding CCG triplet.

Importantly, we cannot explain the observed difference among the three tested Pro triplets by their varying codon optimality, because it simply does not correlate with the amounts of distinct types of Pro-tRNAs specific to these triplets. Hence, we propose that both the presence of proline as the ultimate residue and also some peculiar attributes of the CCG codon beyond codon optimality act together to maximize the inhibitory impact on REI after translation of short uORFs that are not meant to promote efficient resumption of scanning. Consistently, replacing the CCG Pro triplet in uORF3 and uORF4 with the uORF1 TGC cysteine codon relieved the CCG-mediated inhibition of REI after uORF3 and uORF4 translation to some degree (Supplemental Fig. S4).

The proline residue is known for its unusual conformation that, due to its limited spatial rotation during peptide bond formation, slows down the incorporation of this residue into the nascent polypeptide chain and therefore negatively influences the speed of translation (Wohlgemuth et al. 2008; Pavlov et al. 2009). Since uORF1 and uORF2 are very short, the presence of the slowing down Pro as the last residue could theoretically interfere with the time-sensitive formation of the interaction between uORF1 and uORF2 RPEs and their interacting factor eIF3. In support, prolonging the time of uORF1 proteosynthesis by extending its coding region by up to five codons gradually decreased its REI potential (Szamecz et al. 2008). The difference observed among the three tested Pro triplets could then be caused by a specific character of the CCG sequence that might, for example, interfere with proper stop codon recognition for effective translation termination.

The sequence composition of the uORF3 and uORF4 second codon and markedly differing termination efficiency makes the difference in the REI activity between these two uORFs

As mentioned above, we previously established that the inherent REI activity of uORF3 represents ~13%–18% of the maximum REI capacity allowed by uORF1, whereas uORF4 goes down to ~3%–5% (Munzarová et al. 2011; Gunišová and Valášek 2014). Therefore, we wished to uncover what determines the approximately fourfold higher REI activity of uORF3 compared to uORF4. In our earlier work, we demonstrated that the modest REI potential of uORF3 does not depend on any of the uORF1- and/or uORF2-specific RPEs and, accordingly, it does not require intact eIF3 (Gunišová and Valášek 2014). Here we ruled out the possibility that this difference could be caused by the uORF3's ability to utilize the AU-rich motif contained within its 3′ sequence (Fig. 1C; Supplemental Fig. S3). Hence the only option left was the CDS of both uORFs, where only two differences can be found: (i) the second codon that is represented by TAC encoding Tyr in uORF3 and TTT encoding Phe in uORF4, and (ii) the stop codon that is represented by TAG in uORF3 and TAA in uORF4 (Fig. 6A). Looking at their 12-nt sequences per se, these two uORFs differ only by 3 nt.

To investigate what lies behind this difference, we prepared the uORF3- and uORF4-based constructs, where each aspect at which they differ was individually or in combinations swapped between them and examined for REI activity (Fig. 6B). The Tyr to Phe substitution of uORF3 [*uORF3-3333-Tyr* to *Phe (TTT)*] markedly decreased its activity (down to ~55%) (Fig. 6B). A milder decrease down to ~71% was obtained when the stop codon of uORF3 was replaced with that of uORF4 (*uORF3-3333-TAA*), however, a combination of both of these substitutions in *uORF3-3333-Tyr* to *Phe (TTT)-TAA* showed an additive effect by allowing only ~42% of the intrinsic REI activity of wild-type uORF3 (Fig. 6B). Interestingly, whereas the stop codon swap in uORF4 (*uORF4-4444-TAG*) showed no effect, the Phe to Tyr substitution of uORF4 [*uORF4-4444-Phe* to *Tyr (TAC)*] increased the REI activity by ~1.7-fold and their subsequent combination in *uORF4-4444-Phe* to *Tyr (TAC)-TAG* also led to an additive effect by increasing the intrinsic REI potential of uORF4 by approximately twofold (Fig. 6B). Our results thus indicate that the differences in the composition of the uORF3 and uORF4 CDSs are indeed at least partially responsible for their different REI permissiveness.

Next we analyzed the effect of the second sense codon in greater detail because it seemed to have a bigger influence on efficiency of resumption of scanning over the identity of the stop codon. To find out whether it is the encoded amino acid or a particular triplet that makes the difference, we tested both existing Tyr codons (original TAC and synonymous TAT) and both existing Phe codons (original TTT and synonymous TTC) in both uORFs of interest. Luckily, the

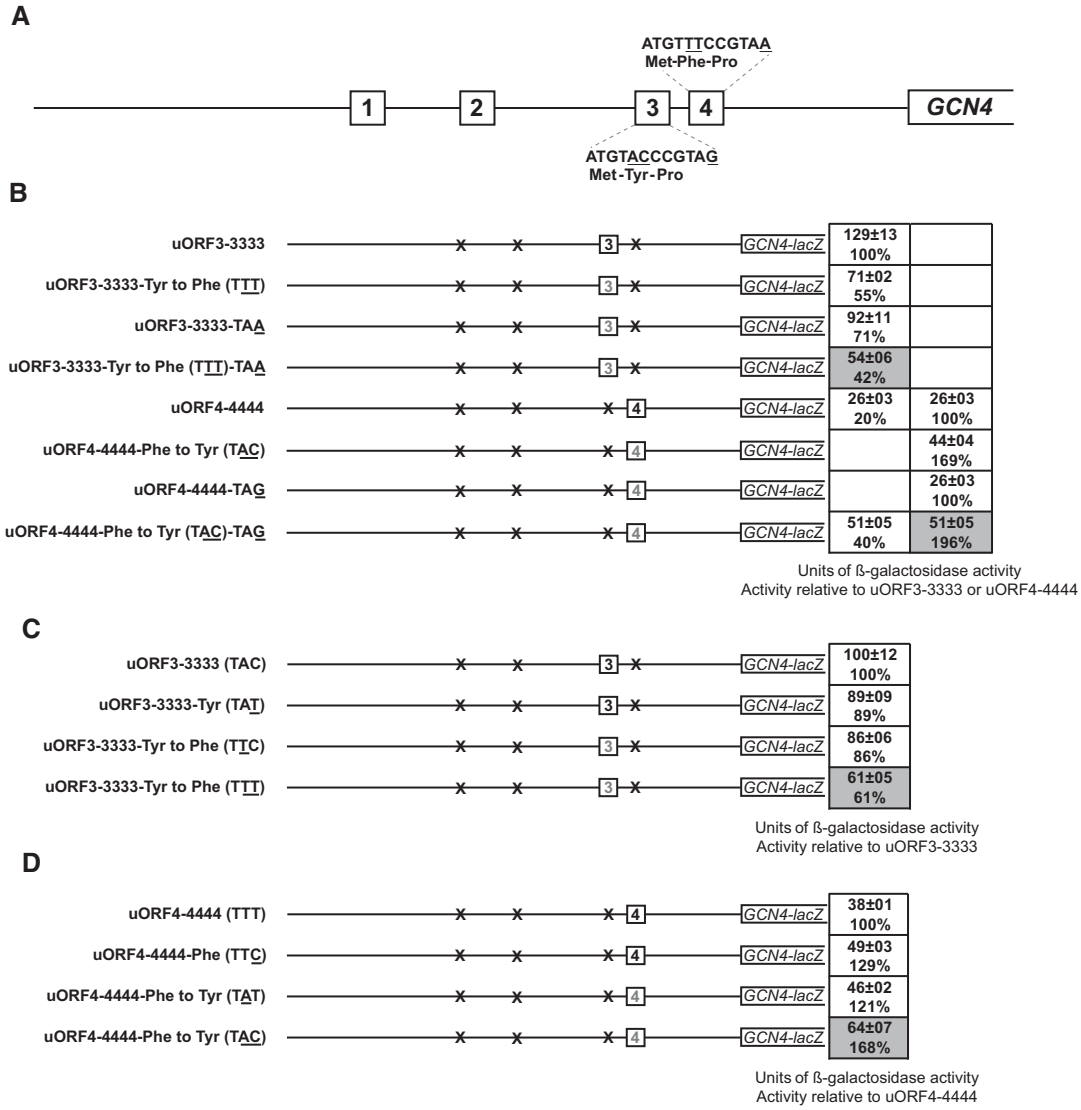

FIGURE 6. The differences in the sequence composition of the uORF3 and uORF4 CDSs are responsible for their varying REI permissiveness. (*A*) Schematic of the *GCN4* leader adapted from Figure 4A. Nucleotide as well as amino acid sequences of only uORF3 and uORF4 are depicted. The different nucleotides between these two uORFs are underlined. (*B*) The CDSs of solitary uORF3 and uORF4 from the *GCN4* mRNA leader in their authentic positions were modified by indicated substitutions and analyzed as described in Figure 1C. Differences in β-galactosidase activities between *uORF3-3333-TAA* and its wt *uORF3-3333*, or *uORF3-3333-Tyr* to *Phe (TTT)* and *uORF3-3333-Tyr* to *Phe (TTT)-TAA*, or *uORF4-4444-Phe* to *Tyr (TAC)* and *uORF4-4444-Phe* to *Tyr (TAC)-TAG* were analyzed by Student's *t*-test and the calculated $P = 0.0609$, 0.0275, or 0.3033, respectively. (*C*) Same as in *B* except that a different set of solitary uORF3 substitutions was used. Differences in β-galactosidase activities between *uORF3-3333-Tyr* to *Phe (TTT)* and its wt *uORF3-3333* were analyzed by Student's *t*-test and the calculated $P = 0.0171$. (*D*) Same as in *B* except that a different set of solitary uORF4 substitutions was used.

interpretation of these analyses is simplified by the fact that both existing Tyr and Phe codons are recognized by a single Tyr- or Phe-tRNA, respectively. Therefore, there should be no unspecific influence on the effect of our substitutions. Out of these three possible substitutions only Phe (TTT), changing two out of three original bases in *uORF3-3333-Tyr* to *Phe (TTT)*, produced by far the most dramatic reduction in the uORF3 REI activity (down to ~61%) (Fig. 6C). Similarly, the Tyr (TAC) substitution, changing two out of three original bases in *uORF4-4444-Phe* to *Tyr (TAC)*, produced by far the largest increase (by ~1.7-fold) in the uORF4 REI activity (Fig. 6D). All other substitutions that changed only one out of three bases of both uORFs [*uORF3-3333-Tyr (TAT)* and *uORF3-3333-Tyr* to *Phe (TTC)* in Fig. 6C, and *uORF4-4444-Phe (TTC)* and *uORF4-4444-Phe* to *Tyr (TAT)* in Fig. 6D] altered the efficiency of REI only modestly. Since the same amino acid encoded by two different triplets that are, however, recognized by the same tRNA produced a marked difference in REI activity, we can conclude that it is not the identity of an amino acid

residue or of a tRNA by which it is delivered, but the sequence composition of the uORF3 and uORF4 second codon that contributes to the difference in the REI potential between these two uORFs.

Because the full remake of uORF3 into uORF4 in the authentic position of uORF3 [*uORF3-3333-Tyr* to *Phe (TTT)-TAA*] reduces its REI activity only approximately twofold, and at the same time the full remake of uORF4 into uORF3 in the authentic position of uORF4 [*uORF4-4444-Phe* to *Tyr (TAC)-TAG*] increases its REI activity also only approximately twofold, there must clearly be some other factor outside of their CDSs that further contributes to the approximately fourfold difference in REI activity between uORF3 and uORF4. We hypothesized that this factor could lie in the identity of the base immediately following the stop codon (the so called +4 nucleotide), which is known to strongly influence the efficiency of stop codon recognition (see, for example, Beznosková et al. 2015b). In particular, cytosine at the +4 position is the leakiest base with respect to efficiency of translation termination among all four bases at all three stop codons (Beznosková et al. 2015a; Dabrowski et al. 2015). Hence, we rationalized that an uORF with a poorer stop codon context allowing increased frequency of stop codon readthrough would extend its translation beyond its genuine stop codon, which would in turn decrease its efficiency of REI. Interestingly, the TAA stop codon of uORF4 is followed by C and TAG of uORF3 by A (Figs. 1A, 7A), and indeed our dual-luciferase reporter assay revealed that uORF4 has ~3.7-fold increased frequency of readthrough compared to uORF3 (Fig. 7B). As a control, we used the TGA stop codon with the C at the +4 position (TGA-C), which is known to allow relatively high levels of readthrough (Beznosková et al. 2015b). Notably, readthrough on uORF4 is even ~1.5-fold higher than readthrough on this very rare terminating tetranucleotide with the so-called programmed readthrough. Hence we propose that the fact that ~3.7-times more ribosomes fail to terminate at uORF4 compared to uORF3 does further contribute to its overall REI nonpermissiveness and thus to the difference in REI activity between these two uORFs.

If true, the combination of the full remake of uORF4 into uORF3 [*uORF4-RT-Phe* to *Tyr (TAC)-TAG*] with a substitution of the +4 nucleotide C of uORF4 for A of uORF3 (*uORF4-RT-TAAA*) into one construct [*uORF4-RT-Phe* to *Tyr (TAC)-TAGA*] should reduce the frequency of readthrough down to the levels observed for wt uORF3; and this is exactly what we observed. Whereas individual mutations reduced readthrough by similar ~2.6-fold, their combination displayed an approximately fourfold decrease [Fig. 7B; compare 24% of *uORF4-RT-Phe* to *Tyr (TAC)-TAGA* with 27% of *uORF3-RT*]. Consistently, the same trend but in a reverse order was seen when we substituted the +4 nucleotide C of uORF4 for A of uORF3 and measured the REI efficiency using the *GCN4-LacZ* construct (*uORF4-4444-TAAA*). It increased the overall REI activity of uORF4 by ~1.6-fold (164%) and the same substitution in the full remake of uORF4 into uORF3 [*uORF4-4444-Phe* to *Tyr (TAC)-TAGA*] increased the overall REI activity from approximately twofold (209%) to approximately threefold (291%), which is now close to the aforementioned approximately fourfold difference between both uORFs (Fig. 7C). We thus conclude that the combination of the sequence composition of the uORF3 and uORF4 second codon and the identity of the stop codon tetranucleotide is what makes the major contribution to the difference in the REI potential between these two uORFs.

Individual and combined effects of all *cis*-elements that determine REI permissiveness of uORF1 and uORF2

To capture our in-depth analysis, we gradually combined mutations in all identified REI-promoting *cis*-determinants of uORF1 as well as uORF2 in an effort to compare their individual contributions to the overall REI potential of both REI-permissive uORFs. First, we side-by-side evaluated individual contributions of (i) the RPEs i.–iv. that are situated in segment A of uORF1 (Munzarová et al. 2011; Gunišová and Valášek 2014), (ii) the CDS of uORF1 and in particular of its third sense codon, and (iii) the 3′ sequence of uORF1. The biggest contribution comes from the RPEs (*uORF1-1111-Δ160*; ~79% drop), some of which like RPE i. and iv. require intact eIF3 for their function. The RPEs are followed by the autonomous 3′ sequence (*uORF1-1114*; ~67% drop), and the uORF1 third sense codon [*uORF1-1111-Cys* to *Pro (CCG)*; ~49% drop] (Fig. 8A). Concurrent removal of the two biggest contributors in *uORF1-1114-Δ160* displayed a robust decrease in the REI activity (down to ~8%), strongly suggesting that their contributions are independent ($0.21 \times 0.33 = 0.07$, which pretty much equals the obtained 8%). A relatively smaller additive effect was observed when the removal of all RPEs was combined with the Cys to Pro substitution in *uORF1-1111-Δ160-Cys* to *Pro (CCG)* (16%), indicating their partial interdependence ($0.21 \times 0.51 = 0.11$, which is smaller than the obtained 16%). Testing the combination of the Cys to Pro substitution with the removal of the uORF1 3′ sequence in the hypothetical *uORF1-only-1114-Cys* to *Pro (CCG)* construct is meaningless, because we previously showed that the otherwise autonomous activity of RPEs follows and in fact requires a prior action of the uORF1 3′ sequences (Munzarová et al. 2011). Therefore, with respect to its minimal activity (~6%), the *uORF1-1144* construct shown in Figure 1C basically mimics the elimination of all three contributors in *uORF1-1114-Δ160-Cys* to *Pro (CCG)* reaching the uORF4-like basal REI activity (~5%) (Fig. 8A).

Finally, removal of the eIF3-independent RPE ii. together with the uORF2-specific, eIF3-dependent RPE v. (Gunišová and Valášek 2014), situated in the uORF2 segment A (*uORF2-2222-Δ233*), reduced the efficiency of REI by a robust ~77%, whereas the Cys to Pro substitution of the

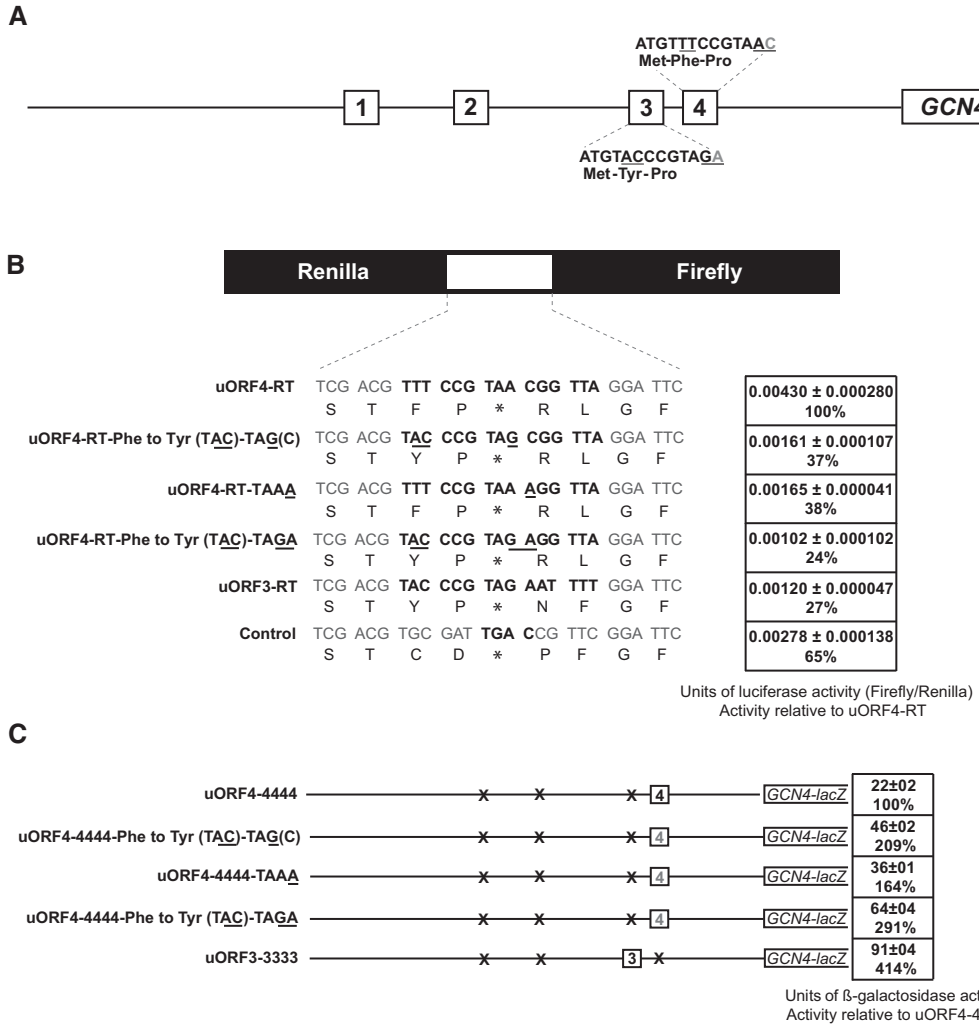

FIGURE 7. Poor termination efficiency at the uORF4 stop codon strongly contributes to the difference in the REI efficiency between uORF3 and uORF4. (*A*) Modified schematic from Figure 6A, in addition depicting the nucleotide following the stop codon of uORF3 and uORF4 (the +4 base; in gray). (*B*) Schematic of the standard dual luciferase readthrough reporter constructs adapted from Keeling et al. (2004). In the linker region, the 15-nt long termination sequences of uORF3 or uORF4 with their derivatives, as well as the control TGA-C terminating tetranucleotide, are shown in bold. The uORF4 derivatives have all their substitutions gradually turning them into wt uORF3 underlined. All indicated constructs were introduced into the PBH156 strain and the resulting transformants were grown in SD and processed for stop codon readthrough measurements as described in Materials and Methods. Values of luciferase activity are represented as mean values and standard deviations obtained from five independent transformants, and each experiment was repeated at least three times. Differences in luciferase activities between *uORF4-RT-Phe* to *Tyr (TAC)-TAG* or *uORF4-RT-TAAA* and their wt *uORF4-RT*, and between *uORF4-RT* and control *TGAC* plasmid were analyzed by Student's *t*-test and the calculated $P = 0.0039$ or 0.0004, and 0.0012, respectively. (*C*) The difference in the nucleotide following the stop codon of uORF3 and uORF4 (the +4 base) contributes to their varying REI permissiveness. Solitary uORF4 from the *GCN4* mRNA leader in its authentic position was modified by indicated substitutions from uORF3 and analyzed as described in Figure 1C. Differences in β-galactosidase activities between *uORF4-4444-TAAA* and its wt *uORF4-4444* were analyzed by Student's *t*-test and the calculated $P = 0.0002$.

uORF2 last coding triplet [*uORF2-2222-Cys* to *Pro (CCG)*] showed a similar reduction to that observed for uORF1 (~56% drop in REI) (Fig. 8B). Hence, as in the case of uORF1, the major contributor to the uORF2 REI potential is represented by its RPEs. Elimination of both of these *cis*-determinants at the same time in *uORF2-2222-Δ233-Cys* to *Pro (CCG)* expectedly reached the uORF4-like basal level of REI (~5%) (Fig. 8B), clearly illustrating the absolute independence of the uORF2 REI activity on its 3′ sequences, as shown above.

Conclusion

Our systematic analysis of all potential *cis*-determinants that either promote or inhibit reinitiation on *GCN4* mRNA revealed the following attributes of individual uORFs (summarized in Fig. 9). The 3′ sequences of uORFs 1–3, in particular the first 12 nt immediately following their stop codons, contain a conserved $AU_{1\text{-}2}A/UUAU_2$ motif that promotes REI independently of other REI-promoting elements but only when situated at the defined distance from the *GCN4* AUG

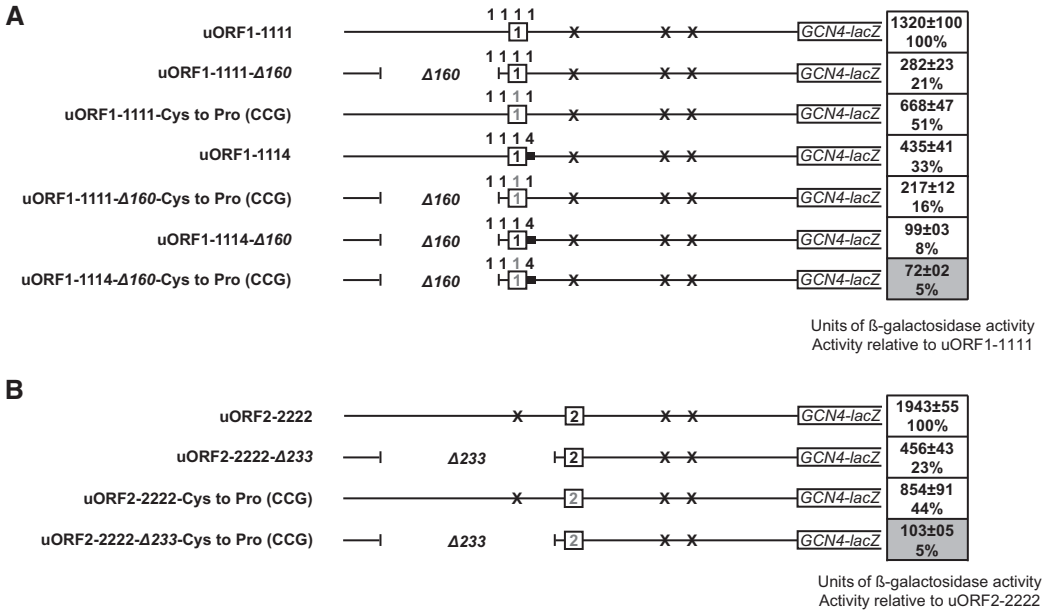

FIGURE 8. Combined effects of mutations in *cis*-determinants of uORF1 and uORF2 on their REI permissiveness. (*A*) The REI permissiveness of uORF1 is determined by three *cis*-factors: RPEs situated in the 5′ sequence, CDS, and the 3′ sequence. Solitary uORF1 from the *GCN4* mRNA leader in its authentic position and its derivatives containing the indicated mutations were analyzed as described in Figure 1C. Differences in β-galactosidase activities between *uORF1-1111-Δ160* and *uORF1-1111-Δ160-Cys* to *Pro (CCG)*, or *uORF1-1114-Δ160* and *uORF1-1114-Δ160-Cys* to *Pro (CCG)* were analyzed by Student's *t*-test and the calculated $P = 0.0369$ or 0.0001, respectively. (*B*) REI permissiveness of uORF2 is determined by two *cis*-factors: RPEs situated in the 5′ sequence and CDS. Solitary uORF2 from the *GCN4* mRNA leader in its authentic position and its derivatives containing the indicated mutations were analyzed as described in Figure 1C.

start codon, in principle corresponding to the position of uORF1. Hence, despite carrying this autonomous motif in their 3′ sequences, uORF2 and uORF3 do not utilize it. Intriguingly, the 3′ sequences of specifically these two uORFs in addition contain inhibitory elements that immediately follow the AU-rich motif and decrease the REI potential of these two uORFs. Interestingly, these inhibitory elements are transferable and function irrespectively of their distance from the *GCN4* start codon. Furthermore, we also revealed that the authentic length of both REI-permissive uORFs has to be maintained for their optimal activity and that the last coding triplet can most probably tolerate a wide range of codons with the exception of the REI-inhibiting proline CCG triplet. Indeed, specifically this Pro triplet occurs as the last triplet in uORF3 and uORF4 and, in fact, features in all ultimate uORFs in the *GCN4* mRNA leaders across yeast species. Finally, we show that the approximately four-fold difference between the REI potential of modestly REI-permissive uORF3 and REI-nonpermissive uORF4 does not lie in the supposedly inhibitory 3′ sequence of uORF4, as suggested before (Gunišová and Valášek 2014), but is manifested through the specific effects of the sequence composition of their second codon and of the identity of their stop codon tetranucleotide, which together impact the efficiency of stop

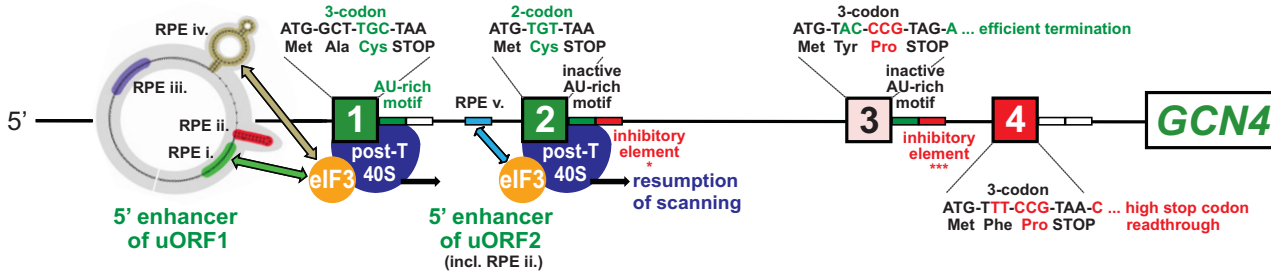

FIGURE 9. Summary of all *cis*-determinants that either promote or inhibit reinitiation on *GCN4* after translation of its four short uORFs. Schematics of the 5′ enhancers of uORF1 and 2 containing their respective RPEs, some of which functionally interact with eIF3 to promote resumption of scanning, were taken from Gunišová and Valášek (2014). Green color-coding generally indicates stimulatory effects of the corresponding *cis*-factors on efficiency of REI, whereas red color-coding indicates inhibitory effects (with the exception of RPE ii. of uORF1, which is also stimulatory); the number of asterisks *below* the inhibitory elements of the uORF2 and uORF3 3′ sequences illustrates the degree of their inhibition as determined experimentally. Please see text for further details.

codon recognition in a positive (uORF3) or negative (uORF4) way. In other words, we demonstrate for the first time that there is a direct negative correlation between the efficiency of reinitiation and efficiency of translation termination. Collectively this comprehensive approach pictures an intriguing complexity of this delicate regulatory system that depends on several REI-promoting as well as inhibiting features that mutually fine-tune their often autonomous effects on the overall efficiency of REI on *GCN4* mRNA in order to keep it as low as possible during nonstarvation conditions or as high as possible during starvation/stress conditions.

Even though there is a prevailing opinion that practically each short uORF is different and there are no generalizable rules that would apply to a majority of them (Wethmar 2014), we can conclude the following. The presence of the CCG triplet encoding proline as the last coding triplet most probably signals very poor REI potential of a given uORF, at least in yeast. Conversely, the presence of the RPE i.-like and/or RPE v.-like sequence motif not far upstream of a given short uORF, as well as the presence of the AU-rich motif immediately following the stop codon, might signal increased permissiveness for REI. An additional indicator of the REI permissiveness could be the presence of a structural element resembling the secondary structure of the uORF1 RPE iv., which can also be found in the 5′ enhancer of the solitary uORF preceding the *YAP1* gene (Munzarová et al. 2011).

MATERIALS AND METHODS

Yeast strains, plasmids, and other biochemical methods

Lists of strains (Supplemental Table S1), plasmids (Supplemental Table S2), and PCR primers (Supplemental Table S3) used in this study and details of their construction can be found in the Supplemental Material. β-Galactosidase assays were conducted as described previously (Mueller et al. 1987; Grant and Hinnebusch 1994). For all β-galactosidase values recorded with mutant constructs that differed from their respective wt constructs by <40%, the *P*-values were calculated and are given in the corresponding figure legends.

Stop codon readthrough assay

Dual luciferase assay was performed using the Dual Luciferase Reporter Assay System (Promega). Briefly, yeast strain PBH156 was transformed with the indicated dual luciferase reporter nonsense control plasmid pTH477 (Fig. 7A) as well as with the sense codon (CAA) plasmid pTH460 and pSG358, pSG362, pSG349, pSG365, or pSG350. The experiments and data analysis were carried out according to the Microtiter plate-based dual luciferase protocol developed by Merritt et al. (2010) and commercially distributed by Promega. Assays were done in quintuplicates ($n = 5$), the data are expressed as the mean ± SD, and each experiment was repeated at least three times. Resulting luciferase activity in each strain was expressed as the firefly/Renilla luciferase activity (nonsense or all indicated pSG plasmids) divided by the firefly/Renilla luciferase activity (sense). For further details, please see Keeling et al. (2004).

SUPPLEMENTAL MATERIAL

Supplemental material is available for this article.

ACKNOWLEDGMENTS

We are thankful to Josef Pánek for computational analysis, to Olga Krýdová for technical and administrative assistance, and to the members of the Valášek laboratory for helpful suggestions. This research was supported by the Czech Science Foundation Grant P305-11-0172.

Received October 26, 2015; accepted December 18, 2015.

REFERENCES

Abastado JP, Miller PF, Jackson BM, Hinnebusch AG. 1991. Suppression of ribosomal reinitiation at upstream open reading frames in amino acid-starved cells forms the basis for *GCN4* translational control. *Mol Cell Biol* **11:** 486–496.

Aylett CH, Boehringer D, Erzberger JP, Schaefer T, Ban N. 2015. Structure of a yeast 40S-eIF1-eIF1A-eIF3-eIF3j initiation complex. *Nat Struct Mol Biol* **22:** 269–271.

Beznosková P, Gunisova S, Valasek LS. 2015a. Rules of UGA-N decoding by near-cognate tRNAs and analysis of readthrough on short uORFs in yeast. *RNA* doi: 10.1261/rna.054452.115.

Beznosková P, Wagner S, Jansen ME, von der Haar T, Valášek LS. 2015b. Translation initiation factor eIF3 promotes programmed stop codon readthrough. *Nucleic Acids Res* **43:** 5099–5111.

Calvo SE, Pagliarini DJ, Mootha VK. 2009. Upstream open reading frames cause widespread reduction of protein expression and are polymorphic among humans. *Proc Natl Acad Sci* **106:** 7507–7512.

Cuchalová L, Kouba T, Herrmannová A, Dányi I, Chiu W-l, Valášek L. 2010. The RNA recognition motif of eukaryotic translation initiation factor 3g (eIF3g) is required for resumption of scanning of posttermination ribosomes for reinitiation on GCN4 and together with eIF3i stimulates linear scanning. *Mol Cell Biol* **30:** 4671–4686.

Cvijović M, Dalevi D, Bilsland E, Kemp GJ, Sunnerhagen P. 2007. Identification of putative regulatory upstream ORFs in the yeast genome using heuristics and evolutionary conservation. *BMC Bioinformatics* **8:** 295.

Dabrowski M, Bukowy-Bieryllo Z, Zietkiewicz E. 2015. Translational readthrough potential of natural termination codons in eukaryotes—the impact of RNA sequence. *RNA Biol* **12:** 950–958.

Davuluri RV, Suzuki Y, Sugano S, Zhang MQ. 2000. CART classification of human 5′ UTR sequences. *Genome Res* **10:** 1807–1816.

Dever TE, Feng L, Wek RC, Cigan AM, Donahue TD, Hinnebusch AG. 1992. Phosphorylation of initiation factor 2 α by protein kinase GCN2 mediates gene-specific translational control of *GCN4* in yeast. *Cell* **68:** 585–596.

Grant CM, Hinnebusch AG. 1994. Effect of sequence context at stop codons on efficiency of reinitiation in *GCN4* translational control. *Mol Cell Biol* **14:** 606–618.

Grant CM, Miller PF, Hinnebusch AG. 1995. Sequences 5′ of the first upstream open reading frame in *GCN4* mRNA are required for efficient translational reinitiation. *Nucleic Acids Res* **23:** 3980–3988.

Gunišová S, Valášek LS. 2014. Fail-safe mechanism of GCN4 translational control–uORF2 promotes reinitiation by analogous mechanism to uORF1 and thus secures its key role in GCN4 expression. *Nucleic Acids Res* **42:** 5880–5893.

Hinnebusch AG. 2005. Translational regulation of GCN4 and the general amino acid control of yeast. *Annu Rev Microbiol* **59:** 407–450.

Hood HM, Neafsey DE, Galagan J, Sachs MS. 2009. Evolutionary roles of upstream open reading frames in mediating gene regulation in fungi. *Annu Rev Microbiol* **63:** 385–409.

Iacono M, Mignone F, Pesole G. 2005. uAUG and uORFs in human and rodent 5′ untranslated mRNAs. *Gene* **349:** 97–105.

Jackson RJ, Hellen CU, Pestova TV. 2012. Termination and post-termination events in eukaryotic translation. *Adv Protein Chem Struct Biol* **86:** 45–93.

Keeling KM, Lanier J, Du M, Salas-Marco J, Gao L, Kaenjak-Angeletti A, Bedwell DM. 2004. Leaky termination at premature stop codons antagonizes nonsense-mediated mRNA decay in *S. cerevisiae*. *RNA* **10:** 691–703.

Kouba T, Dányi I, Gunišová S, Munzarová V, Vlčková V, Cuchalová L, Neueder A, Milkereit P, Valášek LS. 2012. Small ribosomal protein RPS0 stimulates translation initiation by mediating 40S-binding of eIF3 via its direct contact with the eIF3a/TIF32 subunit. *PLoS One* **7:** e40464.

Kozak M. 1987. Effects of intercistronic length on the efficiency of reinitiation by eukaryotic ribosomes. *Mol Cell Biol* **7:** 3438–3445.

Kozak M. 2005. Regulation of translation via mRNA structure in prokaryotes and eukaryotes. *Gene* **361:** 13–37.

Lee YY, Cevallos RC, Jan E. 2009. An upstream open reading frame regulates translation of GADD34 during cellular stresses that induce eIF2α phosphorylation. *J Biol Chem* **284:** 6661–6673.

Merritt GH, Naemi WR, Mugnier P, Webb HM, Tuite MF, von der Haar T. 2010. Decoding accuracy in eRF1 mutants and its correlation with pleiotropic quantitative traits in yeast. *Nucleic Acids Res* **38:** 5479–5492.

Miller PF, Hinnebusch AG. 1989. Sequences that surround the stop codons of upstream open reading frames in *GCN4* mRNA determine their distinct functions in translational control. *Genes Dev* **3:** 1217–1225.

Mueller PP, Harashima S, Hinnebusch AG. 1987. A segment of *GCN4* mRNA containing the upstream AUG codons confers translational control upon a heterologous yeast transcript. *Proc Natl Acad Sci* **84:** 2863–2867.

Munzarová V, Pánek J, Gunišová S, Dányi I, Szamecz B, Valášek LS. 2011. Translation reinitiation relies on the interaction between eIF3a/TIF32 and progressively folded *cis*-acting mRNA elements preceding short uORFs. *PLoS Genet* **7:** e1002137.

Palam LR, Baird TD, Wek RC. 2011. Phosphorylation of eIF2 facilitates ribosomal bypass of an inhibitory upstream ORF to enhance CHOP translation. *J Biol Chem* **286:** 10939–10949.

Pavlov MY, Watts RE, Tan Z, Cornish VW, Ehrenberg M, Forster AC. 2009. Slow peptide bond formation by proline and other *N*-alkylamino acids in translation. *Proc Natl Acad Sci* **106:** 50–54.

Pisarev AV, Hellen CU, Pestova TV. 2007. Recycling of eukaryotic posttermination ribosomal complexes. *Cell* **131:** 286–299.

Pöyry TA, Kaminski A, Jackson RJ. 2004. What determines whether mammalian ribosomes resume scanning after translation of a short upstream open reading frame? *Genes Dev* **18:** 62–75.

Rajkowitsch L, Vilela C, Berthelot K, Ramirez CV, McCarthy JE. 2004. Reinitiation and recycling are distinct processes occurring downstream of translation termination in yeast. *J Mol Biol* **335:** 71–85.

Raveh-Amit H, Maissel A, Poller J, Marom L, Elroy-Stein O, Shapira M, Livneh E. 2009. Translational control of protein kinase Cη by two upstream open reading frames. *Mol Cell Biol* **29:** 6140–6148.

Roy B, Vaughn JN, Kim BH, Zhou F, Gilchrist MA, Von Arnim AG. 2010. The h subunit of eIF3 promotes reinitiation competence during translation of mRNAs harboring upstream open reading frames. *RNA* **16:** 748–761.

Skabkin MA, Skabkina OV, Hellen CU, Pestova TV. 2013. Reinitiation and other unconventional posttermination events during eukaryotic translation. *Mol Cell* **51:** 249–264.

Sundaram A, Grant CM. 2014. A single inhibitory upstream open reading frame (uORF) is sufficient to regulate *Candida albicans* GCN4 translation in response to amino acid starvation conditions. *RNA* **20:** 559–567.

Szamecz B, Rutkai E, Cuchalová L, Munzarová V, Herrmannová A, Nielsen KH, Burela L, Hinnebusch AG, Valášek L. 2008. eIF3a cooperates with sequences 5′ of uORF1 to promote resumption of scanning by post-termination ribosomes for reinitiation on GCN4 mRNA. *Genes Dev* **22:** 2414–2425.

Valášek LS. 2012. 'Ribozoomin'—translation initiation from the perspective of the ribosome-bound eukaryotic initiation factors (eIFs). *Curr Protein Pept Sci* **13:** 305–330.

Valášek L, Mathew AA, Shin BS, Nielsen KH, Szamecz B, Hinnebusch AG. 2003. The yeast eIF3 subunits TIF32/a, NIP1/c, and eIF5 make critical connections with the 40S ribosome in vivo. *Genes Dev* **17:** 786–799.

Vilela C, Linz B, Rodrigues-Pousada C, McCarthy JE. 1998. The yeast transcription factor genes YAP1 and YAP2 are subject to differential control at the levels of both translation and mRNA stability. *Nucleic Acids Res* **26:** 1150–1159.

von Arnim AG, Jia Q, Vaughn JN. 2014. Regulation of plant translation by upstream open reading frames. *Plant Sci* **214:** 1–12.

Wethmar K. 2014. The regulatory potential of upstream open reading frames in eukaryotic gene expression. *Wiley Interdiscip Rev RNA* **5:** 765–778.

Wohlgemuth WA, Safonova O, Engelhardt M, Freitag M, Wölfle K, Kirchhof K. 2008. Improvement of the quality of life concerning the health of patients with peripheral arterial disease (PAD) after successful bypass surgery. *Vasa* **37:** 338–344.

Zhou F, Roy B, von Arnim AG. 2010. Translation reinitiation and development are compromised in similar ways by mutations in translation initiation factor eIF3h and the ribosomal protein RPL24. *BMC Plant Biol* **10:** 193.